RELIABILITY-BASED STRENGTH PREDICTION MODEL FOR CORRODED REINFORCED CONCRETE COLUMNS AND BEAM-COLUMNS

BY

MOHAMMED ALI MOHAMMED AL-OSTA

A Dissertation Presented to the

DEANSHIP OF GRADUATE STUDIES

KING FAHD UNIVERSITY OF PETROLEUM & MINERALS

DHAHRAN, SAUDI ARABIA

In Partial Fulfillment of the

Requirements for the Degree of

DOCTOR OF PHILOSOPHY

In

CIVIL ENGINEERING

MAY 2013

KING FAHD UNIVERSITY OF PETROLEUM & MINERALS

DHAHRAN- 31261, SAUDI ARABIA

DEANSHIP OF GRADUATE STUDIES

This thesis, written by **MOHAMMED ALI MOHAMMED AL-OSTA** under the direction his thesis advisor and approved by his thesis committee, has been presented and accepted by the Dean of Graduate Studies, in partial fulfillment of the requirements for the degree of **DOCTOR OF PHILOSOPHY IN CIVIL ENGINEERING.**

Dr. Abul Kalam Azad
(Advisor)

18 MAY 2013

Dr. Nedal T. Ratrout
Department Chairman

Dr. Shokri Selim
(Co-Advisor)

Dr. Salam A. Zummo
Dean of Graduate Studies

عمادة الدراسات العليا
DEANSHIP OF GRADUATE STUDIES

Dr. Muhammed Baluch
(Member)

21/5/13

Date

Dr. Shamshad Ahmad
(Member)

Dr. Mohammad Maslehuddin
(Member)

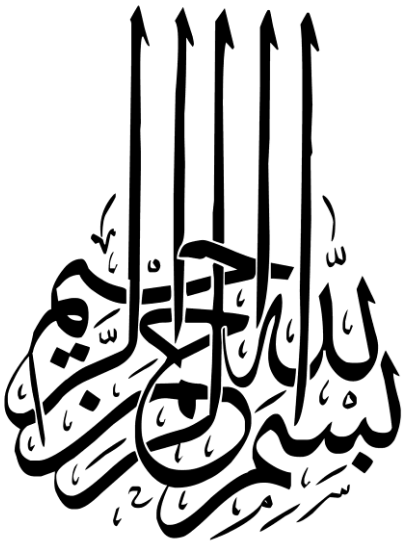
بسم الله الرحمن الرحيم

DEDICATED
TO MY FATHER, MOTHER, WIFE, MY
CHILDREN AND TO MY BROTHERS & SISTER

ACKNOWLEDGMENTS

All praise and thanks are due to my Lord, ALLAH SUBHAN WA TAALA, for giving me the health, knowledge and patience to complete this work. I acknowledge the financial support provided by KFUPM's Civil Engineering Department and Sana'a University during my graduate studies.

My sincerest gratitude goes to my advisor Dr. Abul Kalam Azad and co-advisor Dr. Shokri Selim who guided me with their dedicated attention, expertise and knowledge throughout this research. Thereafter, I deeply indebted and grateful to my Committee Members, Dr. Muhammed Baluch, Dr. Shamshad Ahmad and Dr. Mohammad Maslehuddin, for their extensive guidance, continuous support, and personal involvement in all phases of this research. Thanks are also due to the department's Chairman Dr. Nedal Ratrout and his secretary for providing aid, and to other faculty members and staff.

I also acknowledge the sincere and untiring efforts of Engr. Omer Hussein, Engr. Syed Imran Ali and Mr. M. Mukarram Khan who assisted me during all stages of my experiments. I would like to offer my acknowledgement to Engr. Abbas from the Electrical Engineering Department, who helped me in preparing the experimental set-up utilized in this study. Thanks and acknowledgment is due to Dr. Mohammed H. Essa and Dr. Muhammad K. Rahman for their help and to Mr. Ashhad Imam for his assistance in the experimental work.

Special thanks are due to my colleagues in the Civil Engineering Department, for their aid and support. Thanks are also due to all my friends for their support and encouragement.

My heartfelt gratitude is given to my beloved father, mother, my wife and my children, who always support me with their love, patience, encouragement and constant prayers. I would like to thank my grandmothers, brothers, sisters, and all members of my family in Yemen for their emotional and moral support throughout my study.

TABLE OF CONTENTS

LIST OF TABLES

LIST OF FIGURES

LIST OF SYMBOLS AND ABBREVIATIONS

SYMBOLS:

A_g : Cross-sectional area of concrete

A_{pit} : Cross-sectional area of the pit

A_s : Cross-sectional area of un-corroded reinforcement

A_s' : Cross-sectional area of corroded reinforcement

b_o : Undamaged member section width

b_f : Member width increased by corrosion cracking

B : Constant

β : Reliability index

c : Distance to neutral axis

C_c : $(P_{exu} \times 100 / P_{thu})$

c_{co} : Thickness of the cover layer

D : Diameter of un-corroded reinforcing bar

D' : Diameter of corroded reinforcing bar

d' : Effective cover of compression steel

e : Eccentricity of load applied

ε_1 : Average tensile strain in the cracked concrete perpendicular to the direction of the applied compression

E_c : Modulus of elasticity of concrete

ε_o : Strain at the peak compressive strength f_c'

E_s : Young's modulus of un-corroded longitudinal bar

E_{sc} : Young's modulus of corroded longitudinal bar

ε_y : Yield strain of steel bar

ε_u : Tensile strain of steel bar

F : Faraday's constant

f : Stress at any strain ε

f_1 : Ultimate compressive strength for a state of biaxial compression superimposed on the hydrostatic stress state

f_2 : Ultimate compressive strength for a state of uniaxial compression superimposed on hydrostatic stress state

f_{bc}' : Ultimate biaxial compressive strength

f_c' : 28-day compressive strength of virgin concrete

$f_{cc,cracked}$: Compressive strength of cracked concrete

f_y : Yield strength of un-corroded longitudinal bar

f_{yc} : Yield strength of corroded longitudinal bar

f_{ycp} : Yield strength of corroded longitudinal bar due to pitting corrosion

f_t : Tensile strength of un-cracked concrete

$f_{t,cracked}$: Tensile strength of cracked concrete

f_{ts} : Concrete's splitting tensile strength

f_u : Tensile strengths of steel bar

$\Phi(.)$: Cumulative distribution function (CDF) of the standard normal random variable

γ : (Total depth of cross-section- (effective cover *2))/Total depth of cross-section

h : Depth of cross-section

I_{app} : Applied current density

I_{corr} : Corrosion current density

$I_{corr}T$: Corrosion activity index

J_r : Instantaneous corrosion rate (mass of metal lost/surface area/time)

l : Distance between two adjacent spring elements

M : Bending moment ($P.e$)

M_n : Bending moment ($P_n.e$)

M_{thu} : Nominal ultimate bending moment of un-corroded specimen

μ : Mean of the distribution

$\mu_{p_{res}}$: Mean of the predicted strength

μ_Q : Mean of the required strength

n : Acceptable limit factor

n_{bar} : Number of reinforcement bars in the compression zone

P : Load applied of specimen

P_e : Member perimeter increased by corrosion cracking

P_{exc} : Experimental failure load of corroded specimen

P_{exu} : Experimental failure load of un-corroded specimen

P_f : Probability of failure

P_{fec} : Finite element failure load of corroded specimen

P_{feu} : Finite element failure load of un-corroded specimen

P_o : Undamaged member section perimeter

P_n : Failure axial compressive force

P_r : Penetration rate (penetration depth/time)

P_{res} : Predicted failure load of corroded specimen

P_s : Service load demand

$P(T)$: Maximum pit depth

P_{thu} : Theoretical failure load of un-corroded specimen

P^* : Theoretical failure load of corroded specimen using only the reduced steel area A_s'

P_u : Factored load for design

R : Ratio of bond strength at any corrosion level to the original bond strength for un-corroded specimen

R_c : $(P_{exc} / P_{*)}$

R_f : $(P_{exc} \times 100 / P_{exu})$

R_p : Polarization resistance

S : Slip

S_1 : Maximum slip

σ : Standard deviation of the distribution

σ^2 : Variance of the distribution

σ_h : Hydrostatic pressure

$\sigma_{p_{res}}$: Standard deviation of the predicted strength

σ_Q : Standard deviation of the required strength

$\sigma_{xp}, \sigma_{yp}, \sigma_{zp}$: Principal stresses in the principal directions

T : Duration of corrosion

T_a : Corrosion initiation period

T_c : Critical corrosion time

T_s : Service life period

τ_{bc} : Bond stress of corroded longitudinal bars

τ_{bu} : Bond stress of sound longitudinal bars

$\tau_{\max}$: Maximum bond strength

λ : Metal loss factor = $2P_rT/D$

α : Damage factor

α_1 : Damage factor for column

α_2 : Damage factor for beam-column

$v_{r/s}$: Ratio of volumetric expansion of the oxides with respect to the virgin material

w_{cr} : Crack width for a given corrosion penetration P_rT

W : Equivalent weight of steel

W_i : Initial weight of the bar before corrosion

W_f : Weight after corrosion

ω : Maximum permitted reduction factor for the minimum required residual strength

x_0, x_1, x_2, x_3 : Empirical constants

X_c : Penetration depth and is equal to P_rT

X_p : Precentage weight loss of metal due to induced corrosion

Y : Maximum pitting factor

y' : Distance of geometric centroid

z_0, z_1, z_2, z_3 : Empirical constants

η : Current efficiency

ABBREVIATIONS:

FE : Finite element

FORM : First order reliability method

FOSM : First order second moment

MCS : Monte Carlo simulation

ABSTRACT

Full Name : MOHAMMED A. MOHAMMED AL-OSTA

Thesis Title : RELIABILITY-BASED STRENGTH PREDICTION MODEL FOR CORRODED REINFORCED CONCRETE COLUMNS AND BEAM-COLUMNS

Major Field : CIVIL ENGINEERING

Date of Degree : MAY 2013

The exterior columns and beams-columns are the key load-bearing elements in any structure, such as a building or a bridge and they are the most exposed structural components to chloride attack. This chloride-induced corrosion of steel reinforcement is the single most prevalent cause of concrete deterioration.

This research has three major components: (i) an expanded experimental work in which experimental data on strength reduction of column and beam-column members due to corrosion were collected; (ii) analytical and empirical predictions of residual strength of corroded members and (iii) a reliability analysis to estimate the probability of failure based on Monte Carlo simulation.

For experimental work, a number of reinforced concrete specimens were subjected to accelerated corrosion using impressed current to induct various degrees of corrosion damage. The experimental variables included: corrosion duration, the cross section of a member, the diameter of main reinforcement and the eccentricity of applied load. A total of 20 column specimens and 62 specimens for beam-columns were tested to include all variables. Out of 82 specimens, 14 specimens were repeated specimens, 4 specimens were used for verification and 64 specimens were used in developing the predictive

model. From the experimental data, the reduction in strength of a corroded member is indicated as a function of the degree of corrosion damage. The information on the strength reduction factor is useful in assessing the condition of a deteriorated structure and a timely repair.

The finite element method was used for theoretical prediction of the load carrying capacity of corroded reinforced concrete member based on bond-slip between the steel bars and concrete, the reduction of bars section area, decrease in bars' yielding strength and cracking of concrete for different degree of corrosion. Using all significant parameters that govern strength, a structural reliability analysis is proposed deploying Monte Carlo simulation to estimate the probability of failure based on theoretical prediction.

DOCTOR OF PHILOSOPHY
KING FAHD UNIVERSITY OF PETROLEUM AND MINERALS
DHAHRAN, SAUDI ARABIA

ملخص الرسالة

الاسم الكامل: محمد علي محمد الأسطى

عنوان الرسالة: التقدير الموثوق للقوة المتبقية للأعمدة الخرسانية المركزية و اللامركزية التحميل المعرضة للصدأ.

التخصص : الهندسة المدنية

تاريخ الدرجة العلمية: مايو 2013م

تعتبر الأعمدة الخارجية بنوعيها المركزية و اللامركزية التحميل من العناصر الحاملة الرئيسية في أي منشاة، مثل المبنى أو الجسر، وهي العنصر الأكثر تعرضا لهجوم الكلوريد. ويعتبر الكلوريد المحفز الرئيسي لتآكل حديد التسليح والذي يعتبر السبب الوحيد لتدهور الخرسانة.

يتكون هذا البحث من ثلاثة عناصر رئيسية: (1) العمل التجريبي الواسع التي يتم من خلاله الحصول على البيانات المعملية والخاصة بالقوة المتبقية للأعمدة المركزية و اللامركزية التحميل والناتجة من تآكل حديد التسليح (2) التقديرات التحليلية والتجريبية للقوة المتبقية للعناصر المتآكلة (3) التحليل الموثوق لتقدير احتمالية الفشل باستخدام محاكاة مونت كارلو(MCS).

بالنسبة للعمل التجريبي ، فقد تم تعريض العديد من عينات الخرسانية المسلحة للتآكل المتسارع وذلك باستخدام التيار لعمل درجات مختلفة من التلف الناتج عن التآكل. شملت المتغيرات المعملية: مدة التآكل، والمقطع العرضي للعينة، قطر حديد التسليح الرئيسي و لامركزية التحميل(e). كما تم اجراء الاختبار علي 20 عينه من الأعمدة المركزية التحميل و 62 عينه من الأعمدة اللامركزية التحميل لتشمل جميع المتغيرات المعملية. 14 عينه كانت عينات متكررة من اجمالي 82 عينه، وقد تم استخدام 4 عينات للتحقق النموذج، 64 عينه استخدمت في تطوير نموذج تقدير القوة المتبقية من البيانات المعملية ، و قد تم الاشارة إلى النقص في قوة العنصر المتآكل كدالة في درجه التلف الناتج عن التآكل. ان المعلومات الخاصة بالنقص في قوة العنصر المتآكل مفيدة في تقييم حالة العنصر الانشائي المتدهور والوقت المناسب لإعمال الصيانة.

تم استخدام نموذج العناصر المتناهية في الصغر (FE) للتقدير النظري للقوة المتبقية للعنصر الخرساني المسلح والمعرض لدرجات مختلفة من التلف الناتج عن التآكل بناء على قوة التماسك بين حديد التسليح والخرسانة، نقصان مساحة المقطع لحديد التسليح، نقصان في اجهاد الخضوع لحديد التسليح وتشقق الخرسانة. و باستخدام جميع المتغيرات الهامة التي تحكم قوة المقطع الانشائي، تم اقتراح التحليل الموثوق للعنصر الانشائي باستخدام محاكاة مونتي كارلو لتقدير احتمالية الفشل بالاعتماد علي التقدير النظري للقوة المتبقية.

DOCTOR OF PHILOSOPHY
KING FAHD UNIVERSITY OF PETROLEUM AND MINERALS
DHAHRAN, SAUDI ARABIA

CHAPTER 1

INTRODUCTION

1.1 Reinforcement Corrosion

Corrosion is a major durability problem for reinforced concrete construction. Research work conducted in the Arabian Gulf estimates that the service life of buildings to be between 10 and 15 years and sometimes only five years (MEC, 1987). In addition, corrosion costs millions of dollars for repairing. However, cost is only one problem. Safety is the main problem. Rasheeduzzafar et al. (1984) reported condition surveys of 42 concrete framed structures in the Eastern Province revealing startling degree of concrete damage, which is in the form of cracking and spalling due to corrosion of reinforcement, sulfate attack, salt weathering and cracking due to shrinkage, thermal gradients, and aggregate-cement reactivity. The main causes of concrete damage are the severe environmental conditions, poor construction practices and poor materials used.

Till date, collapse of reinforced concrete structures in Saudi Arabia, due to reinforcement corrosion, has not been reported. However, this is not the case somewhere else. Yeung (1999) reported that reinforcement corrosion contributed to failure of some reinforced concrete structures in Hong Kong.

Chloride-induced corrosion of steel reinforcement is the single most prevalent cause of concrete deterioration. Figure 1.1 shows damage of columns due to corrosion (Aboutaha,

2004). Three types of physical degradation take place simultaneously in a reinforced concrete element due to corrosion: cracking of concrete cover which ultimately leads to spalling of concrete, loss of bond between steel and concrete, and a reduction in the cross-sectional area of the reinforcing steel due to loss of metal from rust formation, all of which combinedly reduces the member's load carrying capacity, thereby compromising its safety to carry the applied loading.

As the residual strength of a corroding member is related to corrosion damage, the strength progressively declines with time due to damage propagation. As part of an inspection and assessment work, it is often necessary to have an expert opinion regarding the load-carrying capacity of the major structural elements which are being corroded. This information is vital to ascertain the prevailing level of safety of the structure to avoid the risk of structural failure. Furthermore, it is necessary to determine the extent of corrosion damage and its implication on safety, so that the necessary repair or restoration work can be planned in time without further compromising the safety of the structure. Based on an analytical model, the residual strength of a corroded reinforced concrete member can be determined to ascertain the level of safety.

The methods for structural reliability being used since recent times are very useful tool for determining the probability of failure and evaluating the safety of complex structures such as buildings and bridges.

Figure 1.1: Corrosion damaged concrete column (Aboutaha, 2004).

There are many reliability methods such as Monte Carlo simulation (MCS), First Order Reliability Method (FORM) and First Order Second Moment (FOSM). In this thesis, MCS was used to estimate the probability of failure for the reinforced concrete beam-columns subjected to corrosion and had different dimensions and bar diameters. In MCS, the statistical distributions which are the source for the input parameters are constructed using numerical methods by fitting the data to theoretical discrete or continuous distribution. It is done by recognizing the most appropriate probability distribution for a given set of data. After that, the random samples are drawn from each distribution, which represent the values of the input. Where, the statistical distributions of some input random variables were used from literature such as the yield strength of steel, f_y etc. (Arun and Pillai, 2006).

1.2 Significance of the Study

A review of literature clearly shows that a considerable body of literature exists on the behavior of corroded beams and on the effect of corrosion of steel on bond between steel and concrete. Some work proposes approaches to predict the residual strength of corroded beams. However, relatively only a few publications are devoted to the study of the strength of the corroded columns and beam-columns. Limited experimental work on the mechanical behavior of corroded columns under concentric and eccentric loading exists, indicating a need for more experimental data, which would help in modeling and understanding the structural behavior. The prediction of the residual strength helps in determining the underlying safety of the corroded columns and beam-columns to decide

when the repairing or strengthening must be undertaken without any further delay.

1.3 Objectives

The primary objective is to develop analytical methods for prediction of residual strength of corroded reinforced concrete columns and beam-columns based on experimental correlation with laboratory-generated test data. Specific objectives are:

(i) Undertake an experimental work to generate substantive data;

(ii) Develop theoretical strength prediction models using empirical approach and finite element analysis in which corrosion damage is captured by modeling various effects;

(iii) Verify of the proposed model using available and newly generated test data, and

(iv) Carry out a reliability analysis using Monte Carlo simulation to estimate probability of failure.

1.4 Scope

The scope of work was limited to the study of corroded reinforced concrete columns and beam-columns which were corroded in laboratory by using accelerated corrosion with

impressed current. The specimen size was limited to two and the eccentricity used for beam-columns was limited to three values.

1.5 Approach

The research work was planned around the following nine tasks:

Task 1: Review of literature

Task 2: Casting and curing of test specimens

Task 3: Preparation for the experimental work

Task 4: Test setup for accelerated corrosion induction

Task 5: Finite element modeling

Task 6: Development of methods for predicting the residual strength

Task 7: Verification of the proposed method

Task 8: Probability of failure of corroded element using (MCS)

Task 9: Results and discussion and writing of dissertation

CHAPTER 2

LITERATURE REVIEW

An extensive literature survey was carried out to review the works of earlier researchers on the topics related to the effect of reinforcement corrosion on the strength, cracking and loss of bond.

The literature review was presented under the following subheadings:

- Effect of reinforced corrosion on the mechanical behavior.
- Effect of loss of bond between steel and concrete.
- Prediction of residual strength.
- Reliability assessment of reinforced concrete elements.
- Modeling of corroded reinforced concrete member.

2.1 Effect of Reinforced Corrosion on the Mechanical Behavior

Ting and Nowak (1991) have developed a method for calculating the effect of the loss of reinforcement area on the moment capacity of corroded beams and slabs using finite difference method. The results showed that the reinforcing steel area loss is a linear function of the loss of material. Cabrera (1996) tested six beams, corroded by accelerated corrosion. The beams had a cross section of 125×160 mm. It was noted that the moment capacity increased by almost 20% when the mass loss is less than 2%. The moment

capacity decreases linearly when the percent of mass loss increases.

Rodriguez et al. (1997) tested six beams, corroded by accelerated corrosion where a constant current of 0.1mA/cm^2 was applied for a period of time ranging between 100 and 200 days. Based on the results, it was noted that the ultimate moment capacity can be predicted using conventional method with a reduced section cross-sectional area of steel only.

Huang and Yang (1997) studied the effect of reinforcing steel area loss on flexural behavior of reinforced concrete beams for 32 corroded reinforced concrete beams. The specimens were corroded using accelerated corrosion by applying an impressed current. It was concluded that a small loss of thickness of bars may significantly reduce load-carrying capacity.

Yoon et al. (2000) have investigated concrete beam specimens having dimensions 100 mm × 150 mm × 1170 mm. It was found that beams having a degree of corrosion greater or equal to 3% weight loss of steel lose load- carrying capacity, and bond failure is likely to occur at higher metal loss. It was stated that the failure mode of the reinforced concrete beams shifted from a shear failure to bond splitting failure as the degree of steel corrosion increased.

Almusallam (2001) reported results to assess the effect of corrosion on mechanical properties of the reinforcing steel bars. It was noted that the tensile strength of steel bars, determined based on the actual area of cross-section, was not influence by the level of reinforcement corrosion.

Apostolopoulos et al. (2006) presented the results of an experimental work for the

gradually accumulating corrosion damage due to laboratory salt spray corrosion on the mechanical behavior of reinforcing steel bars. It was observed that the mass loss increased with increasing duration of exposure. The results showed that the tensile properties of the steel bars go down for laboratory salt spray exposure times to values lying below the limits for using steels in reinforced concrete members.

2.2 Effect of Loss of Bond between Steel and Concrete

Al-Sulaimani et al. (1990) studied corrosion relation of reinforcement to bond deterioration by testing many beams. The beams were of 150×150×1000 mm size, reinforced with 2-10 mm diameter top bars, 2-12 mm diameter bottom bars and links 6 mm diameter at 50 mm spacing. The bottom reinforcement bar was corroded by applying a constant current density of 2.0 mA/cm^2. It was noted that the reduction of strength attributed to the reduction in the bar cross section.

Almusallam et al. (1996) carried out study on the effect of reinforcement corrosion on bond strength. Almusallam et al. reported that bond strength decreased rapidly up-to a certain degree of corrosion and thereafter the rate of decrease was much slower. It was noted that the first corrosion crack appears at about 5% gravimetric weight loss, the bond strength decreased gradually for an additional 1% corrosion, and thereafter decreased rapidly. Fu and Chung (1997) also noted that corrosion of steel bars in concrete initially increased marginally the bond strength, and thereafter with prolonged corrosion bond strength progressively declined. It was concluded that small corrosion (less than 5 weeks) increased the bond strength, but severe corrosion (more than 5 weeks) decreased the bond

strength.

Amleh and Mirza (1999) studied the bond between steel and concrete. The study showed that the bond strength between the steel and concrete decreased rapidly with increasing the corrosion level, especially in the case of any localized corrosion. The result showed that where there was a severe localized corrosion the bond strength and the number of transverse cracks decreases as the level of corrosion increases until it becomes negligible.

Stanish et al. (1999) reported from their study of corrosion effects on bond strength that bond resistance was adversely affected by the accumulation of corrosion products leading to concrete cracking, which, in the absence of confinement, relieves the internal pressure but also weakened the anchorage of the reinforcing steel creating a weak layer of corrosion product that will break off under relatively low stress levels. This soft layer may effectively act as a lubricant, preventing the development of either friction or reinforcement to concrete interlock.

Auyeung et al. (2000) presented the bond behavior of corroded reinforcement bars. It was demonstrated that when the mass loss of the reinforcement due to corrosion reached approximately 2%, the concrete cracked along the bar. A small amount of corrosion increased both the bond strength and bond stiffness, but the slip at failure decreased considerably. It was indicted that when the mass loss exceeded 2%, bond stiffness decreased considerably. Therefore, failure of specimens with corroded bars can be expected to be much more brittle compared to control specimens with un-corroded bars. It was noted that the bond was not completely destroyed even when there was extensive corrosion with considerable cracking of concrete. Measurable bond strength existed even when the mass loss approached 6%.

Coronelli (2002) has developed a model to calculate the pressure around a corroded bar and the bond strength at the onset of pullout in an anchorage. The results showed that considerable bond strength remains available as long as only the primary corrosion cracks had formed across the thinner cover and the corrosion pressure build-up gave some contribution to bond strength. Bond deterioration began when the final cracking took place when the cover was split. The study showed that the stirrups provided some residual confining action together with the concrete remaining around the bar.

Berra et al. (2003) studied the steel-concrete bond deterioration due to corrosion, using finite element analysis for different confinement levels. The numerical results showed that whether or not cover cracking caused by bar corrosion determined a confinement loss, leading to bond deterioration, depends on the amount and arrangement of transverse steel provided. It was found that bond deterioration was limited by confinement: the greater the transverse steel provided, the higher the residual bond strength.

Wang and Liu (2005) carried out the bond strength modeling for corroded reinforcements. It was found that with increasing corrosion level, the bond strength of corroded reinforcement's increased. Thereafter, it decreased until it became negligible with further increase in corrosion level.

Bhargava et al. (2008) suggested simple empirical models to estimate the reduction in bond strength as a function of reinforcement corrosion in reinforced concrete (RC). It was demonstrated that the models could be used to estimate the reduction in bond strength for corroded reinforcement that are in reasonably good agreement with the experimentally observed values.

Lee et al. (2002) have investigated the bond properties between concrete and corroded reinforcement by using the pullout tests and using reinforcements embedded in concrete specimens, which were corroded by an accelerated electric corrosion method. A finite element method (FEM) analysis was also carried out to model the pullout tests. It was noted that the maximum bond strength (τ_{max}) and the bond rigidity (D_s) of specimens decreased in proportion to the increase of corrosion percentage (D_w), respectively. The equations for calculating the maximum bond strength and the bond rigidity necessary for an FEM analysis of RC members with corroded reinforcements were obtained by the experiments and the FEM analysis of the pullout test.

The literature review reveals that the main parameters, which influence the bond strength of corroded bars, are: confinement of concrete cover, strength of concrete, the ratio of rust volume to non-corroded metal, evolution of corrosion pressure due to rust formation, initial geometry of ribbed bars, interface degradation and the reduction of the rib profile of the bars.

2.3 Prediction of Residual Strength

2.3.1 Flexure Strength of Beams

A significant amount of research has been carried out over the past fifteen years or so. Ravindrarajah and Ong (1987) have investigated the effect of the diameter of the steel bar, and the thickness of the cover on the degree of corrosion of mild steel bars embedded in mortar. The specimens were cylindrical in shape and each specimen consisted of a

single mild steel bar placed centrally. A 5V supply was selected to cause a significant intensity of corrosion in steel bars within a reasonable period. The results illustrated that there was significant effect of rebar diameter, cover thickness, and specimen size on the corrosion intensity. It was found that the intensity of corrosion of reinforcing steel in concrete increased with an increase in the bar diameter. For the same diameter of bar, the corrosion intensity of steel increased when the cover thickness was decreased. The surface area of the corrosion specimen through which the chloride ions diffuse was also found as an important parameter in determining the rate and extent of corrosion of embedded steel in concrete.

Uomoto and Misra (1988) carried out a large experimental work with corroded beams and columns to study the load carrying capacity of corroded members. It was observed that beams of 100×100×700 mm, reinforced with 2-10 mm diameter bottom bars failed in shear. The results demonstrated that the deterioration of structures caused by the reinforcement corrosion was not always directly related to loss of strength of the bars due to reduction in cross-sectional area, but some other factors such as crack formation in concrete and loss of bond. This could lead to greater reduction in strength of the structure.

Tachibana et al. (1990) carried out tests with corroded beams of 200×150×2000 mm, reinforced by 2-16 mm diameter bottom bars. The reinforcement was corroded by applying a current density of 0.5 mA/cm^2 up to 15 days. The maximum percentage of weight loss of reinforcement was about 5%. The shear span and the loading span were 300 mm and 1500 mm respectively. The data showed that non-corroded and mildly corroded beams failed in flexure with yielding of steel bars but highly corroded beams

failed in bond shear in a brittle manner.

Cabrera and Ghoddoussi (1992) carried out tests on corroded beams of 160×125×1000 mm. The bottom bars were corroded by applying a current density of unknown value for up to 40 days, using a potentiostatic procedure. It was indicated that a reduction of 9% of the cross section at bottom bar resulted into a reduction of 20% of the ultimate bending moment, and an increase of 40% of the deflection at mid-span at the service load.

Nokhasteh et al. (1992) conducted preliminary flexural tests on three simply supported RC beams. The specimens were of dimensions 130×200×2350 mm with 16 mm smooth mild black steel bars. All beams carried two 6 mm mild steel bars as top steel. The ultimate load capacity of the control specimens was calculated theoretically using the stress-block factors derived from the empirically.

Aziz (1994) has investigated the effect of reinforcement corrosion on the flexural strength of a uniformly loaded and simply supported one-way slab. The specimens were partially immersed in a 5% sodium chloride solution. It was noted that a sharp reduction in the ultimate flexural strength of slabs with up to 20% reinforcement corrosion; thereafter, the strength decreased at a somewhat reduced rate with further increase in reinforcement corrosion. The reduction in the ultimate flexural strength of slabs with 5% reinforcement corrosion was 25%, while it was 60% in the slabs with 25% reinforcement corrosion.

Zhang et al. (1995), Hui et al. (1997), and Jin and Zhao (2001) reported that yield of a corroded bar was expected to increase within the corrosion period. An empirical form of expressions have been suggested for calculations of the reduced steel cross-sectional area, reduced steel yield strength and bond strength based on the test data. No attempt was

made in this study to verify this postulation and the original yield strength of bars has been used in all calculations.

Mangat and Elgarf (1999) carried out a research work on developing relationship between the degree of reinforcement corrosion and the residual strength of flexural members through an experimental scheme. It was found that reinforcement corrosion in concrete has effect on both the flexural load capacity and deflection of beams. The reduction in residual strength was primarily due to the loss or breakdown of the steel-concrete interfacial bond. A trigonometric function has been proposed to predict the residual strength of corroded beams in terms of the rate of corrosion, corrosion time and bar diameter.

Castel et al. (2000 Parts 1 and 2) studied mechanical behavior of corroded reinforced concrete beams. It was illustrated that the concrete cracking created by corrosion of compressive reinforcements does not significantly influence the mechanical characteristics of the reinforced concrete beams in service. It was stated that the residual strength of a corroded beam can be predicted in most cases by taking into consideration only the reduction in tension steel area and discounting the loss of bond.

Li (2003) proposed an exponential form for modeling corrosion deterioration as part of lifecycle modeling of the corrosion affected members. A deterioration factor has also been proposed by Li (2005) for corroded beams.

Based on extensive laboratory generated test data, Azad et al. (2007) proposed a two-step analytical approach for prediction of the residual flexural strength. In this proposed method, first the strength was calculated using conventional theory using only the

reduced tension steel area, and ignoring adverse implication of bond strength. In the next step, this value was corrected to yield the theoretical prediction by multiplying it with a reduction factor developed through a multi-level regression analysis of test data. The size effect of the beams and the bars has been investigated by Azad et al. (2005, 2007) and Al-Gohi (2008), which proposed a modified correction factor for strength prediction that should be used in the approach proposed by Azad et al. (2007).

Torres-Acosta et al. (2007) correlated results from an experimental investigation of flexure capacity loss with steel cross-section loss due to generalized corrosion of the embedded steel in a humid environment. The beams were corroded by applying a nominal 80 $\mu A/cm^2$ constant anodic current for approximately 50–180 days. The results showed that for dry environment, the corrosion-induced concrete crack propagation was enhanced during the accelerated corrosion stage. However, wet environment during corrosion acceleration enhanced pit formation at the rebar surface.

Chung et al. (2008) presented experimental and analytical evaluations on corroded and un-corroded reinforced concrete slabs. From pull-out tests conducted on corroded RC slab, the moment capacity of the slabs was predicted. The results indicated that a good accuracy can be achieved for the behavior of the slabs with corroded reinforcement. This study showed that a small amount of corrosion increased the flexural capacity of the slab as in the case of pull-out tests. However, the capacity reduced considerably when the loss in bar diameter exceeded 2%. The results confirmed that bond damage was the main contributor to the reduction of moment capacity.

Malumbela et al. (2009) presented results of the variation of mass loss of the corroded tensile steel bars in RC beams whilst under a sustained load using an impressed current

and constant wetting cycles (two different drying cycles). It was indicated that for longer drying cycles, the highest level of corrosion occurred. The results showed that the level of sustained load had little effect on the rate of corrosion. The ultimate flexural capacity of beams was found to be best related to the maximum gravimetric mass loss compared to the average mass loss of steel.

Wang and Liu (2010) proposed a simplified methodology to estimates of the residual life of corroded RC beams. The results showed that the ultimate moment capacity of corroded RC beam was not significantly influenced by the partially corroded or un-bonded length and the bond characteristics over this partial length as long as the tensile steel of the beam can reach its yield strength.

Azad et al. (2010) revisited the analytical prediction of residual flexural strength of corroded beams in the context of relatively larger size beams reinforced with larger diameter tension bars to exclude the size-effect of beams in the proposed modeling and to improve further the accuracy of the analytical method. A new correction factor that replaced the previous one by correctly taking into account the size-effect of the tension bars has been accomplished for a more compliant prediction method. The results showed that the proposed method yielded values which were in good agreement with the test data of current and other experiments, lending confidence to the proposed method to serve as a reliable analytical tool to predict the flexural capacity of a corroded concrete beam.

2.3.2 Columns and Beam-Columns

Compared to the amount of published works on beam, the available work on the mechanical behavior of columns and beam-columns (eccentrically loaded columns) are quite limited. Carlsson et al. (2000) presented a reliability analysis of corroded bridge columns, using Monte Carlo simulation and reliability analysis. The result indicated that despite apparently heavy damages the reduction in safety was rather moderate after 32 years. Reliability based evaluation could be a very useful tool as a basis for decision about damaged structures and strategies for repair and inspection.

Lee et al. (2000) presented an experimental study to simulate the corrosion in large-scale reinforced concrete circular columns and their repair using CFRP sheets. Seven columns were corroded by using an accelerated corrosion regime, wrapped using CFRP sheets, then tested to structural failure and (or) subjected to further post-repair accelerated corrosion, monitoring, and testing. In the accelerated corrosion, the specimens were subjected to cyclic wetting and drying. It was clear that the CFRP repair greatly improved the strength of the repaired member and retarded the rate of post-repair corrosion. Furthermore, it was found that subjecting the repaired column to corrosion would not result in loss of strength but only a slight reduction in the ductility of repaired member.

Tapan et al. (2008) proposed a method, using damaged material properties, amount of corrosion, loss of concrete section and bond, and type of stress in corroding bars to assess the condition of deteriorated bridge piers. Various cases of corrosion of longitudinal steel, on tension and compression face, examined, concluding that the proposed method can be applied in practice.

The work of Wang and Liang (2008) can be quoted as the most contributing to the experimental work on eccentrically loaded columns. A total of 12 members were tested using partial length corrosion achieved through accelerated corrosion. Results showed that with larger eccentricity (tension-controlled design) greater reduction in load occurs with corrosion of tension steel compared with the corrosion of the steel on the compression side of the members. But the opposite hold true for small eccentricity (compression-controlled design). No prediction model was proposed.

Revathy et al. (2009) carried out an experimental investigation on corroded reinforced concrete circular columns to evaluate the residual strength and ductility performance of columns. The columns were corroded by using an accelerated corrosion regime to induce different degrees of corrosion damage of 10 and 25%. The columns were tested under uniaxial compression until failure. It was concluded that the axial load carrying capacity of the columns decreased with an increase in corrosion intensity and hence reduction in ductility of the corroded columns.

Saito et al. (2009) presented the fundamental properties of strength and deformation capacity of the corroded RC column subjected to uniaxial compression loading. Twenty two short column specimens were subjected to axial compression load. The parameters were the corrosion part of reinforcements, simulation method of corrosion and corrosion level. It was clear that corrosion of the main bars had an influence on reduction of maximum load, and corrosion of the hoops had an influence on deformation capacity after the maximum load. The compressive stress-strain model was proposed using sectional area of corroded reinforcing bars considering the relationship between minimum sectional area and the yield ratio.

2.4 Reliability Assessment of Reinforced Concrete Elements

Cheung and Kyle (1996) described the use of a reliability-based system to predicate the service life and repair procedures of reinforced concrete structures. This system can be used to establish the levels of reliability in satisfying various governing conditions (also known as limit states) as determined by performance requirements and by using statistical databases and probability theory. It was found that major rehabilitation decisions can be made by using the reliability as a measure of performance requirements, inspection, and preventive maintenance.

Enright and Frangopol (1998) studied the loss of flexural strength in concrete bridge beams due to corrosion of steel reinforcement. The results showed that the mean value of the resistance loss function appeared to increase about linearly with time for the range of parameters and the damage scenarios considered. It was concluded that the results could be used to develop optimal lifetime reliability-based maintenance strategies for reinforced concrete bridges under environmental attack.

Li (2004) presented a methodology to predicate the service life of corrosion affected concrete structures and applied it to flexural members in marine environments. The reliability methods were used to determine the time period for each phase of service life. It was found that corrosion induced concrete cracking would occur in reinforced concrete flexural members at about 18% of its total service life, and that, once reinforced concrete flexural members become unserviceable due to corrosion induced excessive deflection, there was about 13% of the service life remaining before the structures finally become unsafe.

Val (2007) studied the effect of corrosion of reinforcing steel on flexural and shear strength, and subsequently on reliability, of reinforced concrete beams. Two types of corrosion, general and pitting were considered, with particular emphasis on the influence of pitting corrosion of stirrups on the performance of beams in shear. The variability of pitting corrosion along a beam was also considered and the possibility of failure at a number of the beam cross sections was taken into account. The probabilities of failure were evaluated using Monte Carlo simulation, where the uncertainties in material properties, geometry, load, and corrosion modeling were taken into account. The paper showed that corrosion of stirrups, especially pitting corrosion, has a significant influence on the reliability of reinforced concrete beams.

Darmawan (2008) described the accelerated corrosion test designed to obtain a statistical parameter of pit depths distribution. It was concluded that the probability distribution of maximum pit-depths at the completion of an accelerated corrosion test for a given corrosion rate $i_{corr\text{-}exp}$ could be described using the Gumbel distribution. These statistical parameters of maximum pit-depths distribution were combined with statistical parameters of RC beams to determine the effect of corrosion on flexural and shear strength of RC beam. The analysis showed that pitting corrosion has a lesser detrimental effect on flexural and shear strength of a RC beam than general corrosion.

Stewart (2009) has developed a spatial time-dependent reliability model for a RC beam subject to corrosion-induced pitting corrosion, for shear and flexural limit states. This study considered the spatial and time-dependent variability of pitting corrosion, structural resistance and load effects. The amount of corrosion loss can significantly affect the mechanical behavior of reinforcement, namely low corrosion loss can result in ductile

yielding, whereas a higher corrosion loss can result in brittle fracture. The structural resistance of reinforcement was modeled as either (i) perfectly ductile parallel system or (ii) perfectly brittle parallel system. The results showed that the probability of failure assuming brittle reinforcement behavior was up to 450% higher than assuming ductile behavior.

Araujo (2001) presented the probabilistic finite element analysis of reinforced concrete columns. In this paper, the concrete properties were represented as homogeneous Gaussian random fields. The yield stress and position of steel reinforcement, dimensions of the column cross-section and axial load were considered as random variables. The Monte Carlo method was employed to obtain expected values and standard deviations of the rupture load. The reliability index was investigated by main parameters. It was shown that the correlation length of random fields for concrete properties may have a significant effect on reliability.

The two-part study of Bhargava et al. (2011) addressed time-dependent reliability analyses of RC beams affected by reinforcement corrosion. The effects of time to corrosion initiation and its variability on the failure probability of the considered RC beam were discussed. In the second part, the estimation of time-dependent failure probability was presented by using Monte Carlo simulation (MCS) that provides an insight about the dependence of failure probability of beam on the variability associated with the time-dependent strengths. Then, analytical formulations were presented for estimating time-dependent failure probability considering the variability in degradation functions. The results showed reasonably good agreement between the failure probabilities evaluated from analytical formulations and MCS.

Review of the literature implies that many researchers have been working in this direction to find the reliability or safety index by determining the probability of failure for corroded elements but most of them focused on the corroded beams. Thus far, reliability modeling of columns and beam-columns has received limited attention.

2.5 Modeling of Corroded Reinforced Concrete Member

Coronelli and Gambarova (2004) studied the effect of corrosion on the behavior of reinforced concrete beams by developing a suitable numerical procedure. It was considered many aspects of the progressive damage in an existing structure (cracking and crushing, bar yielding, bond failure), and the assessment of the actual safety level. The effect of corrosion in nonlinear finite element analysis was modeled by reducing the geometry of the finite elements and by modifying the constitutive laws of the materials (steel and concrete) and of their interface (bond). It was found that the introduction of a specific model for bond deterioration appeared to be of paramount importance in order to evaluate the residual ductility of a structure.

Thomas and Ramaswamy (2006) reported the finite element analysis of eleven shear critical partially prestressed concrete T-beams having steel fibers over partial or full depth. Prestressed T-beams were analyzed using the 'ANSYS' program. It was modeled by taking into account the nonlinearity, such as, bond-slip of longitudinal reinforcement, post-cracking tensile stiffness of the concrete, stress transfer across the cracked blocks of the concrete and load sustenance through the bridging action of steel fibers at crack interface. The concrete was modeled using'SOLID65'- eight-node brick element and the

reinforcement such as deformed bars, prestressing wires and steel fibers was modeled discretely using 'LINK8'-3D spar element. A 'COMBIN39'- nonlinear spring element was used to model the slip between the reinforcement (rebars, fibers) and the concrete.

Val et al. (2009) demonstrated the effect of corrosion on deflections of RC beams and the probability of failure due to excessive deflection. A nonlinear finite element 2D model was used to describe the structural behavior of RC beams with corroding reinforcement. Uncertainties associated with the model and available data were taken into account. The results indicated that an increase in deflections due to corrosion had a lesser effect on serviceability of RC beams than corrosion induced cracking.

Wang et al. (2011) focused on the residual strengths of reinforced concrete beams with heavy deterioration. This work was based on experimental investigation of reinforced concrete beams naturally corroded over 30years. The residual bending strengths obtained from the test results were compared with design strengths of un-corroded beam. It was found that the corroded beams lost most of their strengths. Finite element model was developed to further investigate the behavior of corroded reinforced concrete beams. The effect of concrete cover spalling, rebar corrosion and mid-span vertical crack on the residual strength of corroded reinforced concrete beams were analyzed using the developed model.

Mohammed et al. (2011) presented a nonlinear elasto-plastic numerical model to simulate bridge columns under the combined effects of reinforcement corrosion and seismic excitation. It was noted that the model was efficient in simulating the behavior of the column under corrosion and seismic loads. From the case study, it was clear that the load carrying capacity of the corroded column was much lower than that of non-corroded

columns. The results illustrated significant reduction in the column displacement capacity and energy dissipation capability due to rebar corrosion. The corrosion-induced damage could result in accelerated degradation of the bridge columns and reduce its ultimate strength.

Shang et al. (2011) examined the axial nonlinearity in corroded RC members under tension and showed that fewer transverse cracks with greater spacing occurred as steel corrosion progressed. The open-slip coupled model, which took into account the transverse action associated with longitudinal bond stress transfer in the bond transition zone, was extended to cover corroded reinforcement and is successfully used to simulate the behavior of RC members in tension. It was clear that modeling of the bond transition zone and of the layer of corrosion products is found to be crucial to understanding residual bond performance after corrosion had occurred.

Hanjari et al. (2011) presented a methodology to analyze the mechanical behavior and remaining load-carrying capacity of corroded reinforced concrete (RC) structures. The effect of corrosion was modeled as a change in geometry and properties of corroded reinforcement and surrounding concrete that were, a reduction of steel area and ductility, removal of spalled concrete, modification of concrete response due to corrosion cracks, and modification of bond-slip properties. A comparison of the results with available experiments from the literature indicated that the changes in failure mode and failure load caused by uniform and pitting corrosion of reinforcement could be predicted reasonably well by using the proposed methodology.

Potisuket al. (2011) have developed finite element (FE) modeling techniques to isolate the different contributions of corrosion damage to structural response of experimental

reinforced concrete beams with shear-dominated behavior. Corrosion-damage parameters included concrete cover spalling due to the expansion of corrosion products; uniform stirrup cross-sectional loss from corrosion; localized stirrup cross-sectional loss due to pitting; de-bonding of corrosion-damaged stirrups from the concrete. Both individual and combined damages were performed by FE analyses. It was observed that the FE results matched experimental results well and quantitatively estimated capacity reduction of the experimental specimens.

A review of literature clearly showed that a considerable body of literature exists on the behavior of corroded beams and on the effect of corrosion of steel on bond between steel, some work proposing approaches to predict the residual strength of corroded beams.

However, relatively only a few publications are devoted to the study of the strength of the corroded columns and beam-columns. Limited experimental work on the mechanical behavior of corroded columns under concentric and eccentric loading exists, indicating a need for more experimental data, which would help researchers in modeling and understanding the structural behavior. Also, work on strength prediction has not been well executed and needs a fresh exploration and attempt. The proposed work therefore aims to shed further light in this area.

The review also highlights that almost all investigators have used accelerated corrosion in the laboratory studies to study the behavior of corroded concrete members and generate test data, despite the general perception that there is a difference in the two corrosion processes, the natural and the artificial galvanostatic corrosion induction process. This is because the natural process is too slow and therefore time demanding. Accelerated corrosion through impressed current is a faster way to introduce corrosion damage and

has gained wider acceptance in corrosion study.

CHAPTER 3

EXPERIMENTAL PROGRAM

3.1 Test Variables

The experimental program was planned to generate sufficient data for modeling of corrosion damage for columns and beam-columns (member subjected to axial load and bending moment). The following four test variables were used:

1. Diameter of main longitudinal bars, *D*: (Two diameters 18 mm and 20 mm)
2. Cross-section, *h*×*h*: (Two cross-sections 180×180 mm and 220×220 mm).
3. Periods of accelerated corrosion, *T*: (Three different corrosion durations)
4. Eccentricity for eccentric loading, *e*: (Three different values).

3.2 Test Specimens

The specimens were divided into two groups. A total of 18 specimens for Group I and 60 specimens for Group II were cast to include all variables. Group I specimens were tested as columns and Group II specimens, which had enlarged ends (Figure 3.1), were used as beam-columns by subjecting them to eccentric loads.

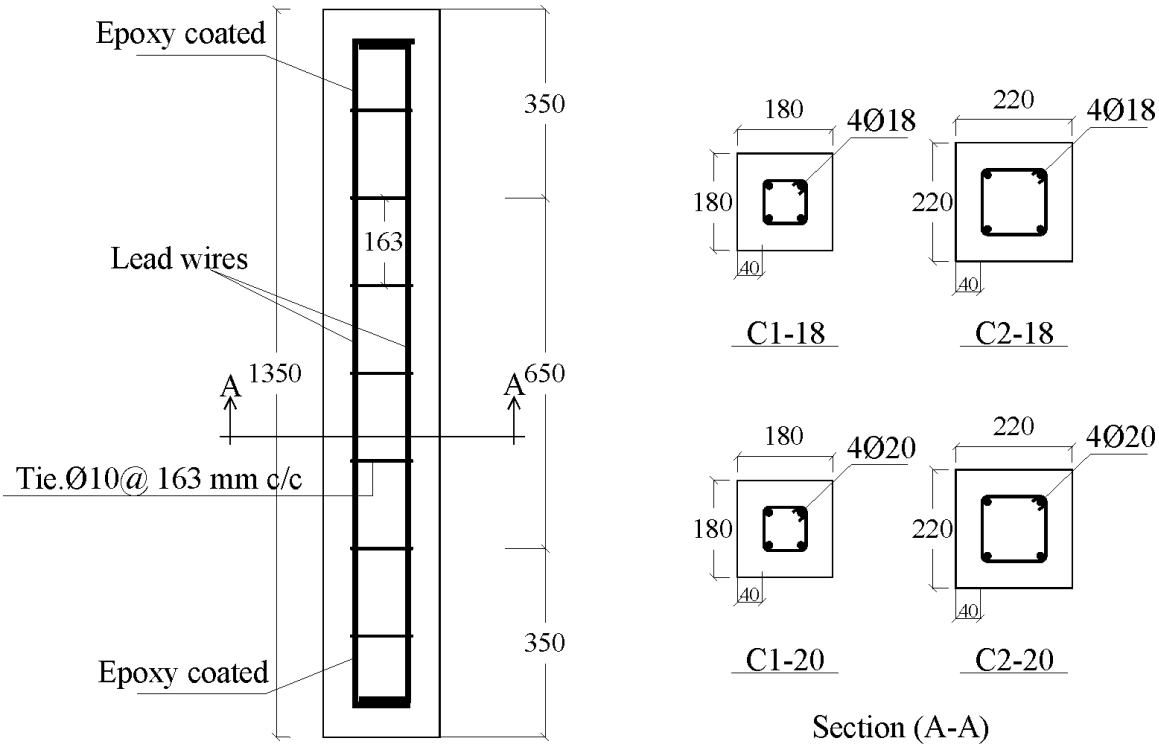

a) Column

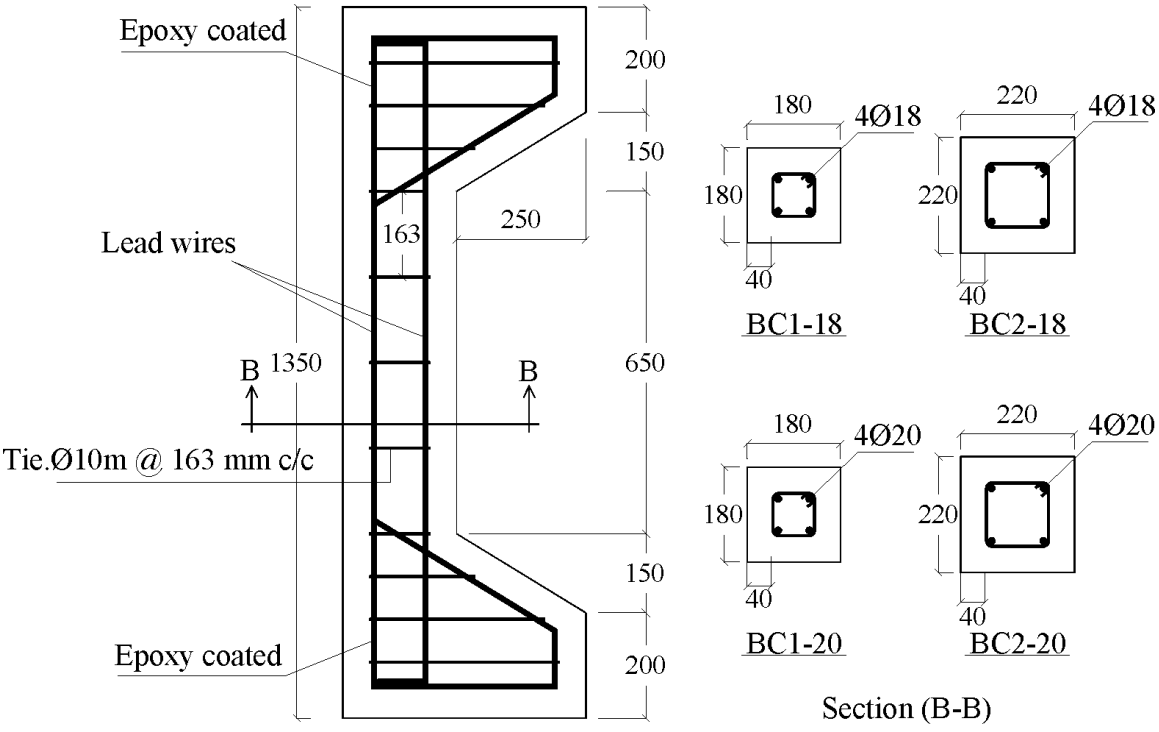

b) Beam-column

Figure 3.1: Details of test specimens.

Table 3.1 gives the test variables and the corresponding number of test specimens, which were used in generating experimental data. Out of 78 specimens, 14 specimens were repeated specimens and 64 specimens were used to develop the predictive model.

In addition, there were two columns and two beam-column specimens, each of 210×210 mm in section and reinforced with 4-bars of 18 mm. These four specimens were subjected to accelerated corrosion. The test data from these four specimens was not used in modeling but was utilized as independent data to verify the proposed method.

Table 3.1: Test Variables and number of test specimens.

<table>
<tr><th rowspan="3">Variables</th><th rowspan="3">Level</th><th colspan="4">Number of Test Specimens</th></tr>
<tr><th colspan="2">Controlled Specimens</th><th colspan="2">Corroded Specimens</th></tr>
<tr><th>Gr. I</th><th>Gr. II</th><th>Gr. I</th><th>Gr. II</th></tr>
<tr><td>Rebar dia. (D)</td><td>2</td><td rowspan="4">2×2
= 4</td><td rowspan="4">2×2×3
= 12</td><td rowspan="4">2×2×3
= 12</td><td rowspan="4">2×2×3×3
= 36</td></tr>
<tr><td>Cross-section
(h×h)</td><td>2</td></tr>
<tr><td>Period (T)</td><td>3</td></tr>
<tr><td>Eccentricity (e)</td><td>3</td></tr>
<tr><td>Repeated specimens</td><td colspan="5">Gr. I = 2 and Gr. II = 12</td></tr>
<tr><td>Specimens for verification</td><td colspan="5">Gr. I = 2 and Gr. II = 2</td></tr>
<tr><td>Total No.</td><td colspan="5">Gr. I = 20 and Gr. II = 62</td></tr>
</table>

3.3 Details of Test Specimens

Square reinforced concrete columns and beam-columns specimens of size 180 × 180 × 1350 mm and 220 × 220 × 1350 mm, respectively, were used in this research. Figure 3.1 shows the reinforcement details of the test specimens for both Group I and Group II specimens.

The clear cover of the specimens was 40 mm. The main reinforcement consisted of four steel bars. The ties were of double-legged 10 mm diameter steel bars spaced uniformly at 163 mm center to center throughout the length of each columns and beam-column. The main steel was epoxy-coated at the both ends of bars to avoid corrosion and the ties at the middle of the specimens were left uncoated so that they would be affected by corrosion along with the main bars. The ties were subjected to corrosion to reflect practical case.

3.3.1 Materials and Concrete Mix Proportions

Type I Portland cement (ASTM C150) was used in the preparation of concrete specimens. The coarse aggregate used in this study was crushed limestone processed from the quarries on Riyadh highway. Based on ASTM C 127, the average values of specific gravity and absorption of the coarse aggregates are 2.5, and 1.4%, respectively. For fine aggregate, medium coarse sand was used. The fine aggregate has specific gravity and absorption of 2.6 and 0.45%, respectively. For mixing and curing of concrete, potable water was used.

The mix proportions used are as follows:

Water-cement ratio = 0.45

Cement content = 350 kg/m^3

Coarse to fine aggregate ratio = 1.50

Table 3.2 gives the grading of coarse aggregate. The weights of constituent per cubic meter of concrete are given in Table 3.3.

Table 3.2: Grading of coarse aggregates.

Sieve opening	% Weight Retained
1/2"	35
3/8"	35
3/16"	20
3/32"	10

Table 3.3: Weights of components in a cubic meter of concrete.

Constituent	Weight (kg)
Cement	350
Water	157.5
Fine aggregate	752
Coarse aggregate	1128

3.3.2 Casting and Curing of Test Specimens

A total of 20 columns and 62 beam-columns specimens were cast. From each batch of concrete mix, three cylindrical concrete specimens were cast to determine the compressive strength of concrete. Figure 3.2 shows the specimens during and after casting. The specimens were un-molded after 24 hours of casting and then covered with wet burlap and plastic sheet to cure at laboratory temperature of 18 to 20°C (Figure 3.2). For a period of seven days, moist curing was carried out followed by air curing at room temperature. Figure 3.3 shows the view of the test specimens ready for testing.

Figure 3.2: Casting and curing of concreter specimens.

Figure 3.3: Test specimens.

3.4 Designation of Specimens

Forty six column and beam-column specimens were divided into groups based on cross-section dimensions and rebars diameter. The designations of the un-corroded specimens are given in Table 3.4. These un-corroded specimens were not subjected to accelerated corrosion. Specimens marked with 'C' stand for columns and 'BC' represents beam-columns. The designations used in Table 3.4 reflect also the bar diameter and the eccentricities. For example, specimen BC1-18-30 had 18 mm diameter bars and was tested with eccentricity of 30 mm.

Table 3.4: Designation of un-corroded specimens.

Gr.I Specimens (Columns)			
Cross-section (180 x 180 mm)		Cross-section (220 x 220 mm)	
Rebar Dia. (18 mm)	Rebar Dia. (20 mm)	Rebar Dia. (18 mm)	Rebar Dia. (20 mm)
C1-18	C1-20	C2-18	C2-20
Gr.II Specimens (Beam-Columns)			
BC1-18-30	BC1-20-30	BC2-18-35	BC2-20-35
BC1-18-60	BC1-20-60	BC2-18-65	BC2-20-65
BC1-18-95	BC1-20-95	BC2-18-115	BC2-20-115

Table 3.5 gives the designation for the corroded columns and beam-columns. This designation indicates, in addition to rebar diameter and the eccentricity, the duration of the applied current in days for inducing corrosion as the last suffix.

Table 3.5: Designation of corroded specimens.

Gr.I Specimens (Columns)			
Cross-section (180 x 180 mm)		Cross-section (220 x 220 mm)	
Rebar Dia. (18 mm)	Rebar Dia. (20 mm)	Rebar Dia. (18 mm)	Rebar Dia. (20 mm)
C1-18-7d	C1-20-7d	C2-18-7d	C2-20-7d
C1-18-10d	C1-20-10d	C2-18-10d	C2-20-8d
C1-18-13d	C1-20-13d	C2-18-13d	C2-20-10d
Gr.II Specimens (Beam-Columns)			
BC1-18-30-7d	BC1-20-30-7d	BC2-18-35-6d	BC2-20-35-7d
BC1-18-30-10d	BC1-20-30-6d	BC2-18-35-8d	BC2-20-35-6d
BC1-18-30-12d	BC1-20-30-13d	BC2-18-35-9d	BC2-20-35-9d
BC1-18-60-7d	BC1-20-60-7d	BC2-18-65-4d	BC2-20-65-7d
BC1-18-60-10d	BC1-20-60-10d	BC2-18-65-7d	BC2-20-65-6d
BC1-18-60-13d	BC1-20-60-13d	BC2-18-65-10d	BC2-20-65-9d
BC1-18-95-7d	BC1-20-95-7d	BC2-18-115-7d	BC2-20-115-7d
BC1-18-95-10d	BC1-20-95-10d	BC2-18-115-8d	BC2-20-115-6d
BC1-18-95-11d	BC1-20-95-13d	BC2-18-115-9d	BC2-20-115-9d

3.5 Experimental Techniques

3.5.1 Compressive Strength of Concrete

The compressive strength of concrete, f_c' after 28 days was determined by testing cylindrical specimens in accordance with ASTM C39 with dimension of 75 × 150 mm and 150 x 150 x 150 mm cubic specimens under test machines. The average of six cylinders tested for each batch was taken as the applicable value of f_c' for that batch. In addition, 8-75 mm diameter cores extracted from un-damage specimens were tested to verify the concrete strength.

3.5.2 Tensile Strength of Reinforcing Bars

The yield and tensile strength of tension bars were determined by testing bar specimens of 18 mm and 20 mm in tension in a Universal Testing Machine (Figure 3.4) and the load-elongation (stress-strain) plot was obtained. Thereafter, the yield strength and tensile strength of the bars was obtained from the stress-strain plots.

Figure 3.4: Arrangement for measuring the tensile strength of steel bars.

3.5.3 Test Setup for Corrosion Induction

After completion of immersion in water to ensure full saturation, the specimens were subjected to corrosion by applying a constant current intensity for specified time periods. The accelerated corrosion was achieved by using a small DC power supply with a built-in ammeter to check the current and a potentiometer to control the current intensity. The middle part of the concrete specimens was sprayed with 3% sodium chloride solution every one hour as shown in Figure 3.5. The current was applied so that a stainless steel plate placed around the middle part of the concrete specimen acted a cathode and reinforcing steel served as an anode (Figure 3.6). Figure 3.7 shows the power supply step up.

Although the corrosion of specimens using the accelerated corrosion does corrode the bars and leads to crack formation, the actual corrosion in structures differs considerably in rate and characteristics. The cracks due to corrosion in existing structures may not always form in surrounding concrete because of concrete creep. However, Uomoto et al. (1988) reported that the cracks developed by accelerated corrosion are quite similar to those developed during exposure tests. As most researches have used the accelerated corrosion test to induce corrosion, accelerated corrosion induction method was chosen in this work to cause a significant amount of corrosion for specified time periods.

From previous work, it has been noted that the applied impressed current densities in accelerated corrosion tests have ranged from, as low as 0.1 mA/cm^2 (Rodriguez et al., 1997) to as high as 4 mA/cm^2 (Mangat et al., 1999). In this work, the impressed current intensities chosen were 2 mA/cm^2 and 2.5 mA/cm^2.

The total amount of current required was calculated based on the steel surface area for each specimen, as given in Tables 3.6 and 3.7 for 18 mm and 20 mm, ϕ steel bars, respectively.

Figure 3.5: Specimens subjected to accelerated reinforcement corrosion.

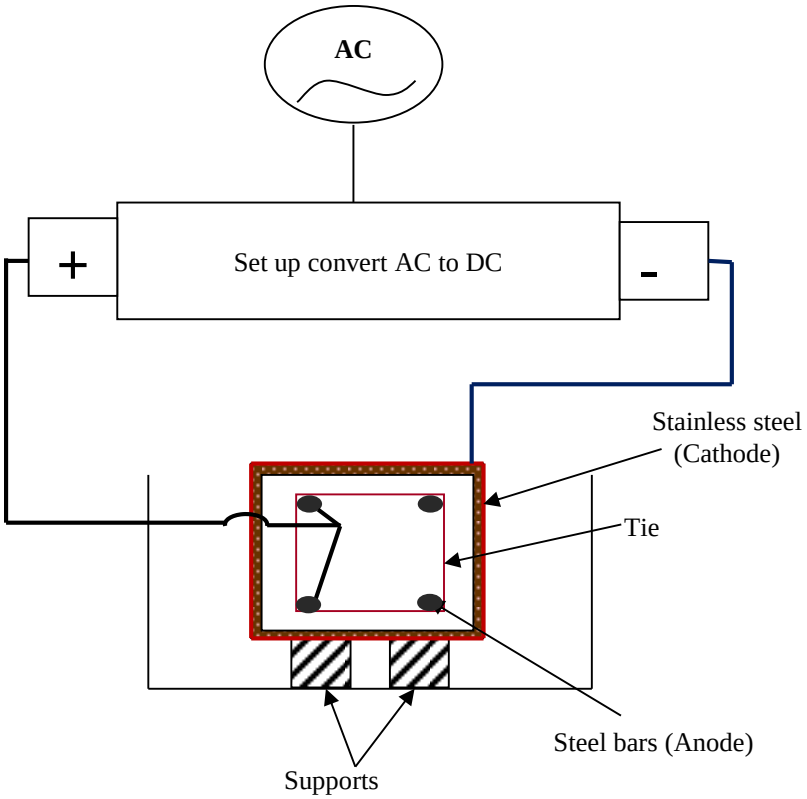

Figure 3.6: Schematic diagram of accelerated corrosion test.

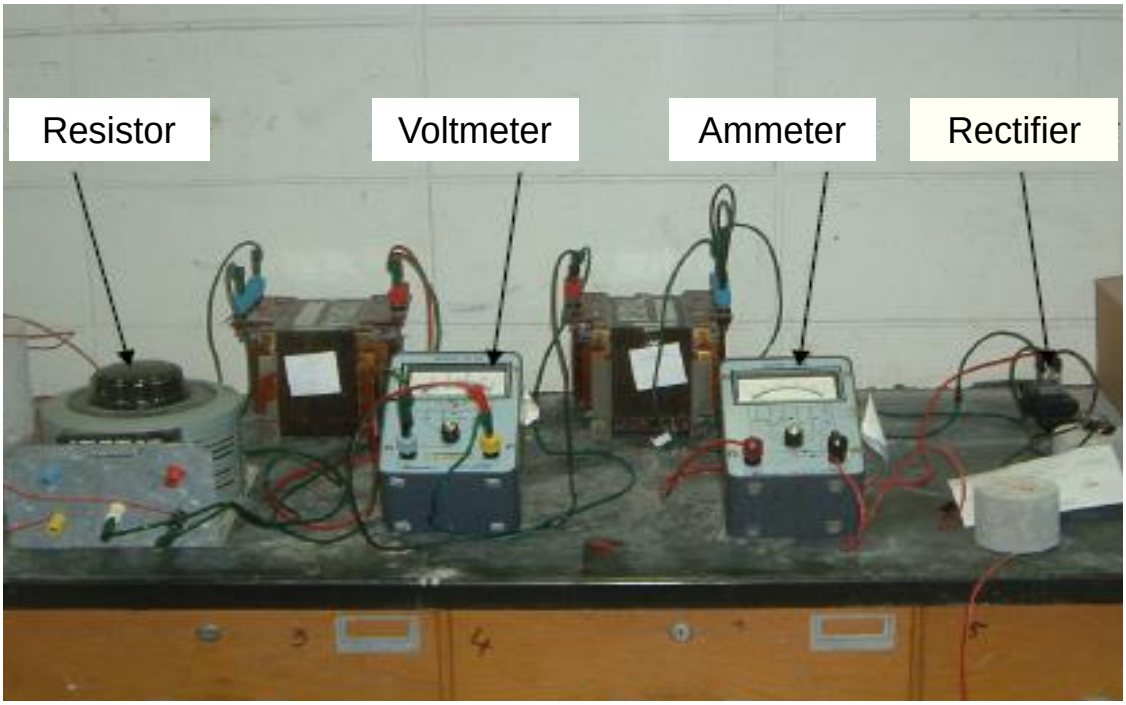

Figure 3.7: Power supply set up.

Table 3.6: Total current applied to column and beam-column specimens with 18 mm diameter bars.

Specimen Type	*D* (mm)	Total surface area of steel and stirrups (cm^2)	Total current I (Amps) @ $2mA/cm^2$	Total current I (Amps) @ $2.5mA/cm^2$
C1-18-7d	10 and 18	1972.9	3.946	-
C1-18-10d	10 and 18	1972.9	-	4.932
C1-18-13d	10 and 18	1972.9	-	4.932
BC1-18-30-7d	10 and 18	1972.9	-	4.932
BC1-18-30-10d	10 and 18	1972.9	-	4.932
BC1-18-30-12d	10 and 18	1972.9	-	4.932
BC1-18-60-7d	10 and 18	1972.9	-	4.932
BC1-18-60-10d	10 and 18	1972.9	-	4.932
BC1-18-60-13d	10 and 18	1972.9	-	4.932
BC1-18-95-7d	10 and 18	1972.9	-	4.932
BC1-18-95-10d	10 and 18	1972.9	-	4.932
BC1-18-95-11d	10 and 18	1972.9	-	4.932
C2-18-7d	10 and 18	2224.3	-	5.561
C2-18-10d	10 and 18	2224.3	-	5.561
C2-18-13d	10 and 18	2224.3	-	5.561
BC2-18-35-6d	10 and 18	2224.3	-	5.561
BC2-18-35-8d	10 and 18	2224.3	-	5.561
BC2-18-35-9d	10 and 18	2224.3	-	5.561
BC2-18-65-4d	10 and 18	2224.3	-	5.561
BC2-18-65-7d	10 and 18	2224.3	-	5.561
BC2-18-65-10d	10 and 18	2224.3	-	5.561
BC2-18-115-7d	10 and 18	2224.3	-	5.561
BC2-18-115-8d	10 and 18	2224.3	-	5.561
BC2-18-115-9d	10 and 18	2224.3	-	5.561

Table 3.7: Total current applied to column and beam-column specimens with 20 mm diameter bars.

Specimen Type	D (mm)	Total surface area of steel and stirrups (cm^2)	Total current I (Amps) @ $2mA/cm^2$	Total current I (Amps) @ $2.5mA/cm^2$
C1-20-7d	10 and 20	2136.3	-	5.341
C1-20-10d	10 and 20	2136.3	-	5.341
C1-20-13d	10 and 20	2136.3	-	5.341
BC1-20-30-7d	10 and 20	2136.3	-	5.341
BC1-20-30-6d	10 and 20	2136.3	-	5.341
BC1-20-30-13d	10 and 20	2136.3	-	5.341
BC1-20-60-7d	10 and 20	2136.3	-	5.341
BC1-20-60-10d	10 and 20	2136.3	-	5.341
BC1-20-60-13d	10 and 20	2136.3	-	5.341
BC1-20-95-7d	10 and 20	2136.3	-	5.341
BC1-20-95-10d	10 and 20	2136.3	-	5.341
BC1-20-95-13d	10 and 20	2136.3	-	5.341
C2-20-7d	10 and 20	2387.6	-	5.969
C2-20-8d	10 and 20	2387.6	-	5.969
C2-20-10d	10 and 20	2387.6	-	5.969
BC2-20-35-7d	10 and 20	2387.6	-	5.969
BC2-20-35-6d	10 and 20	2387.6	-	5.969
BC2-20-35-9d	10 and 20	2387.6	-	5.969
BC2-20-65-7d	10 and 20	2387.6	-	5.969
BC2-20-65-6d	10 and 20	2387.6	-	5.969
BC2-20-65-9d	10 and 20	2387.6	-	5.969
BC2-20-115-7d	10 and 20	2387.6	-	5.969
BC2-20-115-6d	10 and 20	2387.6	-	5.969
BC2-20-115-9d	10 and 20	2387.6	-	5.969

On a regular basis, the current applied to each specimen was checked for any drift and corrected. The drift generally occurred within the first 24-36 hrs. Thereafter, the system becomes fully stable with constant current passing through the circuit.

3.5.4 Linear Polarization Resistance (LPR) Method

After accelerated corrosion, some of the corroded columns and beam-columns were tested by using the linear polarization resistance (LPR) method to measure corrosion current density (I_{corr}). To perform the test, an external stainless steel plate and a saturated calomel reference electrode placed very near to the concrete specimen were connected to a Potentiostat/Galvanostat. The steel bar was polarized to +10 mV of the corrosion potential at the scan rate of 0.2 mV/s and the resulting current was recorded. The potential-current curve was used to evaluate the resistance to linear polarization (R_p) (Maslehuddin et al., 2010). The I_{corr} was obtained by the following formula:

$$I_{corr} = {}^{B}/_{R_p} \tag{3.1}$$

where:

I_{corr} is the corrosion current density, B the constant and R_p is the polarization resistance (Ω cm^2).

The corrosion current density values of embedded steel bars in concrete, obtained from the LPR method, are difficult in large part because determining the actual corroding area of steel is almost impossible and usually causes underestimation of the actual corrosion current density in the areas of active corrosion (Esmaeilpoursaee, 2007). Figure 3.8 shows the LPR method for the corroded columns and beam-columns specimens.

(a) Column

(b) Beam-column

Figure 3.8: Linear polarization resistance (LPR) method of corroded specimens.

3.5.5 Testing of Column and Beam-Column Specimens

The 4 control column and 12 beam-column specimens, which were not subjected to corrosion, were tested for determining the reference strength. The other 48 column and beam-column specimens that were subjected to accelerated reinforcement corrosion were tested, after the expiry of corrosion period, to determine their residual strength.

Prior to testing, the column specimens were prepared by attaching surface strain gauges on opposite faces using a quick set epoxy to help ensure that the applied load is concentric. They were placed under a loading frame, and the compressive load was applied through hydraulic jack (Figures 3.9 and 3.10). The speed of application of load was maintained at a constant speed of about 5 kN/sec. Initially a load of 25-30 kN was applied and the strains on opposite faces of the specimen were monitored to check the eccentricity of load. If the strains on opposite faces differed by more than 5 %, the load center was adjusted to ensure uniform stress as evident by the strain readings. All load and deformation data were recorded at load increments of 10 kN using automated computer controlled data loggers.

The beam-column specimens were tested with eccentricities given in Table 3.8. From each test, the failure load was recorded.

Table 3.8: The Eccentricities of applied load for beam-column specimens.

Cross-section (180 x 180 mm)		Eccentricities, *e* (mm)	*e/h*
Rebar Dia. (18 mm)	Rebar Dia. (20 mm)		
BC1-18-30	BC1-20-30	30	0.17
BC1-18-60	BC1-20-60	60	0.33
BC1-18-95	BC1-20-95	95	0.53
Cross-section (220 x 220 mm)			
BC2-18-35	BC2-20-35	35	0.16
BC2-18-65	BC2-20-65	65	0.30
BC2-18-115	BC2-20-115	115	0.52

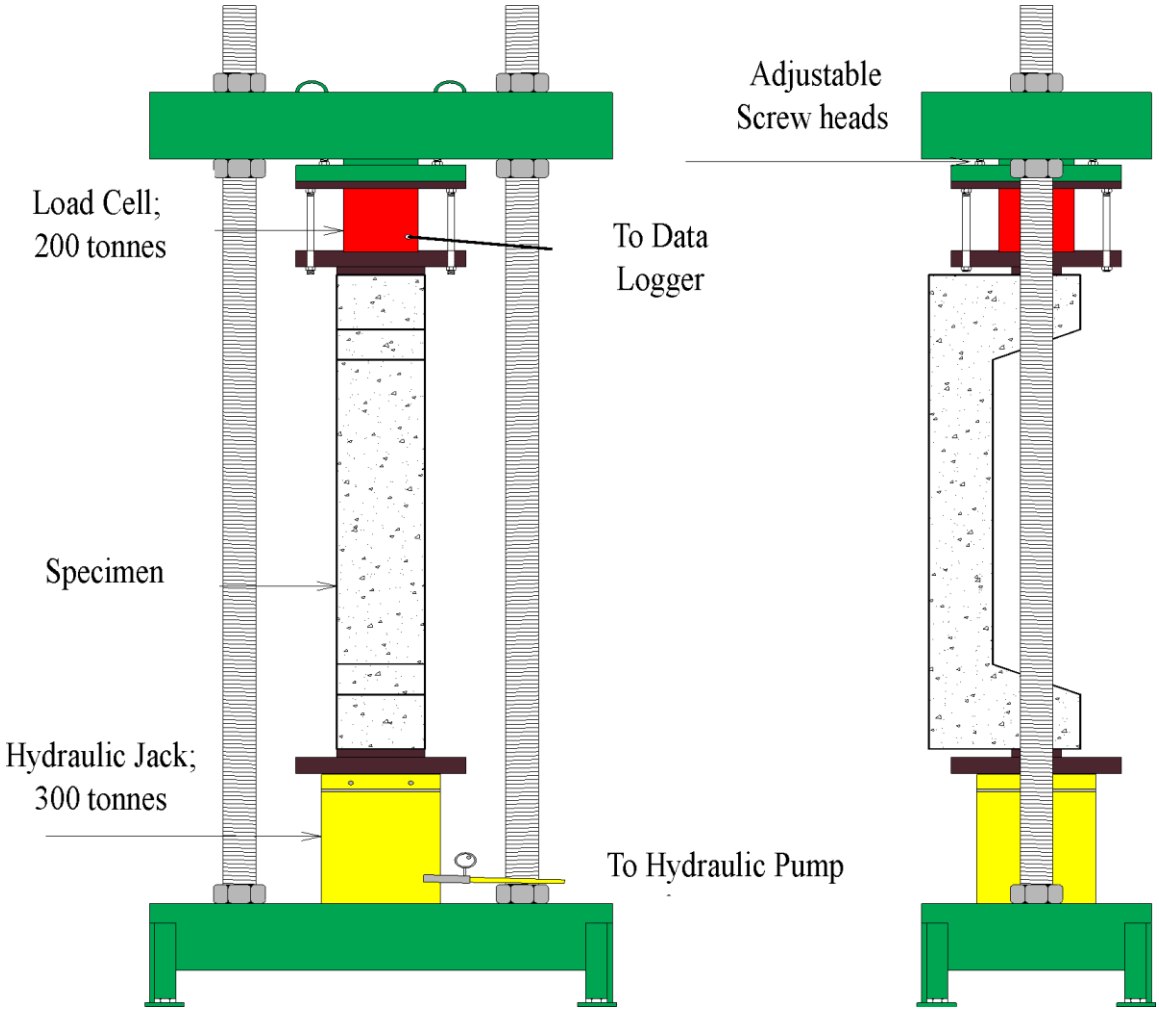

Figure 3.9: Schematic view of compressive strength test setup.

(a) Un-corroded specimens

(b) Corroded specimens

Figure 3.10: Un-corroded and corroded specimens being tested for its load capacity.

3.5.6 Gravimetric Weight Loss

Each corroded specimen, after testing, was broken to remove the longitudinal bars. The bars were cut into pieces and then cleaned of all concrete and rust products manually. Then, it was cleaned using Clarke's solution to completely remove all rust products from the bars. Finally, it was rinsed with water, dried and then weighed to find average weight. The loss of metal can be calculated by comparing with the weight of the original bars of same length. Preparation, cleaning and evaluation of weight loss were carried out in accordance with ASTM G1.

The percentage weight loss was calculated as:

$$\text{Precentage weight Loss } (X_p) = \frac{W_i - W_f}{W_i} \times 100 \tag{3.2}$$

where

W_i = initial weight of the bar before corrosion

W_f= weight after corrosion.

Figure 3.11 shows some of the steel samples after cleaning. It can be seen that the loss of rebars at some sections is higher at others. This reconfirms the notion that corrosion, in general, is non-uniform throughout the length of the bar.

Figure 3.11: 20 mm diameter corroded bars.

CHAPTER 4

FINITE ELEMENT ANALYSIS

The corroded member was modeled by taking into account the following corrosion-induced phenomena:

- Reduction of bond-slip properties;
- Reduction of steel area;
- Reduction in yield strength of steel and its modulus of elasticity; and
- Cracking of concrete.

4.1 Bond-slip

The bond between the bar-concrete interfaces is governed by the friction between the reinforcement and the concrete and by splitting stresses. Since corrosion of reinforcement causes volume expansion which ultimately results into splitting of the surrounding concrete, the bond is degraded. Tests have reported that bond of the corroded reinforcement and concrete is slightly improved at relatively low level of corrosion. However, the bond strength decreases when weight loss is greater than 4% and the loss becomes significant when corrosion cracks develop (Almusallam et al., 1996).

The effect of corrosion on the bond at bar-concrete interface has been studied through

experiments and analyses by several researchers. Al-Sulaimani et al. (1990), Cabrera and Ghoddoussi (1992), Auyeung et al. (2000) and Rodriguez et al. (1995a) experimentally studied the bond of corroded bars. The pull-out tests on corroded steel bars have been studied by Saether (2009a) and Bhargava (2008). Rodriguez et al. (1994) and Chernin et al. (2010) proposed relationships to account for the effect of corrosion on the bond strength between the concrete and reinforcement.

In this analysis, the bond-slip between steel and concrete for corroded members has been simulated using a three-dimensional nonlinear spring element. The nonlinearity of spring element was defined by inputting the load displacement relationship.

4.1.1 Empirical Equations of Bond Strength for Un-corroded Members

Bhaskar et al. (2010) estimated the bond stress-slip behavior of un-corroded member as:

$$\tau_{bu} = \tau_1 \left(\frac{S}{S_1}\right)^{\frac{1}{4}} \qquad \text{and} \qquad 0 \leq S \leq S_1 \tag{4.1}$$

where

$$\tau_1 = 0.9\tau_{max} \tag{4.2}$$

τ_{bu} is the bond strength between the sound longitudinal bars and the concrete and S = slip, less or equal to the maximum value S_1, taken as 0.3 mm.

The maximum bond strength is obtained as

$$\tau_{max} = 20 \left(\frac{f_c'}{D}\right)^{\frac{1}{3}} \tag{4.3}$$

where

f_c' is mean compressive strength of concrete in MPa.

D is the diameter of un-corroded rebar in mm

Xiaoming et al. (2012) suggested relationship between local bond force *F(S)* and slip at the non-corroded bar-concrete interface along the longitudinal direction as follows:

$$F(S) = \left[\langle 61.5S - 659S^2 + 3.14 \times 10^3 S^3 - 0.478 \times 10^4 S^4 \rangle f_{ts} \sqrt{\frac{c_{co}}{D}}\right] \times \pi D l \quad (4.4)$$

where

S is the slip value (mm),

c_{co} is the thickness of the cover layer (mm),

D is the diameter of un-corroded reinforcement (mm),

f_{ts} is the concrete's splitting tensile strength (MPa), and

l is the distance between two adjacent spring elements (mm)

The bond strength between the longitudinal bars and the concrete, given by Xue and Seki (2010), as:

$$\tau_{bu} = f_t \left[5\left(\frac{S}{S_o}\right) 4.5\left(\frac{S}{S_o}\right)^2 + 1.4\left(\frac{S}{S_o}\right)^3\right] \qquad \text{if } 0 \le S \le S_o \quad (4.5a)$$

$$\tau_{bu} = 1.9 f_t \qquad \text{if } S \ge S_o \quad (4.5b)$$

where

τ_{bu} is the bond strength between the sound longitudinal bars and the concrete.

S_o= 0.06 mm.

f_t is tensile strength of concrete.

4.1.2 Loss of Bond Strength for Corroded Members

Lee et al. (2002) suggested the bond strength as a function of corrosion level as:

$$\tau_{bc} = 5.12\, e^{(-0.0561 X_p)} \tag{4.6}$$

where

τ_{bc} is the residual bond strength and

X_p is the loss of weight of reinforcing bar expressed as a percentage of original rebars weight (%).

Chung et al. (2004) gave the bond strength as a normalized bond strength ratio 'R' expressed as:

$$R = 2.09 X_p^{(-1.06)} \quad \text{for} \quad X_p > 2\ \% \tag{4.7}$$

where: R is the ratio of bond strength at any corrosion level to the original bond strength for un-corroded specimen.

Cabrera (1996) presented the bond strength for normal Portland cement concrete τ_{bc} based on pullout test on RC specimens as a function of corrosion level X_p as follows:

$$\tau_{bc} = 23.478 - 1.313 X_p \tag{4.8}$$

Bhargava et al. (2008) determined the progressive bond degradation between the concrete and the reinforcing steel based on experimental data for the specimens without stirrups as (Figures 4.1 and 4.2):

$$R = 1 \qquad X_p \leq 1.5\ \% \qquad (4.9)$$

Pullout test:

$$R = 1.192e^{(-0.117X_p)} \qquad X_p > 1.5\ \% \qquad (4.10)$$

Flexural test:

$$R = 1.346e^{(-0.198X_p)} \qquad X_p > 1.5\ \% \qquad (4.11)$$

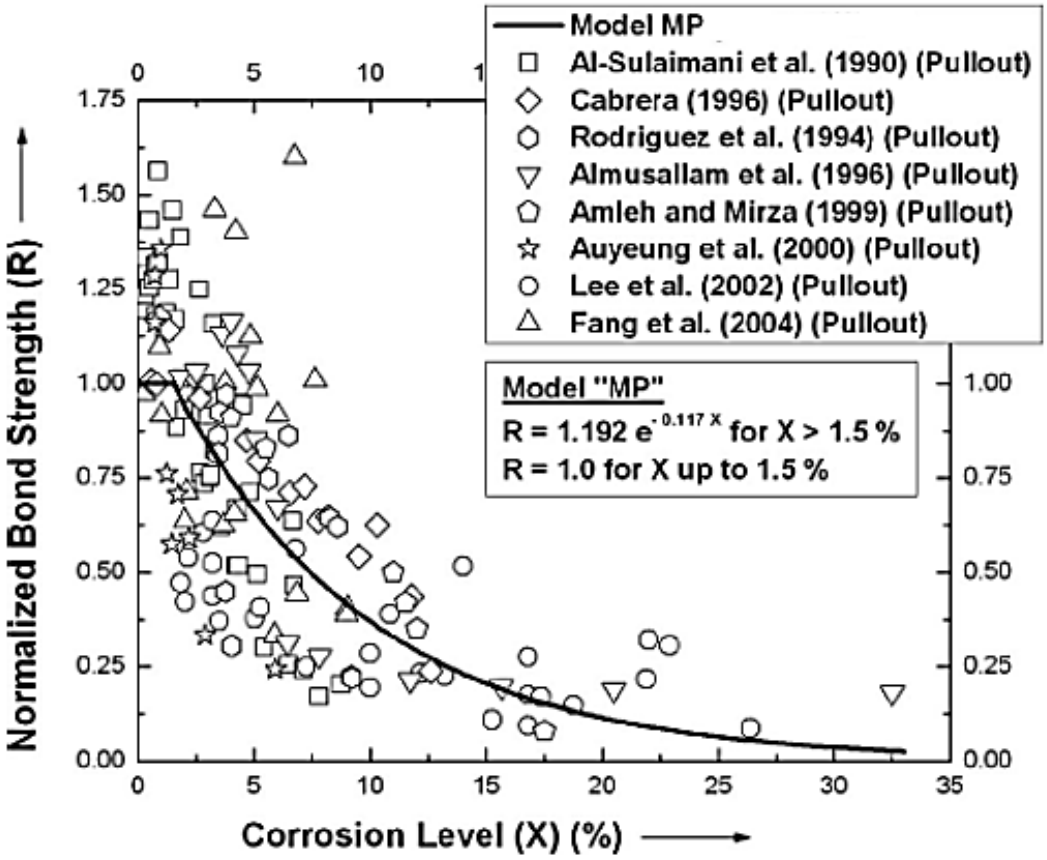

Figure 4.1: Normalized bond strength as function of corrosion level for experimental data of pullout testing (Bhargava et al., 2008).

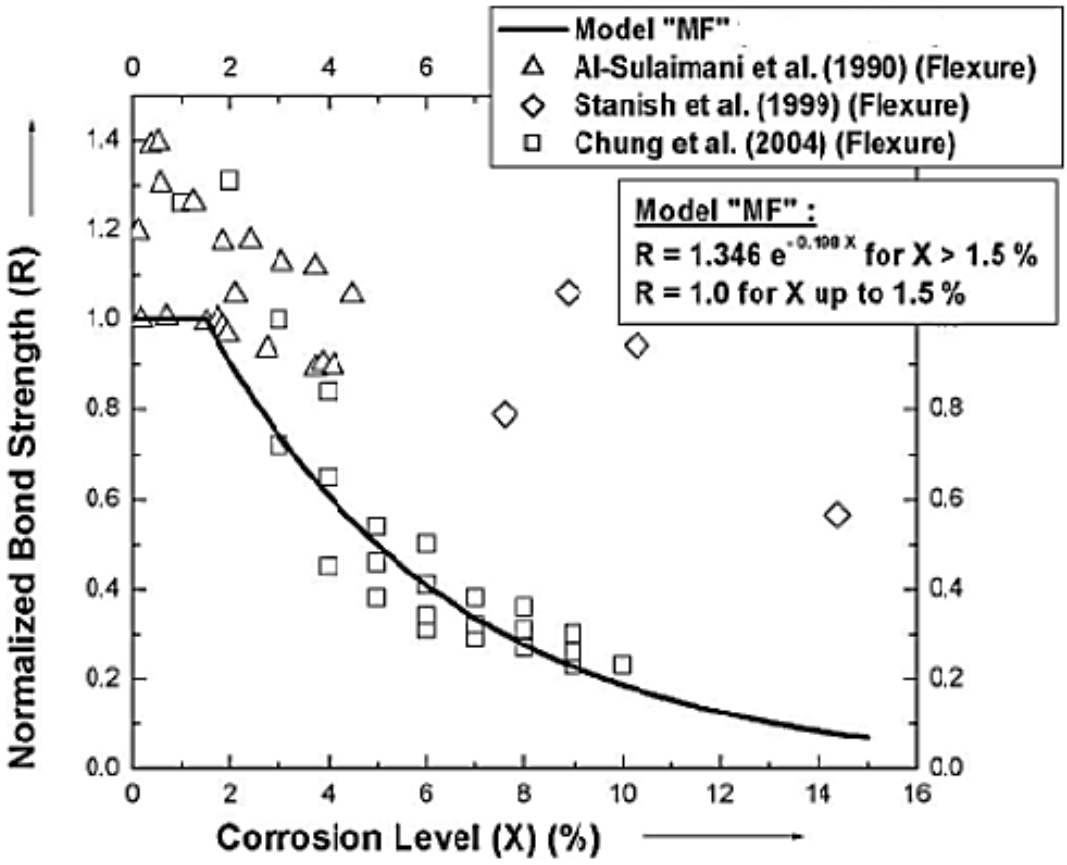

Figure 4.2: Normalized bond strength as function of corrosion level for experimental data of flexural testing (Bhargava et al., 2008)

When the corrosion level is X_p, Xiaoming et al. (2012) suggested the reduction factor R of the bond strength at the corroded bar-concrete interface as:

$$R = 1 + 0.5625X_p - 0.3357{X_p}^2 + 0.055625{X_p}^3 - 0.003{X_p}^4 \quad X_p \leq 7\% \tag{4.12a}$$

$$R = 2.0786{X_p}^{-1.0369} \qquad X_p > 7\% \tag{4.12b}$$

Xin et al. (2010) used the reduction of the bond strength due to corrosion based on the following equation:

$$\tau_{bc}/\tau_{bu} = e^{(-0.0607X_p)} \tag{4.13}$$

where

τ_{bc} is the bond stress of corroded longitudinal bars;

$\tau_{bu}$is the bond stress of sound longitudinal bars;

Auyeung et al. (2000) determined normalized bond stress R for corroded reinforcing steel based on experimental data of pull out test as:

$$R = 1.161e^{(-0.3251X_p)} \tag{4.14}$$

The prediction equations for loss of bond due to corrosion proposed by various researchers are collectively listed in Table 4.1 and plotted in Figure 4.3. As seen from Figure 4.3, some of the empirical equations predict an almost linear reduction in bond strength and the others show a non-linear reduction with increasing corrosion level. Also, there is a considerable divergence in the values of residual bond strength given by different equations proposed by the research. Hence, the use of one of the proposed equations may result in either overestimation or underestimation of the reduction of bond

strength between concrete and steel. Therefore, in this study, the average value of reduction of bond strength of all available formulations except the one proposed by Auyeung et al. (2000) was used to obtain a reasonably good estimate of the reduction factor *R*. The solid curve in Figure 4.3 represents the average value of *R*, which can be estimated as:

$$R = 1 \qquad X_p \leq 1.5\ \% \tag{4.15}$$

$$R = 1.2e^{(-0.14X_p)} \qquad X_p > 1.5\ \% \tag{4.16}$$

Table 4.1: Summary of empirical equations for loss of bond strength for corroded members.

References	Loss of Bond Strength for Corroded Members
Lee et al. (2002)	$\tau_{bc} = 5.12\, e^{(-0.0561 X_p)}$
Chung et al. (2004)	$R = 2.09 {X_p}^{(-1.06)} \quad for \quad X_p \geq 2\%$
Cabrera (1996)	$\tau_{bc} = 23.478 - 1.313 X_p$
Bhargava et al. (2008) (Pullout test)	$R = 1 \qquad X_p \leq 1.5\ \%$ $R = 1.192 e^{(-0.117 X_p)} \qquad X_p > 1.5\ \%$
Bhargava et al. (2008) (Flexural test)	$R = 1 \qquad X_p \leq 1.5\ \%$ $R = 1.346 e^{(-0.198 X_p)} \qquad X_p > 1.5\ \%$
Xiaoming et al. (2012)	$R = 1 + 0.5625 X_p - 0.3357 {X_p}^2 + 0.055625 {X_p}^3 - 0.003 {X_p}^4 \qquad X_p \leq 7\%$ $R = 2.0786 {X_p}^{-1.0369} \qquad X_p > 7\%$
Xin et al. (2010)	${\tau_{bc}}/{\tau_{bu}} = e^{(-0.0607 X_p)}$
Auyeung et al. (2000)	$R = 1.161 e^{(-0.3251 X_p)}$
Average Value	$R = 1 \qquad X_p \leq 1.5\ \%$ $R = 1.2 e^{(-0.14 X_p)} \qquad X_p > 1.5\ \%$

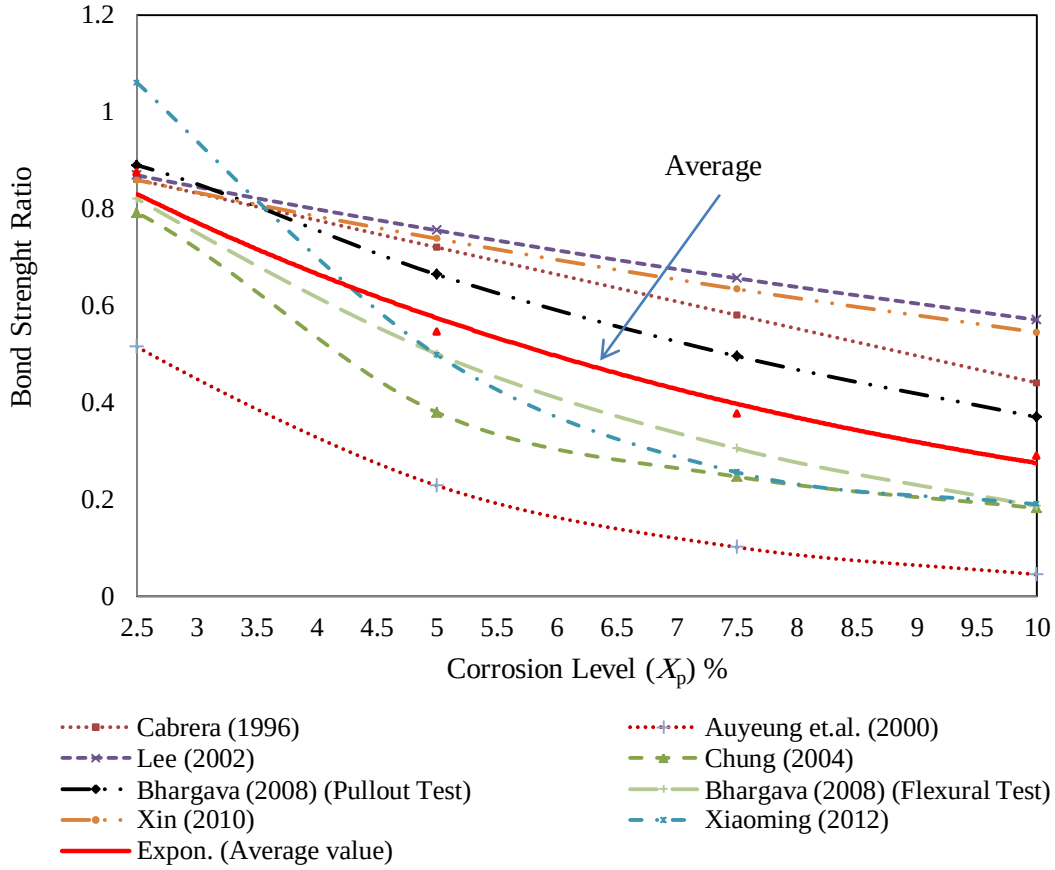

Figure 4.3: Effect of corrosion on bond strength ratio.

4.2 Reduction in Steel Cross-Sectional Area

4.2.1 Uniform Reduction in Cross-Sectional Area

In FEM, the uniform loss of metal from rust formation was modeled by using reduced cross-sectional areas of the longitudinal steel. The reduced area was calculated based on the net diameter of the bars, after allowing the average depth of penetration as (Ijsseling, 1986)

$$D' = D(1 - \frac{2P_r T}{D}) \tag{4.17}$$

where

P_r = metal loss rate or penetration rate,

D= original diameter of bar,

T = time corrosion period and

D' is the net diameter after metal loss.

4.2.2 Effect of Pitting on Reinforcement Cross-Section

In general, the corrosion is non-uniform throughout the length of the bar. The effect of pitting on reinforcement can be estimated by calculating the maximum pit depth based on Stewart (2009) model as:

$$P(T) = 0.0116 \times I_{corr} \times Y \times T \tag{4.18}$$

where: I_{corr} is the corrosion current density (normally expressed in ($\mu A/cm^2$); T is time since corrosion initiation in years; and $P(T)$ is in mm.

Gonzalez et al. (1995) suggested the maximum pitting factor *Y* from 4 to 8 for reinforced concrete specimens exposed to natural environments.

Val et al. (1997) estimated the following equations to predict the cross-sectional area of the pit (A_{pit}) for the pit configuration shown in Figure 4.4.

$$A_{pit}(T) = \begin{cases} A_1 + A_2 & P(T) \le \frac{D}{\sqrt{2}} \\ \frac{\pi D^2}{4} - A_1 + A_2 & \frac{D}{\sqrt{2}} < P(T) \le D \\ \frac{\pi D^2}{4} & P(T) > D \end{cases} \tag{4.19}$$

where

$$b_p = 2P(T)\sqrt{1 - \left(\frac{P(T)}{D}\right)^2} \tag{4.20}$$

$$A_1 = 0.5\left[\theta_1 \left(\frac{D}{2}\right)^2 - b_p \left|\frac{D}{2} - \frac{P(T)^2}{D}\right|\right] \tag{4.21}$$

$$A_2 = 0.5\left[\theta_2 P(T)^2 - b_p \frac{P(T)^2}{D}\right] \tag{4.22}$$

$$\theta_1 = 2arcsin\frac{b_p}{D}; \quad \theta_2 = 2arcsin\left(\frac{b_p}{2P(T)}\right) \tag{4.23}$$

and where *D* is the initial diameter of the reinforcing bar.

The cross-sectional area of an un-corroded reinforcing bar is $\frac{\pi D^2}{4}$

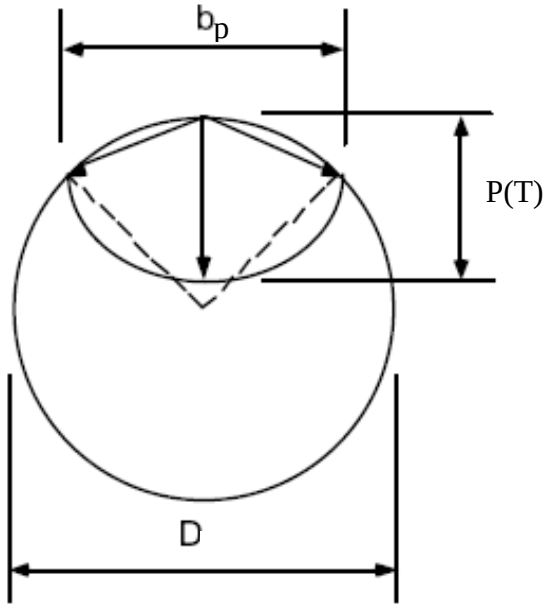

Figure 4.4: Pit configuration Val et.al. (1997).

4.3 Effect of Corrosion on Yield Strength and Modulus of Elasticity of Corroded Steel Bars

4.3.1 Empirical Formulations

Xue et al. (2010) reported the effect of corrosion on Young's modulus and the yield strength of corroded longitudinal bars. It is calculated using the following equation:

$$\frac{f_{yc}}{f_y} = 1 - 0.0217X_p \tag{4.24}$$

$$\frac{E_{sc}}{E_s} = 1 - 0.0113X_p \tag{4.25}$$

where: f_y and E_s are the yield strength and Young's modulus of un-corroded longitudinal bars; f_{yc} and E_{sc} are those of corroded longitudinal bars and X_p is the percent average mass loss given by Eq. (3.2).

Xiaoming et al. (2012) proposed yield strength of corroded bars as

$$f_{yc} = \frac{1-0.01077X_p}{1-0.01X_p} f_y \tag{4.26}$$

where

f_y and f_{yc} are the yield strength of corroded and un-corroded longitudinal bars in MPa.

Xiao-hui et al. (2008) used the following relationship for f_{yc} based on Lee's (1998) work and assuming uniform corrosion:

$$f_{yc} = \left(1 - 0.0124X_p\right)f_y \quad \text{Uniform corrosion} \tag{4.27}$$

Modulus of elasticity:

$$E_{sc} = \left(1 - 0.0075X_p\right)E_s \quad \text{Uniform corrosion} \tag{4.28}$$

Zhang and Lu (1995) proposed the following relationship:

$$f_{yc} = \left(0.986 - 0.011992X_p\right)f_y \tag{4.29}$$

Kallias et al. (2010) considered the effect of pitting corrosion by a linear reduction in yield strength of the corroded rebars at increasing levels of pitting corrosion proposed by Stewart (2009):

$$f_{ycp} = \left[1 - \alpha_y \left(\frac{A_{pit}}{A_s}\right) 100\right] f_y \tag{4.30}$$

where

f_{ycp} and f_y are the reduced and initial yield strengths respectively;

A_s is the area of the un-corroded rebar = $\frac{\pi D^2}{4}$;

A_{pit} is the area of the pit which can be calculated from Eq. (4.19); and

α_y = 0.005 based on Du et al. (2005).

4.3.2 Test Data from this Study

The reinforcing bars, 18 mm and 20 mm in diameter, extracted from corroded specimens, were tested in direct tension test to obtain stress-strain plots. Figures 4.5 through 4.7 show such plots for 18 mm diameter bars. The results of the tensile strength for 18-mm diameter bars are listed in Table 4.2 with varying degree of corrosion as percent of loss weight. The tensile stresses were calculated using Eq. (4.17) based on corroded diameter bar D' assuming uniform corrosion. The results show that the total elongation and the ductility of corroded bar decreases as degree of corrosion X_p increases, and the corroded bars had well-define yield point. The effects of degree of corrosion on the ultimate tensile

load for bars are presented in Figure 4.8. From Table 4.2 and Figure 4.8, it is observed that the ultimate tensile load for the corroded bars decreases with increasing the degree of corrosion. The typical stress-strain plots for 20-mm diameter steel bars are plotted in Figures 4.9 through 4.11 with different degree of corrosion. The tensile strength data for 20-mm diameter bars with varying degree of reinforcement corrosion as percent of loss weight are plotted and recoded in Figure 4.12 and Table 4.3.

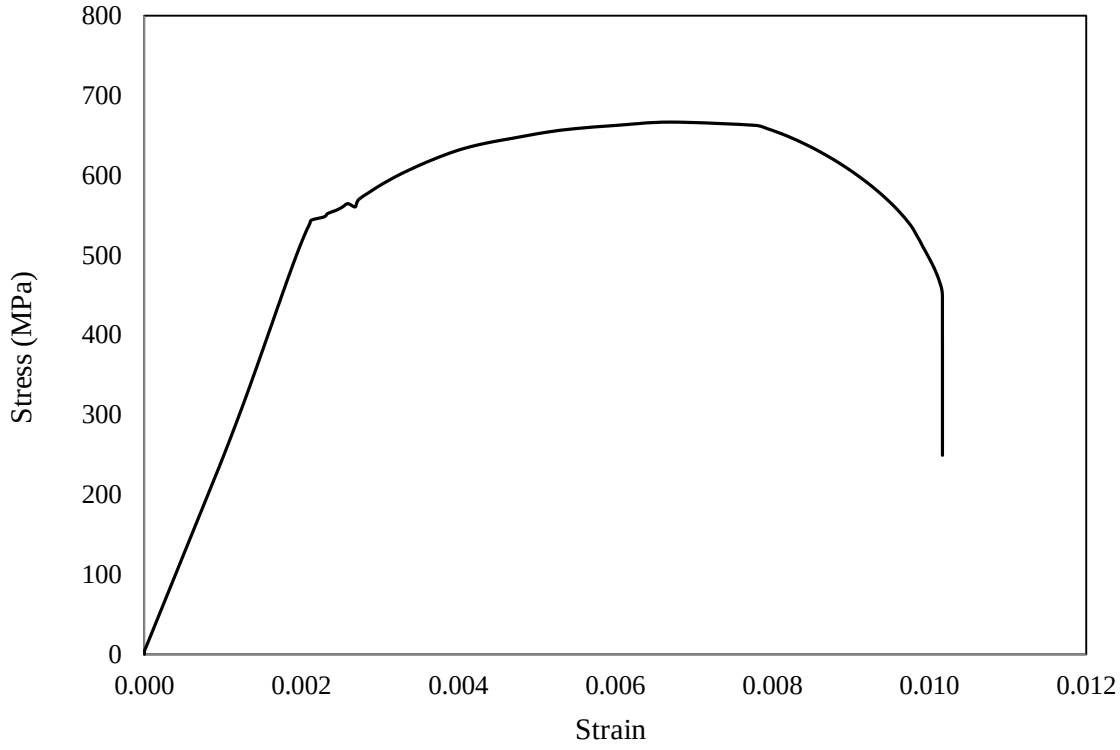

Figure 4.5: Stress-strain curve for 18-mm diameter steel bar with 3.9 % corrosion.

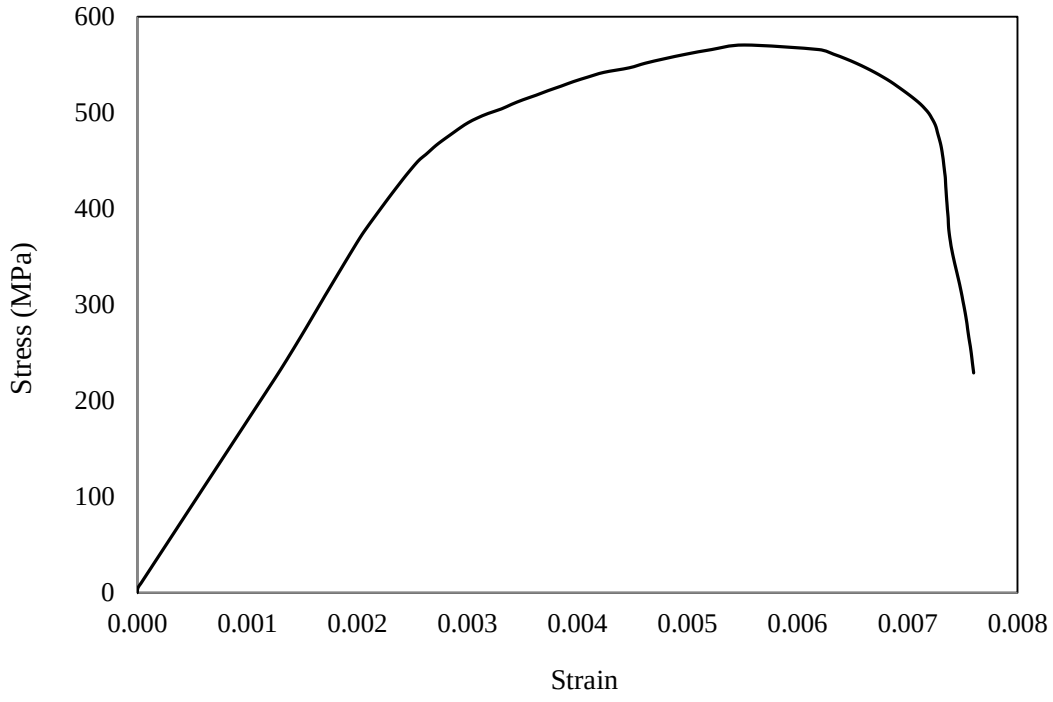

Figure 4.6: Stress-strain curve for 18-mm diameter steel bar with 18.1% corrosion.

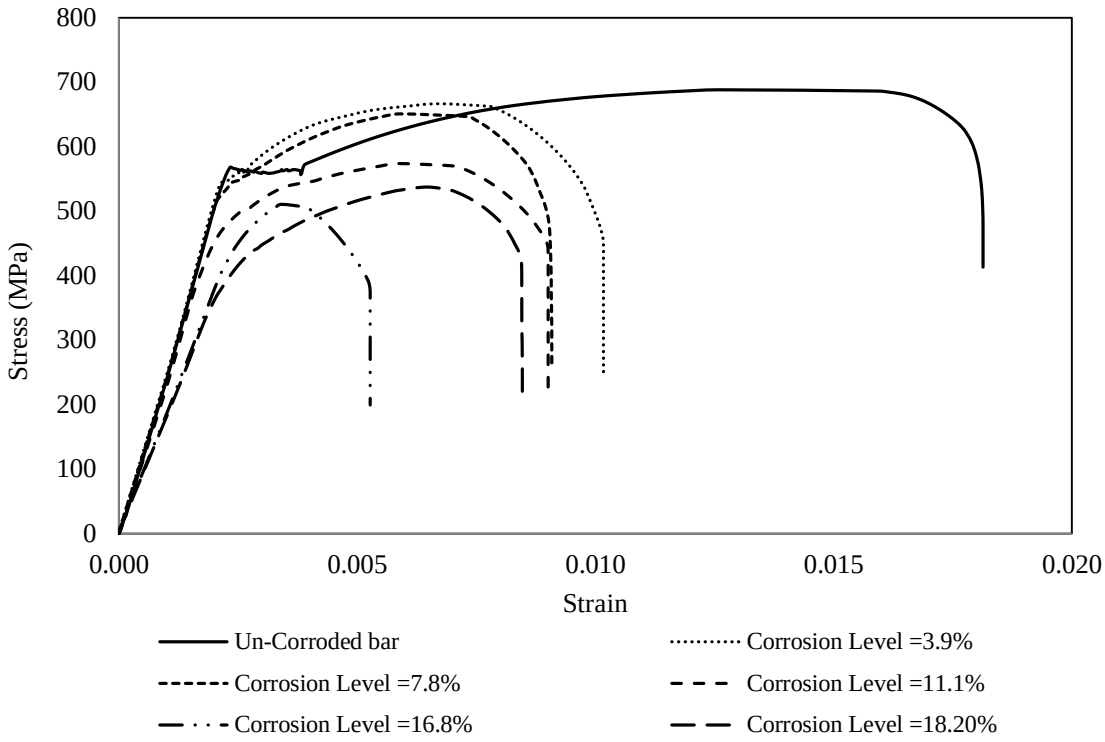

Figure 4.7: Stress-strain curves for 18-mm diameter steel bars with varying degree of corrosion.

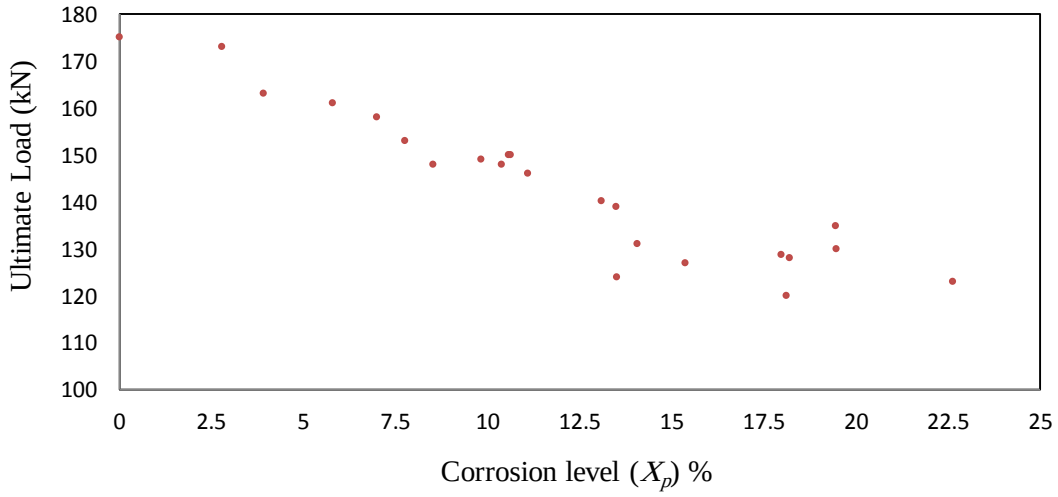

Figure 4.8: Variation of ultimate load with the corrosion level X_p (as percent loss weight) in 18-mm diameter steel bars.

Table 4.2: Tensile strength of 18-mm diameter bars.

Specimen No.	Corrosion %	D' Eq.(4.17) (mm)	Ultimate Load (kN)	Tensile Stress (MPa)
1	0.0	18.00	175	688
2	3.9	17.65	163	667
3	5.8	17.48	161	671
4	7.0	17.37	158	667
5	7.8	17.30	153	651
6	8.5	17.23	148	635
7	9.8	17.12	149	648
8	10.4	17.07	148	647
9	10.6	17.05	150	657
10	10.6	17.04	150	658
11	11.1	17.00	146	643
12	13.1	16.82	140	631
13	13.5	16.79	139	628
14	13.5	16.78	124	561
15	14.1	16.73	131	596
16	15.4	16.62	127	586
17	18.0	16.38	129	611
18	18.1	16.37	120	570
19	18.2	16.36	128	609
20	19.5	16.25	135	651
21	19.5	16.25	130	627
22	22.6	15.96	123	615

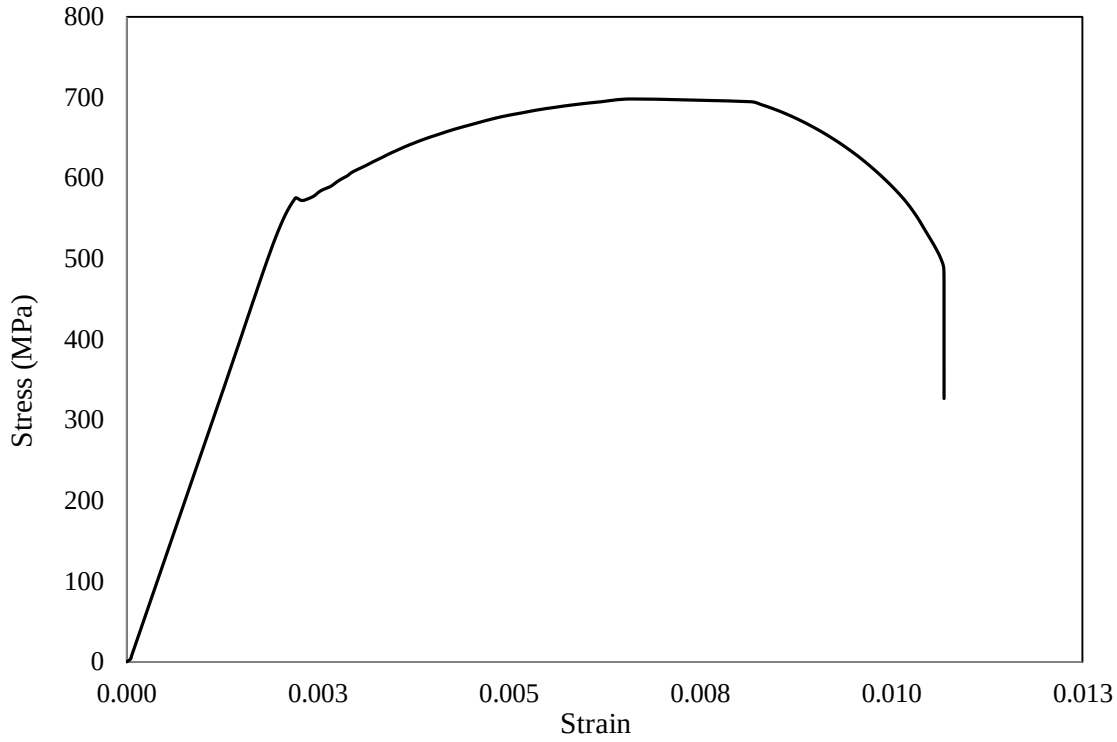

Figure 4.9: Stress-strain curve for 20-mm diameter steel bar with 6.6 % corrosion.

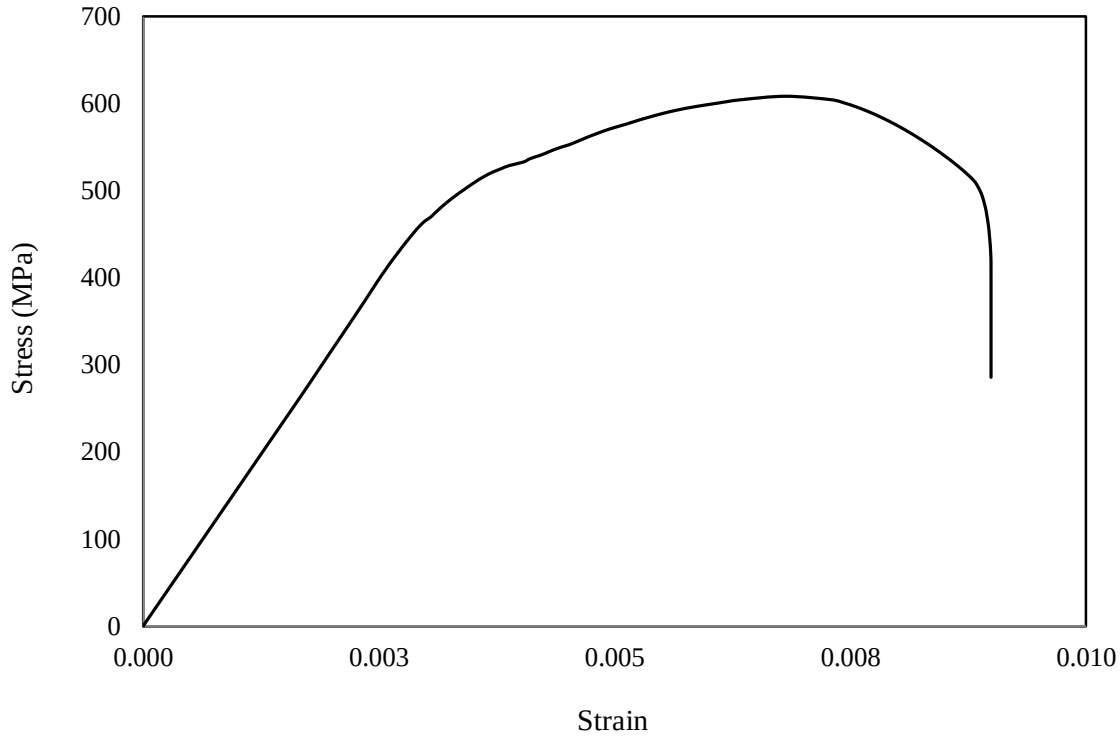

Figure 4.10: Stress-strain curve for 20-mm diameter steel bar with 21 % corrosion.

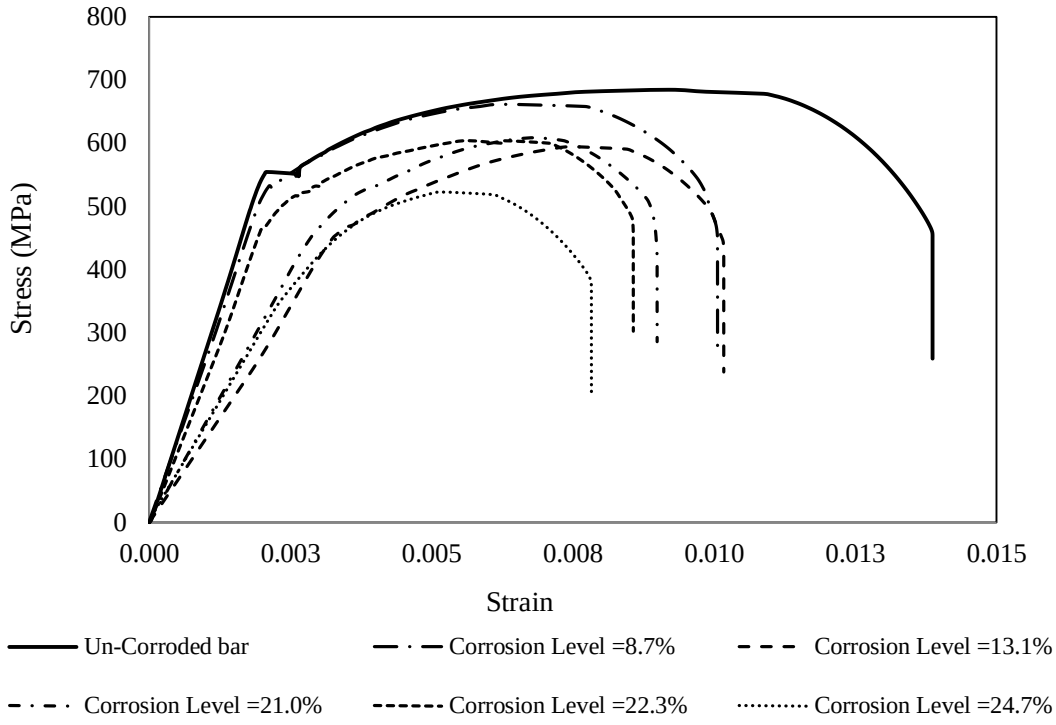

Figure 4.11: Stress-strain curves for 20-mm diameter steel bars with varying degree of corrosion.

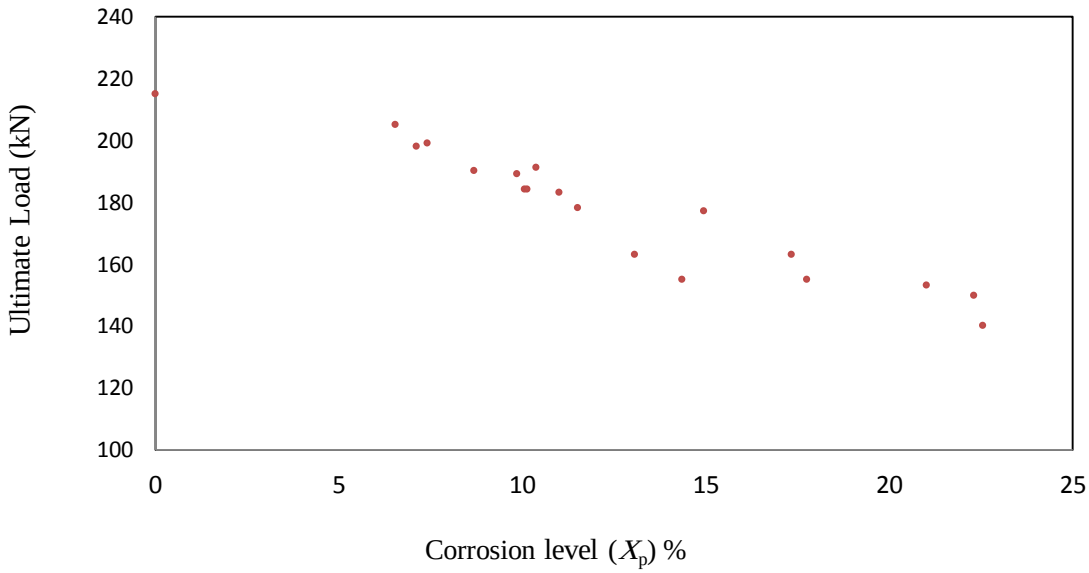

Figure 4.12: Variation of ultimate load with the corrosion level X_p (as percent loss weight) in 20-mm diameter steel bars.

Table 4.3: Tensile strength of 20-mm diameter bars.

Specimen No.	Corrosion %	D' Eq.(4.17) (mm)	Ultimate Load (kN)	Tensile Stress (MPa)
1	0.00	20.00	215	684
2	7.12	19.29	198	678
3	7.42	19.26	199	684
4	8.69	19.13	190	661
5	9.85	19.02	189	666
6	10.07	18.99	184	650
7	10.37	18.96	191	677
8	11.01	18.90	183	653
9	11.51	18.85	178	638
10	13.07	18.69	163	594
11	14.35	18.57	155	573
12	14.94	18.51	177	658
13	17.34	18.27	163	622
14	17.75	18.22	155	594
15	21.02	17.90	153	608
16	22.31	17.77	150	604
17	22.55	17.75	140	566

Based on the above experimental data of the tensile strength test of the corroded bars used in this work and using D' for calculating the stresses (Lee, 1998), new formulations of f_{yc} and modulus of elasticity of the corroded bars E_{sc} are proposed.

$$f_{yc} = \left(1 - 0.011X_p\right)f_y \tag{4.31a}$$

$$E_{sc} = \left(1 - 0.007X_p\right)E_s \tag{4.31b}$$

The empirical formulas for f_{yc} and E_{sc} for the corroded bars proposed by researchers are collectively listed in Table 4.4 and plotted in Figures 4.13 and 4.14. The plot of Eqs. 4.31a and 4.31b are shown in Figures 4.13 and 4.14. It can be seen that the value of f_{yc}

and E_{sc} given by Eqs. 4.31a and 4.31b falls a little above Lee's formulas.

Table 4.4: Summary of empirical models for effect of corrosion on f_y and modulus of elasticity of corroded steel bars.

References	Yield strength of corroded steel bar	Modulus of elasticity of corroded steel bar
Xue et.al. (2010)	$\frac{f_{yc}}{f_y} = 1 - 0.0217X_p$	$\frac{E_{sc}}{E_s} = 1 - 0.0113X_p$
Xiaoming et.al. (2012)	$f_{yc} = \frac{1-0.01077X_p}{1-0.01X_p} f_y$	-
Lee (1998) (Uniform corrosion)	$f_{yc} = (1 - 0.0124X_p)f_y$	$E_{sc} = (1 - 0.0075X_p)E_s$
Zhang and Lu (1995)	$f_{yc} = (0.986 - 0.01992X_p)fy$	-
Kallias et al. (2010) (Pitting corrosion)	$f_{ycp} = \left[1 - \alpha_y \left(\frac{A_{pit}}{A_s}\right) 100\right] f_y$	-
Proposed model	$f_{yc} = (1 - 0.011X_p)fy$	$E_{SC} = (1 - 0.007X_p)E_S$

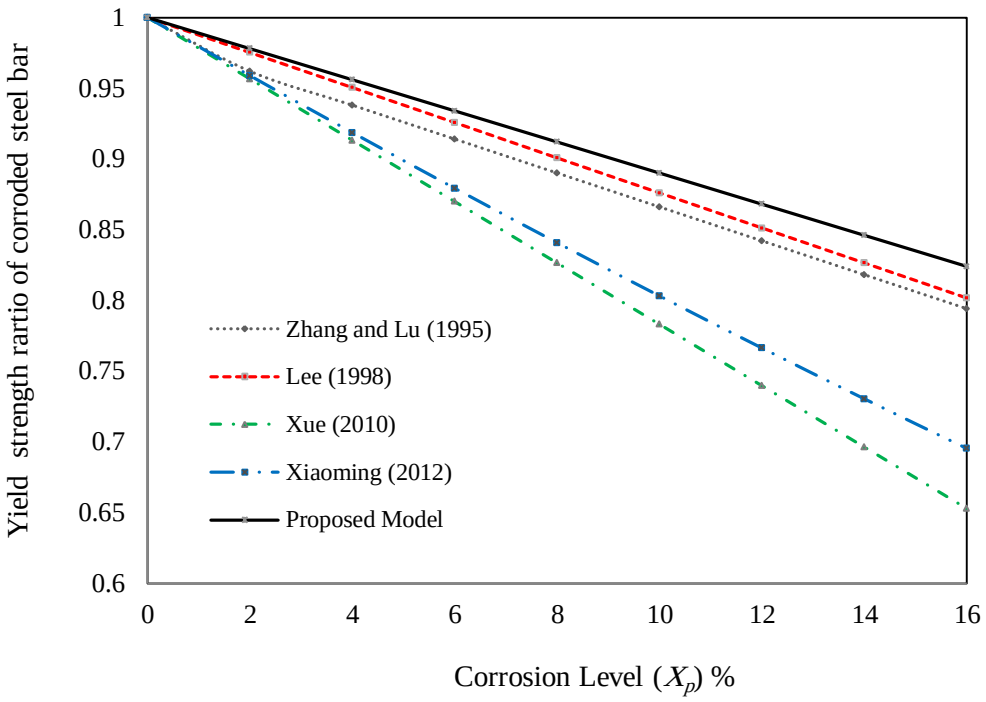

Figure 4.13: Effect of corrosion on yield strength of bars.

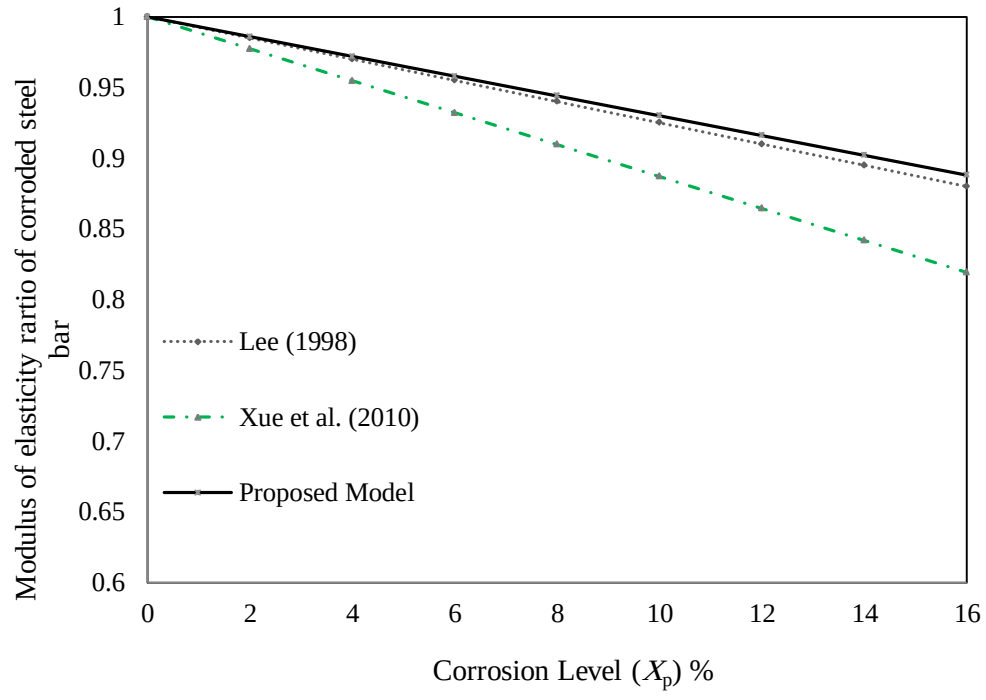

Figure 4.14: Effect of corrosion on modulus of elasticity of bars.

4.4 Cracking of Concrete

The literature review showed that a limited number of studies investigated the effect of corrosion damage in the compressive region of RC member. Capozucca et al. (2003); Coronelli and Gambarova (2004) and Du et al. (2007) proposed a method to include damage of concrete due to corrosion. Many researchers have used the method proposed by Coronelli and Gambarova (2004) for concrete damage in compression due to corrosion such as Kallias et al. (2010) and Hanjari et al. (2011).

Coronelli and Gambarova (2004) reported that the rust of the corrosion process will result into volume expansion that generates splitting stresses in the concrete and may cause the surrounding concrete cover to crack. In regions with high levels of confinement, the concrete cracks and the un-cracked parts in between the cracks contributes to the stiffness and load-carrying capacity. It is proposed to use the following equations to reduce concrete strength of cracked concrete due to corrosion in compression zone (Figure 4.15):

$$f_{cc,cracked} = \frac{f_c'}{1+K\frac{\varepsilon_1}{\varepsilon_o}} \tag{4.32}$$

where f_c' is the compressive strength of virgin concrete; K is coefficient related to bar roughness and diameter (K = 0.1 for medium-diameter ribbed bars (Capé, 1999)); ε_o is strain at the peak compressive strength f_c'; ε_1 is average tensile strain in the cracked concrete perpendicular to the direction of the applied compression and can be calculated as:

$$\varepsilon_1 = \frac{(b_f - b_o)}{b_o} \tag{4.33}$$

where: b_o is the undamaged member section width and b_f is the member width increased by corrosion cracking. The increase of beam width (b_f- b_o), can be approximated as:

$$(b_f - b_o) = n_{bar} w_{cr} \tag{4.34}$$

w_{cr} can be estimated by using the crack width proposed by Molina et al. (1993) :

$$\sum w_{cr} = 2\pi(v_{r/s} - 1) P_r T \tag{4.35}$$

where n_{bar} is the number of reinforcement bars in the compression zone; w_{cr} is the crack width for a given corrosion penetration P_rT; T = time corrosion period and $v_{r/s}$ is the ratio of volumetric expansion of the oxides with respect to the virgin material.

The ratios of volumetric expansion of different typical oxides with respect to the virgin material given in the literature (Liu and Weyers, 1998) vary between $v_{r/s}$ = 1.7 for FeO and $v_{r/s}$ = 6.15 for Fe $(OH)_3 3H_2O$. While the value of $v_{r/s}$ = 2.0 proposed by Molina et al. (1993) is frequently used in numerical analysis of corroded concrete, Bhargava et al. (2008) suggested a value of $v_{r/s}$ = 3.39357 based on the available published experimental data. In this study, the value of $v_{r/s}$ = 3.113 is chosen for all the analyses.

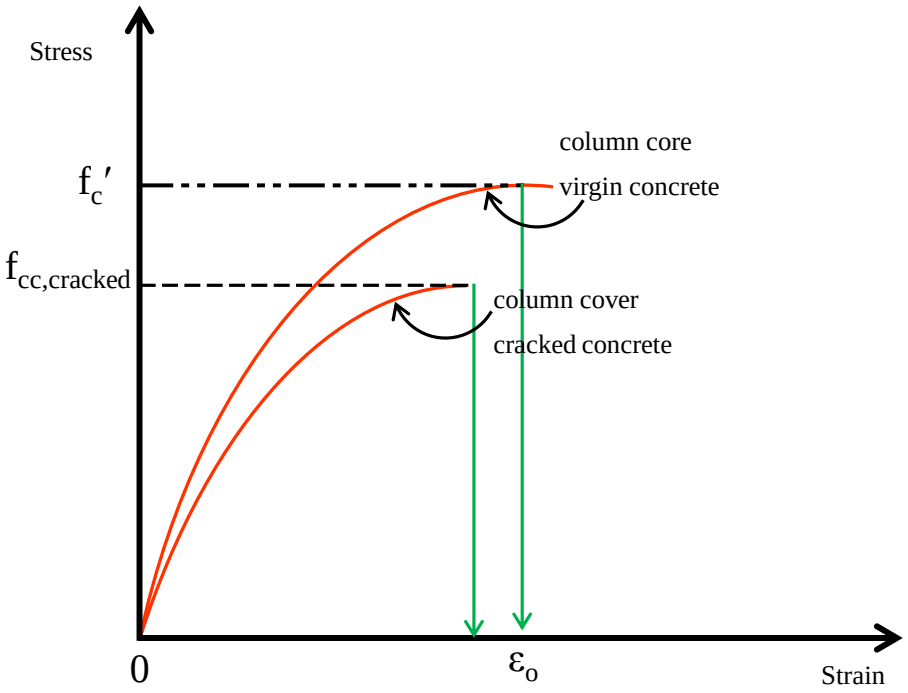

Figure 4.15: Reduced concrete strength in compression zone due to corrosion.

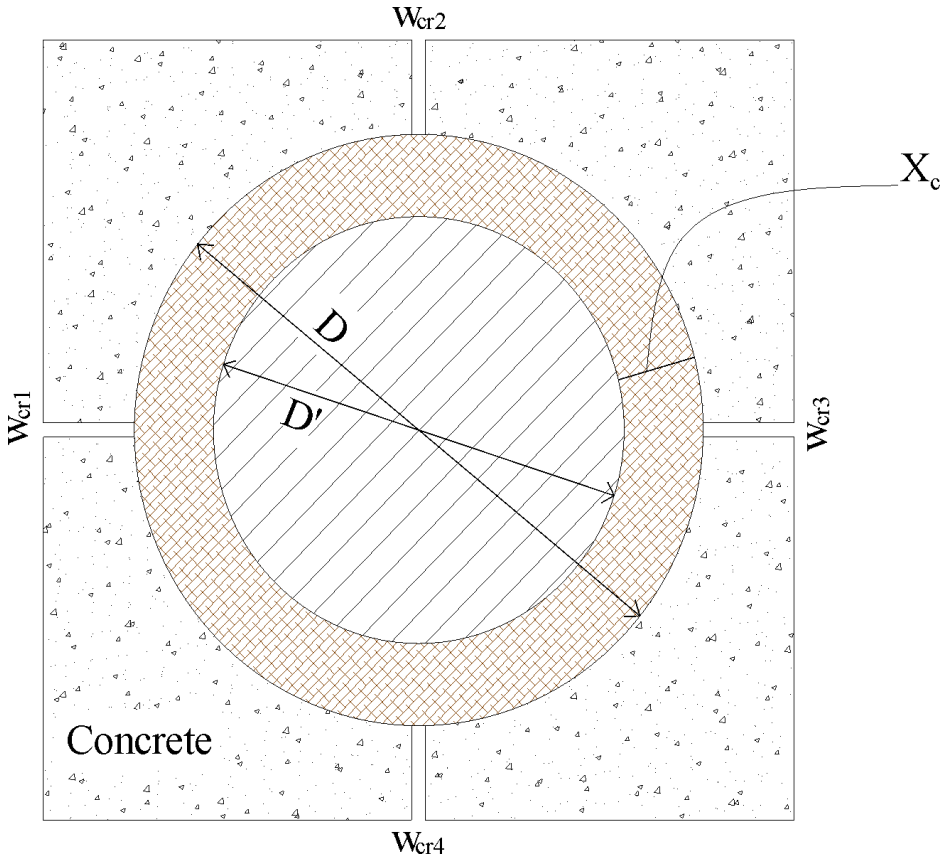

Figure 4.16: Corrosion product accumulation around a bar and corrosion crack width.

Eq. (4.35) can be derived from Figure 4.16 as follows.

The volume of steel rust/ unit length =

$$\frac{\pi}{4}(D^2 - (D - 2X_c)^2) = \pi D X_c \tag{4.36}$$

Equating increase in volume due to rust = $(v_{r/s} - 1)\,\pi D X_c$ and the increase in volume due to crack

$$\frac{\pi}{4}\left(D + \frac{\sum w_{cri}}{\pi}\right)^2 - \frac{\pi}{4}D^2 = \frac{D\sum w_{cri}}{2\pi} \tag{4.37}$$

The total width of cracks becomes

$$\sum w_{cri} = 2\pi(v_{r/s} - 1)X_c \tag{4.38}$$

where:

D is the original diameter of rebar;

D′ is the diameter of corroded rebar;

X_c is penetration depth and is equal to $P_r T$;

P_r is metal loss rate or penetration rate;

T is time corrosion period;

$v_{r/s}$ is the volume ratio between rust and steel and

$\sum w_{cri}$ is the total corrosion crack width

For columns and beam-columns with square or circular cross-section, ε_1 can be calculated as an average based on the perimeter as:

$$\varepsilon_1 = \frac{(P_e - P_o)}{P_o} = \frac{((4b_0 + n_{bar}\sum w_i) - 4b_0)}{4b_0} = \frac{n_{bar}\sum w_{cri}}{4b_0} \quad (4.39)$$

where:

P_o is the undamaged member section perimeter and

P_e is the member perimeter increased by corrosion cracking.

The reduction in the tensile strength of concrete in tension zone due to corrosion can be determined based on the reduction in compressive strength (Hanjari et al., 2011) as:

$$f_{t,cracked} = \frac{f_{cc,cracked}}{f_{c'}} f_t \quad (4.40)$$

where f_t is the tensile strength of virgin concrete.

To illustrate the effect of corrosion on the compressive strength, the concrete strength ratio in compression zone versus metal loss X_p is plotted in Figure 4.17 using Eq. 4.32. It is observed that the concrete strength ratio in compression zone decreases with increasing the mass loss X_p due to corrosion.

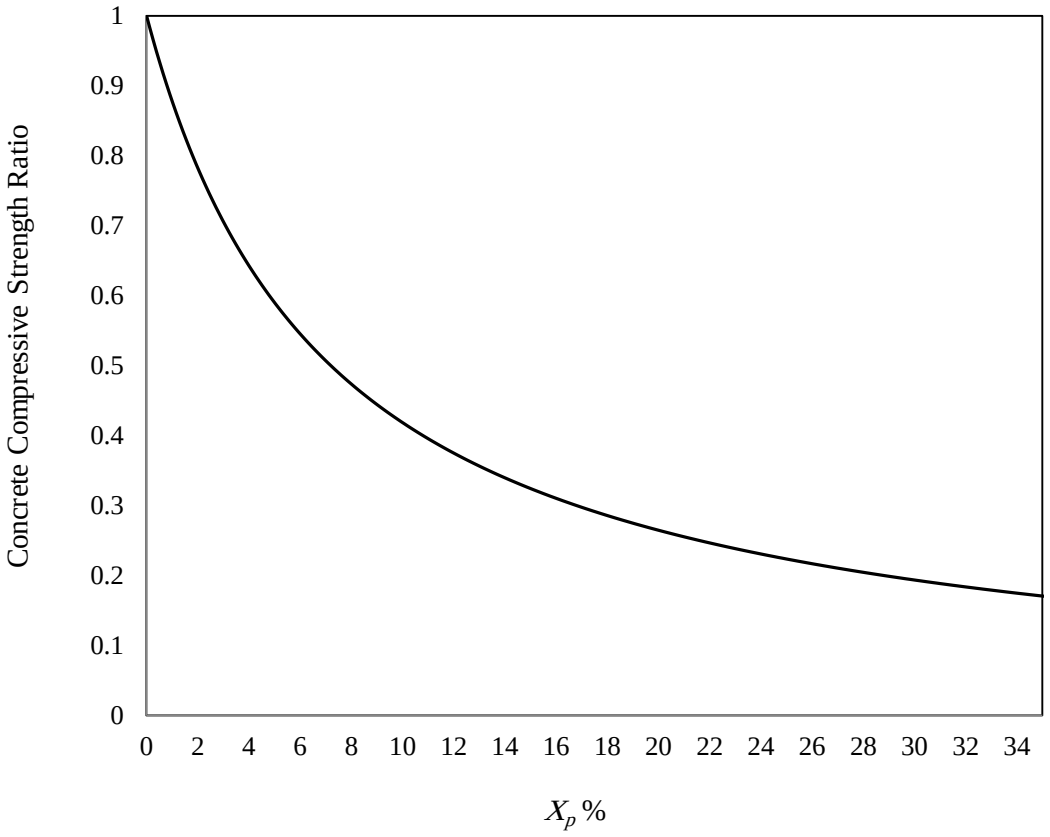

Figure 4.17 Effect of corrosion on compressive strength of concrete.

4.5 Finite Element Model

The FEA model using ANSYS consists of modeling the un-corroded columns and beam-columns with the dimensions and material properties corresponding to specimen tested. The corroded columns and beam-columns were modeled by adjusting the material properties that are affected by the corrosion. For the corroded specimens, it is assumed that the concrete core within the confinements of longitudinal bars is not affected by corrosion (Figure 4.18). The cracked and spilling in the compressed concrete cover were defined by reducing the strength of the concrete elements belonging to the cover using Eq. (4.32) (Coronelli and Gambarova, 2004).

In ANSYS, there are two methods to create the model, either by using command prompt line input (Advanced Parametric Design Language (APDL)) or the Graphical User Interface. Furthermore, the amount of time needed for solving the model can be reduced by taking advantage of the symmetry of member and loads and test setup. In this study, command prompt line input was applied to create the entire model, as Monte Carlo simulation (MCS) was used to vary the input parameters (f_c', f_y, etc.).

4.5.1 Element Types for Un-corroded and Corroded Specimens

Table 4.5 gives the element types used in the model. The concrete was modeled by using the Solid65 element. This element is three-dimensional and is defined by eight nodes having three degrees of freedom at each node (translations in the nodal x, y, and z directions). Solid65 element has capable of plastic deformation, cracking in three orthogonal directions, crushing in compression and creep. Soild65 element is shown in

Figure 4.19 (SAS, 2009).

Table 4.5**:** Element types for the model.

Material Type	ANSYS Element
Concrete	Solid65
Steel Plates	Solid45
Steel Reinforcement	Link8
Bond Interface	COMBIN39

To avoid localization of stress at ends of the model, a Solid45 element was used for steel plates at the ends of columns and beam- columns to apply the load. The element is capable of creep, swelling, stress stiffening, large deflection, large strain and plasticity. This element is defined by eight nodes similar to the Solid65. Figure 4.20 shows 3D view of this element (SAS, 2009).

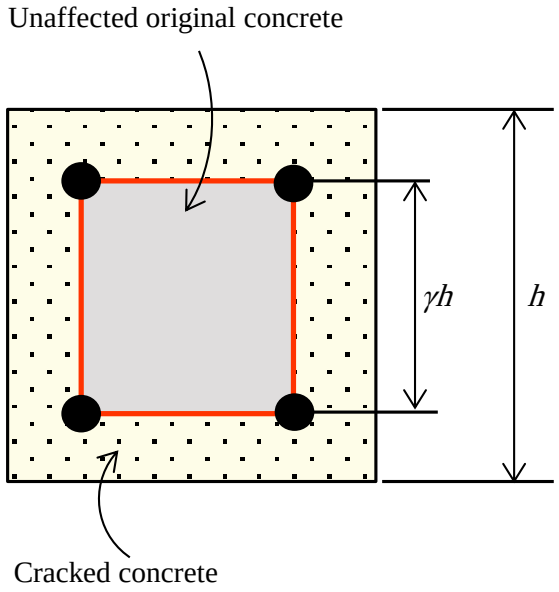

Figure 4.18: Effect of corrosion on column concrete.

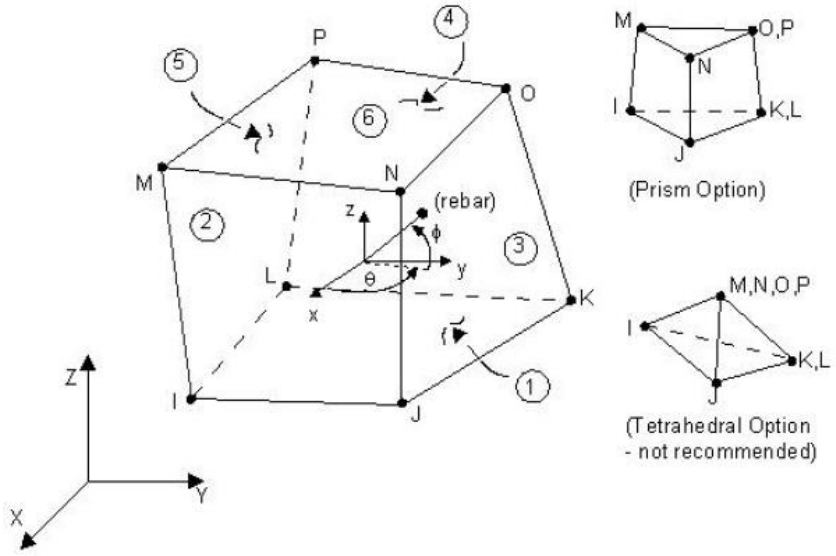

Figure 4.19: Solid65 element (SAS, 2009).

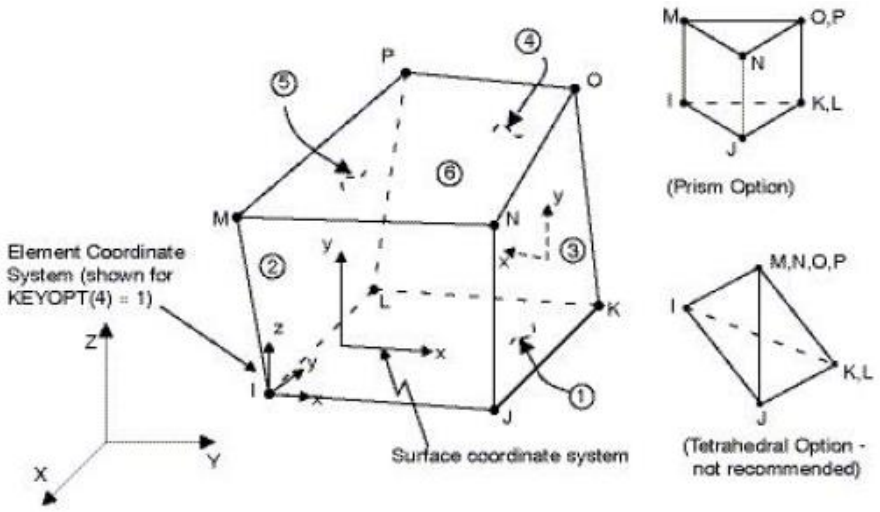

Figure 4.20: Solid45 element (SAS, 2009).

The steel reinforcement for longitudinal bars and ties was modeled by using a Link8 element which is a 3-D spar element (Figure 4.21).This element has two nodes with three degrees of freedom – translations in the nodal x, y, and z directions and also capable of plastic deformation (SAS, 2009).

COMBIN39 element was used to model the bond between concrete and steel. This element is a unidirectional element with nonlinear generalized force-deflection capability that can be used in any analysis. The element has longitudinal or torsional capability in 1-D, 2-D, or 3-D applications. The longitudinal option is a uniaxial tension-compression element with up to three degrees of freedom at each node: translations in the nodal x, y, and z directions. No bending or torsion is considered. The element also has large displacement capability for which there can be two or three degrees of freedom at each node. This element is shown in Figure 4.22 (SAS, 2009).

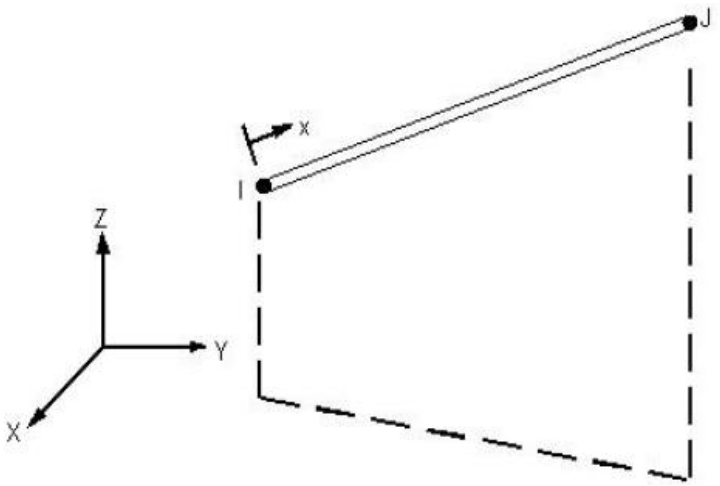

Figure 4.21: Link8 element (SAS, 2009).

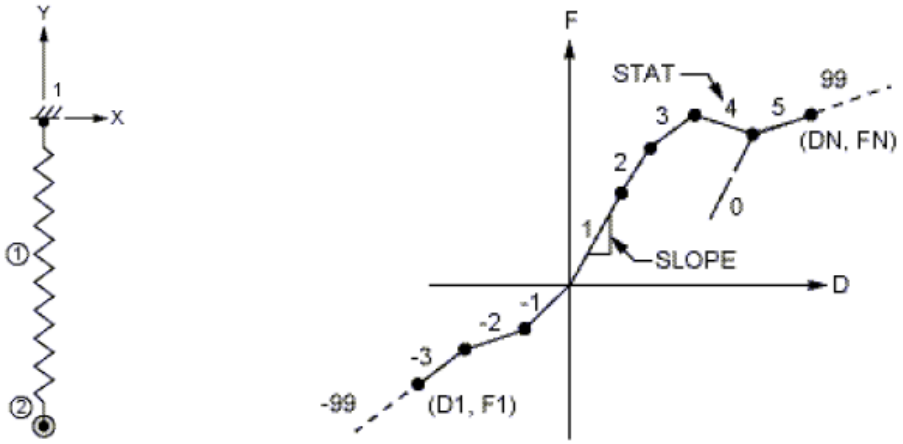

Figure 4.22: COMBIN39 element defined by a tension-compression force-deflection curve (SAS, 2009).

4.5.2 Real Constants for Un-corroded and Corroded Specimens

The model has many real constants as given in Table 4.6 where each of those elements has different real constants. The Solid45 element does not have real constant.

The real constant for the Solid65 element for the rebar is used assuming a smeared model. As seen from Table 4.6, the real constant for Solid65 needs to enter Material Number, Volume Ratio, and Orientation Angles. The volume ratio refers to the ratio of steel to concrete in the element and the orientation angles refer to the orientation of the reinforcement in the smeared model (Figure 4.23b). ANSYS allows the user to enter three rebar materials in the concrete. Each material corresponds to x, y, and z directions in the element (Figure 4.19).

The reinforcement has uniaxial stiffness and the directional orientation is defined by the user. In this study, the columns and beam-columns were modeled using discrete reinforcement so a value of zero was used for all real constants.

Real Constant Sets 2 and 3 are defined for the Link8 elements which are for the main longitudinal reinforcement and ties respectively. Values are entered for cross-sectional area and initial strain.

Real Constant Sets 4 is defined for the COMBIN39 element. Values are entered for forces versus deflections for the elements which are calculated based on the bond strength and slip for the concrete steel interface.

Table 4.6: Real constants of model.

Real Constant	Set Element	Type Constants			
1	Solid65		Real Constant for Rebar 1	Real Constant for Rebar 2	Real Constant for Rebar 3
		Material Number	0	0	0
		Volume Ratio	0	0	0
		Orientation Angles	0	0	0
2	Link8	Cross-Sectional Area of Longitudinal Rebar		Initial strain	
3	Link8	Cross-Sectional Area of Tie		Initial strain	
4	COMBIN39	Forces versus deflections			

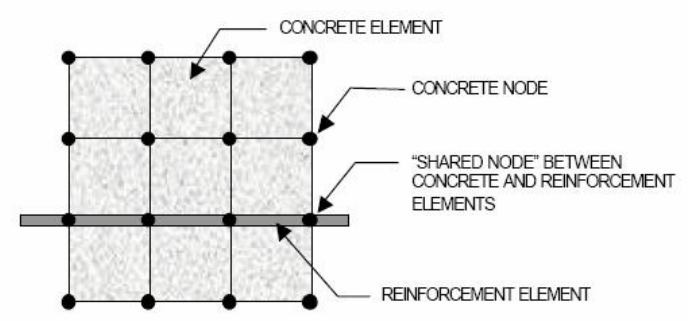

(a)

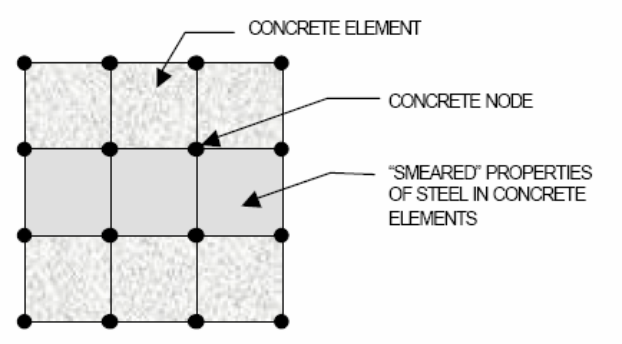

(b)

Figure 4.23: Models for reinforcement in reinforced concrete (Tavarez, 2001): (a) discrete; and (b) smeared.

4.5.3 Material Properties for Un-corroded and Corroded Specimens

Table 4.7 gives all the parameters that used to define the material models. It can be seen from Table 4.7 that there are many parts for each element should be inputted.

The material properties for the Solid65 element (concrete) require linear isotropic and multilinear isotropic material properties in ANSYS. The failure of concrete can be defined by the multilinear isotropic material along with the Willam and Warnke (1974) model. The modulus of elasticity of the concrete (E_c) is referred as E_X, and PRXY is the Poisson's ratio (v) (Wolanski, 2004). The modulus of elasticity of the concrete (E_c) is given as:

$$E_c = 4733\sqrt{fc'} \tag{4.41}$$

where f_c' is uniaxial compressive strength of concrete after 28 days (MPa).

The relationship of compressive uniaxial stress-strain for the concrete model can be found by using the following equations (Figure 4.24) (MacGregor, 1992).

$$f = \varepsilon E_c \qquad \text{if} \quad 0 \leq \varepsilon \leq \varepsilon_1 \tag{4.42}$$

$$f = \frac{E_c \varepsilon}{1+\left(\frac{\varepsilon}{\varepsilon_o}\right)^2} \qquad \text{if} \quad \varepsilon_1 \leq \varepsilon \leq \varepsilon_o \tag{4.43}$$

$$f = f_c' \qquad \text{if} \quad \varepsilon_o \leq \varepsilon \leq \varepsilon_{cu} \tag{4.44}$$

where:

$$\varepsilon_o = \frac{2f_c'}{E_c} \tag{4.45}$$

$$\varepsilon_1 = \frac{0.3f_c'}{E_c} \tag{4.46}$$

where

f is stress at any strain ε, and ε_o is strain at the ultimate compressive strength f_c'.

This curve is used by ANSYS to help the nonlinear solution logarithm with convergence.

Point 1 on the curve in Figure 4.24, defined as $0.30f_c'$ is calculated in the linear range by using Eq. (4.42). The remaining points 2 to 4 are calculated from Eq. (4.43) and ε_o determined from Eq. (4.45). The stress is calculated for each strain that selected .Point 5 is obtained at f_c' and ε_o to indicate traditional crushing strain for unconfined concrete (Wolanski, 2004). The above model for concrete has been used by a number of researchers such as Kachlakev et al. (2001), Jia (2003), Wolanski (2004) and Zangeneh (2011).

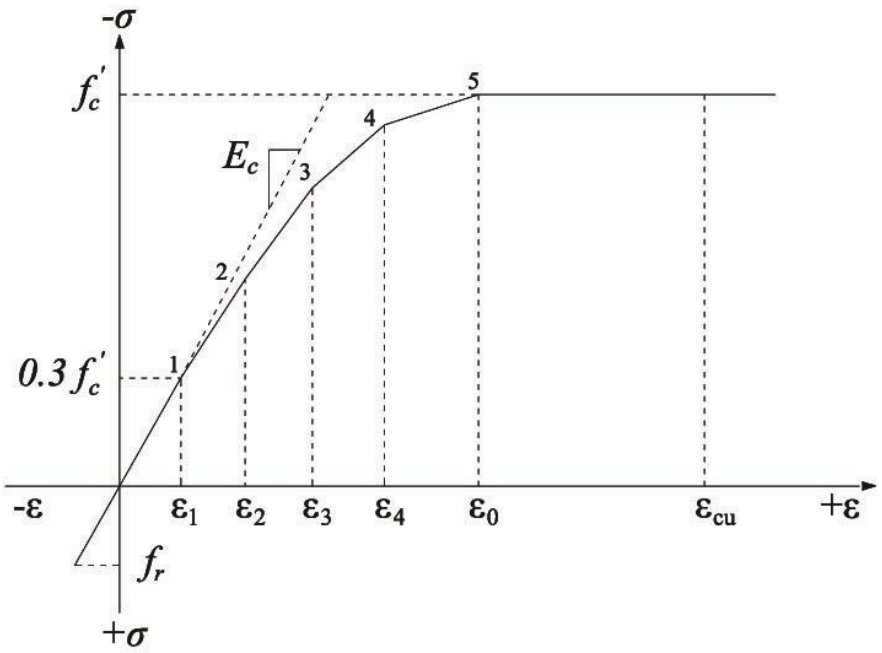

Figure 4.24: Uniaxial stress-strain curve.

Table 4.7: Material models of corroded and un-corroded specimens.

Element Type	Material Properties		
Solid65	Linear Isotropic		
	E_X PRXY		
	Multilinear Isotropic		
		Strain	Stress
	Point 1		
	….		
	Point 5		
	Concrete ShrCf-Op ShrCf-Cl UnTensSt UnCompSt BiCompSt HydroPrs BiCompSt UnTensSt TenCrFac		
Solid45	Linear Isotropic		
	E_X PRXY		
Link8	Linear Isotropic		
	E_X PRXY		
	Bilinear Isotropic		
	Yield Stss Tang Mod		
COMBIN39	-		

The Willam and Warnke (1974) material model implementation in ANSYS needs different constants to be defined. These nine constants are (SAS, 2009):

1. Shear transfer coefficients for an open crack (ShrCf-Op);
2. Shear transfer coefficients for a closed crack (ShrCf-Cl);
3. Uniaxial tensile cracking stress (UnTensSt);
4. Uniaxial crushing stress (positive) (UnCompSt);
5. Biaxial crushing stress (positive) (BiCompSt);
6. Ambient hydrostatic stress state for use with constants 7 and 8 (HydroPrs);
7. Biaxial crushing stress (positive) under the ambient hydrostatic stress state (BiCompSt);
8. Uniaxial crushing stress (positive) under the ambient hydrostatic stress state (UnTensSt); and
9. Stiffness multiplier for cracked tensile condition (TenCrFac).

The coefficients of shear transfer range from 0.0 to 1.0. The value of this coefficient equals to 0.0 to represent a smooth crack (complete loss of shear transfer) and 1.0 to indicate a rough crack (no loss of shear transfer). Kachlakev et al. (2001) determined these coefficients for open and closed cracks (Wolanski, 2004). It was noted that convergence problems appeared when the shear transfer coefficient for the open crack below 0.2. In this study, the uniaxial cracking and crushing stresses were determined based upon the modulus of rupture concrete and uniaxial unconfined compressive strength, and denoted as f_t and f_c', respectively.

The stress-strain behavior of the concrete in tension was assumed to be linearly elastic with slope E_c up to f_t modulus of rupture, based on (ACI-318):

$$f_t = 0.623\sqrt{f_c'} \tag{4.47}$$

where f_c' is uniaxial compressive strength of concrete after 28 days (MPa).

The biaxial crushing stress refers to the ultimate biaxial compressive strength (f_{cb}'). The hydrostatic pressure is denoted as σ_h. This stress state is defined as:

$$\sigma_h = \frac{1}{3}(\sigma_{xp} + \sigma_{yp} + \sigma_{zp}) \tag{4.48}$$

where σ_{xp} , σ_{yp} , and σ_{zp} are the principal stresses in the principal directions.

The biaxial crushing stress under the ambient hydrostatic stress state refers to the ultimate compressive strength for a state of biaxial compression superimposed on the hydrostatic stress state (f_1). The ultimate compressive strength for a state of uniaxial compression superimposed on hydrostatic stress state is denoted as f_2. The failure surface can be described with a minimum of two constants, f_t and f_c'. The other constants in the concrete model are default to Willam and Warnke. (SAS, 2009)

These constants can be obtained by the following equations:

$$f_{cb}' = 1.2f_c' \tag{4.49}$$

$$f_1 = 1.45f_c' \tag{4.50}$$

$$f_2 = 1.725f_c' \tag{4.51}$$

These above stress states are only used for stress states satisfying the following condition:

$$|\sigma_h| \leq \sqrt{3} f_c' \tag{4.52}$$

The Willam and Warnke (1974) triaxial failure surface model for unconfined plain concrete is used in the software as failure model for concrete. The three dimensional failure surfaces are plotted in Figure 4.25a in which σ_1, σ_2 and σ_3 are the principal stresses. The ANSYS uses a simpler way to define the concrete failure criteria by "biaxial principal stresses" which needs only the strength of concrete in tension and compression (SAS, 2009). The projection of the failure surface of Figure 4.25a is also plotted in Figure 4.25b. It represents failure surface in biaxial principal stress plane of σ_1 and σ_2 in which σ_{zp} is the same as σ_3. In ANSYS, the concrete will crack when any of the principal tensile stresses are located outside the failure surface. On the other hand, the concrete will fail due to crushing when both σ_1 and σ_2 lie outside the surface in the compression-compression part. In this case, the ANSYS would set the stiffness of the failed element to zero and would proceed to the next sub-step and result into a non-convergence state indicating that the concrete has failed completely (Zangeneh, 2011).

In this study, material model numbers 1 and 5 to 12 were used for concrete core and cover, respectively as shown in Figure 4.26.The model was created with different material numbers of the concrete so that Monte Carlo simulation can be used to vary the input parameters as well as to reflect damage due to corrosion on concrete cover.

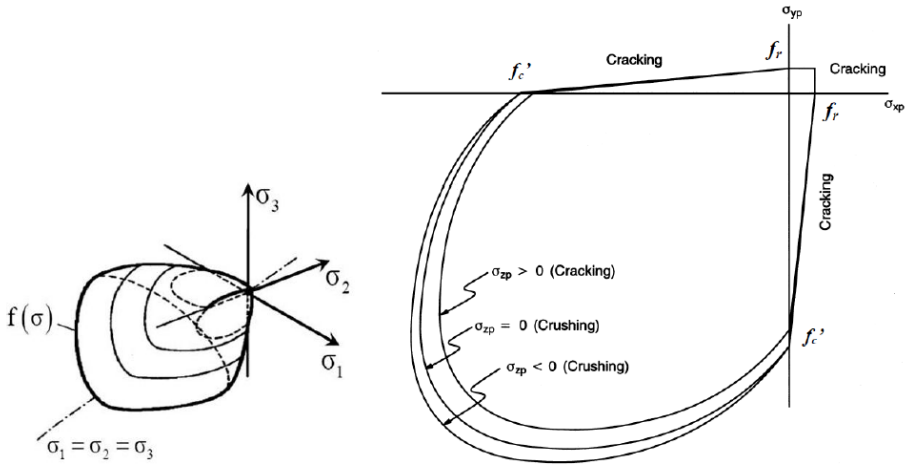

(a) (b)

Figure 4.25: (a) Failure surface of plain concrete proposed by Willam and Warnke (1974) (b) Failure surface in principal stress space with nearly biaxial stresses (Zangeneh, 2011).

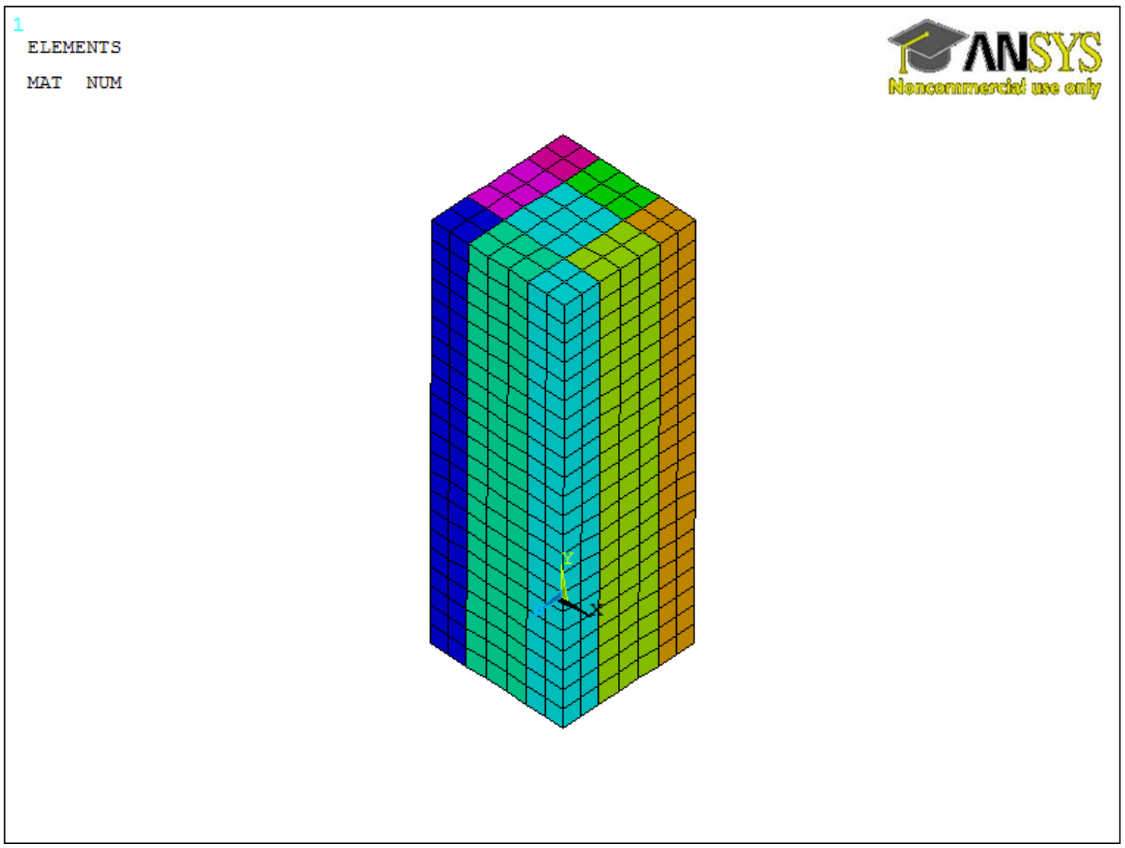

Figure 4.26: Material model for concrete.

Material Model Number 2 was used for the steel plates at loading points on the column and beam-column (Solid45 element). This element was modeled as a linear isotropic element with a modulus of elasticity for the steel (E_s = 200000 MPa), and Poisson's ratio (0.3).

Material Model Numbers 3 and 4 were used for the main reinforcements and ties (Link8 element), respectively. It was assumed to be bilinear isotropic material and identical in tension and compression (Figure 4.27). The Bilinear isotropic material is based on the Von Mises failure criteria and needs the yield stress (f_y) and the hardening modulus of the steel to be given. In this study, the reinforcing steel was assumed as perfectly elastic-plastic.

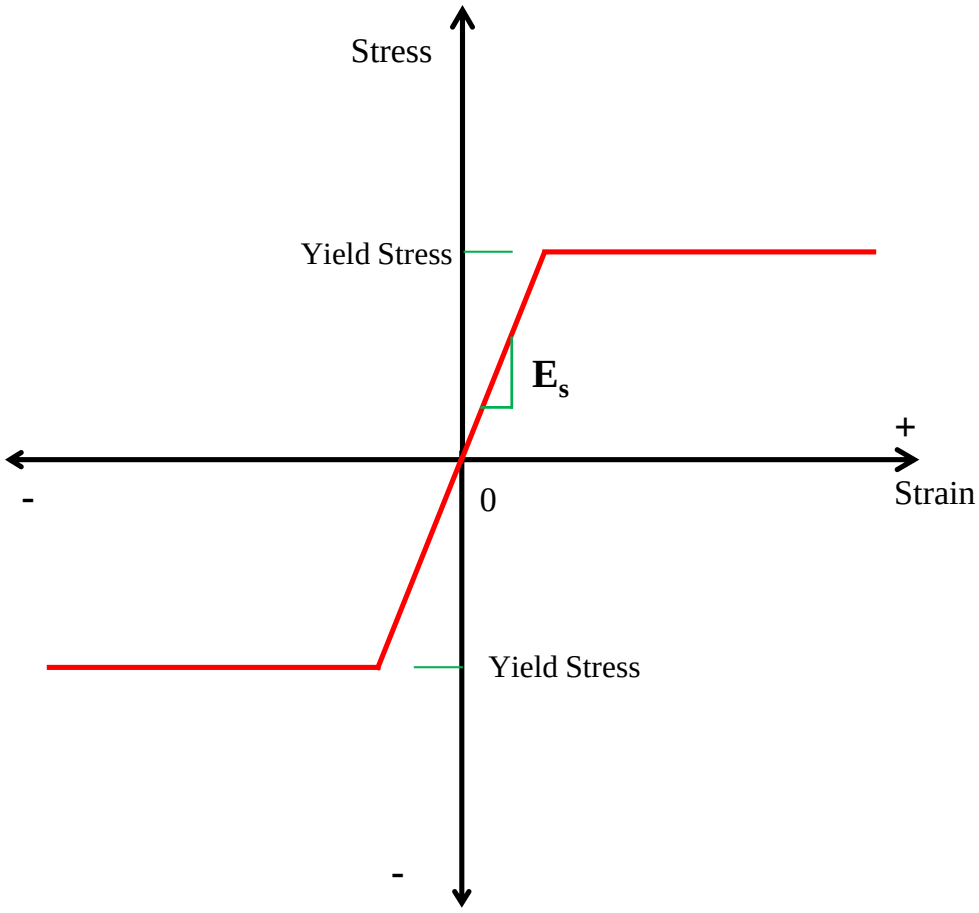

Figure 4.27: Stress-strain for steel in finite element.

4.5.4 Meshing

Good results can be achieved by using a rectangular mesh for the Solid65 element. Consequently, the mesh was made such that square or rectangular elements were created as shown in Figure 4.28. Thereafter, the reinforcement elements were connected to the COMBIN39 element .Thus, COMBIN39 elements were created in the modeling through the nodes created by the mesh of the concrete volume to act as bond element between concrete and steel (Figure 4.29). Therefore, the necessary mesh for the concrete element as described above need to be set before each section of the reinforcement is created. Each concrete mesh element was about a prism with 30x30x30 mm.

4.5.5 Algorithm Implementation in ANSYS

The model of un-corroded and corroded members was implemented in ANSYS by using command prompt line input (APDL). APDL enables users to carry out reliability analysis by using Monte Carlo simulation to estimate the probability of failure.

Figure 4.30 outlines the flowchart of FE model for un-corroded and corroded members.

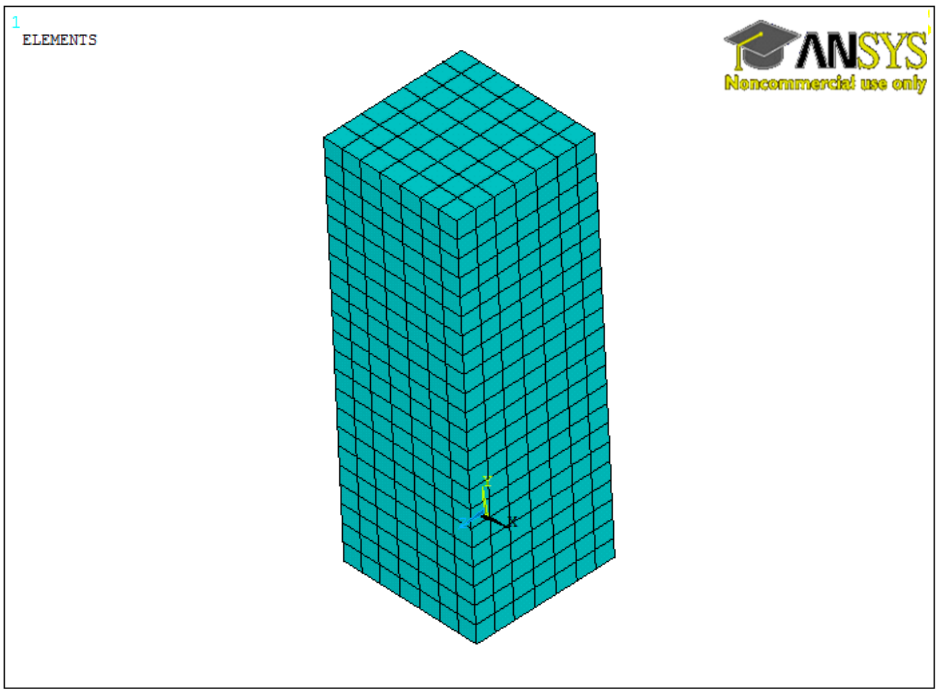

(a) Column mesh

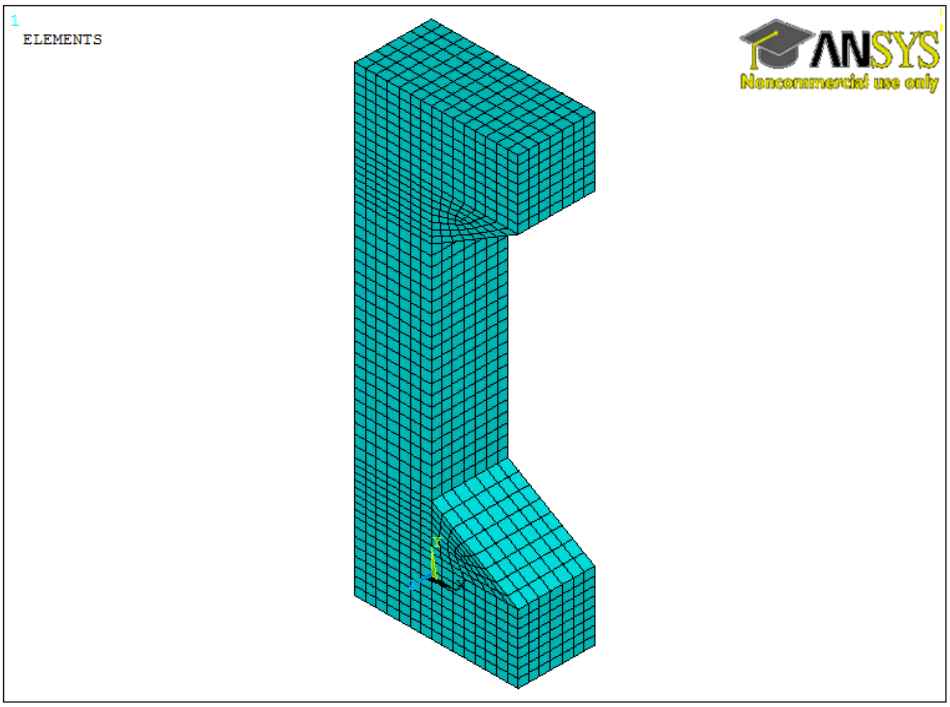

(b) Beam-column mesh

Figure 4.28: Finite element mesh for concrete.

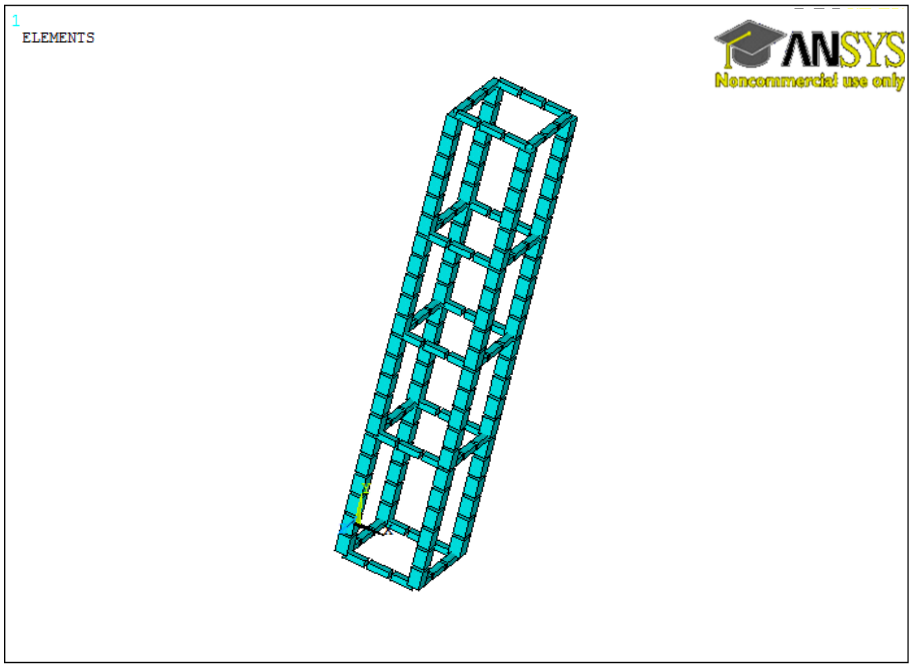

(a) Column steel

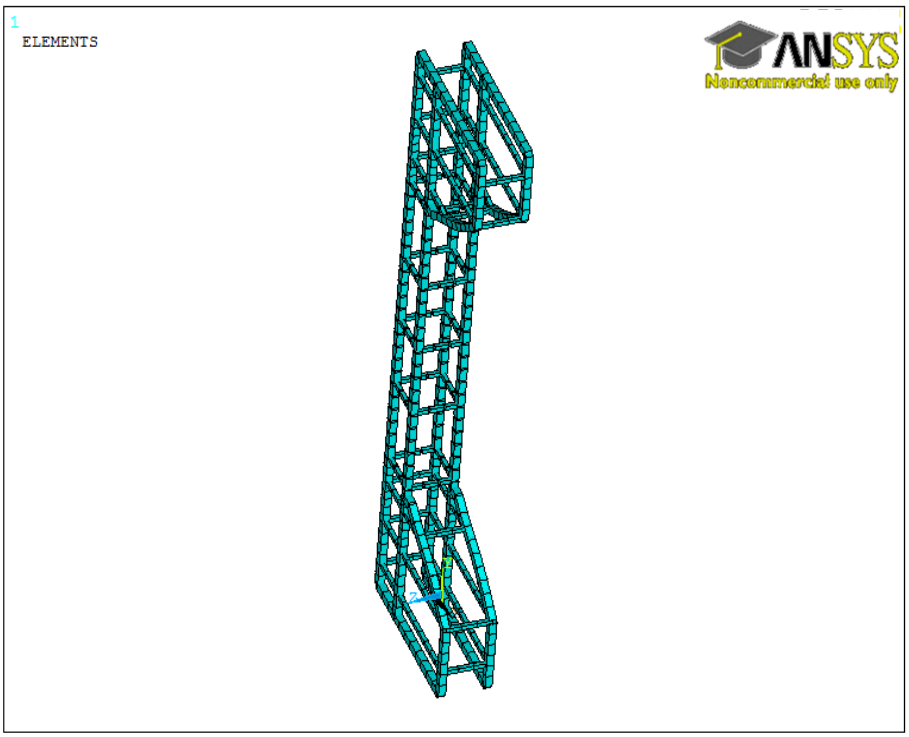

(b) Beam-column steel

Figure 4.29: Finite element mesh for steel.

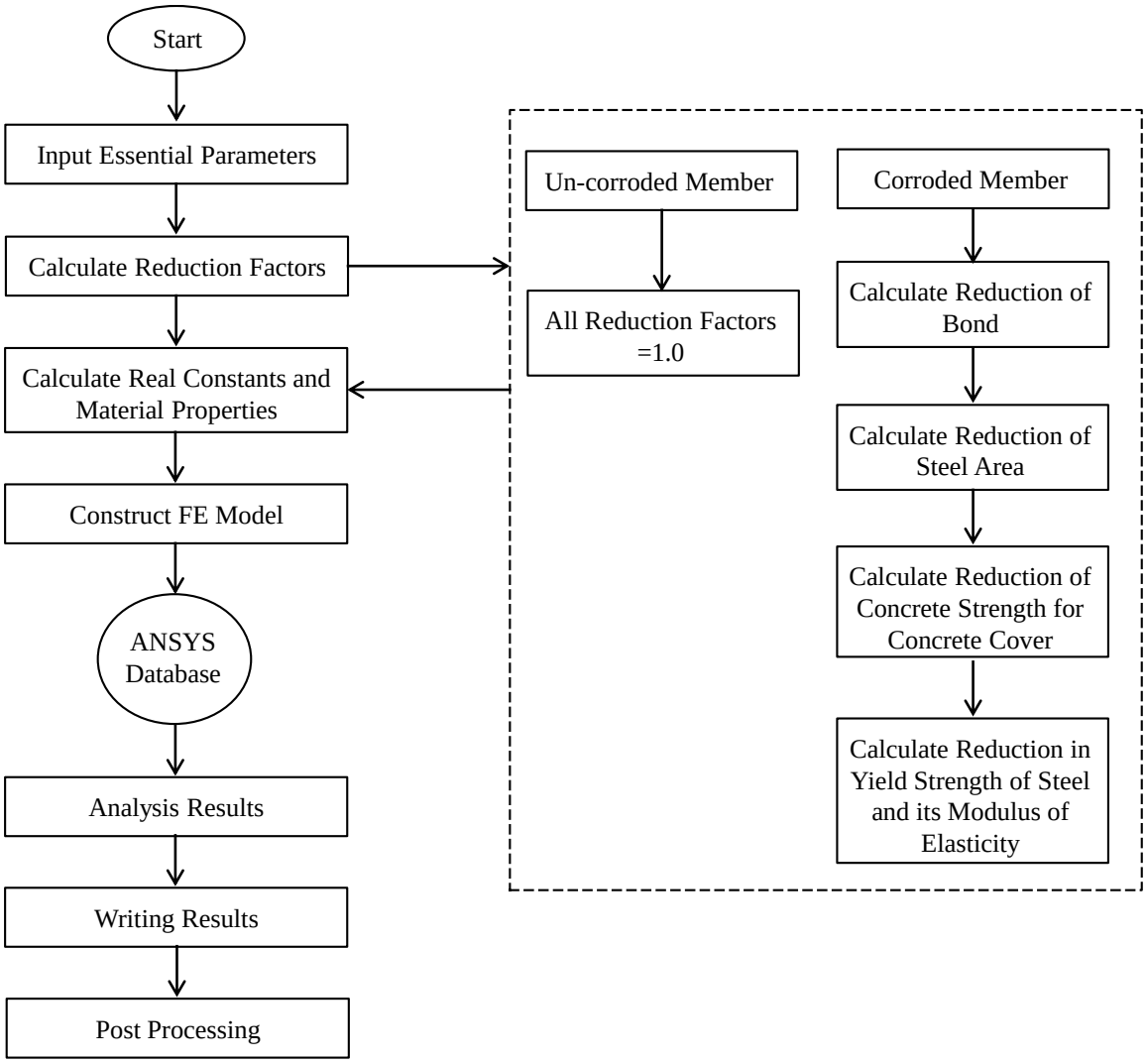

Figure 4.30: Flowchart of FE model for un-corroded and corroded members.

CHAPTER 5

RESULTS AND DISCUSSION

5.1 Material Strength

5.1.1 Concrete Strength f_c'

The values of 28-day cylinder strength of concrete, f_c', for six 75 × 150 mm was varied within the acceptable range, from a maximum of 32.7MPa to a minimum of 30.1MPa and from batch to batch. Therefore, the values of f_c' used in computation of column and beam-column strength are 30 MPa for big specimens (220 x 220 mm) and 32MPa for small cross-section (180 x 180 mm). These were checked by testing cores extracted from actual specimens. The core strength was found to be close to those values. Figure 5.1 shows the stress-strain relationship for the core specimens.

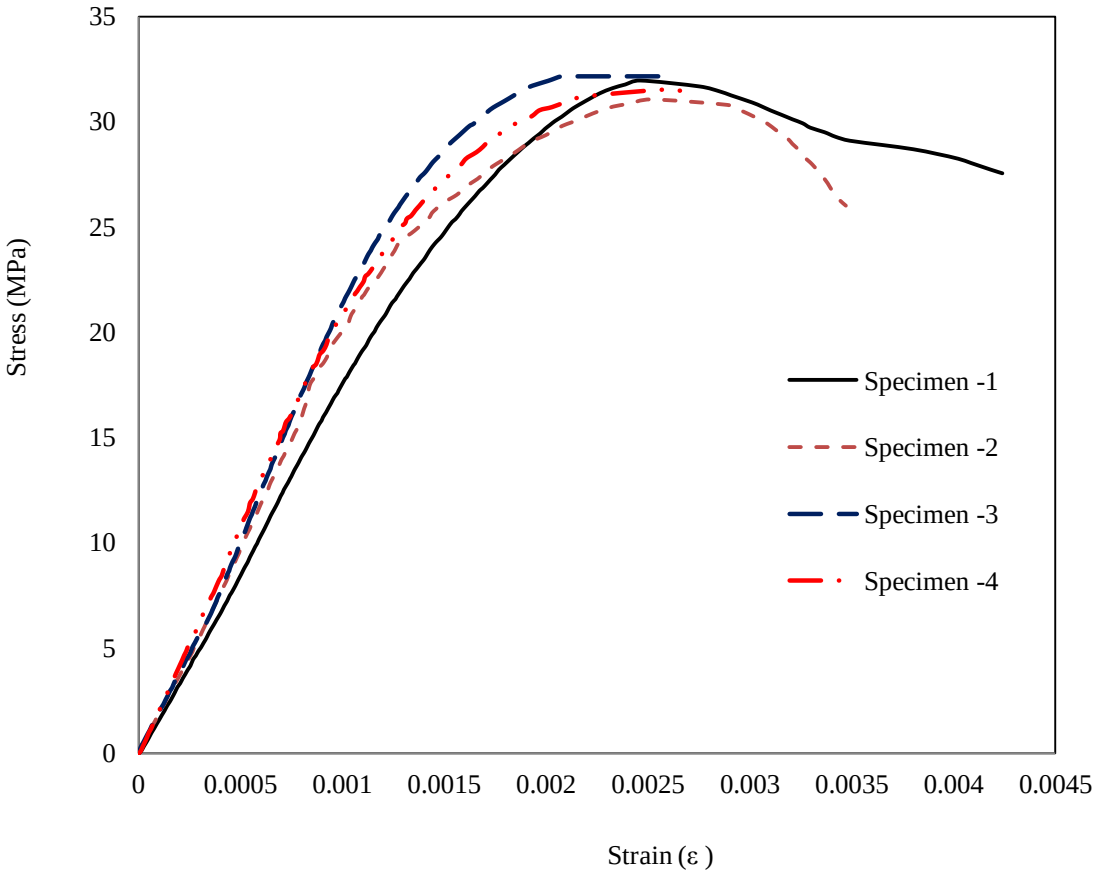

Figure 5.1: Stress-strain plot for concrete.

5.1.2 Steel Strength

From the tension test, the stress-strain curves for the reinforcing bars, 18 mm and 20 mm in diameter, are obtained and plotted in Figures 5.2 and 5.3. The plots show that the stress-strain diagrams have a clear yield point and strain-hardening zones. The values of yield and tensile strengths of steel bars (f_y and f_u) are determined from these plots and given in Table 5.1. It can be seen that the value of yield strengths for both bars are nearly identical. Therefore, a value of 555 MPa was used for f_y in computation of column and beam-column strength for both bars.

Table 5.1: Yield and tensile strength and strain of steel bars.

Diameter, D (mm)	Yield Strength, f_y (MPa)	Yield Strain, ε_y (mm/mm)	Tensile Strength, f_u (MPa)	Tensile Strain, ε_u (mm/mm)
18	557	0.00279	688.5	0.016
20	555	0.00278	684	0.014

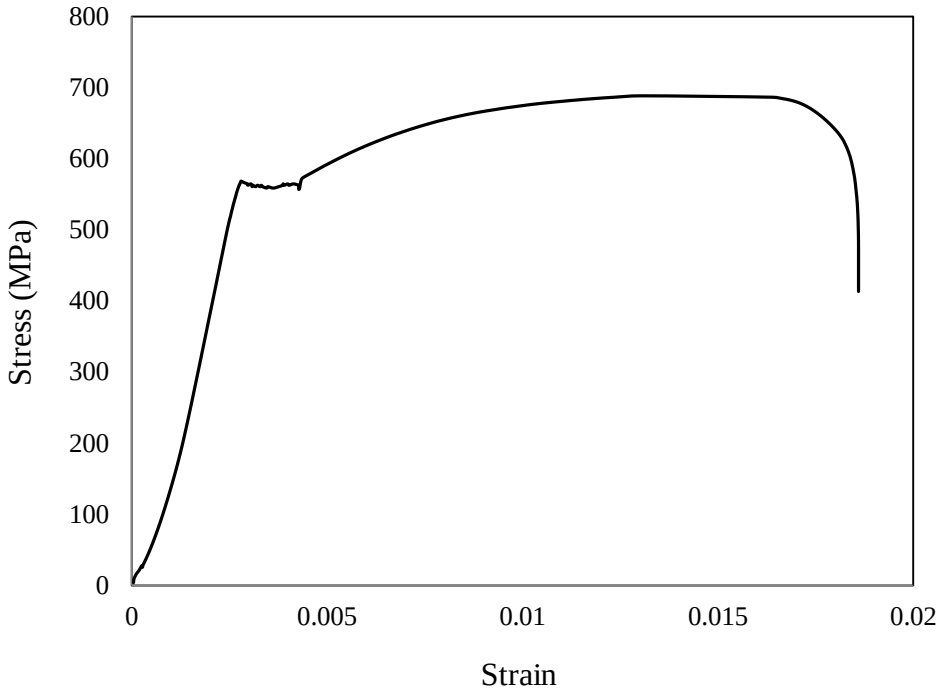

Figure 5.2: Stress-strain plot for 18 mm diameter bar.

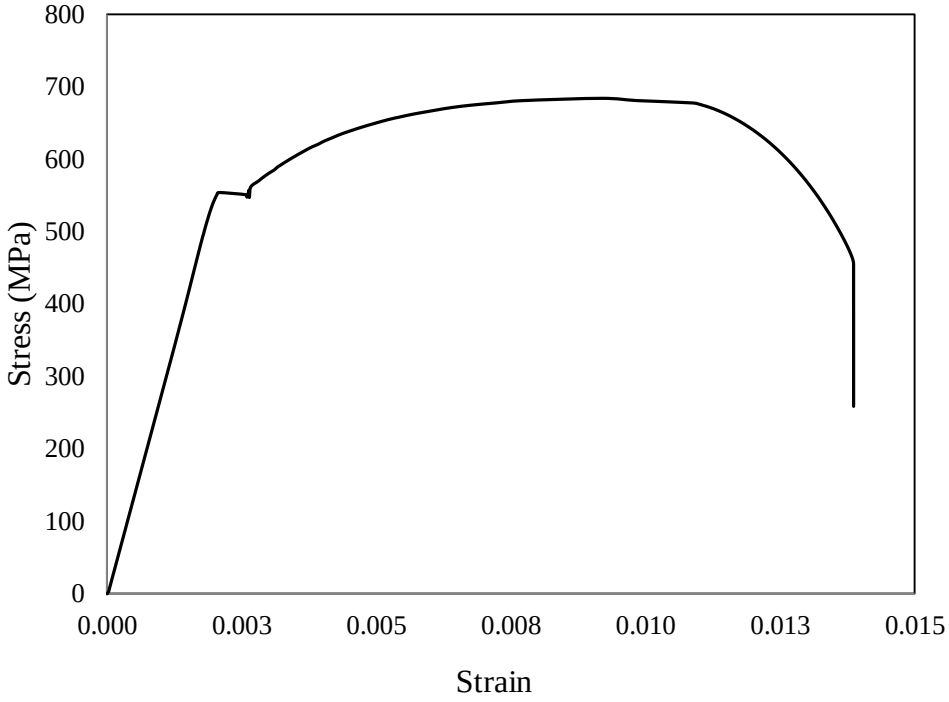

Figure 5.3: Stress-strain plot for 20 mm diameter bar.

5.2 Mechanistic Strength of Control Columns and Beam-Columns

The theoretical values of nominal ultimate capacity of the control columns and beam-columns, P_{thu}, and M_{thu} were calculated using conventional mechanics and the values of f_c' and f_y as specified in Sections 5.1.1 and 5.1.2. The values are presented in Table 5.2. The values of P_{thu}, and M_{thu} are calculated according to the following method:

5.2.1 Short Axially Loaded Columns

The theoretical values of nominal ultimate load of the control columns P_{thu} were calculated using ACI 318-08 Code provision as follows:

$$P_{thu} = 0.85 f_c'(A_g - A_{st}) + f_y A_{st} \quad (5.1)$$

where:

P_{thu} is the nominal ultimate load;

f_c' and A_g are the compression strength of concrete and area of cross-section, respectively;

f_y and A_{st} are the yield strength of steel and total area of steel, respectively.

5.2.2 Short Columns subjected to Axial Load and Moment

The nominal ultimate load of the control beam-columns P_{thu}, and M_{thu} were determined from mechanics as follows:

1. For a known cross-section shown in Figure 5.4 and eccentricity e, the value of the distance to the neutral axis c is assumed.

2. The depth of compression block is calculated by

$$a = \omega_1 c \tag{5.2}$$

3. f_s and f_s' are calculated as

$$f_s = E_s \varepsilon_s = E_s \frac{0.003(d-c)}{c} \leq f_y \tag{5.3a}$$

$$f_s' = E_s \varepsilon_s' = E_s \frac{0.003(c-d')}{c} \leq f_y \tag{5.3b}$$

4. Using the assumed value of *c*, calculate the total axial load P_{thu} as

$$P_{\text{thu}} = 0.85 f_c' b.a + A_s'(\text{f}_s' - 0.85 f_c') - A_s \text{f}_s \tag{5.4}$$

5. Calculate the eccentricity corresponding to the calculated load P_{thu} in step 4

$$e = {}^{M_{\text{thu}}}/_{P_{\text{thu}}} \tag{5.5}$$

where

$$M_{\text{thu}} = 0.85 f_c' ba\left(y' - \frac{a}{2}\right) + A_s'(\text{f}_s' - 0.85 f_c')(y' - d') + A_s \text{f}_\text{s}(d - y') \tag{5.6}$$

6. The calculated eccentricity *e* should contest the given one. If not, steps 1 to 6 has to repeat till the calculated eccentricity *e* match the given.

In Eqs. 5.2 to 5.6,

P_{thu} is the nominal ultimate load;

f_c' and f_y are the compression strength of concrete and the yield strength of steel, respectively.

c is distance to neutral axis

y' is distance of geometric centroid

e is eccentricity of load to geometric centroid

d' is effective cover of compression steel

β_1= 0.836 for f_c' = 30 MPa and 0.821 for f_c' = 32 MPa (ACI 318-08)

The other variables are as defined in Figure 5.4.

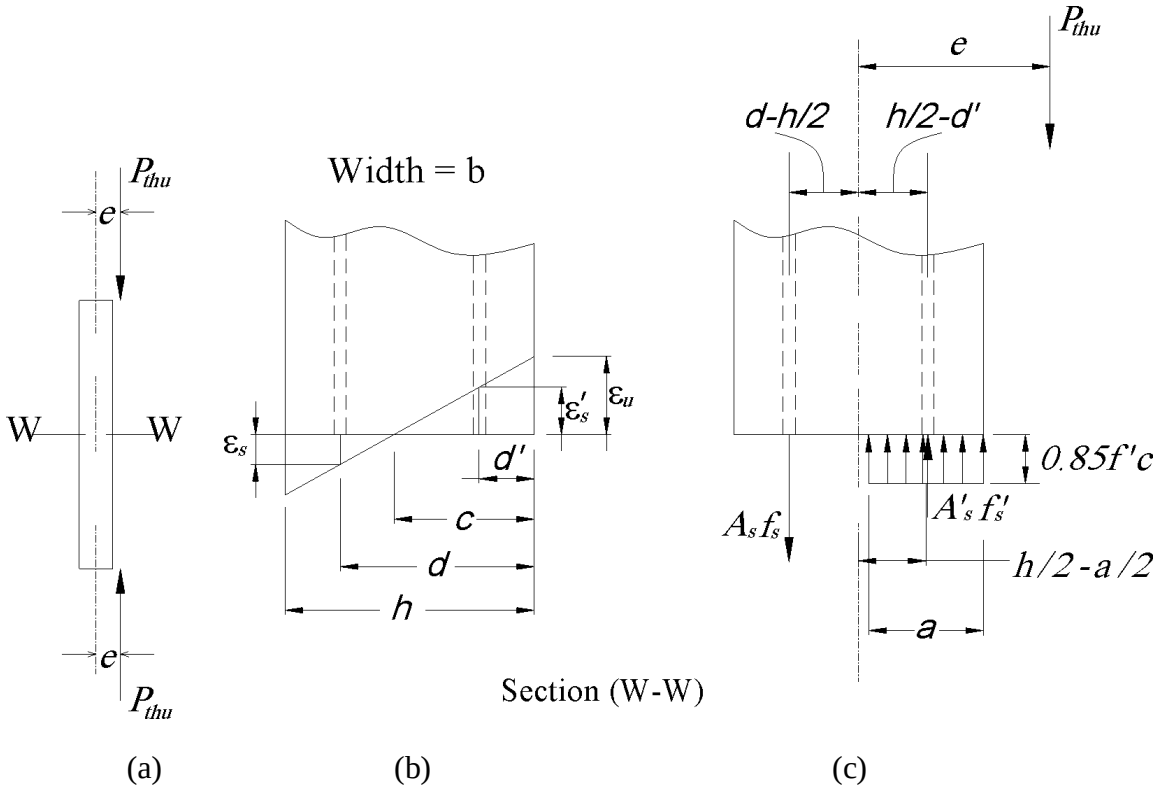

Figure 5.4: Column subject to eccentric compression: (a) loaded column; (b) strain distribution at section W-W; (c) stresses and forces at nominal ultimate strength.

Table 5.2: Theoretical capacity of control column and beam-column specimens.

Specimen	Eccentricity, e (mm)	f_c' (MPa)	Failure Load, P_{thu} (kN)	Moment, M_{thu} (kN.m)
C1-18	0	32	1414	0
BC1-18-30	30	32	746	22
BC1-18-60	60	32	414	25
BC1-18-95	95	32	262	25
C2-18	0	30	1769	0
BC2-18-35	35	30	1068	37
BC2-18-65	65	30	693	45
BC2-18-115	115	30	405	47
C1-20	0	32	1539	0
BC1-20-30	30	32	782	23
BC1-20-60	60	32	434	26
BC1-20-95	95	32	277	26
C2-20	0	30	1894	0
BC2-20-35	35	30	1122	39
BC2-20-65	65	30	730	47
BC2-20-115	115	30	433	50

5.3 Experimental Strength of Column and Beam-Column Specimens

5.3.1 Control Specimens

The failure load, P_{exu} for the control column and beam-column specimens were obtained from the results of test of each specimen, and are presented in Table 5.3.

The ratio between the experimental and theoretical strengths of the sixteen control specimens, C_c presented in Table 5.3 shows small difference between the theoretical and experimental capacities of the specimens. The values of C_c in Table 5.3 which ranged from 86 % to 109 % illustrate that the theoretically predicted capacities of the columns

and beam-columns were mostly lower than and reasonably closer to the experimental values. Therefore, for comparison purposes, the experimental strength of the control specimens was used as the strength of un-corroded columns and beam-columns.

Table 5.3: Comparison test results of un-corroded columns and beam-columns.

Specimen	Eccentricity, e (mm)	f_c' (MPa)	Failure Load, (kN)		$C_c = P_{exu}/P_{thu}$ (%)
			P_{exu}	P_{thu}	
C1-18	0	32	1272	1414	90
BC1-18-30	30	32	675	746	90
BC1-18-60	60	32	453	414	109
BC1-18-95	95	32	260	262	99
C2-18	0	30	1605	1769	91
BC2-18-35	35	30	940	1068	88
BC2-18-65	65	30	595	693	86
BC2-18-115	115	30	350	405	86
C1-20	0	32	1350	1539	88
BC1-20-30	30	32	690	782	88
BC1-20-60	60	32	460	434	106
BC1-20-95	95	32	271	277	98
C2-20	0	30	1780	1894	94
BC2-20-35	35	30	962	1122	86
BC2-20-65	65	30	645	730	88
BC2-20-115	115	30	419	433	97

5.3.2 Corroded Specimens

The experimentally determined values of the load carrying capacity of all corroded specimens, P_{exc}, are presented in Tables 5.4 and 5.5 for specimens with 18 mm and 20 mm diameter bars, respectively. Also given in Tables 5.4 and 5.5 the values of R_f which is the ratio between the experimental strengths of corroded specimen P_{exc} and un-corroded specimen P_{exu} multiplied by 100. R_f represents the residual strength as percentage of the original strength, after loss due to reinforcement corrosion. The results indicate that the reduction in capacity of corroded specimens is more for columns than for beam-columns within the range of eccentricities considered. This is because the cracking and de-bonding of concrete cover have more adverse effect on the strength of columns, as the strength of concrete section accounts for much of the axial load capacity. For a beam-column with e that produces small compressive stress or tensile stress on the moment-producing tension face, the effect of the concrete cover is not as critical as for a column.

Table 5.4: Experimental load capacity of corroded and un-corroded specimens with 18 mm diameter bars.

Specimen	e (mm)	f_c' (MPa)	I_{app} (mA/cm^2)	T (Day)	Failure Load, (kN)		$R_f = P_{exc} / P_{exu}$ ×100
					P_{exc}	P_{exu}	
C1-18-7d	0	32	2	7	515	1272	40
C1-18-10d	0	32	2.5	10	480	1272	38
C1-18-13d	0	32	2.5	13	390	1272	31
BC1-18-30-7d	30	32	2.5	7	561	675	83
BC1-18-30-10d	30	32	2.5	10	472	675	70
BC1-18-30-12d	30	32	2.5	11.5	348	675	52
BC1-18-60-7d	60	32	2.5	7	386	453	85
BC1-18-60-10d	60	32	2.5	10	300	453	66
BC1-18-60-13d	60	32	2.5	13	252	453	56
BC1-18-95-7d	95	32	2.5	7	236	260	91
BC1-18-95-10d	95	32	2.5	10	214	260	82
BC1-18-95-11d	95	32	2.5	10.5	177	260	68
C2-18-7d	0	30	2.5	7	700	1605	44
C2-18-10d	0	30	2.5	10	665	1605	41
C2-18-13d	0	30	2.5	13	550	1605	34
BC2-18-35-6d	35	30	2.5	6	667	940	71
BC2-18-35-8d	35	30	2.5	8	589	940	63
BC2-18-35-9d	35	30	2.5	9	575	940	61
BC2-18-65-4d	65	30	2.5	4	548	595	92
BC2-18-65-7d	65	30	2.5	7	482	595	81
BC2-18-65-10d	65	30	2.5	10	442	595	74
BC2-18-115-7d	115	30	2.5	7	278	350	79
BC2-18-115-8d	115	30	2.5	8	256	350	73
BC2-18-115-9d	115	30	2.5	9	246	350	70

Table 5.5: Experimental load capacity of corroded and un-corroded specimens with 20 mm diameter bars.

Specimen	e (mm)	f_c' (MPa)	I_{app} (mA/cm^2)	T (Day)	Failure Load, (kN)		$R_f = P_{exc} / P_{exu}$ ×100
					P_{exc}	P_{exu}	
C1-20-7d	0	32	2.5	7	456	1350	34
C1-20-10d	0	32	2.5	10	375	1350	28
C1-20-13d	0	32	2.5	13	330	1350	24
BC1-20-30-7d	30	32	2.5	7	475	690	69
BC1-20-30-6d	30	32	2.5	6	495	690	72
BC1-20-30-13d	30	32	2.5	13	384	690	56
BC1-20-60-7d	60	32	2.5	7	431	460	94
BC1-20-60-10d	60	32	2.5	10	284	460	62
BC1-20-60-13d	60	32	2.5	13	258	460	56
BC1-20-95-7d	95	32	2.5	7	209	271	77
BC1-20-95-10d	95	32	2.5	10	197	271	73
BC1-20-95-13d	95	32	2.5	13	168	271	62
C2-20-7d	0	30	2.5	7	670	1780	38
C2-20-8d	0	30	2.5	8	620	1780	35
C2-20-10d	0	30	2.5	9.5	580	1780	33
BC2-20-35-7d	35	30	2.5	7	631	962	66
BC2-20-35-6d	35	30	2.5	6	731	962	76
BC2-20-35-9d	35	30	2.5	9	582	962	60
BC2-20-65-7d	65	30	2.5	7	497	645	77
BC2-20-65-6d	65	30	2.5	6	519	645	80
BC2-20-65-9d	65	30	2.5	9	460	645	71
BC2-20-115-7d	115	30	2.5	7	301	419	72
BC2-20-115-6d	115	30	2.5	5.5	336	419	80
BC2-20-115-9d	115	30	2.5	9	280	419	67

5.4 Weight Loss of Bars and Equivalent Corrosion Current Density

The weight of corroded bar for column and beam-column specimens were compared with the original (un-corroded) bar.

The instantaneous corrosion rate (J_r) was calculated by using the measured weight loss as follows:

$$J_r = \frac{weight\ loss}{surface\ area\ of\ bar \times corrsion\ period} \tag{5.7}$$

Calculated values of J_r were used to determine the equivalent corrosion current density (I_{corr}), using the following expression (Ijsseling (1986)).

$$J_r = \left(\frac{W}{F}\right) I_{corr} \tag{5.8}$$

where

W = equivalent weight of steel

F = Faraday's constant

By substituting W = 55.85/2 = 27.925 g and F = 96487 coulombs (A-sec) in Eq. (5.8), the following simplified equation for calculating I_{corr} from the value of J_r is obtained:

$$I_{corr} = 0.1096 J_r \tag{5.9}$$

where: I_{corr} is in mA/cm^2 and J_r is in gm/cm^2/year.

By combining Eqs. (5.7) and (5.8), the weight loss of a bar can be expressed as

Weight loss /surface area of a bar = $\left(\frac{W}{F}\right) I_{corr} T = 0.289 I_{corr}\ T$ (5.10)

where: I_{corr} is in mA/cm^2 and T is time in seconds.

It is clear from Eq. (5.10) that the weight loss of a given bar is directly proportional to $I_{corr}T$, since W/F for steel is a constant.

The percentage of weight loss, X_p can be obtained as follows:

$$X_p = \frac{Weight\ Loss(g)}{Original\ Weight} \times 100 \tag{5.11}$$

The values of the equivalent I_{corr} calculated using Eq. (5.9) for all corroded specimens are given in Tables 5.6 and 5.7. As seen from table, the highest weight loss (18.09%) was in corroded rebars of column specimen, while it was the lowest (4.96%). It is observed that the equivalent I_{corr} values calculated from gravimetric analysis are always lower than the applied current density, I_{app}. Yubun et al. (2000) and Ballim et al. (2003) reported the same observations. This difference between I_{corr} and I_{app} can be attributed to several factors. These factors are the diameter of bars being corroded, quality of concrete and concrete cover. The values of I_{corr} and I_{app} will be equal for bars suspended in liquid. For the bars embedded in concrete, Yubun et al. (2000) found that the resistance provided by the concrete needed a certain amount of energy to initiate the corrosion. To reflect the difference between I_{corr} and I_{app}, the current efficiency, η is calculated and presented in Tables 5.8 and 5.9 as follows:

$$\eta = Efficiency\ applied\ current = \frac{I_{corr}}{I_{app}} \times 100 \tag{5.12}$$

Table 5.6: Gravimetric weight loss and I_{corr} for specimens with 18 mm diameter bars.

Specimen	D (mm)	I_{app} (mA/cm^2)	T (Day)	Gravimetric test results			J_r (g/cm^2/yr)	I_{corr} (mA/cm^2)
				Avg. original wt. of sample (g)	Avg. wt. Loss (g)	X_p, wt. loss %		
C1-18-7d	18	2	7	479.04	30.21	6.29	11.11	1.22
C1-18-10d	18	2.5	10	516.14	53.84	10.49	12.87	1.41
C1-18-13d	18	2.5	13	570.49	103.14	18.09	17.16	1.88
BC1-18-30-7d	18	2.5	7	459.41	31.08	6.76	11.92	1.31
BC1-18-30-10d	18	2.5	10	545.65	66.66	12.36	15.07	1.65
BC1-18-30-12d	18	2.5	11.5	552.39	77.84	14.13	15.12	1.66
BC1-18-60-7d	18	2.5	7	470.16	36.96	7.86	13.85	1.52
BC1-18-60-10d	18	2.5	10	559.5	71.85	12.93	15.84	1.74
BC1-18-60-13d	18	2.5	13	640.73	101.82	15.92	15.08	1.65
BC1-18-95-7d	18	2.5	7	477.32	36.95	7.75	13.64	1.49
BC1-18-95-10d	18	2.5	10	582.92	64.04	10.96	13.55	1.49
BC1-18-95-11d	18	2.5	10.5	488.77	60.86	12.34	14.63	1.6
C2-18-7d	18	2.5	7	597.8	39.41	6.57	11.62	1.27
C2-18-10d	18	2.5	10	610.99	70.15	11.52	14.16	1.55
C2-18-13d	18	2.5	13	601.79	100.38	16.68	15.83	1.73
BC2-18-35-6d	18	2.5	6	583.97	34.34	5.86	12.09	1.33
BC2-18-35-8d	18	2.5	8	518.65	49.13	9.52	14.61	1.6
BC2-18-35-9d	18	2.5	9	543.38	62.02	11.42	15.64	1.71
BC2-18-65-4d	18	2.5	4	634.64	31.48	4.96	15.3	1.68
BC2-18-65-7d	18	2.5	7	521.28	32.86	6.32	11.11	1.22
BC2-18-65-10d	18	2.5	10	583.97	70.44	11.96	14.88	1.63
BC2-18-115-7d	18	2.5	7	555.8	35.09	6.35	11.13	1.22
BC2-18-115-8d	18	2.5	8	559.41	47.26	8.42	13.03	1.43
BC2-18-115-9d	18	2.5	9	544.81	62.8	11.47	15.8	1.73

Table 5.7: Gravimetric weight loss and I_{corr} for specimens with 20 mm diameter bars.

Specimen	D (mm)	I_{app} (mA/cm^2)	T (Day)	Gravimetric test results			J_r (g/cm^2/yr)	I_{corr} (mA/cm^2)
				Avg. original wt. of sample (g)	Avg. wt. Loss (g)	X_p, wt. loss %		
C1-20-7d	20	2.5	7	720.12	70.03	9.74	19.36	2.12
C1-20-10d	20	2.5	10	668	79.26	11.82	16.53	1.81
C1-20-13d	20	2.5	13	661.97	100.34	15.18	16.25	1.78
BC1-20-30-7d	20	2.5	7	689.35	65.05	9.44	18.79	2.06
BC1-20-30-6d	20	2.5	6	640.48	48.68	7.98	17.65	1.93
BC1-20-30-13d	20	2.5	13	694.75	99.1	14.22	15.29	1.68
BC1-20-60-7d	20	2.5	7	723.53	61.53	8.48	16.93	1.86
BC1-20-60-10d	20	2.5	10	730.88	89.5	12.27	17.06	1.87
BC1-20-60-13d	20	2.5	13	740.47	118.5	15.88	17.15	1.88
BC1-20-95-7d	20	2.5	7	726.68	65.67	9.03	17.99	1.97
BC1-20-95-10d	20	2.5	10	739.58	89.1	12.05	16.79	1.84
BC1-20-95-13d	20	2.5	13	679.66	101.08	14.75	15.94	1.75
C2-20-7d	20	2.5	7	800.44	69.83	8.71	17.37	1.9
C2-20-8d	20	2.5	8	839.27	79.35	9.47	16.47	1.8
C2-20-10d	20	2.5	9.5	832.53	89.62	10.81	15.79	1.73
BC2-20-35-7d	20	2.5	7	708.9	60.81	8.6	17.08	1.87
BC2-20-35-6d	20	2.5	6	736.43	52.04	7.06	16.41	1.8
BC2-20-35-9d	20	2.5	9	751.96	79.37	10.55	16.34	1.79
BC2-20-65-7d	20	2.5	7	700.74	63.78	9.02	18.12	1.99
BC2-20-65-6d	20	2.5	6	681.37	51.36	7.51	17.51	1.92
BC2-20-65-9d	20	2.5	9	763.95	84.29	11.03	17.08	1.87
BC2-20-115-7d	20	2.5	7	696.55	69.51	9.97	19.87	2.18
BC2-20-115-6d	20	2.5	5.5	724.43	48.4	6.56	16.93	1.86
BC2-20-115-9d	20	2.5	9	725.18	79.51	10.96	16.98	1.86

Table 5.8: Relationship between I_{corr} and I_{app} for specimens with 18 mm diameter bars.

Specimen	%Weight Loss (X_p) (Gravimetric)	I_{corr} (mA/cm^2)	I_{app} (mA/cm^2)	Current Efficiency η (%)	Average Efficiency η (%)
C1-18-7d	6.29	1.22	2	61	62
C1-18-10d	10.49	1.41	2.5	56	
C1-18-13d	18.09	1.88	2.5	75	
BC1-18-30-7d	6.76	1.31	2.5	52	
BC1-18-30-10d	12.36	1.65	2.5	66	
BC1-18-30-12d	14.13	1.66	2.5	66	
BC1-18-60-7d	7.86	1.52	2.5	61	
BC1-18-60-10d	12.93	1.74	2.5	69	
BC1-18-60-13d	15.92	1.65	2.5	66	
BC1-18-95-7d	7.75	1.49	2.5	60	
BC1-18-95-10d	10.96	1.49	2.5	59	
BC1-18-95-11d	12.34	1.60	2.5	64	
C2-18-7d	6.57	1.27	2.5	51	
C2-18-10d	11.52	1.55	2.5	62	
C2-18-13d	16.68	1.73	2.5	69	
BC2-18-35-6d	5.86	1.33	2.5	53	
BC2-18-35-8d	9.52	1.60	2.5	64	
BC2-18-35-9d	11.42	1.71	2.5	69	
BC2-18-65-4d	4.96	1.68	2.5	67	
BC2-18-65-7d	6.32	1.22	2.5	49	
BC2-18-65-10d	11.96	1.63	2.5	65	
BC2-18-115-7d	6.35	1.22	2.5	49	
BC2-18-115-8d	8.42	1.43	2.5	57	
BC2-18-115-9d	11.47	1.73	2.5	69	

Table 5.9: Relationship between I_{corr} and I_{app} for specimens with 20 mm diameter bars.

Specimen	%Weight Loss (X_p) (Gravimetric)	I_{corr} (mA/cm^2)	I_{app} (mA/cm^2)	Current Efficiency η (%)	Average Efficiency η (%)
C1-20-7d	9.74	2.12	2.5	85	
C1-20-10d	11.82	1.81	2.5	72	
C1-20-13d	15.18	1.78	2.5	71	
BC1-20-30-7d	9.44	2.06	2.5	82	
BC1-20-30-6d	7.98	1.93	2.5	74	
BC1-20-30-13d	14.22	1.68	2.5	67	
BC1-20-60-7d	8.48	1.86	2.5	74	
BC1-20-60-10d	12.27	1.87	2.5	75	
BC1-20-60-13d	15.88	1.88	2.5	75	
BC1-20-95-7d	9.03	1.97	2.5	79	
BC1-20-95-10d	12.05	1.84	2.5	74	
BC1-20-95-13d	14.75	1.75	2.5	70	75
C2-20-7d	8.71	1.90	2.5	76	
C2-20-8d	9.47	1.80	2.5	72	
C2-20-10d	10.81	1.73	2.5	69	
BC2-20-35-7d	8.60	1.87	2.5	75	
BC2-20-35-6d	7.06	1.80	2.5	72	
BC2-20-35-9d	10.55	1.79	2.5	72	
BC2-20-65-7d	9.02	1.99	2.5	79	
BC2-20-65-6d	7.51	1.92	2.5	77	
BC2-20-65-9d	11.03	1.87	2.5	75	
BC2-20-115-7d	9.97	2.18	2.5	87	
BC2-20-115-6d	6.56	1.86	2.5	74	
BC2-20-115-9d	10.96	1.86	2.5	74	

It is can be seen that the average value of η for 18 mm and 20 mm diameter bars is 62% and 75%, respectively. Yubun et al. (2000) reported current efficiency of 30% for 19 mm diameter.

5.5 Effect of Chosen Variables on Reinforcement Corrosion

The variables in this study include: the diameter of main longitudinal bars, D, the cross-section, $h \times h$, the periods of accelerated corrosion, T and eccentricity for eccentric loading, e.

In laboratory or field tests of corroded members, the value of I_{corr} is determined through Galvanostatic or Potentiostatic measurement. This value is considered as the key parameter of corrosion activity. Therefore, I_{corr} as calculated from gravimetric analysis is taken as the important value of corrosion current density for all computations.

It is noted from Eq. (5.10) that the weight loss of a bar is directly proportional to the product $I_{corr}T$. This implies that a higher corrosion current density, I_{corr} for a lesser period of corrosion would be as damaging as a lesser value of I_{corr} for a longer corrosion period in terms of metal loss of a corroding bar. The product $I_{corr}T$ was termed as 'corrosion activity index' by Azad et al. (2007).

The values of $I_{corr}T$ and corresponding percentage weight loss, X_p of all specimens are presented in Tables 5.10 and 5.11. These values are plotted in Figure 5.5 to show the effect of $I_{corr}T$ on X_p.

Table 5.10: $I_{corr}T$ versus X_p data for specimens with 18 mm diameter bars.

Specimen	T (day)	%Weight Loss (X_p) (Gravimetric)	I_{corr} (mA/cm^2)	$I_{corr}T$ (mA-days/cm^2)
C1-18-7d	7	6.29	1.22	8.53
C1-18-10d	10	10.49	1.41	14.10
C1-18-13d	13	18.09	1.88	24.44
BC1-18-30-7d	7	6.76	1.31	9.15
BC1-18-30-10d	10	12.36	1.65	16.52
BC1-18-30-12d	11.5	14.13	1.66	19.05
BC1-18-60-7d	7	7.86	1.52	10.63
BC1-18-60-10d	10	12.93	1.74	17.36
BC1-18-60-13d	13	15.92	1.65	21.49
BC1-18-95-7d	7	7.75	1.49	10.46
BC1-18-95-10d	10	10.96	1.49	14.85
BC1-18-95-11d	10.5	12.34	1.60	16.83
C2-18-7d	7	6.57	1.27	8.91
C2-18-10d	10	11.52	1.55	15.52
C2-18-13d	13	16.68	1.73	22.55
BC2-18-35-6d	6	5.86	1.33	7.95
BC2-18-35-8d	8	9.52	1.60	12.81
BC2-18-35-9d	9	11.42	1.71	15.43
BC2-18-65-4d	4	4.96	1.68	6.71
BC2-18-65-7d	7	6.32	1.22	8.52
BC2-18-65-10d	10	11.96	1.63	16.31
BC2-18-115-7d	7	6.35	1.22	8.54
BC2-18-115-8d	8	8.42	1.43	11.42
BC2-18-115-9d	9	11.47	1.73	15.58

Table 5.11: $I_{corr}T$ versus X_p data for specimens with 20 mm diameter bars.

Specimen	T (day)	%Weight Loss (X_p) (Gravimetric)	I_{corr} (mA/cm^2)	$I_{corr}T$ (mA-days/cm^2)
C1-20-7d	7	9.74	2.12	14.85
C1-20-10d	10	11.82	1.81	18.12
C1-20-13d	13	15.18	1.78	23.15
BC1-20-30-7d	7	9.44	2.06	14.41
BC1-20-30-6d	6	7.98	1.93	11.61
BC1-20-30-13d	13	14.22	1.68	21.78
BC1-20-60-7d	7	8.48	1.86	12.99
BC1-20-60-10d	10	12.27	1.87	18.70
BC1-20-60-13d	13	15.88	1.88	24.44
BC1-20-95-7d	7	9.03	1.97	13.80
BC1-20-95-10d	10	12.05	1.84	18.40
BC1-20-95-13d	13	14.75	1.75	22.71
C2-20-7d	7	8.71	1.90	13.32
C2-20-8d	8	9.47	1.80	14.44
C2-20-10d	9.5	10.81	1.73	16.44
BC2-20-35-7d	7	8.60	1.87	13.10
BC2-20-35-6d	6	7.06	1.80	10.79
BC2-20-35-9d	9	10.55	1.79	16.12
BC2-20-65-7d	7	9.02	1.99	13.90
BC2-20-65-6d	6	7.51	1.92	11.51
BC2-20-65-9d	9	11.03	1.87	16.85
BC2-20-115-7d	7	9.97	2.18	15.24
BC2-20-115-6d	5.5	6.56	1.86	10.20
BC2-20-115-9d	9	10.96	1.86	16.74

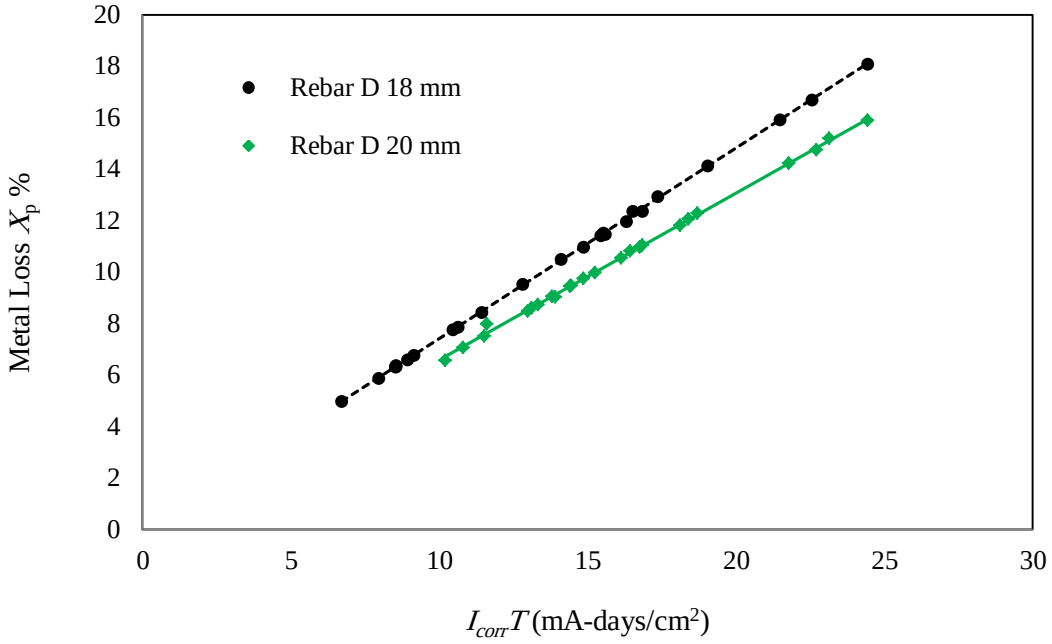

Figure 5.5: Percentage metal loss X_p versus $I_{corr}T$.

Figure 5.5, confirms the linear relationship between $I_{corr}T$ and X_p. For the same value of $I_{corr}T$, it is noted that X_p is higher for 18 mm diameter bars than for 20 mm diameter bars. Similar observations were reported by Azher (2005) and Al-Gohi (2008). Banic et al. (2008) stated bars with smaller diameter achieve equal negative electrochemical potentials faster than bars with large diameter. Therefore, the small diameter rebar corrodes faster than the large diameter rebar in an equally aggressive environment in concrete.

5.6 Effect of Corrosion on the Strength of Specimens

To show the effect of the degrees of corrosion (% weight loss X_p) and the corrosion activity index' ($I_{corr}T$) on the residual strength of corroded columns and beam-columns, the values of the percentage of residual strength of the corroded specimens R_f and the corresponding $I_{corr}T$ and X_p for all corroded specimens are gathered collectively in Tables 5.12 and 5.13. In addition, the data in Tables 5.12 and 5.13 is used to plot $I_{corr}T$ versus R_f in Figures 5.6 and 5.7 to study the effect of $I_{corr}T$ on R_f with changing eccentricity e. In general, it can be observed that the beam-column with higher eccentricity has greater value of R_f than beam-column with lower eccentricity. The test results also reveal an important observation. The reduction in strength, as reflected by R_f, is much higher for columns than for beam-columns for similar $I_{corr}T$. This is however, not unexpected, as the strength of a pure column depends to a large extent on the strength of the concrete section. Any damage to the concrete cover reduces the effective concrete strength area and hence diminishes the axial load capacity. For a beam-column with an appreciable

value of *e*, the concrete cover on the tension side is not so critical like a column. The strength reduction is therefore much lesser than those for columns (Figures 5.6 and 5.7). As seen from Tables 5.12 and 5.13, the column had R_f in the range of 25-45% for different $I_{corr}T$ values. For similar $I_{corr}T$ values, bam-columns had R_f values exceeding 50%, depending up *e*-values.

Table 5.12: Effect of percentage weight loss on load carrying capacity of specimens with 18 mm diameter bars.

Specimen	*e* (mm)	%Weight Loss (X_p)	$I_{corr}T$ (mA-days/cm^2)	Failure Load, (kN)		$R_f = P_{exc} / P_{exu}$ ×100
				P_{exc}	P_{exu}	
C1-18-7d	0	6.29	8.53	515	1272	40
C1-18-10d	0	10.49	14.10	480	1272	38
C1-18-13d	0	18.09	24.44	390	1272	31
BC1-18-30-7d	30	6.76	9.15	561	675	83
BC1-18-30-10d	30	12.36	16.52	472	675	70
BC1-18-30-12d	30	14.13	19.05	348	675	52
BC1-18-60-7d	60	7.86	10.63	386	453	85
BC1-18-60-10d	60	12.93	17.36	300	453	66
BC1-18-60-13d	60	15.92	21.49	252	453	56
BC1-18-95-7d	95	7.75	10.46	236	260	91
BC1-18-95-10d	95	10.96	14.85	214	260	82
BC1-18-95-11d	95	12.34	16.83	177	260	68
C2-18-7d	0	6.57	8.91	700	1605	44
C2-18-10d	0	11.52	15.52	665	1605	41
C2-18-13d	0	16.68	22.55	550	1605	34
BC2-18-35-6d	35	5.86	7.95	667	940	71
BC2-18-35-8d	35	9.52	12.81	589	940	63
BC2-18-35-9d	35	11.42	15.43	575	940	61
BC2-18-65-4d	65	4.96	6.71	548	595	92
BC2-18-65-7d	65	6.32	8.52	482	595	81
BC2-18-65-10d	65	11.96	16.31	442	595	74
BC2-18-115-7d	115	6.35	8.54	278	350	79
BC2-18-115-8d	115	8.42	11.42	256	350	73
BC2-18-115-9d	115	11.47	15.58	246	350	70

Table 5.13: Effect of percentage weight loss on load carrying capacity of specimens with 20mm diameter bars.

Specimen	e (mm)	%Weight Loss (X_p)	$I_{corr}T$ (mA-days/cm^2)	Failure Load, (kN)		$R_f = P_{exc} / P_{exu}$ ×100
				P_{exc}	P_{exu}	
C1-20-7d	0	9.74	14.85	456	1350	34
C1-20-10d	0	11.82	18.12	375	1350	28
C1-20-13d	0	15.18	23.15	330	1350	24
BC1-20-30-7d	30	9.44	14.41	475	690	69
BC1-20-30-6d	30	7.98	11.61	495	690	72
BC1-20-30-13d	30	14.22	21.78	384	690	56
BC1-20-60-7d	60	8.48	12.99	431	460	94
BC1-20-60-10d	60	12.27	18.70	284	460	62
BC1-20-60-13d	60	15.88	24.44	258	460	56
BC1-20-95-7d	95	9.03	13.80	209	271	77
BC1-20-95-10d	95	12.05	18.40	197	271	73
BC1-20-95-13d	95	14.75	22.71	168	271	62
C2-20-7d	0	8.71	13.32	670	1780	38
C2-20-8d	0	9.47	14.44	620	1780	35
C2-20-10d	0	10.81	16.44	580	1780	33
BC2-20-35-7d	35	8.60	13.10	631	962	66
BC2-20-35-6d	35	7.06	10.79	731	962	76
BC2-20-35-9d	35	10.55	16.12	582	962	60
BC2-20-65-7d	65	9.02	13.90	497	645	77
BC2-20-65-6d	65	7.51	11.51	519	645	80
BC2-20-65-9d	65	11.03	16.85	460	645	71
BC2-20-115-7d	115	9.97	15.24	301	419	72
BC2-20-115-6d	115	6.56	10.20	336	419	80
BC2-20-115-9d	115	10.96	16.74	280	419	67

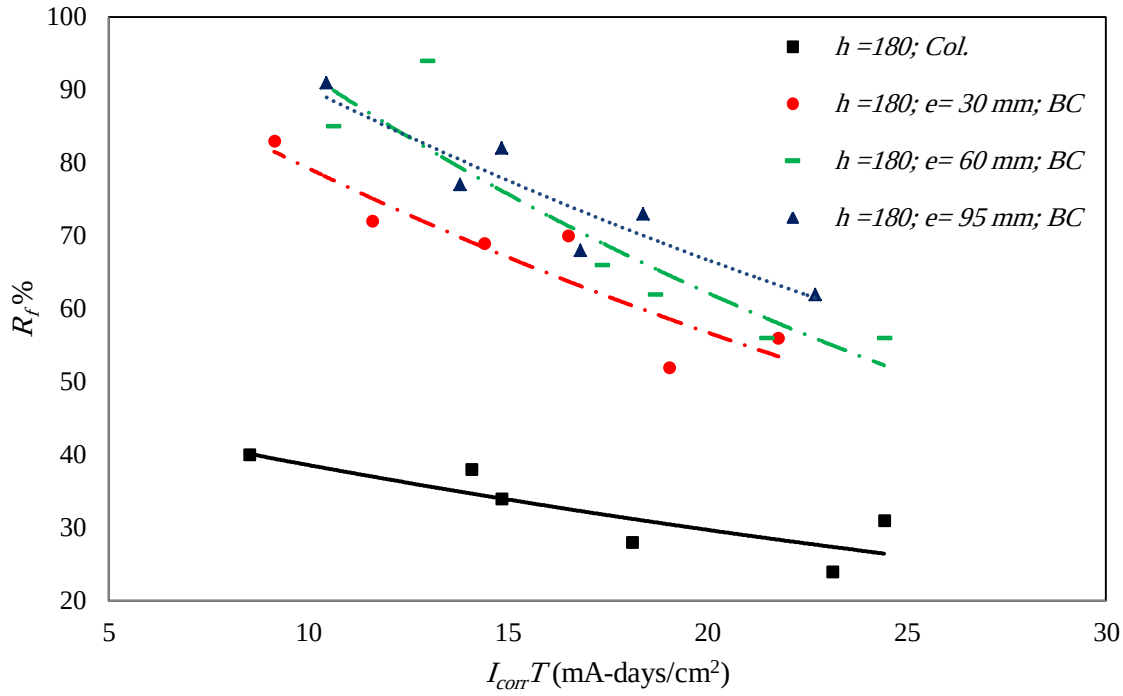

Figure 5.6: Variation of R_f % with $I_{corr}T$ and e for cross-section (180 x1800 mm).

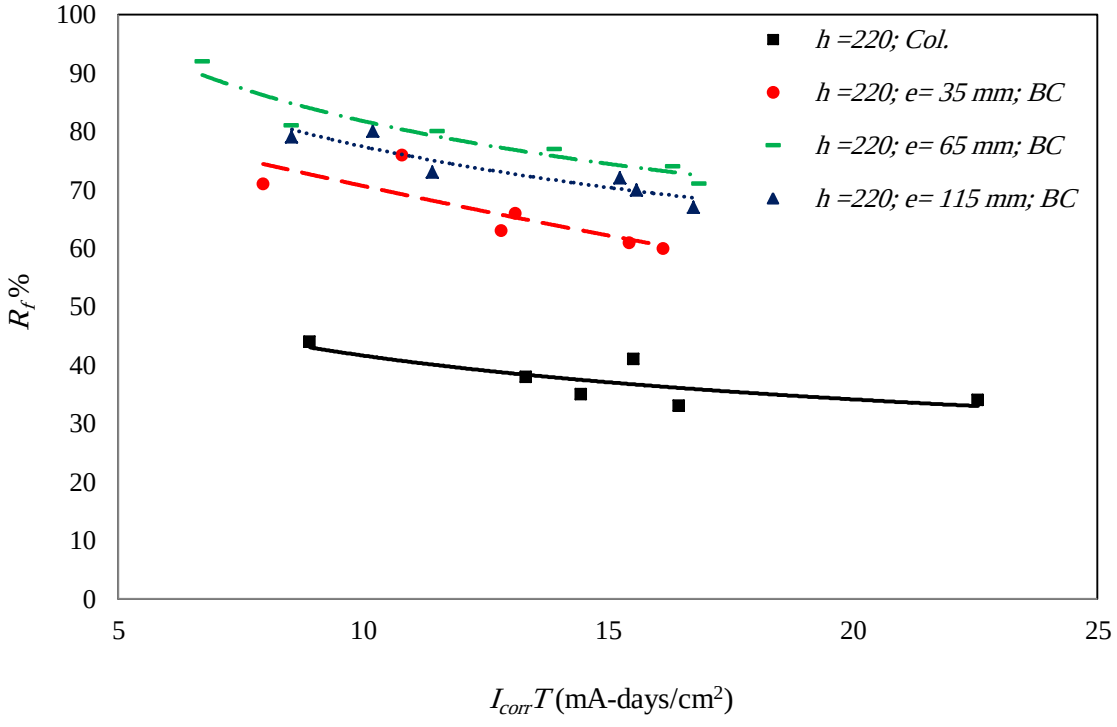

Figure 5.7: Variation of R_f % with $I_{corr}T$ and e for cross-section (220 x220 mm).

5.7 Interaction Diagrams for Corroded and Un-Corroded Specimens

The failure axial compressive force, P_n and corresponding bending moment, M_n for both corroded and un-corroded specimen can generally be related to each other by means of an interaction diagram (*P-M* interaction diagram), which represents the actual resisting capacity of a specimen, under combined P_n and M_n. The data for three values of eccentricity were used to plot the trend of an interaction diagram.

5.7.1 Comparison of Interaction Diagram of Corroded and Un-Corroded Specimens

For the corroded specimens, an ideal interaction plot of *M-P* requires that $I_{corr}T$ should approximately be a constant for all specimens considered in a plot so that the corrosion damage, represented by $I_{corr}T$, is similar. However, that is not the case for the test specimens, as each corroded specimens had slightly different $I_{corr}T$. For the purpose of plotting *M-P* diagram as illustrations, Tables 5.14 and 5.15 are constructed from Tables 5.12 and 5.13 using specimens having similar $I_{corr}T$. The plots of the interaction diagrams for un-corroded and corroded specimens are shown in Figures 5.8 to 5.11. Average $I_{corr}T$ for specimens is 9.7 mA-day/cm^2, 8.5 mA-day/cm^2, 23 mA-day/cm^2 and 14.2 mA-day/cm^{2}for Figures 5.8 to 5.11, respectively. The solid plots represent the strength of the theoretical un-corroded members obtained from mechanics. It was observed that the theoretical values were mostly higher than the experimental value by about 10% to 16% of the experimental values. This perhaps explains the higher strength reduction factors that are normally used in columns and beam-columns.

As expected, corrosion decreases the envelope of safe area for the interaction diagram of the column. The results showed that the corroded columns and beam-columns with lower eccentricity have greater reduction in failure load than beam-column with higher eccentricity. This is shown by the *e/h* lines in Figures 5.8 to 5.11and explained earlier.

Table 5.14: Failure load of corroded specimens with similar $I_{corr}T$ (18mm dia. bars).

Specimen	e (mm)	%Weight Loss (X_p)	$I_{corr}T$ (mA-days/cm^2)	Experimental Failure Load, (kN)		P_{thu} (kN)
				P_{exc}	P_{exu}	
C1-18-7d	0	6.29	8.53	515	1272	1414
BC1-18-30-7d	30	6.76	9.15	561	675	746
BC1-18-60-7d	60	7.86	10.63	386	453	414
BC1-18-95-7d	95	7.75	10.46	236	260	262
Average $I_{corr}T$ (mA-days/cm^2)			9.7			
C2-18-7d	0	6.57	8.91	700	1605	1769
BC2-18-35-6d	35	5.86	7.95	667	940	1068
BC2-18-65-7d	65	6.32	8.52	482	595	693
BC2-18-115-7d	115	6.35	8.54	278	350	405
Average $I_{corr}T$ (mA-days/cm^2)			8.5			

Table 5.15: Failure load of corroded specimens with similar $I_{corr}T$ (20mm dia. bars).

Specimen	e (mm)	%Weight Loss (X_p)	$I_{corr}T$ (mA-days/cm^2)	Experimental Failure Load, (kN)		P_{thu} (kN)
				P_{exc}	P_{exu}	
C1-20-13d	0	15.18	23.15	330	1350	1539
BC1-20-30-13d	30	14.22	21.78	384	690	782
BC1-20-60-13d	60	15.88	24.44	258	460	434
BC1-20-95-13d	95	14.75	22.71	168	271	277
Average $I_{corr}T$ (mA-days/cm^2)			23			
C2-20-8d	0	9.47	14.44	620	1780	1894
BC2-20-35-7d	35	8.6	13.1	631	962	1122
BC2-20-65-7d	65	9.02	13.9	497	645	730
BC2-20-115-7d	115	9.97	15.24	301	419	433
Average $I_{corr}T$ (mA-days/cm^2)			14.2			

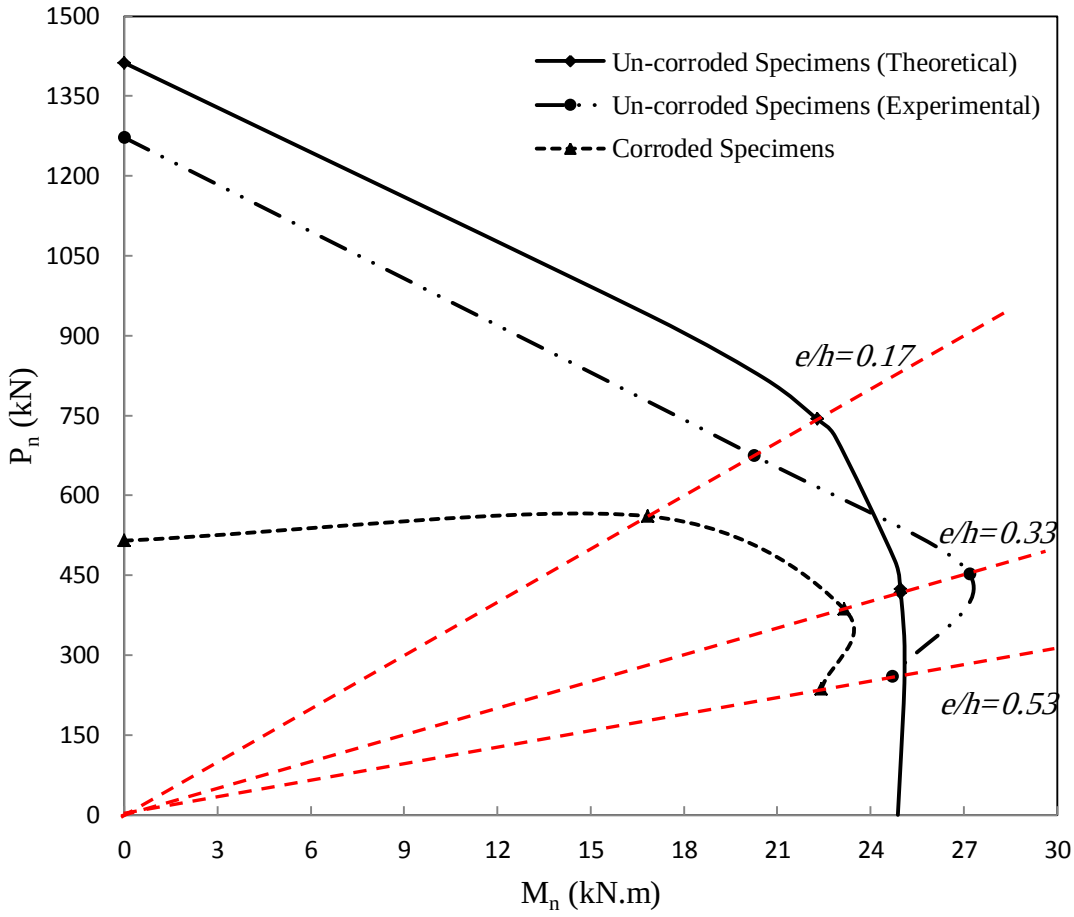

Figure 5.8: Interaction diagram for failure load of specimens (cross-section 180 x 180 mm) with 18 mm diameter bars and average value of $I_{corr}T$ (9.7 mA-day/cm^2).

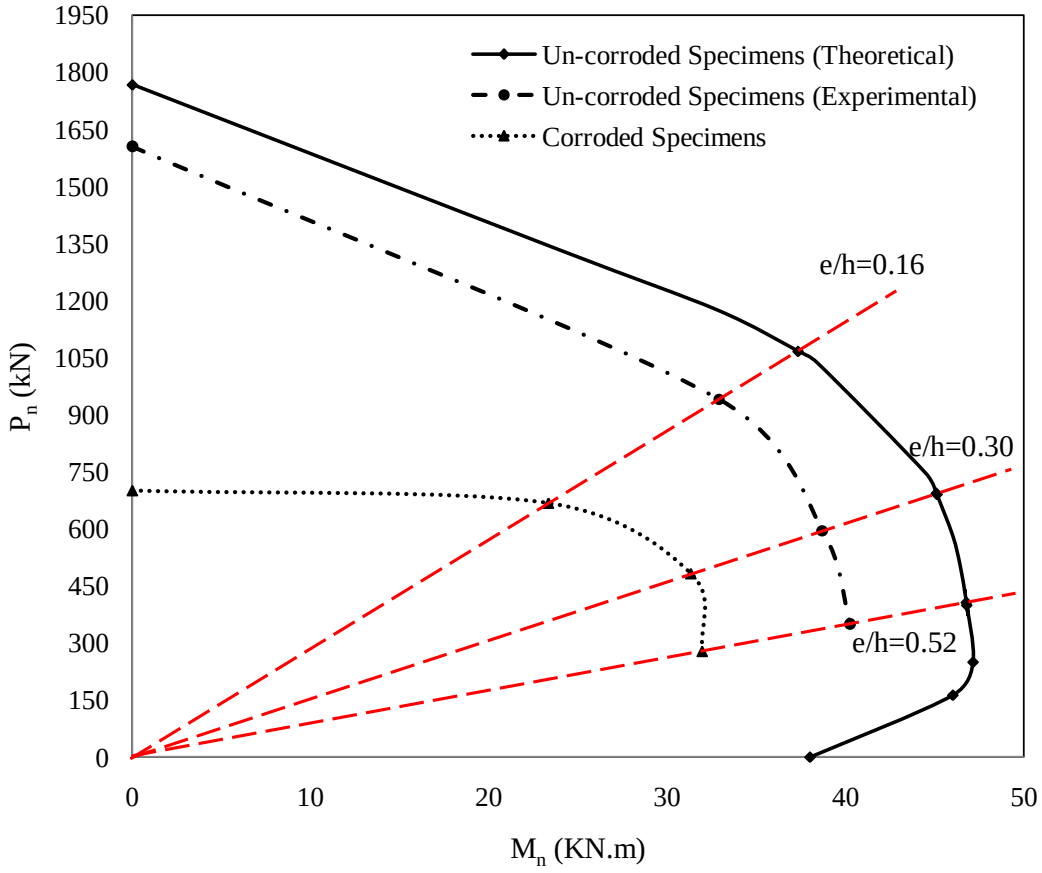

Figure 5.9: Interaction diagram for failure load of specimens (cross-section 220 x 220 mm) with 18 mm diameter bars and average value of $I_{corr}T$ (8.5 mA-day/cm^2).

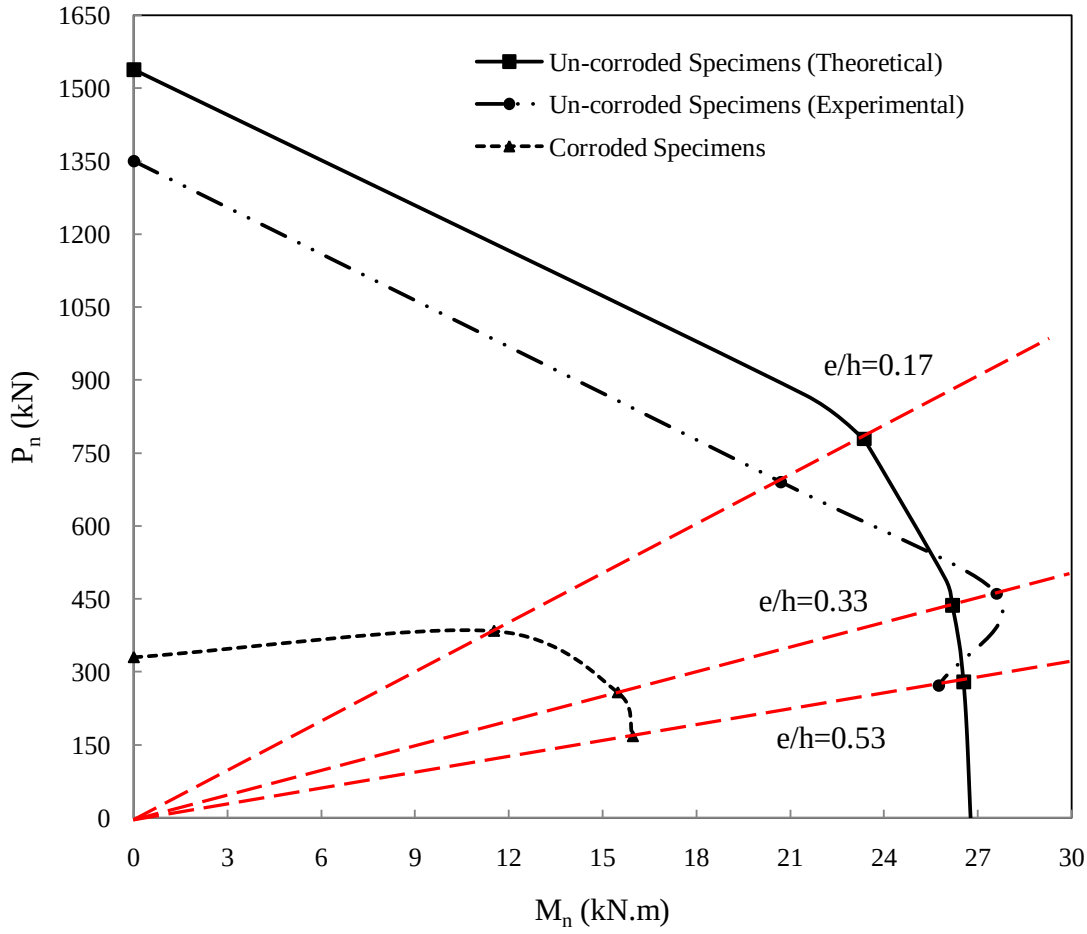

Figure 5.10: Interaction diagram for failure load of specimens (cross-section 180 x 180 mm) with 20 mm diameter bars and average value of $I_{corr}T$ (23 mA-day/cm^2).

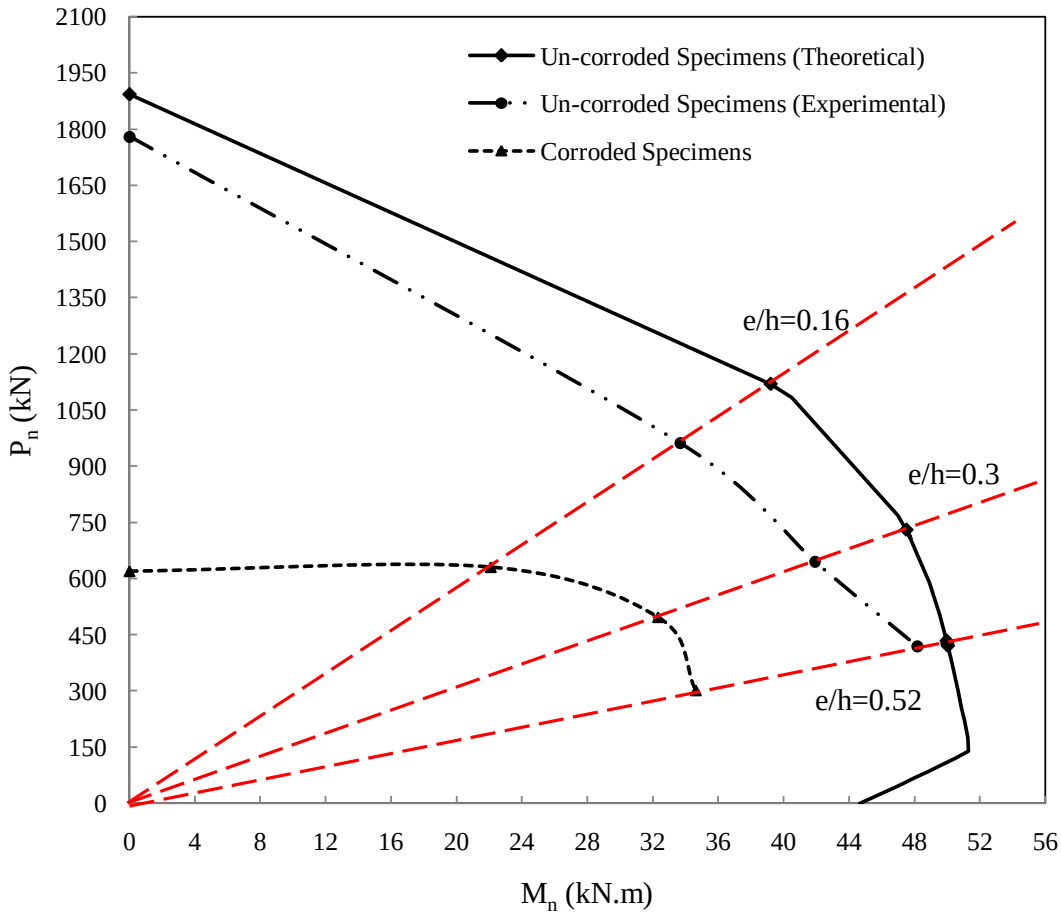

Figure 5.11: Interaction diagram for failure load of specimens (cross-section 220 x 220 mm) with 20 mm diameter bars and average value of $I_{corr}T$ (14.2 mA-day/cm^2).

5.8 Results for FE Analysis and Comparison with Experimental Values

5.8.1 Member Strength

The proposed FE model using the input material properties was used to analyze all test specimens corroded and un-corroded and to determine the load-carrying capacities. These theoretically predicted values were compared with the experimentally determined load capacities to examine the validity of the proposed FE models.

(a) Control (Un-Corroded) Specimens

The predicted failure loads, P_{feu} obtained from the finite element model using ANSYS for the control (un-corroded) columns and beam-columns are listed in Table 5.16. The ratio between the experimental P_{exu} and predicted failure load P_{feu} of the control specimens, C_f are illustrated in it. Table 5.16 shows that there is a small difference between the finite element and experimental capacities of the un-corroded member. The ranges of C_f in Table 5.16 are 83 % to 106 % demonstrate that the predicted capacities of the columns and beam-columns using ANSYS software were reasonably closer to the experimental values. The theoretical load capacities P_{thu} of the control (un-corroded) specimens were compared with predicted failure load P_{feu} and experimental failure load P_{exu} by means of interaction diagrams as shown in Figures 5.12 to 5.15. The solid plots in these figures represent the theoretical failure load P_{thu} of the un-corroded specimens obtained from mechanics. It can be seen that the theoretical values are almost matching to the predicted failure load $P_{feu.}$

This indicates that ANSYS model predicted the capacities of un-corroded specimens with

reasonable accuracy. Figures 5.15 and 5.16 show the crunching of concrete and principle stresses for the un-corroded column (C1-18), respectively.

Table 5.16: Values of P_{exu}, P_{feu} and P_{thu} for un-corroded columns and beam-columns.

Specimen	Eccentricity, e (mm)	f_c' (MPa)	Failure Load, (kN)			$C_f = P_{exu} / P_{feu}$ (%)
			P_{exu}	P_{thu}	P_{feu}	
C1-18	0	32	1272	1414	1426	89
BC1-18-30	30	32	675	746	757	89
BC1-18-60	60	32	453	414	428	106
BC1-18-95	95	32	260	262	266	98
C2-18	0	30	1605	1769	1773	91
BC2-18-35	35	30	940	1068	1026	92
BC2-18-65	65	30	595	693	697	85
BC2-18-115	115	30	350	405	420	83
C1-20	0	32	1350	1539	1498	90
BC1-20-30	30	32	690	782	799	86
BC1-20-60	60	32	460	434	436	106
BC1-20-95	95	32	271	277	272	100
C2-20	0	30	1780	1894	1881	95
BC2-20-35	35	30	962	1122	1118	86
BC2-20-65	65	30	645	730	756	85
BC2-20-115	115	30	419	433	440	95

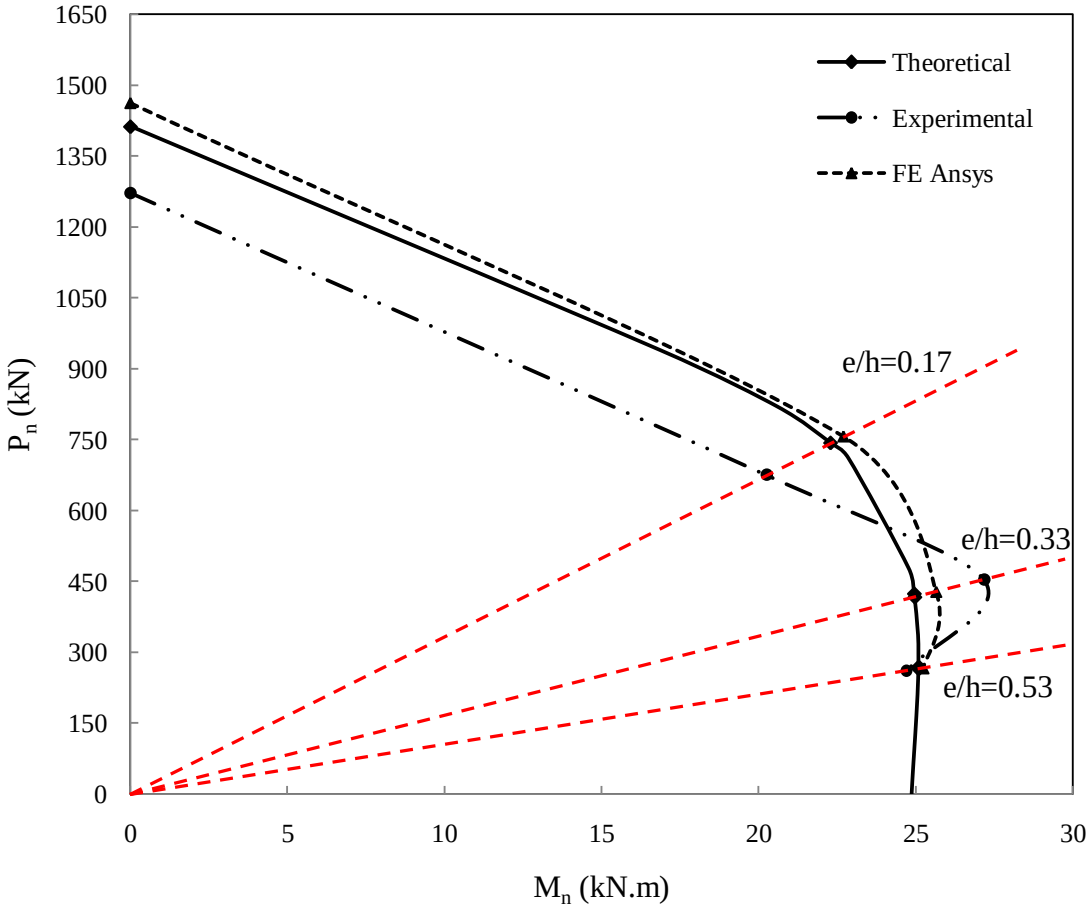

Figure 5.12: Interaction diagram for failure load of controlled (un-corroded) specimens (cross-section 180 x 180 mm) with 18 mm diameter bars.

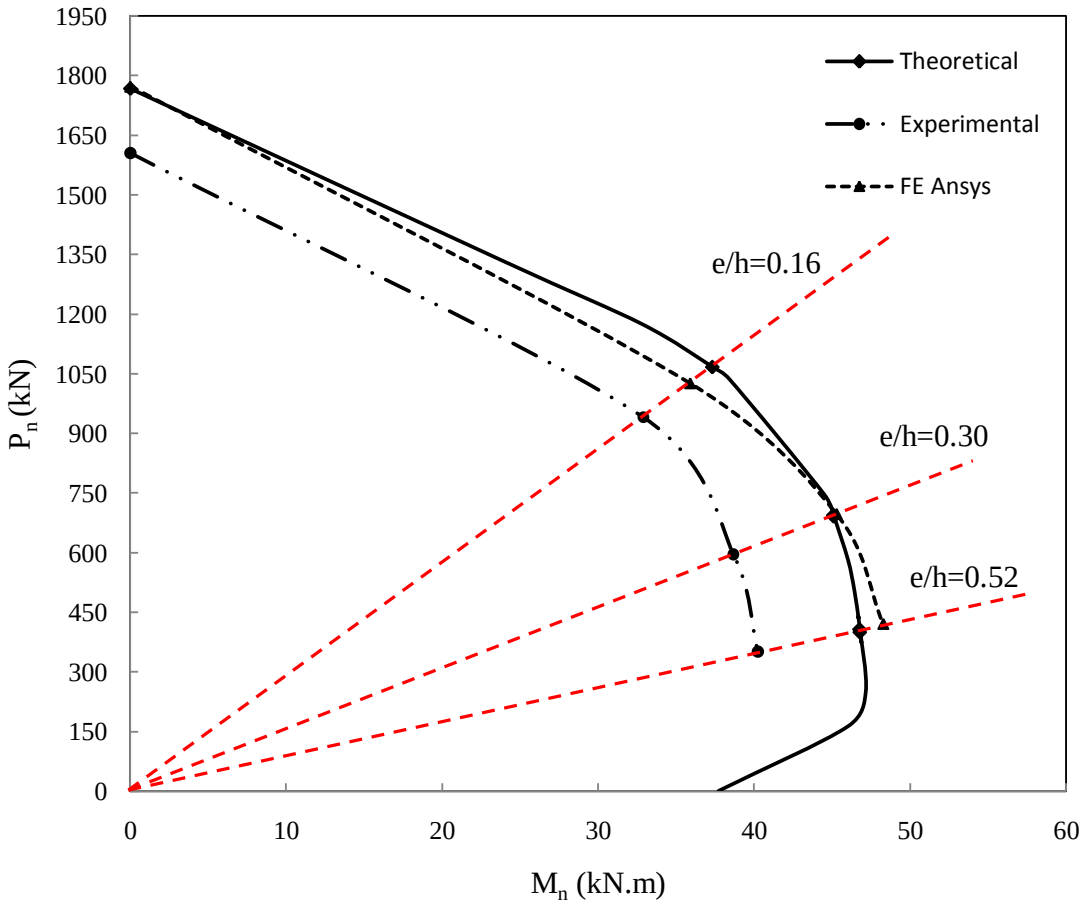

Figure 5.13: Interaction diagram for failure load of controlled (un-corroded) specimens (cross-section 220 x 220 mm) with 18 mm diameter bars.

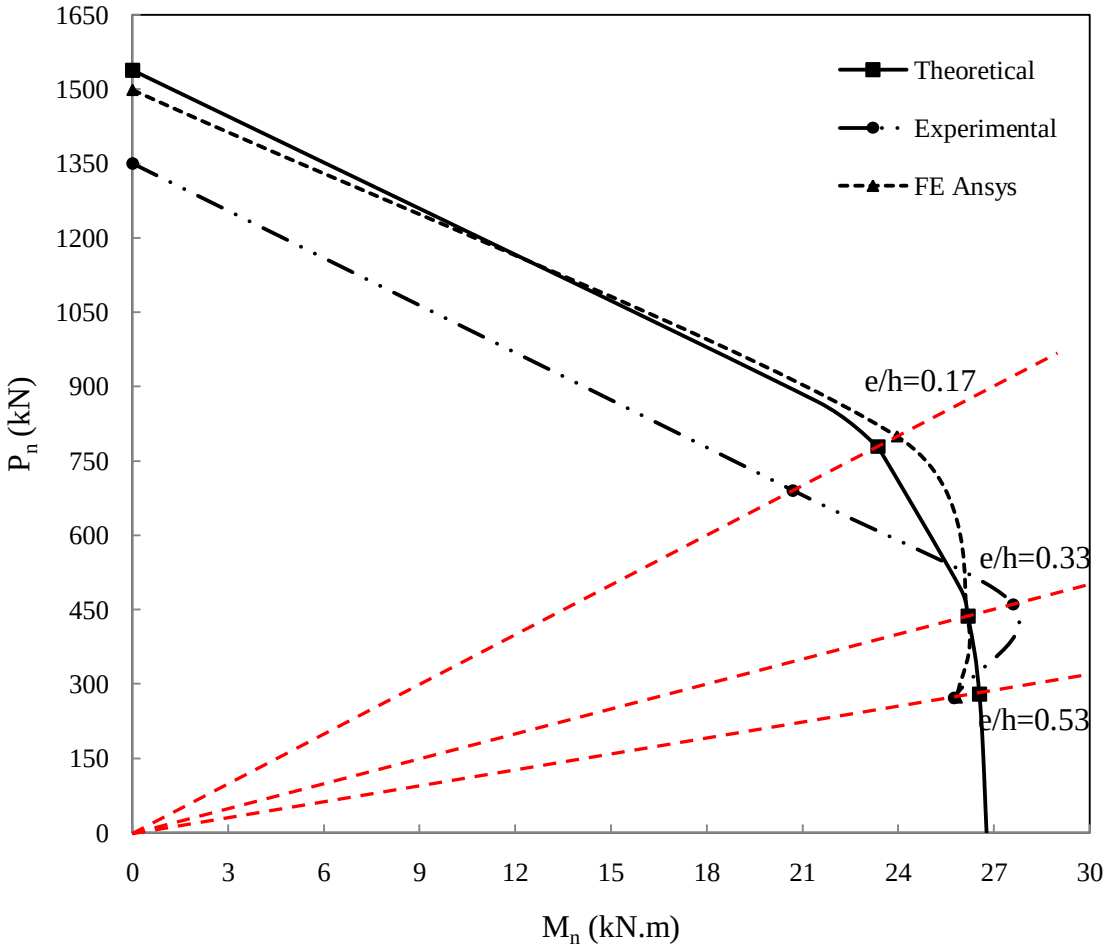

Figure 5.14: Interaction diagram for failure load of controlled (un-corroded) specimens (cross-section 180 x 180 mm) with 20 mm diameter bars.

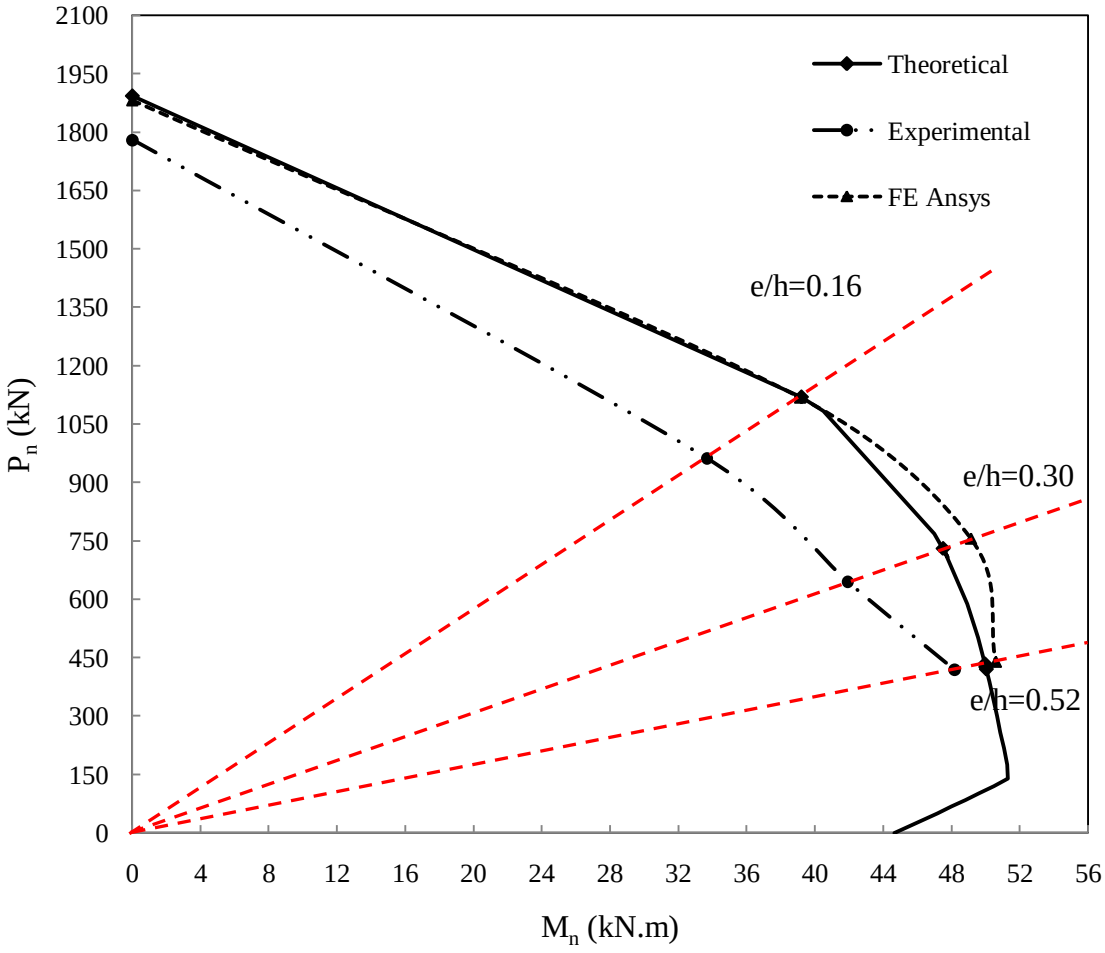

Figure 5.15: Interaction diagram for failure load of controlled (un-corroded) specimens (cross-section 220 x 220 mm) with 20 mm diameter bars.

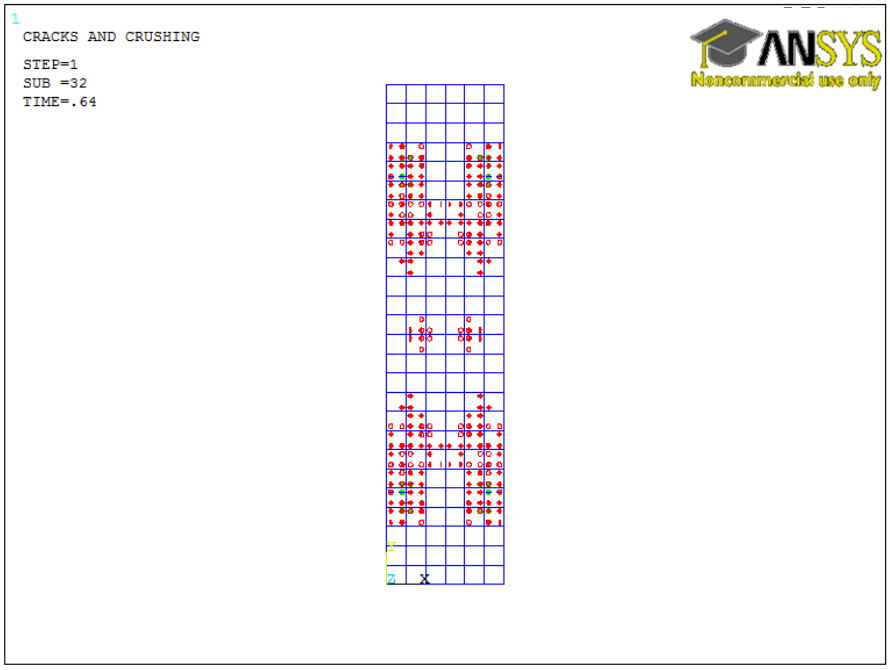

Figure 5.16: Cracking at 1024 kN for controlled specimen C1-18.

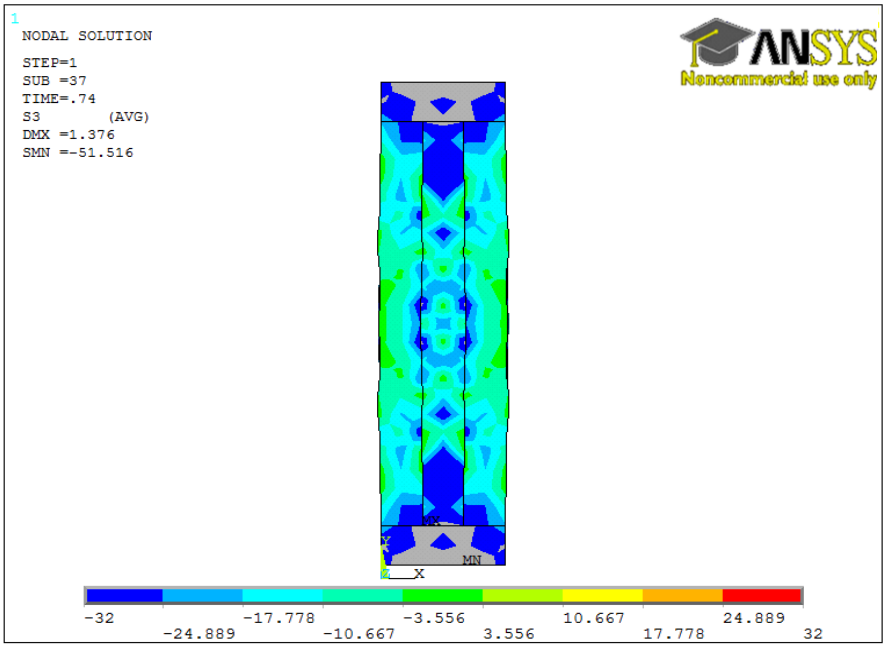

Figure 5.17: Principle stress for controlled specimen C1-18.

(b) Corroded Specimens

Since cracking in concrete due to corrosion is random, the modeling of the corroded member is quite difficult. The predicted failure loads of the corroded columns and beam-columns using FE analysis were obtained by changing the material properties and real constants of the un-corroded one for different degrees of corrosion damage.

The real constants for un-corroded specimens were modified to reflect the damage due to corrosion as follows:

- The steel cross-sectional area of longitudinal rebars and ties was reduced by using Eq. (4.17).
- The bond between concrete and steel which represented by the input data of COMBIN39 was modified by using Eq. (4.16).

The material properties for corroded specimens were determined by adjusting the material properties of the un-corroded specimens by factors based on the degree of corrosion as given below:

- The yield strength of steel and its modulus of elasticity were reduced by using Eqs. (4.31a) and (4.31b), respectively.
- The effect of corrosion damage on concrete is assumed to be confined within the concrete cover and no damage occurs on the core of the concrete. Therefore, a reduction in the strength of the concrete was applied to concrete cover only by using Eqs. (4.32) and (4.40).

Based on the above concept, the finite element failure load of all corroded specimens, P_{fec}, are obtained and presented in Tables 5.17 and 5.18. The failure load from finite element P_{fec} values was compared with the experimental failure load P_{exc} to note the divergence between the two sets of results. The values of error of experimental failure load P_{exc} and predicted finite element failure load of all corroded specimens multiplied by 100 are calculated and listed in Tables 5.17 and 5.18. The results show that for all corroded columns, about 75% of data is between 3% and -11% and the remaining data of columns above -20%. However, most of corroded beam-columns data is between 10% and -15%. Therefore, it can be concluded that FE can be used to have a reasonable estimate of the residual strength of corroded columns and beam-columns.

Table 5.17: Values of P_{exc} and P_{fec} for corroded specimens and with 18-mm diameter bars.

Specimen	e (mm)	%Weight Loss (X_p)	$I_{corr}T$ (mA-days/cm^2)	Failure Load, (kN)		Error*
				P_{exc}	P_{fec}	
C1-18-7d	0	6.29	8.53	515	527	2
C1-18-10d	0	10.49	14.1	480	372	-23
C1-18-13d	0	18.09	24.44	390	279	-28
BC1-18-30-7d	30	6.76	9.15	561	593	6
BC1-18-30-10d	30	12.36	16.52	472	378	-20
BC1-18-30-12d	30	14.13	19.05	348	331	-5
BC1-18-60-7d	60	7.86	10.63	386	330	-15
BC1-18-60-10d	60	12.93	17.36	300	233	-22
BC1-18-60-13d	60	15.92	21.49	252	208	-17
BC1-18-95-7d	95	7.75	10.46	236	215	-9
BC1-18-95-10d	95	10.96	14.85	214	211	-1
BC1-18-95-11d	95	12.34	16.83	177	164	-7
C2-18-7d	0	6.57	8.91	700	684	-2
C2-18-10d	0	11.52	15.52	665	589	-11
C2-18-13d	0	16.68	22.55	550	437	-21
BC2-18-35-6d	35	5.86	7.95	667	718	8
BC2-18-35-8d	35	9.52	12.81	589	586	-1
BC2-18-35-9d	35	11.42	15.43	575	534	-7
BC2-18-65-4d	65	4.96	6.71	548	527	-4
BC2-18-65-7d	65	6.32	8.52	482	510	6
BC2-18-65-10d	65	11.96	16.31	442	334	-24
BC2-18-115-7d	115	6.35	8.54	278	295	6
BC2-18-115-8d	115	8.42	11.42	256	281	10
BC2-18-115-9d	115	11.47	15.58	246	231	-6

* (100 x (P_{fec}-P_{exc})/P_{exc})

Table 5.18: Values of P_{exc} and P_{fec} for corroded specimens and with 20-mm diameter bars.

Specimen	e (mm)	%Weight Loss (X_p)	$I_{corr}T$ (mA-days/cm^2)	Failure Load, (kN)		Error*
				P_{exc}	P_{fec}	
C1-20-7d	0	9.74	14.85	456	425	-7
C1-20-10d	0	11.82	18.12	375	391	4
C1-20-13d	0	15.18	23.15	330	323	-2
BC1-20-30-7d	30	9.44	14.41	475	418	-12
BC1-20-30-6d	30	7.98	11.61	495	516	4
BC1-20-30-13d	30	14.22	21.78	384	354	-8
BC1-20-60-7d	60	8.48	12.99	431	380	-12
BC1-20-60-10d	60	12.27	18.7	284	276	-3
BC1-20-60-13d	60	15.88	24.44	258	223	-14
BC1-20-95-7d	95	9.03	13.8	209	221	6
BC1-20-95-10d	95	12.05	18.4	197	180	-9
BC1-20-95-13d	95	14.75	22.71	168	161	-4
C2-20-7d	0	8.71	13.32	670	660	-1
C2-20-8d	0	9.47	14.44	620	640	3
C2-20-10d	0	10.81	16.44	580	600	3
BC2-20-35-7d	35	8.6	13.1	631	663	5
BC2-20-35-6d	35	7.06	10.79	731	742	2
BC2-20-35-9d	35	10.55	16.12	582	610	5
BC2-20-65-7d	65	9.02	13.9	497	438	-12
BC2-20-65-6d	65	7.51	11.51	519	468	-10
BC2-20-65-9d	65	11.03	16.85	460	405	-12
BC2-20-115-7d	115	9.97	15.24	301	243	-19
BC2-20-115-6d	115	6.56	10.2	336	260	-23
BC2-20-115-9d	115	10.96	16.74	280	220	-21

* (100 x $(P_{fec}-P_{exc})/P_{exc}$)

5.8.2 Load Deflection Plots

The bond-slip between steel and concrete for corroded members was simulated using a three-dimensional nonlinear spring element as mentioned before (in section 4.5.1). Many researchers have used non-linear spring element (COMBIN39) as bond-slip at the concrete-steel interface for corroded members. Therefore, this element was chosen to simulate the bond between concrete and corroded steel. In finite element model, the 'COMBIN39' non-linear spring elements that have a very small dimension were connected between the steel nodes 'LINK8' and concrete nodes 'SOLID65' as shown in Figure 5.18.The input values of load-deflection of the 'COMBIN39' element were determined based on the model that suggested by the Xiaoming et al. (2012).

In ANSYS, the un-corroded columns and beam-columns were modeled as follows:

- By connecting the steel nodes 'LINK8' and concrete nodes 'SOLID65' without nonlinear spring elements (perfectly bonded to the surrounding concrete).
- Using'COMBIN39' non-linear spring elements as bonding element between steel and concrete interface.

The plots of the load-defection for un-corroded specimens for perfect bond and using non-linear spring element (COMBIN39) are shown in Figures 5.19 and 5.20 to confirm that the element (COMBIN39) worked well as bonding element at the bar-concrete interface. It can be seen that there is a good agreement between the curves of load-deflection for perfect bond and bond using non-linear spring element (COMBIN39).

Furthermore, the results from finite element model were compared with the experimental results to check that the model (material properties, real constants and chosen failure

criteria) are suitable to express the behavior of the un-corroded and corroded specimens. The results obtained by the numerical finite element model for the un-corroded columns and beam-columns (control specimens) are compared with the experimental results as shown in Figures 5.21 to 5.24. Similarly, the experimental and numerical finite element model results for corroded specimens are plotted in Figures 5.25 to 5.27. Figure 5.28 is plotted for the un-corroded and corroded specimens. Figure 5.28 shows that there is degradation in stiffness of the specimens due to corrosion. In general, it is observed from figures that there is a good agreement between the finite element results and experimental results. Therefore, the ANSYS model using the reduction of steel area, modification of the concrete strength due to cracking of concrete, modification of bond-slip properties, the reduction in yield strength of steel and its modulus of elasticity predicted the load-strain for columns and load-deflection for beam-columns quite accurately.

5.8.3 Crack Pattern

A comparison between the cracks pattern from finite element model and experimental observation is shown in Figure 5.29. As seen from Figure, a good agreement is found between the cracks predicted using the finite element model and the experimental observation for flexural cracks and compressive cracks (crushing of concrete).

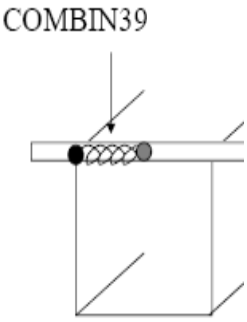

Figure 5.18: Concrete-steel Interface (with gray steel node and black concrete node) (Pozolo A. M., 2010).

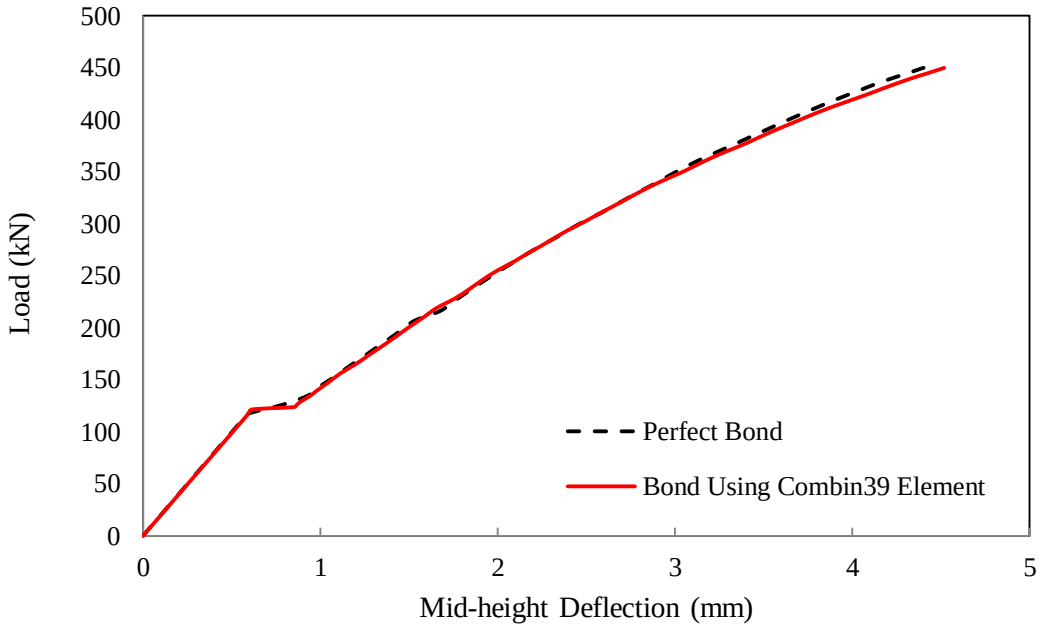

Figure 5.19: Comparison of the load-deflection of the controlled specimen (BC1-20-30) with perfect bond (without spring elements) and with spring element (COMBIN39 element).

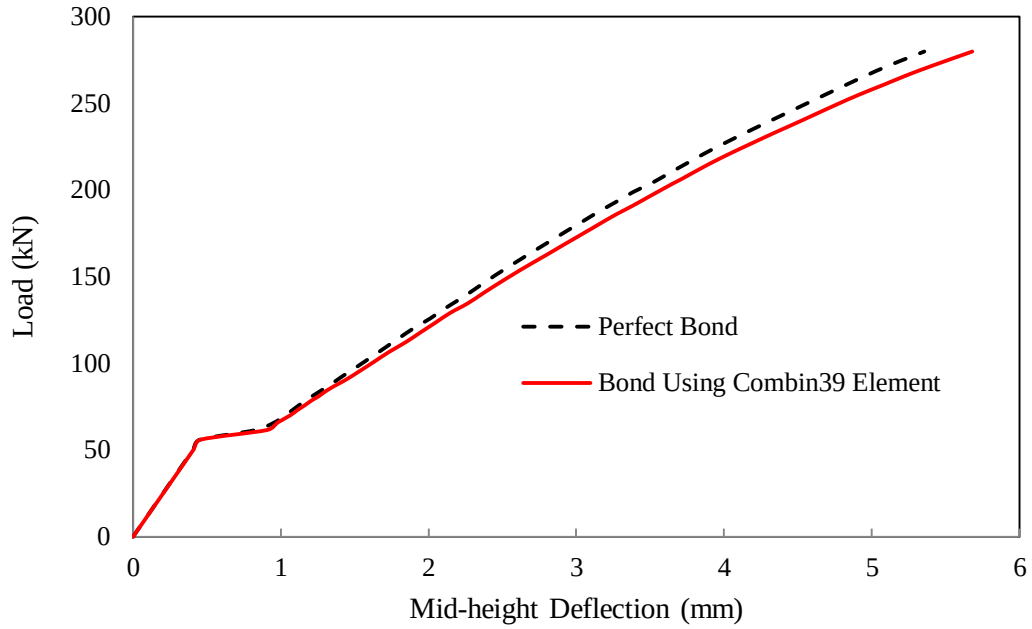

Figure 5.20: Comparison of the load-deflection of the controlled specimen (BC1-20-95) with perfect bond (without spring elements) and with spring element (COMBIN39 element).

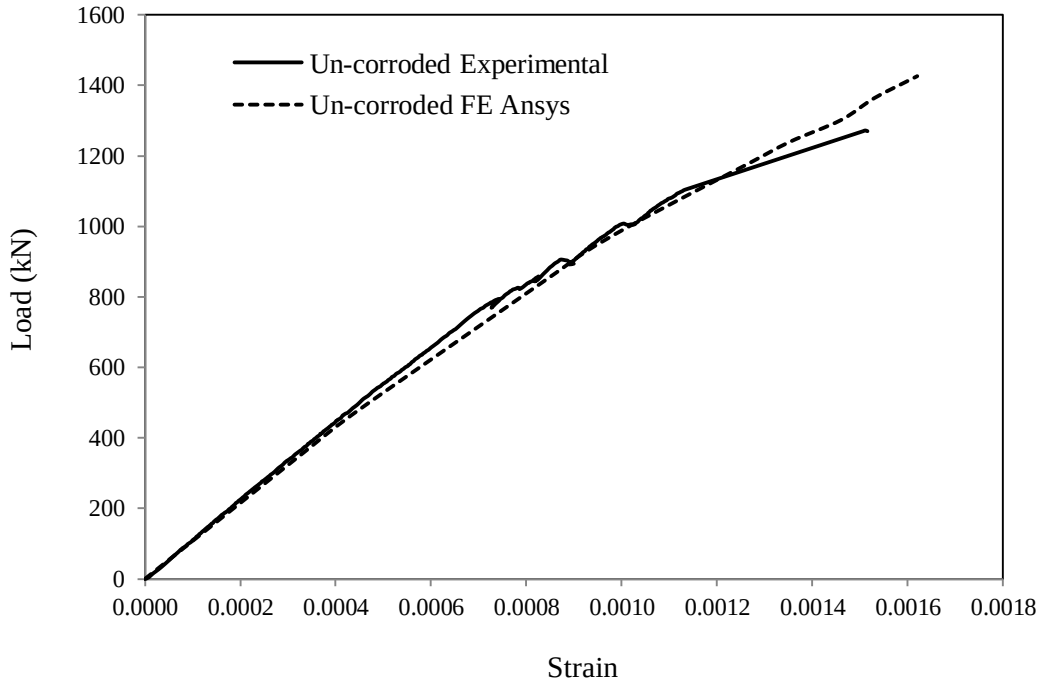

Figure 5.21: Comparison of the load-strain of the controlled specimen C1-18 and finite element.

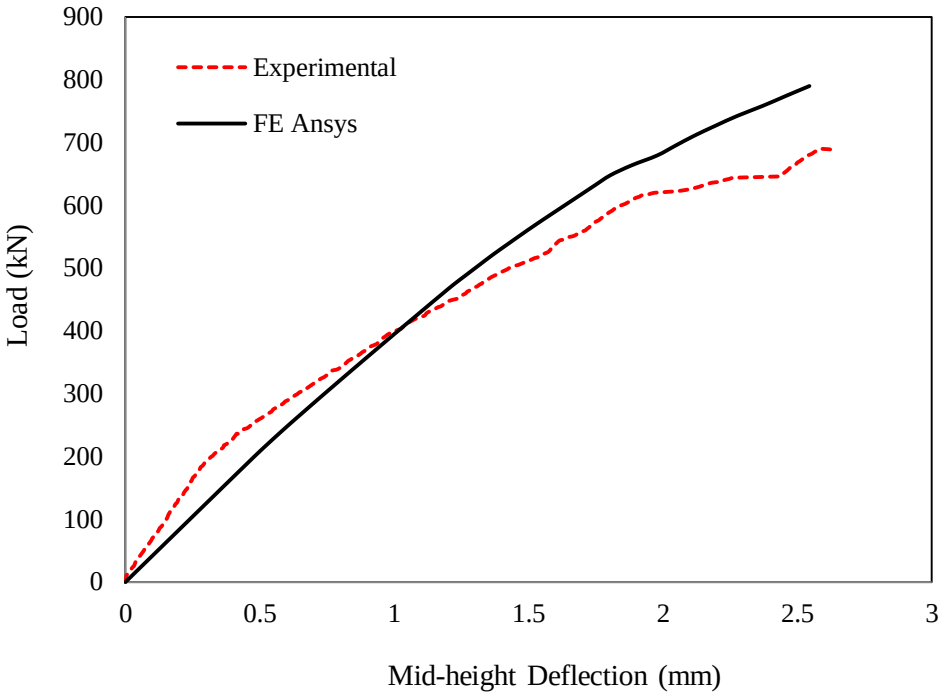

Figure 5.22: Comparison of the load-deflection of the specimen BC1-20-30 and finite element.

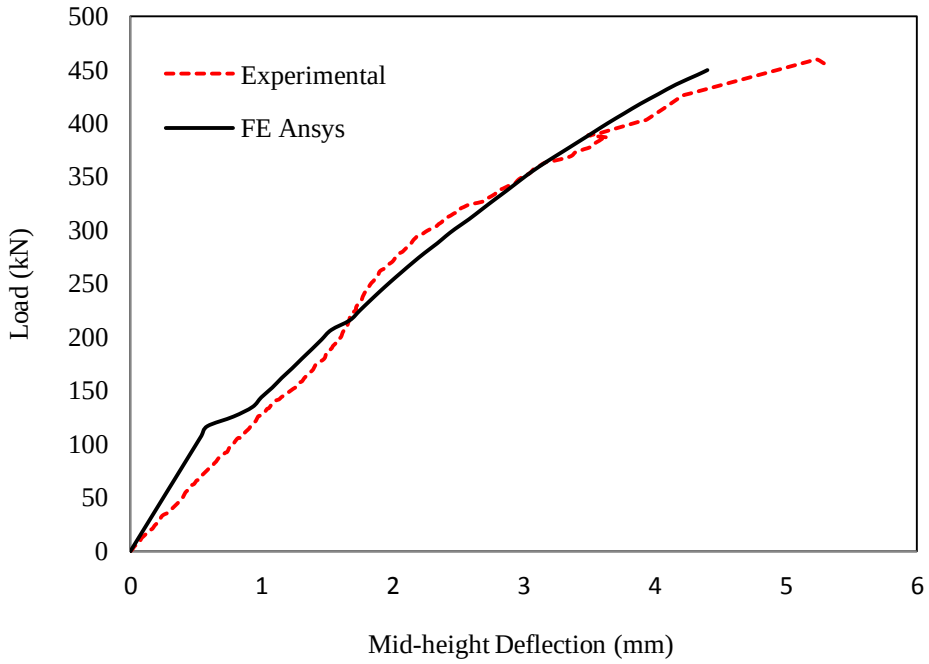

Figure 5.23: Comparison of the load-deflection of the specimen BC1-20-60 and finite element.

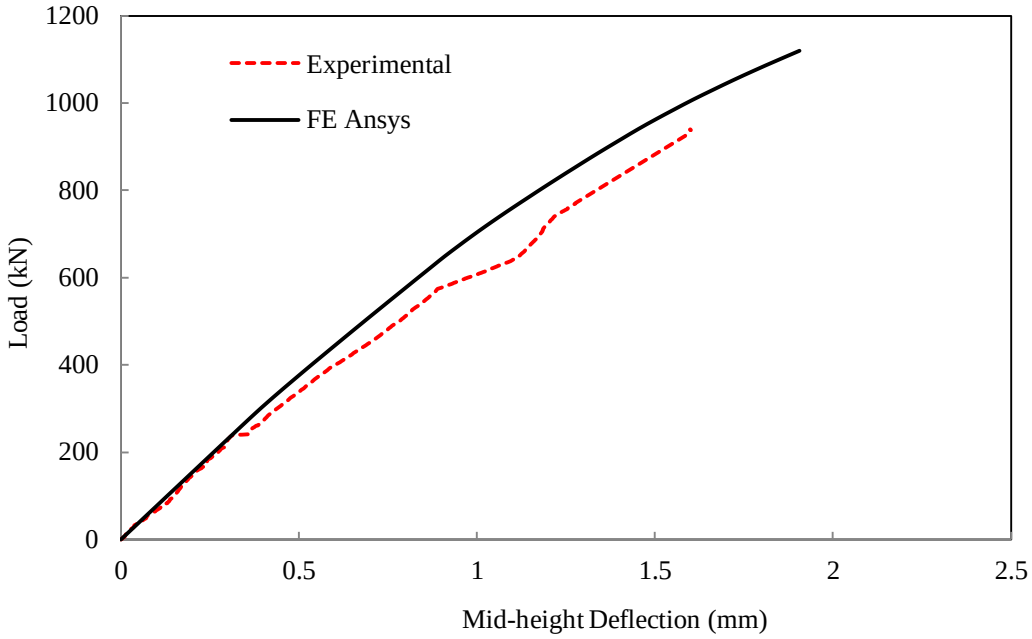

Figure 5.24: Comparison of the load-deflection of the specimen BC2-20-35 and finite element.

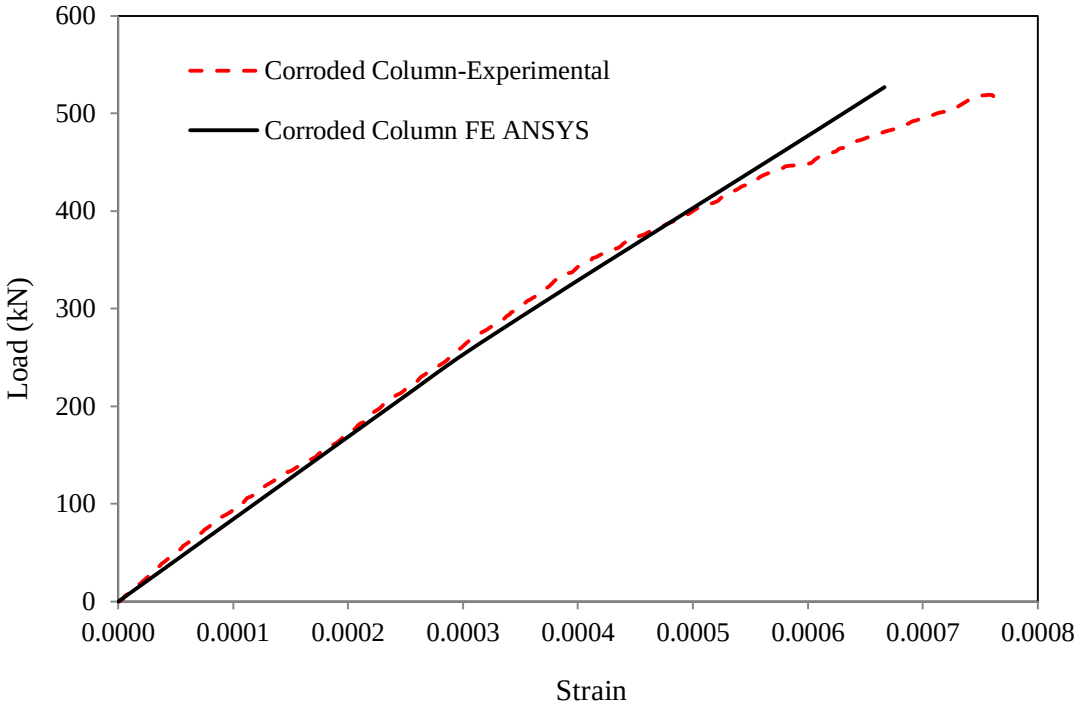

Figure 5.25: Comparison of the load-strain of the specimen C1-18-7d and finite element.

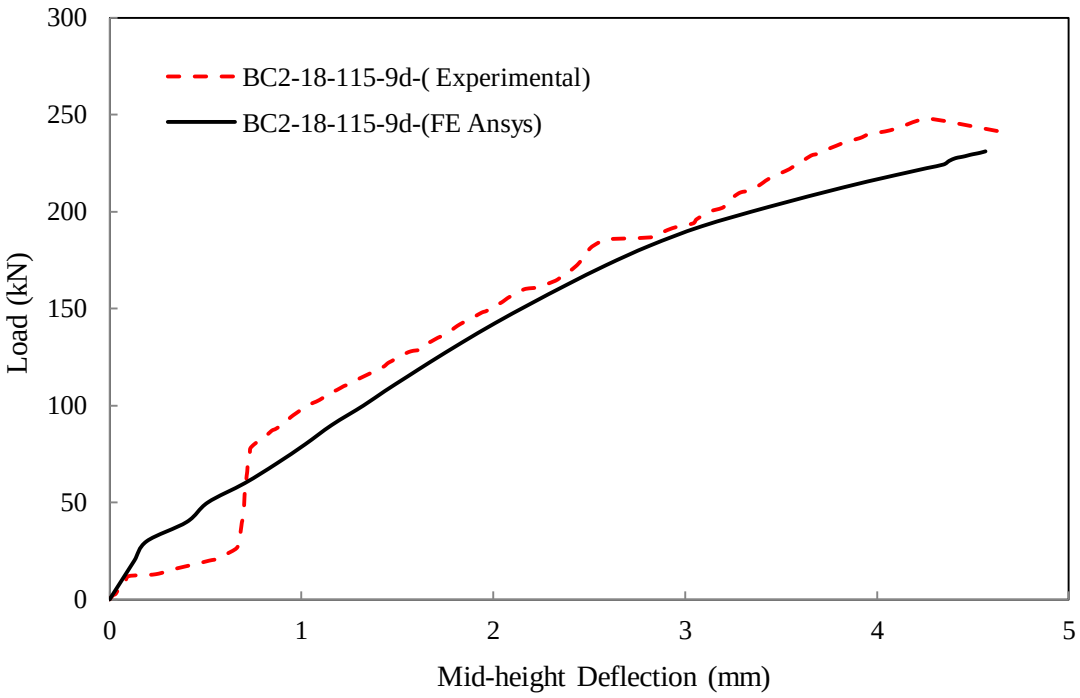

Figure 5.26: Comparison of the load-deflection of the specimen BC2-18-115-9d and finite element.

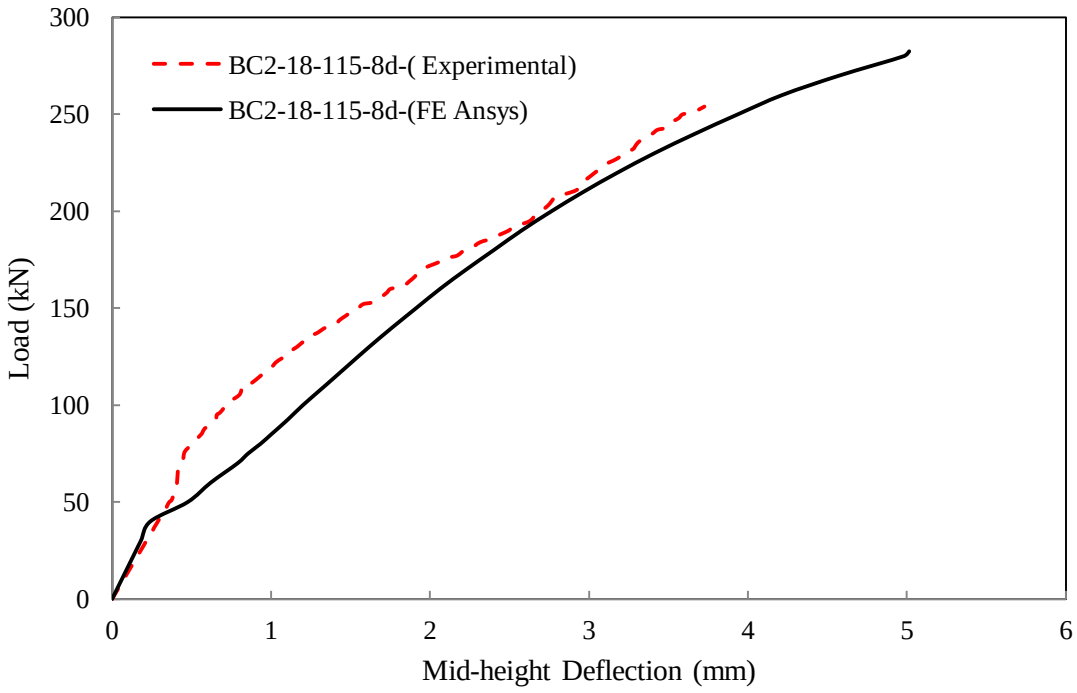

Figure 5.27: Comparison of the load-deflection of the specimen BC2-18-115-8d and finite element.

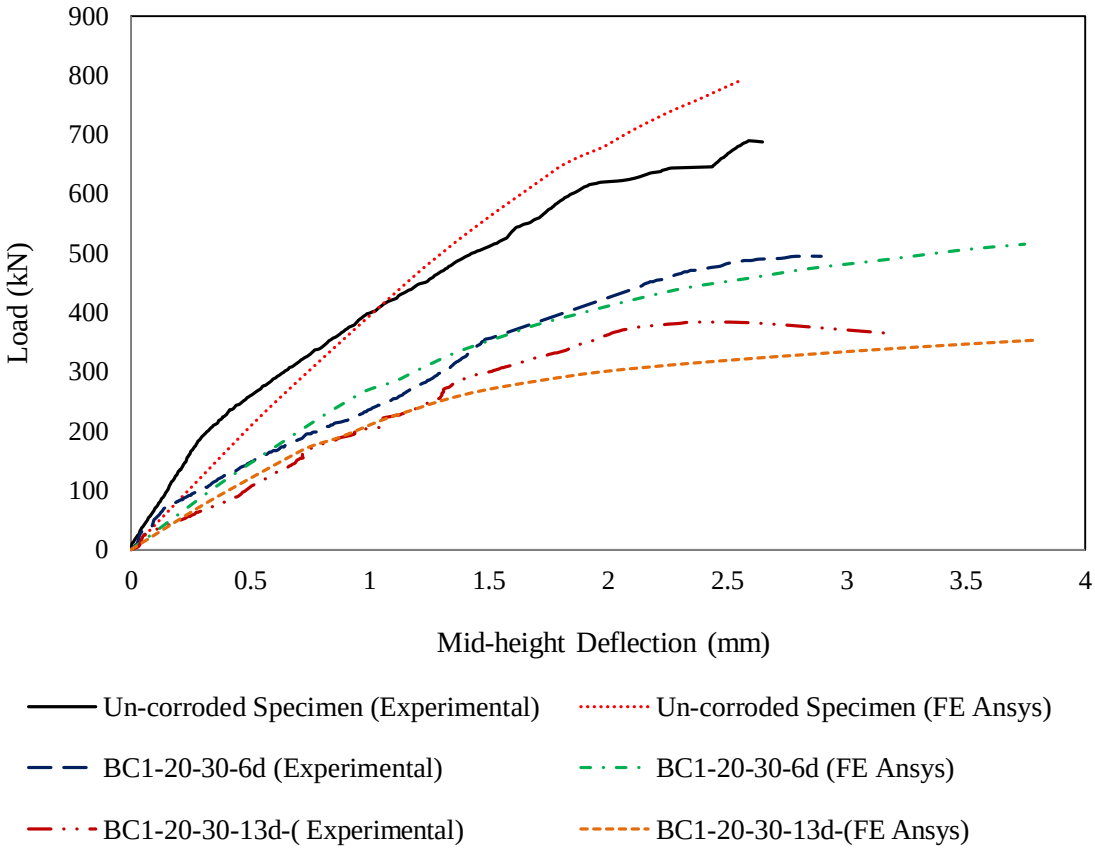

Figure 5.28: Comparison of the load-deflection of the specimens BC1-20-30 and finite element.

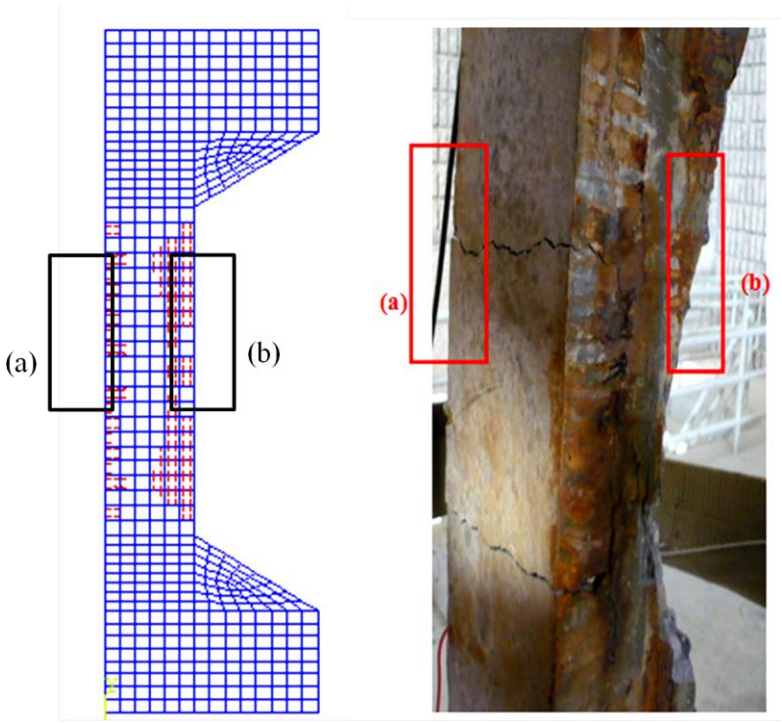

Cross-section (180 x 180 mm)

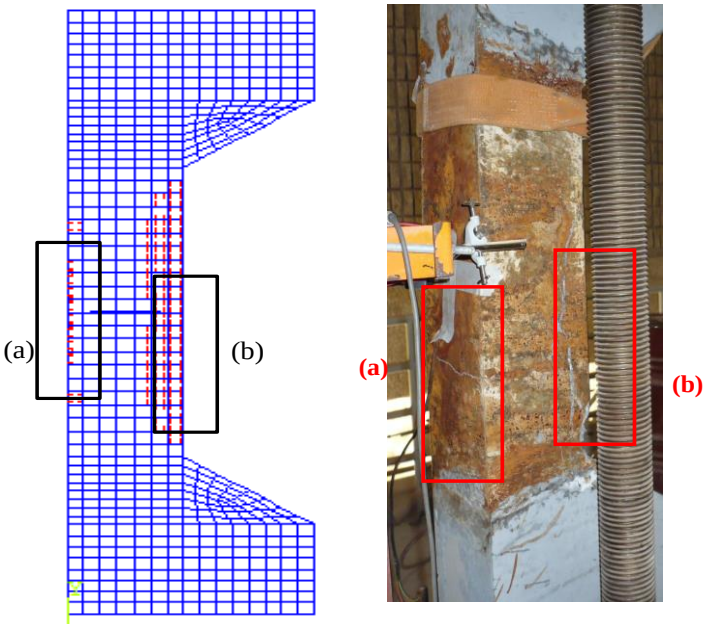

Cross-section (220 x 220 mm)

Figure 5.29: Cracking in finite element model: (a) flexural cracks, (b) compressive cracks (crushing of concrete).

CHAPTER 6

PREDICTION OF RESIDUAL STRENGTH

An effort has been made to utilize the experimental data developed in this study to predict the residual strength of corroded columns and beam-columns.

6.1 Prediction of Residual Strength: Empirical Approach

The load carrying capacity of corroded members is affected by:

(i) Loss of reinforcement area due to corrosion that result in reduction of the cross-sectional area of a bar.

(ii) Loss of bond between reinforcement and concrete. Previous research has experimentally shown that reinforcement corrosion leads to loss of bond, following a small increase in strength at the early stage of corrosion (Section 2.2).

(iii) Cracking of concrete cover due to corrosion. The material property of concrete progressively degrades with build-up of crack-induced damage.

(iv) Possible reduction in yield stress of steel.

In order to develop an approach to predict the residual strength, the capacity of a corroded column and beam-column is first calculated in the same manner as the un-corroded specimens by using reduced diameter of bars D' due to corrosion in place of the

original diameter, D and ignoring the effect of possible bond loss between reinforcement and concrete, effect of cracking of concrete from corrosion and no change in the yield strength of steel (Azad et al., 2007). The aim of this is to examine the role effect of reduction in steel area on the strength of corroded members.

6.1.1 Capacity of Corroded Specimens Using Reduced Area of Reinforcement

The penetration rate, P_r of the corroded bars for calculating the reduced diameter D' is given as (Ijsseling, 1986):

$$P_r = 0.003185 I_{corr} \quad (cm/day) \tag{6.1}$$

Therefore, the reduction in bar diameter due to corrosion with steady-state corrosion current density I_{corr} for corrosion period T is $2P_rT$.

The reduced net diameter of a corroded bar, D' is then determined as:

$$D' = D(1 - \frac{2P_rT}{D}) \tag{6.2}$$

For $\lambda = \frac{2P_rT}{D}$, the reduced cross-sectional area of the bar, A_s' can be calculated as (Azad et al., 2007)

$$A_s' = A_s(1 - \lambda) \tag{6.3}$$

where D is the original bar diameter in cm and A_s is the original cross-sectional area of the bar.

The theoretical capacity of corroded specimens P^*, are calculated using A_s' and presented

in Tables 6.1 and 6.2. The values of R_c, calculated as the ratio between the experimental failure load of the corroded specimens P_{exc} and the calculated failure load of the corroded specimens P^*, are shown in the tables.

From Tables 6.1 and 6.2, the following two noteworthy observations can be drawn:

(i) A comparison of the theoretical values P_{thu} with A_s (Table 5.3) and P^* with A_s' (Tables 6.1 and 6.2) show that P^* are only slightly less, being in the range of about 1% to 7%. Even with higher $I_{corr}T$ the reduction is no more than 7%.

(ii) In most case, the value of R_c is significantly less than 1.0. For columns, in general, R_c values are much lower than the beam-columns. This implies that the residual strength of columns and beam-columns with appreciable amount of axial loads cannot be predicted by simply considering reduced area of steel, A_s', and ignoring other corrosion-induced damage factors.

Table 6.1: D', P_{exc}, P^*, and R_c for the corroded specimens with diameter of bars 18 mm.

Specimen	D (mm)	D' (mm)	%Weight Loss (X_p)	$I_{corr}T$ (mA-days/cm^2)	Failure Load (kN)		$R_c = \frac{P_{exc}}{P^*}$
					P_{exc}	P^*	
C1-18-7d	18	17.46	6.29	8.53	515	1383	0.37
C1-18-10d	18	17.1	10.49	14.1	480	1362	0.35
C1-18-13d	18	16.44	18.09	24.44	390	1326	0.29
BC1-18-30-7d	18	17.42	6.76	9.15	561	736	0.76
BC1-18-30-10d	18	16.95	12.36	16.52	472	729	0.65
BC1-18-30-12d	18	16.79	14.13	19.05	348	726	0.48
BC1-18-60-7d	18	17.32	7.86	10.63	386	408	0.95
BC1-18-60-10d	18	16.89	12.93	17.36	300	404	0.74
BC1-18-60-13d	18	16.63	15.92	21.49	252	401	0.63
BC1-18-95-7d	18	17.33	7.75	10.46	236	257	0.92
BC1-18-95-10d	18	17.05	10.96	14.85	214	255	0.84
BC1-18-95-11d	18	16.93	12.34	16.83	177	254	0.7
C2-18-7d	18	17.43	6.57	8.91	700	1735	0.4
C2-18-10d	18	17.01	11.52	15.52	665	1711	0.39
C2-18-13d	18	16.56	16.68	22.55	550	1687	0.33
BC2-18-35-6d	18	17.49	5.86	7.95	667	1056	0.63
BC2-18-35-8d	18	17.18	9.52	12.81	589	1048	0.56
BC2-18-35-9d	18	17.02	11.42	15.43	575	1044	0.55
BC2-18-65-4d	18	17.57	4.96	6.71	548	685	0.8
BC2-18-65-7d	18	17.46	6.32	8.52	482	683	0.71
BC2-18-65-10d	18	16.96	11.96	16.31	442	675	0.66
BC2-18-115-7d	18	17.46	6.35	8.54	278	398	0.7
BC2-18-115-8d	18	17.27	8.42	11.42	256	395	0.65
BC2-18-115-9d	18	17.01	11.47	15.58	246	392	0.63

Table 6.2: D', P_{exc}, P^*, and R_c for the corroded specimens with diameter of bars 20 mm.

Specimen	D (mm)	D' (mm)	%Weight Loss (X_p)	$I_{corr}T$ (mA-days/cm^2)	Failure Load (kN)		$R_c = \frac{P_{exc}}{P^*}$
					P_{exc}	P^*	
C1-20-7d	20	19.05	9.74	14.85	456	1479	0.31
C1-20-10d	20	18.85	11.82	18.12	375	1466	0.26
C1-20-13d	20	18.53	15.18	23.15	330	1446	0.23
BC1-20-30-7d	20	19.08	9.44	14.41	475	765	0.62
BC1-20-30-6d	20	19.26	7.98	11.61	495	768	0.64
BC1-20-30-13d	20	18.61	14.22	21.78	384	757	0.51
BC1-20-60-7d	20	19.17	8.48	12.99	431	426	1.01
BC1-20-60-10d	20	18.81	12.27	18.7	284	422	0.67
BC1-20-60-13d	20	18.44	15.88	24.44	258	418	0.62
BC1-20-95-7d	20	19.12	9.03	13.8	209	270	0.77
BC1-20-95-10d	20	18.83	12.05	18.4	197	268	0.73
BC1-20-95-13d	20	18.55	14.75	22.71	168	266	0.63
C2-20-7d	20	19.15	8.71	13.32	670	1839	0.36
C2-20-8d	20	19.08	9.47	14.44	620	1835	0.34
C2-20-10d	20	18.95	10.81	16.44	580	1827	0.32
BC2-20-35-7d	20	19.17	8.6	13.1	631	1099	0.57
BC2-20-35-6d	20	19.31	7.06	10.79	731	1103	0.66
BC2-20-35-9d	20	18.97	10.55	16.12	582	1094	0.53
BC2-20-65-7d	20	19.11	9.02	13.9	497	713	0.7
BC2-20-65-6d	20	19.27	7.51	11.51	519	716	0.73
BC2-20-65-9d	20	18.93	11.03	16.85	460	709	0.65
BC2-20-115-7d	20	19.03	9.97	15.24	301	419	0.72
BC2-20-115-6d	20	19.35	6.56	10.2	336	424	0.79
BC2-20-115-9d	20	18.93	10.96	16.74	280	418	0.67

6.1.2 The Approach

The important parameters for developing the model for the residual strength of corroded reinforced concrete columns and beam-columns were based on the following observations:

- The strength of corroded column and beam-column decreases with increasing $I_{corr}T$, which plays a significant role in strength degradation.
- At given $I_{corr}T$, the loss of strength for corroded columns is larger than that for corroded beam-columns.
- The values of R_c, determined on the basis of theoretical structural mechanics, using reduced cross-sectional area A_s' from Eq. (6.3), show that such theoretical prediction would not be accurate, as it does not take into account the other adverse effects due to corrosion.

As it is difficult to quantify corrosion damage precisely through a mechanistic model, it is perhaps prudent to seek an experimentally dependent correlation to capture the overall impact of damage on the strength. For limit state of failure of a corroded member, the maximum axial load P_{res} that a column can carry and a beam-column can sustain with a prescribed eccentricity e (the applied moment is $P_{res}\,e$) is assumed to be the resistance or residual strength of a corroded member.

The value of P_{res} was computed in two-steps: First, the theoretical capacity of a corroded member, P^* is calculated based on conventional mechanics using only the reduced steel area A_s' from corrosion. The combined effect of the bond-slip, crack-damage and possible variation in yield strength of reinforcement can collectively be accounted for by a reduction factor, α, referred to as 'corrosion damage factor'. An empirical expression for

the correction factor is developed through a multi-level regression of test data using the most significant variables that have impact on damage and loss of strength. This way, a closer and acceptable convergence of the theoretical and actual values can be achieved. The predicted strength then equals the values calculated on the basis of reduced steel area only multiplied by the correction factor α developed in this study. Thus,

$$P_{res} = \alpha P^* \tag{6.4}$$

where, α is the correction factor which reflects the combined effect of possible bond-slip, crack-induced damage and reduction in yield strength of reinforcement.

6.1.3 Development of the Correction Factor

The value of α is taken as a nonlinear function of several variables such as I_{corr} (corrosion current density), time (T), diameter of the bar (D), member size and eccentricities e. For columns, α is represented as α_1 and for beam-columns, it is represented as α_2. Based on the experimental observations and several trials, α_1 and α_2 are taken in the following empirical forms:

For columns:

$$\alpha_1 = z_0 \frac{(\gamma)^{z_1}\left(\frac{D'}{D}\right)^{z_2}}{(I_{corr}T)^{z_3}} \tag{6.5a}$$

and for beam-columns

$$\alpha_2 = x_0 \frac{(e/h)^{x_1} \cdot \left(\frac{D'}{D}\right)^{x_2}}{(I_{corr}T)^{x_3}} \quad (6.5b)$$

where

z_0 to z_3 and x_0 to x_3 are all constants to be determined through a multi-level regression of test data.

e = eccentricity.

h = depth of cross-section.

γ = ratio of concrete core to the depth of cross-section (Figure 4.18).

D = diameter of un-corroded rebar.

D' = diameter of corroded rebar as determined from Eq. (6.2).

I_{corr}= corrosion current density in mA/cm^2

T = duration of corrosion in days

The proposed form of α_1 and α_2 are taken as a function of important variables namely, $I_{corr}T$, γ, D, D' and e/h. The rationale behind the choice of these variables and the proposed forms is the following observations, reported in Chapter 5:

- The percentage loss of metal X_p increases with increasing $I_{corr}T$, and therefore capacity of a corroded column and beam-column decreases with increasing $I_{corr}T$. Thus α_1 and α_2 values should be inversely related to $I_{corr}T$. Furthermore, the original diameter of bar D reduces to D' with $I_{corr}T$. The reduction factors are therefore linked to (D'/D).

- Damage to the concrete cover due to corrosion reduces the strength of the column. The ratio of concrete core to the depth of cross-section, γ, (Figure 4.18) indicates the proportion of the column area which is undamaged. Therefore, the residual strength of corroded column depends on γ.
- For beam-column, *e/h* ratio is an important factor that determines whether the failure is ′compression-controlled′ or ′tension-controlled′. For α_2, *e/h* is therefore an important factor.

The values of the constants z_0 to z_3 and x_0 to x_3 were determined by satisfying the imposed condition that the predicted failure load of members will be lower than the experimental failure load in over 70% of the samples for safer prediction and should not exceed 10% the experimental values.

Based on the above criteria, regression analysis of 48 test data yielded

z_0 = 2.542; z_1= 0.841; z_2= 0.25; z_3= 0.499

x_0 = 1.323; x_1= 0.14; x_2= 1.48; x_3=0.192

The empirical equations for the reduction factors α_1 and α_2 are then:

For columns

$$\alpha_1 = 2.542 \frac{(\gamma)^{0.841} \left(\frac{D'}{D}\right)^{0.25}}{(I_{corr}T)^{0.499}} \quad (6.6a)$$

For beam-columns

$$\alpha_2 = 1.323 \frac{(e/h)^{0.14} \cdot \left(\frac{D'}{D}\right)^{1.48}}{(I_{corr}T)^{0.192}} \quad (6.6b)$$

By substituting the values of *e*, *h*, *D*, D', and $I_{corr}T$, the values of α_1 and α_2 for all 48 corroded columns and beam-columns are calculated and listed in Tables 6.3 and 6.4. The predicted residual capacity of all test specimens, P_{res}, are then calculated using Eq. (6.4) and are tabulated in Tables 6.3 and 6.4. It can be seen that all the predicted values of P_{res} have an error less than 10%.

The experimental value of failure load P_{exc} for the corroded specimens and the predicted value P_{res} are plotted in Figure 6.1. It can be seen that there is a reasonably good correlation between the predicted and experimental values of failure load. The ratio between the predicted values of the residual strength P_{res} and the P_{exc} experimental values for all corroded specimens are plotted in Figure 6.2, which shows that about 83% of the data are under the value of 1.0, and 90% of data are between 1.1 and 0.8. For only four specimens, the ratios of P_{res}/P_{exc} fall below 0.8.

Figures 6.1 and 6.2 lend confidence to the applicability of the correction factors α_1 and α_2 for prediction purposes. The two-step approach for prediction of residual strength of corroded columns and beam-columns seems satisfactory.

Table 6.3: Values of α_1, α_2, P^*, P_{exc} and P_{res} for corroded specimens with 18-mm diameter bars.

Specimen	h (mm)	e/h	γ	$\alpha^{\dagger}$	Failure Load, (kN)			Error** %
					P^*	P_{exc}	P_{res}	
C1-18-7d	180	0	0.34	0.35	1383	515	489	-5
C1-18-10d				0.27	1362	480	373	-22
C1-18-13d				0.21	1326	390	273	-30
BC1-18-30-7d	180	0.17	0.34	0.64	736	561	472	-16
BC1-18-30-10d				0.55	729	472	400	-15
BC1-18-30-12d				0.53	726	348	383	10
BC1-18-60-7d		0.33		0.68	408	386	278	-28
BC1-18-60-10d				0.60	404	300	241	-20
BC1-18-60-13d				0.56	401	252	225	-11
BC1-18-95-7d		0.53		0.73	257	236	187	-21
BC1-18-95-10d				0.67	255	214	170	-21
BC1-18-95-11d				0.64	254	177	163	-8
C2-18-7d	220	0	0.46	0.44	1735	700	770	10
C2-18-10d				0.33	1711	665	572	-14
C2-18-13d				0.28	1687	550	465	-16
BC2-18-35-6d	220	0.16	0.46	0.66	1056	667	695	4
BC2-18-35-8d				0.59	1048	589	613	4
BC2-18-35-9d				0.56	1044	575	581	1
BC2-18-65-4d		0.30		0.75	685	548	512	-7
BC2-18-65-7d				0.71	683	482	483	0
BC2-18-65-10d				0.60	675	442	403	-9
BC2-18-115-7d		0.52		0.76	398	278	304	9
BC2-18-115-8d				0.71	395	256	281	10
BC2-18-115-9d				0.66	392	246	257	4

$\dagger$ $\alpha=\alpha_1$ for columns; $\alpha=\alpha_2$ for beam-columns

** (100 x (P_{res}-P_{exc})/P_{exc})

Table 6.4: Values of α_1, α_2, P^*, P_{exc} and P_{res} for corroded specimens with 20-mm diameter bars.

Specimen	h (mm)	e/h	γ	$\alpha^{\dagger}$	Failure Load, (kN)			Error** %
					P^*	P_{exc}	P_{res}	
C1-20-7d	180	0	0.33	0.26	1479	456	384	-16
C1-20-10d				0.23	1466	375	343	-8
C1-20-13d				0.21	1446	330	298	-10
BC1-20-30-7d	180	0.17	0.33	0.58	765	475	440	-7
BC1-20-30-6d				0.61	768	495	467	-6
BC1-20-30-13d				0.51	757	384	388	1
BC1-20-60-7d		0.33	0.33	0.65	426	431	277	-36
BC1-20-60-10d				0.59	422	284	249	-12
BC1-20-60-13d				0.54	418	258	228	-12
BC1-20-95-7d		0.53	0.33	0.68	270	209	185	-12
BC1-20-95-10d				0.63	268	197	170	-14
BC1-20-95-13d				0.59	266	168	158	-6
C2-20-7d	220	0	0.45	0.36	1839	670	654	-2
C2-20-8d				0.34	1835	620	627	1
C2-20-10d				0.32	1827	580	584	1
BC2-20-35-7d	220	0.16	0.45	0.59	1099	631	644	2
BC2-20-35-6d				0.62	1103	731	678	-7
BC2-20-35-9d				0.55	1094	582	607	4
BC2-20-65-7d		0.30	0.45	0.63	713	497	449	-10
BC2-20-65-6d				0.66	716	519	472	-9
BC2-20-65-9d				0.60	709	460	424	-8
BC2-20-115-7d		0.52	0.45	0.67	419	301	279	-7
BC2-20-115-6d				0.74	424	336	312	-7
BC2-20-115-9d				0.65	418	280	271	-3

$\dagger \alpha=\alpha_1$ for columns; $\alpha=\alpha_2$ for beam-columns

** (100 x (P_{res}-P_{exc})/P_{exc})

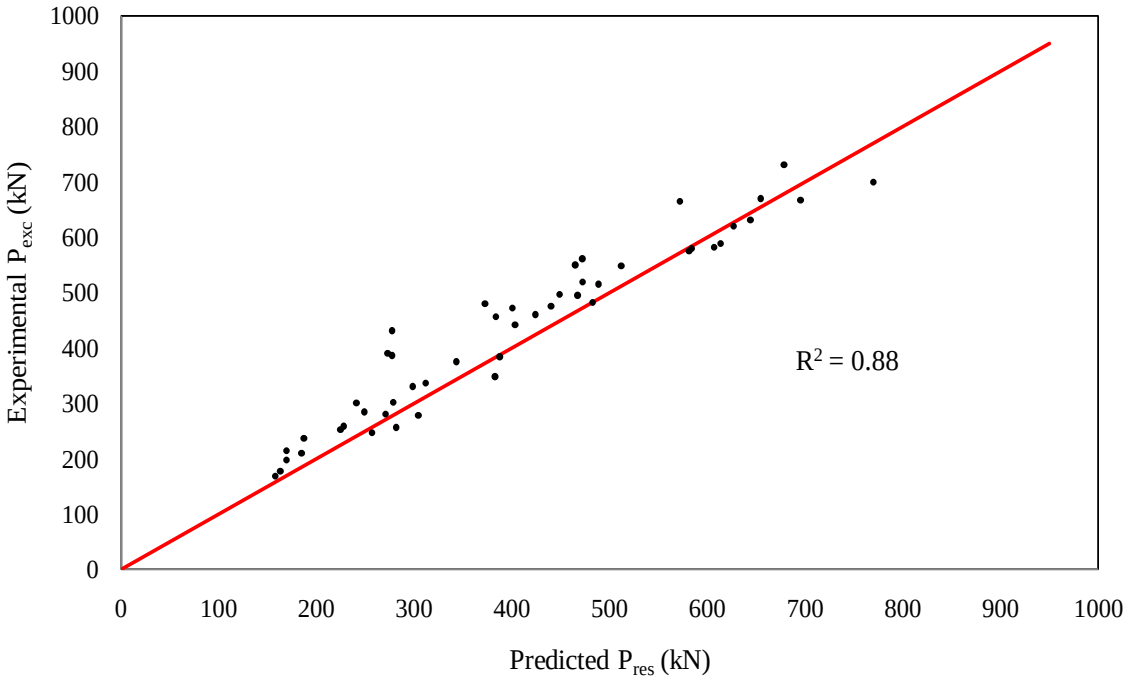

Figure 6.1: Comparison of experimental P_{exc} and the predicted P_{res}.

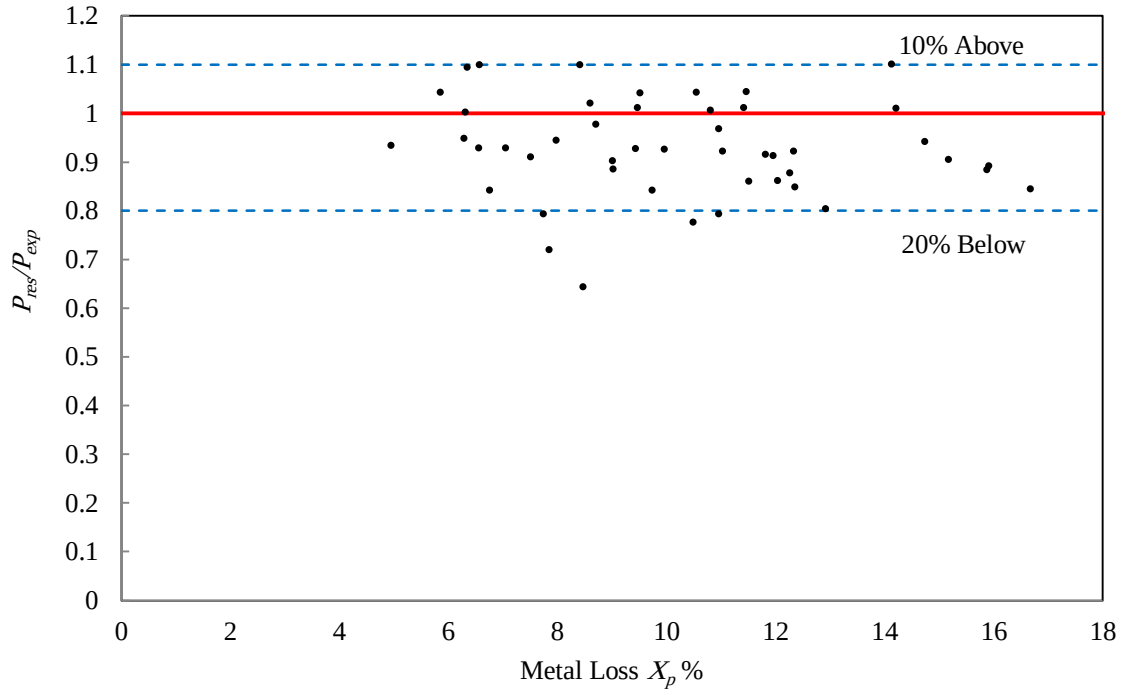

Figure 6.2: Comparison of the ratio of the predicted P_{res} and experimental P_{exc}.

6.1.4 The Suggested Method

The proposed methodology for the prediction of the residual strength of corroded columns and beam-columns comprise of a two-step calculation process as mentioned in Section 6.1:

In the first step, the theoretical strength of corroded member, P^*, is calculated by using the reduced steel area A_s' from corrosion (Eq. 6.3). In the second step, the correction factor α_1 and α_2 as applicable (α_1 for column and α_2 for beam-column) is calculated by using Eq. 6.6 to reflect the combined effect of possible bond-slip, crack-induced damage and reduction in yield strength.

Finally, the predicted strength P_{res} is then equal to:

$$P_{res} = \alpha_1 P^* \qquad \text{for columns} \qquad (6.7a)$$

$$= \alpha_2 P^* \qquad \text{for beam-columns} \qquad (6.7b)$$

6.1.5 Verification of the Accuracy of the Proposed Method

(a) New Test Data

The tests data for two columns and two beam-column specimens, each of 210×210 mm in section and reinforced with 4-bars of 18 mm, was used for verification. The test data for these four specimens given in Table 6.5 was used as independent data to verify the proposed method. Table 6.6 gives the details of the comparison between the experimental values of the residual strength and the predicted values P_{res}. In addition, the ratio between the predicted values of the residual strength P_{res} and the P_{exc} experimental values for all corroded specimens are plotted in Figure 6.3.

Table 6.5: Corrosion data of new tested specimens.

Specimen	D mm	D' mm	T day	%Weight Loss (X_p) (Gravimetric)	$I_{corr}T$ (mA-days/cm^2)
C3-18-9d	18	17.21	9	9.20	12.42
C3-18-13d	18	16.68	13	15.34	20.73
BC3-18-105-9d	18	17.18	9	9.48	12.80
BC3-18-45-13d	18	16.92	13	12.58	17.00

Table 6.6: Comparison of the proposed model results with additional specimens

Specimens	h (mm)	e (mm)	γ	$\alpha^{\dagger}$	Failure Load, (kN)			% Error **
					P*	P_{exc}	P_{res}	
C3-18-9d	210	0	0.44	0.36	1613	524	576	10
C3-18-13d		0	0.44	0.27	1583	440	435	-1
BC3-18-105-9d		105	0.44	0.69	372	272	256	-6
BC3-18-45-13d		45	0.44	0.56	794	433	448	3

$\dagger$ $\alpha=\alpha_1$ for columns; $\alpha=\alpha_2$ for beam-columns

** (100 x (P_{res}-P_{exc})/P_{exc})

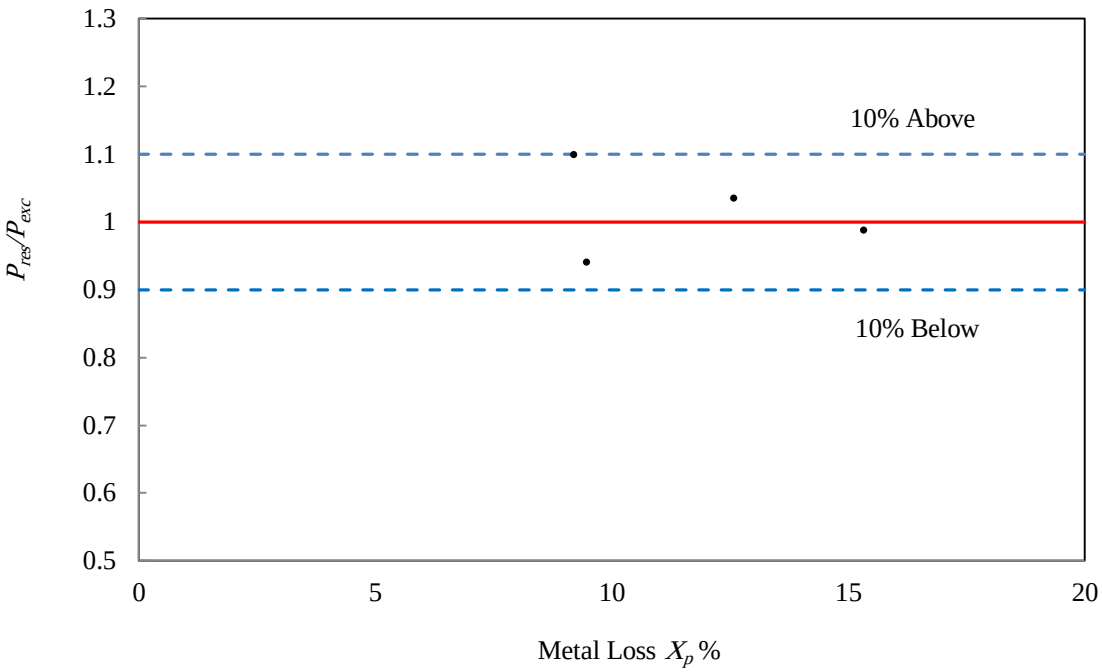

Figure 6.3: Comparison of the ratio of the predicted P_{res} and experimental P_{exc} of new specimens.

Table 6.6 shows that the proposed model predicts good results for the P_{res} by comparison with the experimental values P_{exc}. It is clear from Figure 6.3 that all points are around the value of 1.0, showing good correlation between predicted and actual strengths.

(b) Data of Wang and Liang

The work done by Wang and Liang (2008) can be quoted as the most contributing experimental work on eccentrically loaded columns. A total of 12 members were tested using partial length corrosion achieved through accelerated corrosion as given in Table 6.7. Table 6.8 gives the details of the comparison between the experimental and predicted failure loads of corroded specimens using Eq.6.7.

Table 6.7: Corrosion data of Wang and Liang (2008).

Specimens	*b* (mm)	*h* (mm)	*e/h*	Average wt. loss, X_p %	Average $I_{corr}T$ (mA-days/cm^2)
ZD0	203	185	0.85	0	0
ZDL700-1	201	201	0.74	2.86	4.04
ZDL700-2	208	190	0.82	4.68	6.61
ZDL350-3	205	201	0.75	4.85	6.85
ZDY700-1	200	198	0.76	3.29	4.65
ZDY350-2	204	192	0.79	3.65	5.16
ZDY350-3	204	190	0.83	5.51	7.79
ZXY700-1	205	195	0.27	1.98	2.79
ZXY350-2	204	200	0.27	4.31	6.09
ZXY350-3	204	204	0.23	7.07	9.99
ZXL700-1	206	198	0.26	2.9	4.09
ZXL350-3	204	200	0.26	4.59	6.49

Table 6.8: Values of α, P_{exc} and P_{res} (Wang and Liang, 2008).

Specimens	*e/h*	$\alpha^{\dagger}$	Failure Load (corroded), (kN)			% Error**
			*P**	P_{exc}	P_{res}	
ZD0	0.85	1.00	234	239.1	234	-2
ZDL700-1	0.74	0.953	274	255.3	261	2
ZDL700-2	0.82	0.864	257	232.8	222	-4
ZDL350-3	0.75	0.85	293	240.1	249	4
ZDY700-1	0.76	0.926	284	269.2	263	-2
ZDY350-2	0.79	0.91	263	223.9	239	7
ZDY350-3	0.83	0.836	250	266	209	-22
ZXY700-1	0.27	0.893	795	741.2	710	-4
ZXY350-2	0.27	0.754	792	696.5	597	-14
ZXY350-3	0.23	0.655	936	613.1	613	0
ZXL700-1	0.26	0.818	839	756.5	686	-9
ZXL350-3	0.26	0.737	874	647.7	644	-1

† $\alpha=\alpha_2$ for beam-columns

** (100 x (P_{res}-P_{exc})/P_{exc})

In addition, the ratio between the predicted values of the residual strength P_{res} and the experimental values P_{exc}, (P_{res}/P_{exc}) versus metal loss X_p for all corroded specimens of Wang and Liang data are plotted in Figure 6.4. As seen from figure, most points are between 1.1 and 0.9, showing good agreement between predicted and experimental values.

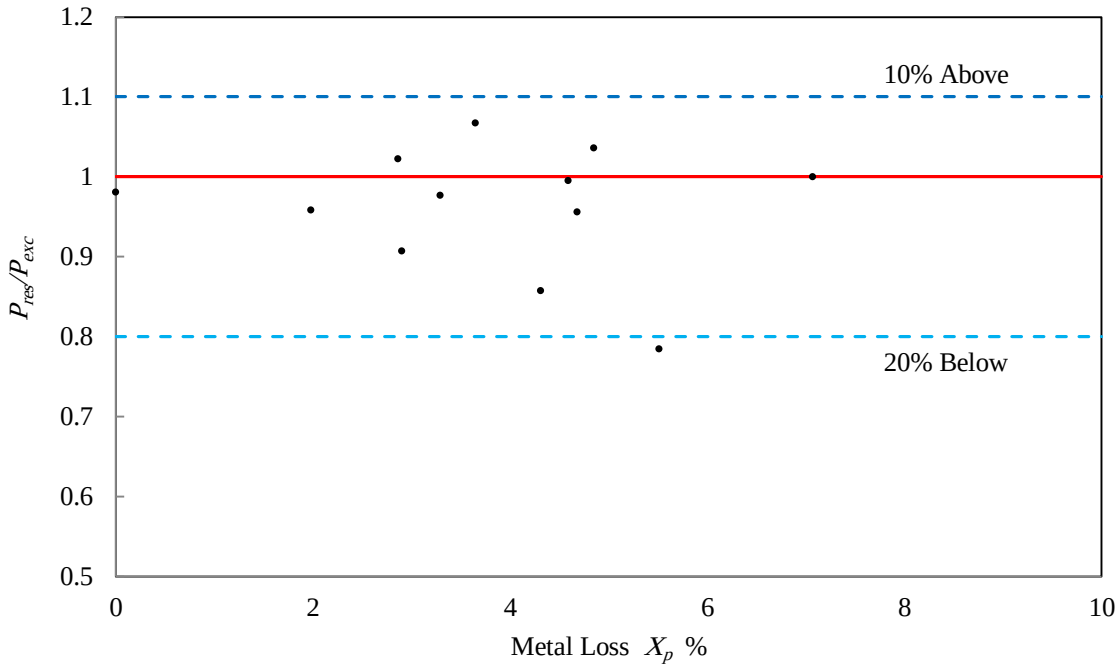

Figure 6.4: Comparison of the ratio of the predicted P_{res} and experimental P_{exc} of Wang and Liang, 2008.

6.2 Prediction of Residual Strength: FE Model

The proposed finite element method for prediction of the residual strength of corroded columns and beam-columns requires idealization and adjustment of the material properties of concrete and steel reinforcement. ANSYS-based model for nonlinear analysis was calibrated with the experimental data to establish a value of $v_{r/s}$ for the rust volume of the type of steel used in this work. Using $v_{r/s}$ = 3.113, the predicted failure loads from FE model P_{fec} were computed and compared with the experimental values, P_{exc}. The comparison presented in Chapter 5 have revealed that proposed FE model can be used as an analytical tool to estimate the residual capacities of corroded columns and beam-columns.

The only one requirement for application to members reinforced with different types of steel is an appropriate value of $v_{r/s}$. Although, literature has reported a wide ranging value of $v_{r/s}$ from 1.7 to 6.15 (Liu and Weyers, 1998), it is suggested that unless more accurate value available, $v_{r/s}$ = 3.113 can be used. It should however be noted that higher value of $v_{r/s}$ will lead to more reduction in capacity, although results are not highly sensitive to a small change in the value of $v_{r/s}$.

CHAPTER 7

PROBABILITY OF FAILURE OF CORRODED ELEMENTS

The reliability of deterioration of reinforced concrete columns and beam-columns has been, and still is, a widely targeted research field. However, a review of literature shows that no reliable analytical model for predicting residual strength of corroded columns and beam-columns has been developed till now. In this chapter, an attempt has been made to use the model for prediction of the residual strength of a corroded concrete member presented in chapter 6 in developing a reliability analysis using Monte Carlo simulation (MCS), and to calculate the reliability or safety index by estimating the probability of failure.

As residual strength of a corroded member is related to corrosion damage, the strength progressively declines with time due to damage propagation as shown in Figure 7.1. As part of an inspection and assessment work, it is often necessary to have an expert opinion of the load-carrying capacity of corroded members. This information is vital to ascertain the prevailing level of safety of the structure to avoid the risk of structural failure. Furthermore, it is also necessary to determine the extent of corrosion damage and its implication on safety so that the necessary repair or restoration work can be planned in time without further compromising the safety of the structure.

Since the problems associated with corrosion of reinforced concrete are, in general, complex and random, the probability of failure of corroded reinforced concrete columns

and beam-columns depends on the possible combination of the random variables in the function governing safety.

For such an analysis, a large number of system parameters that govern the strength need to be considered as random variables. Monte Carlo simulation is chosen for the probability analysis of this complex problem, from which reliability can be assessed.

7.1 Damage Propagation and Structural Safety

Once corrosion is initiated, a member's original load carrying capacity P_{thu} is progressively reduced with corrosion as indicated in Figure 7.1 due to progressive built-up of damage. The plot of residual strength $P_{res}(T)$ can be achieved using Eq. (6.7). In strength design method, the value of P_{thu} is greater than or equal to P_u, the factored load for design. The use of load factors results in P_{thu} values much greater than the service load requirements. Because of this built-in margin of safety above the service load, some loss of P_{thu} due to corrosion will not cause a member to fail, as long as the reduced strength, P_{res} is greater than the service load, although the original factor of safety will be reduced.

To ensure an acceptable minimum factor of safety above the service load demand P_s, $P_{res}(T)$ must not fall below an acceptable limit ωP_{thu} (Figure 7.1), when ω is the maximum permitted reduction factor for the minimum required residual strength ($\omega P_{thu} > P_s$).

The ratio of the reduced original strength to the service load demand, $\omega P_{thu}/ P_s$ represents the minimum safety factor considered permissible. The critical time at which ωP_{thu} equals P_{res} is T_c as shown in Figure 7.1 beyond which the member is declared as ′unsafe′ or potentially hazardous. The member can be considered as ′safe′ when $T \leq T_c$, i.e. when $P_{res}(T)$ is greater or equal to ωP_{thu}. A corroded member must therefore be repaired to restore its strength prior to the critical corrosion time T_c.

An estimation of T_c is necessary to establish a safe service life of a member. Thus useful service life of a member prior to repair T_s is: $T_s = T_a + T_c$, when T_a = corrosion initiation period.

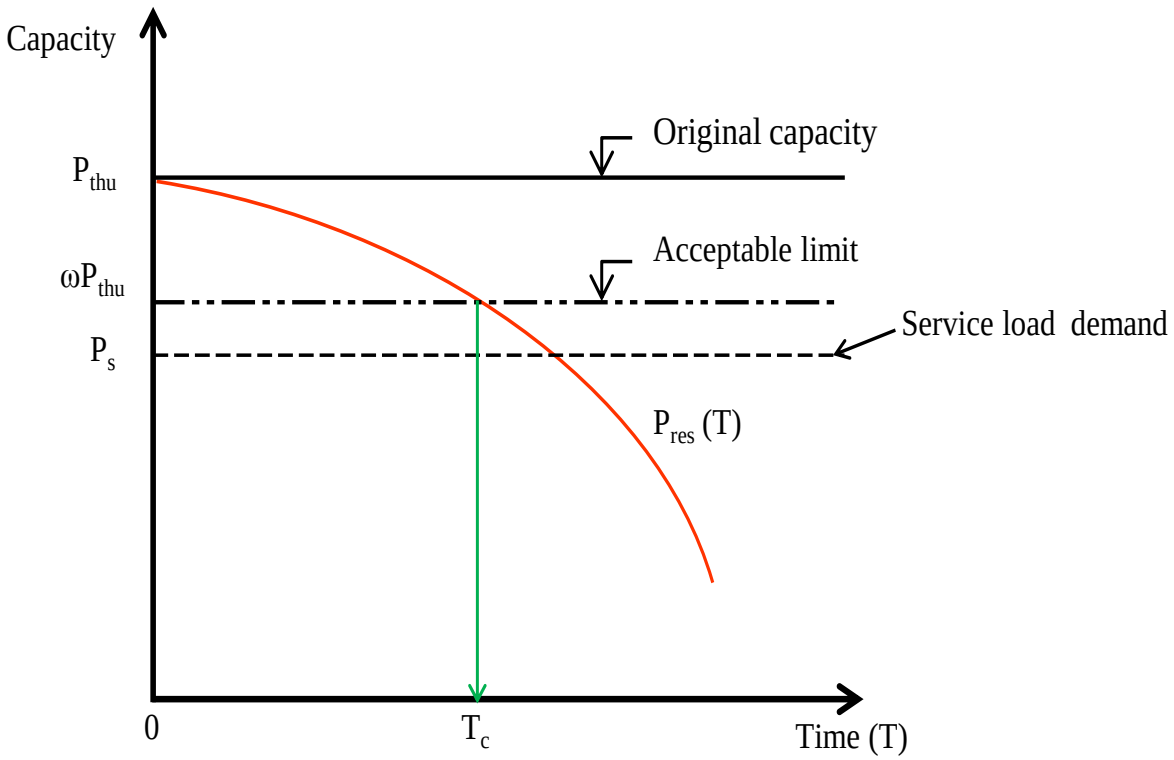

Figure 7.1: Deterioration model.

7.1.1 Illustration of Damage Propagation Model

Determination of the critical corrosion time T_c when the residual strength of a member equals the acceptable limit ωP_{thu}, is illustrated for a column and a beam-column using the following assumed data:

Cross-section: 300 x 300 mm

Main reinforcement: 8-16 mm dia. bars

Effective cover = 58 mm

γ = (Total depth of cross-section- (effective cover *2))/Total depth of cross-section

Concrete compressive strength, f_c' = 30 MPa

Yield strength of steel, f_y = 460 MPa

I_{corr}= 1.0 μA/cm^2 and 1.5 μA/cm^2 where the first value corresponds to a moderate corrosion risk (Stewart and Rosowsky, 1998).

Maximum permitted reduction factor ω = 0.714

Figure 7.2a shows a plot of $P_{res}(T)$ for the column section using values calculated from Eq. (6.7a) with I_{corr} = 1.0 μA/cm^2. The original strength of the un-corroded section, P_{thu} = 2995 kN at T= 0.0 The value of ωP_{thu} is taken as 2138 kN, using a value of ω = 0.714. The critical T_c is determined as about 15 years (Figure 7.2a).

For beam-column member of the same section with e/h = 0.25, the plot of $P_{res}(T)$ is shown in Figure 7.2b. Using the residual strength values obtained from Eq. (6.7b) with

I_{corr} = 1.0 μA/cm^2. P_{thu} = 1605 kN at e/h = 0.25 and based on ωP_{thu}, T_c is approximately 19 years.

To demonstrate the influence of I_{corr} on T_c, Figure 7.3 is plotted for I_{corr} = 1.0 and 1.5 μA/cm^2. Results for the column show that an increase in the I_{corr} from 1.0 to 1.5 μA/cm^2 will result in a drop in the critical corrosion time, T_c from about 15 years to about 9.9 years. For the beam-column with e/h = 0.25, T_c reduces to 12.8 from 19 years, when I_{corr} is increased to 1.5 from 1.0 μA/cm^2. The results show that with increasing I_{corr}, the critical time T_c decreases, reducing the service life prior to repair, as damage intensifies with higher I_{corr}.

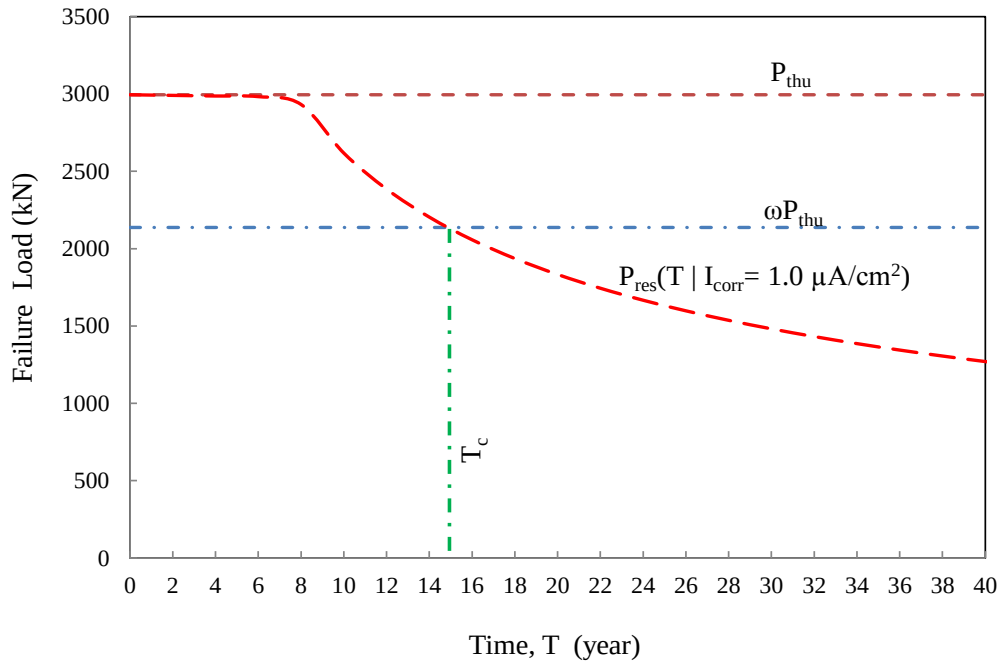

(a) Column

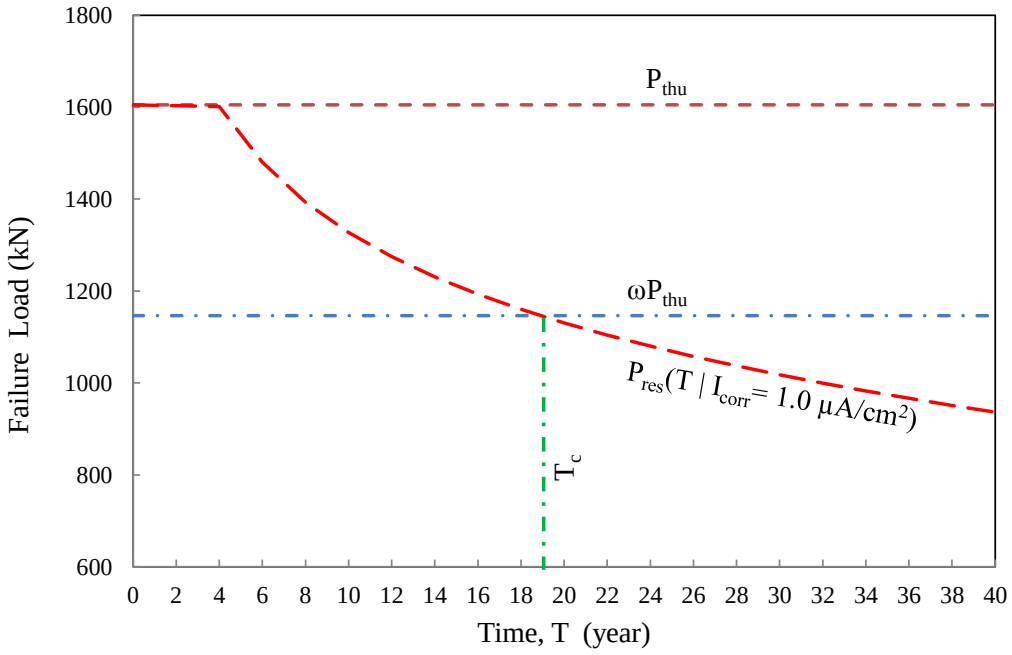

(b) Beam-column (e/h = 0.25)

Figure 7.2: Critical time T_c for corrosion damage of column and beam-column.

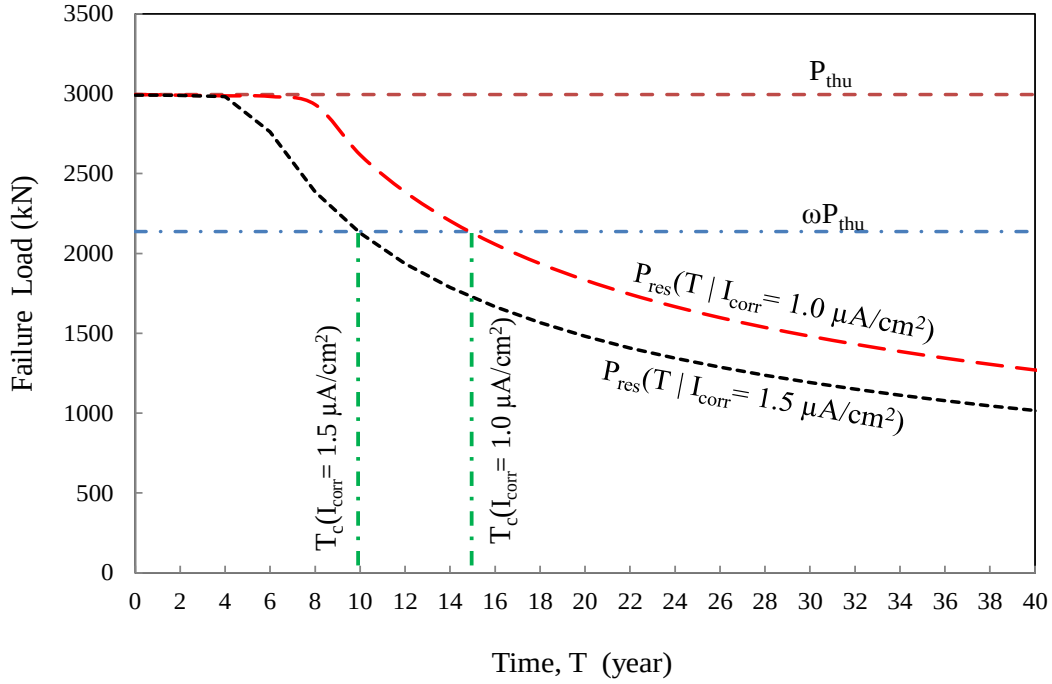

(a) Column

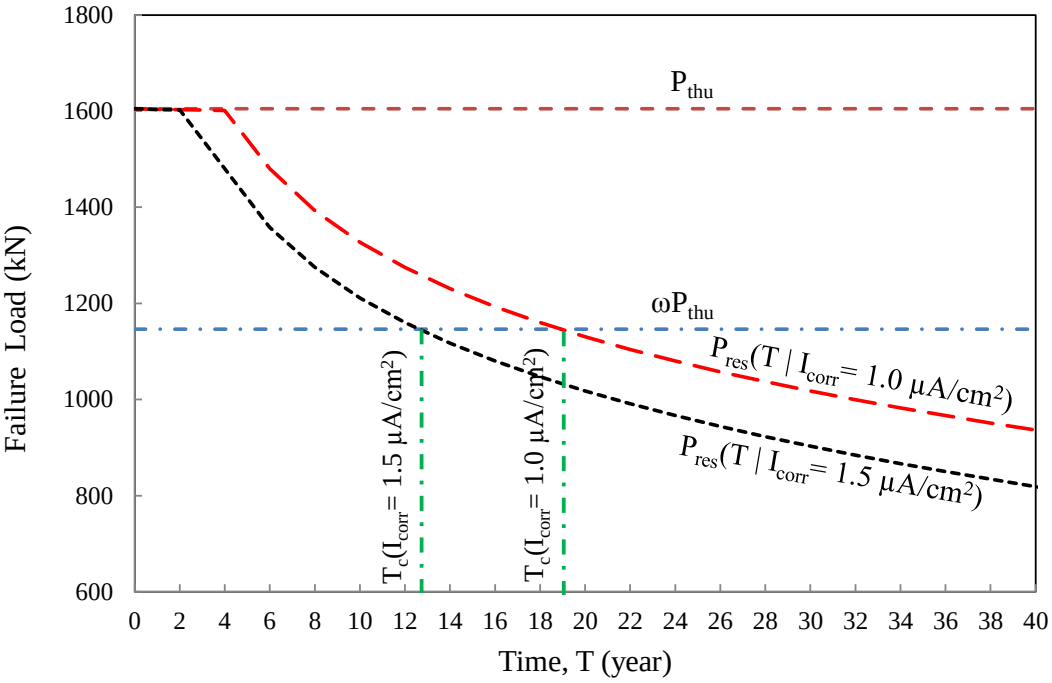

(b) Beam-column (e/h = 0.25)

Figure 7.3: Critical time T_c for corrosion damage of columns and beam-columns with different values of I_{corr}.

7.2 Computing the Probability of Failure using Monte Carlo Simulation (MCS)

In this section, the probability of failure of corroded columns and beam-columns is evaluated by MCS approach. It is important to know that this evaluation of probability is indeed only an estimate. However the estimate improves as the number of simulations increases (Nowark and Collins, 2000).

7.2.1 Limit State Function for Strength and Safety

For structural safety, the residual capacity of strength of a corroded member at a prescribed corrosion period T must be greater than or equal to ωP_{thu}, which is the demand on load capacity. The limit state function is then $P_{res} \geq \omega P_{thu}$. Thus, a corroded structure can be declare safe if P_{res} - $\omega P_{thu} \geq 0$. Both P_{res} and ωP_{thu} values are governed by a set of design variables that may vary randomly within upper and lower limits. Thus P_{res} and ωP_{thu} can have a large number of values depending upon the random combination of the design variables within the range of possible distribution.

The limit state function g, for corroded member can be expressed as

$$g(P_{res}, \omega P_{thu}) = P_{res}(\mathbf{X}) - \omega P_{thu}(\mathbf{X}) \quad (7.1)$$

where, **X** = vector of random variables which effect the strength;

P_{res} = the predicted strength (residual strength) of corroded member using Eq. (6.7);

P_{thu} = the original load capacity of the un-corroded member and

ω is the maximum permitted reduction factor for the minimum required residual strength.

The following conditions can be used to describe the state of a corroded member (Figure 7.4):

$g(P_{res}, \omega P_{thu}) < 0$ Unsafe.

$g(P_{res}, \omega P_{thu}) > 0$ Safe.

$g(P_{res}, \omega P_{thu}) = 0$ Critical situation.

7.2.2 Probability of Failure

The probability of failure P_f for a given limit state function g is then

$$P_f = P\,[g \leq 0] = P\,[P_{res}(\mathbf{X}) - \omega P_{thu}(\mathbf{X}) \leq 0] \tag{7.2a}$$

$$\text{Or } P_f = P\left[g' \geq \frac{1}{\omega}\right] = P\left[\frac{P_{thu}(\mathbf{X})}{P_{res}(\mathbf{X})} \geq n\right] \tag{7.2b}$$

where, $n = \frac{1}{\omega}$ is the acceptable limit factor.

The probability of failure estimated from Monte Carlo simulation is:

$$P_f = \frac{\text{number of times } g \leq 0}{\text{total number of simulated g values}} \tag{7.3a}$$

$$P_f = \frac{\text{number of times } g' \geq n}{\text{total number of simulated } g' \text{ values}} \tag{7.3b}$$

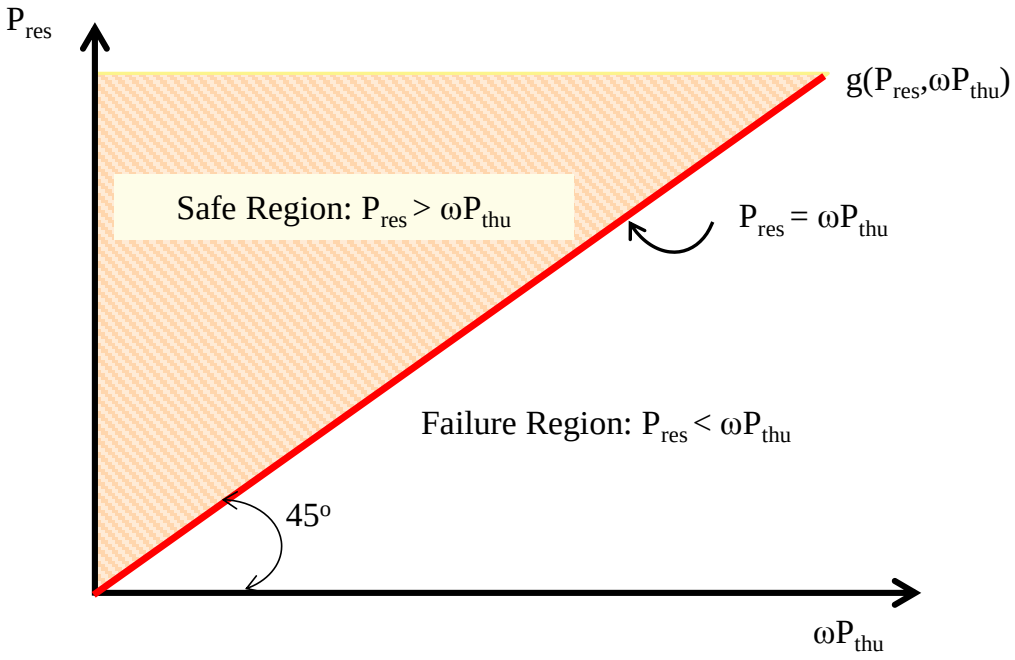

Figure 7.4: Representation of limit state function *g* (P_{res}, ωP_{thu}).

7.2.3 Random Variables and Distribution

For determination of the probability of failure of corroded members, different random variables are introduced. Each of the random variables has a probability distribution function either discrete or continuous. A suitable distribution of a random variable can be estimated from a set of available data for that variable. Most often normal and lognormal probability distributions are used. The random variables (input parameters) used in this study are: corrosion current density I_{corr}, yield strength of steel f_y, compressive strength of concrete f_c', the bar diameter, member size, clear concrete cover and eccentricity.

(a) Normal Distribution

The normal distributions are frequently used in engineering of random variables whose distributions are not known. The continuous probability density function for the normal (or Gaussian) distribution is defined as (Figure 7.5a):

$$\mathrm{P(x)} = \frac{1}{\sigma\sqrt{2\pi}} \mathrm{e}^{-\frac{(x-\mu)^2}{2\sigma^2}}, -\infty < \mathrm{x} < \infty \qquad (7.4)$$

where: μ is the mean of the distribution; σ is the standard deviation of the distribution and its variance is σ^2.

(b) Lognormal Distribution

It is a continuous distribution of random variables in which the logarithm of a variable has a normal distribution. The Lognormal distributions can be used to model a random

variable X where log(X) is normally distributed. The continuous probability density function for the lognormal distribution shown in Figure 7.5b is given as:

$$P(x) = \frac{1}{\sigma x\sqrt{2\pi}} e^{-\frac{(lnx-\mu)^2}{2\sigma^2}} \qquad x > 0 \tag{7.5}$$

where

$E(x) = e^{\mu+\sigma^2/2}$ is the mean of the distribution;

$V(x) = (e^{\sigma^2} - 1)e^{2\mu+\sigma^2}$ is the variance of the distribution.

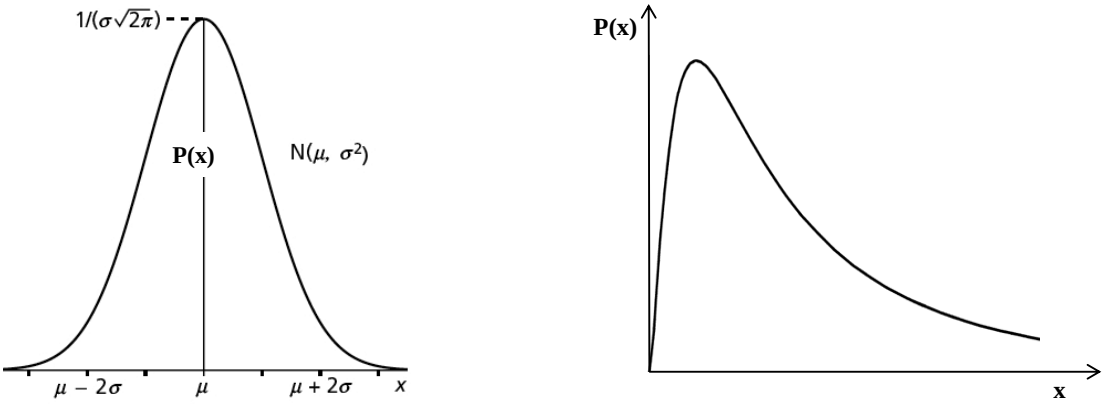

(a) Normal distribution (b) Lognormal distribution

Figure 7.5: Probability densities for the random variable.

The statistical parameters adopted or proposed by some researchers for several variables are given in Table 7.1.

Table 7.1: Statistical parameters by other researchers.

Variables	Mean (μ)	Coefficient of Variation (CV= σ/μ)	Distribution	Reference
f_c' (MPa)	26.2	0.18	Lognormal	Mirza et al. (1979)
f_y (MPa)	490 460	0.10	Lognormal	Mirza and MacGregor (1979) Val and Chernin (2009)
h (mm)	nominal	0.05	Normal	Val and Chernin (2009)
Initial diameter of steel reinforcement D (mm)	nominal	0.02	Lognormal	Enright et al. (1998)
Corrosion current density				
I_{corr} (μA/cm^2)	5	0.3	Normal	Stewart and Rosowsky (1998)
	1	0.2	Normal	Vu and Stewart (2000)
	3.0	0.1; 0.2 and 0.3	Normal	Bhargava et al. (2011)

7.2.4 Determination of Probability of Failure Using Proposed Strength Prediction Approach

The probability of failure or the reliability index of corroded columns and beam-columns has been numerically estimated by using Monte Carlo simulation (MCS). MCS approach is often used because the limit state function g is complex and it has several uncertain

parameters (random variables). The general procedures of estimating the probability of failure is shown in Figure 7.6. Figure 7.7 represents the flowchart for estimating the probability of failure by using Monte Carlo method.

The basic procedure is as follows:

1. Construct a limit state function, g
2. Define a statistical distribution for each random variable (input parameter) and a domain of possible inputs.
3. From the statistical distributions for the input parameters, generate inputs randomly over the domain.
4. Calculate $g = P_{res}(X) - \omega P_{thu}(X)$.
5. Repeat steps 3-4 until a sufficient number of g values have been generated.
6. Estimate the probability of failure (Eq. 7.3) or reliability index.

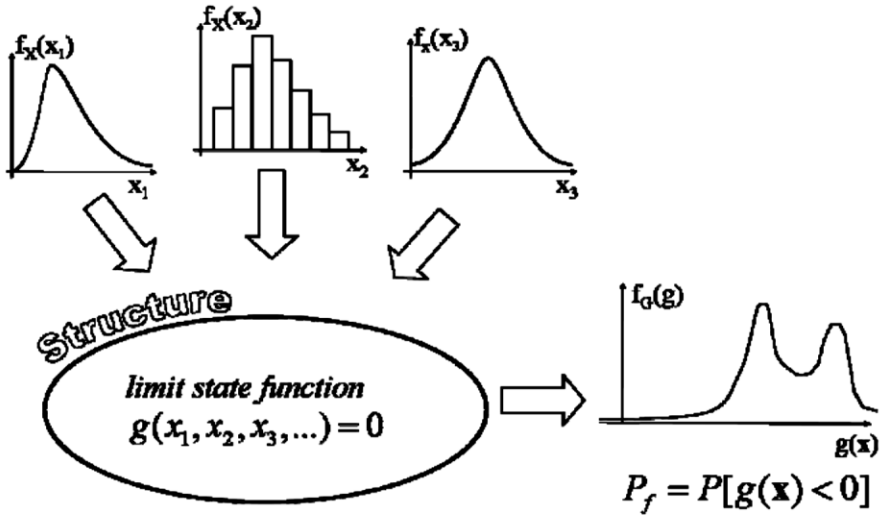

Figure 7.6: General procedure for estimating probability of failure of a structure with random parameters (Emhamed (2010)).

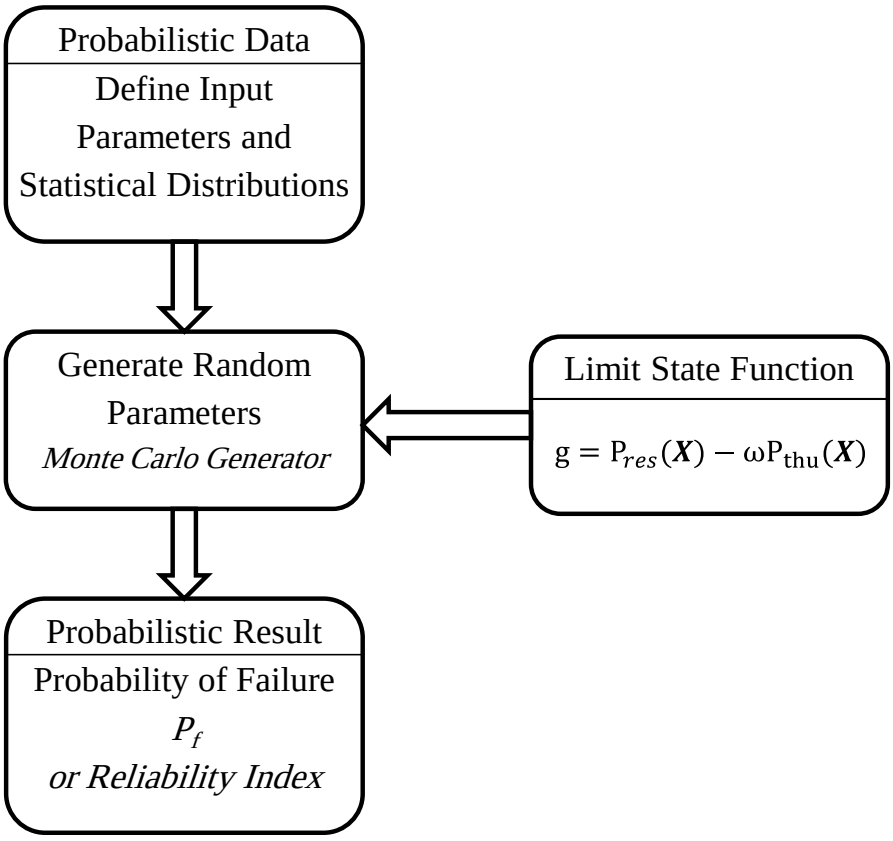

Figure 7.7: Flowchart representation for estimating the probability of failure by Monte Carlo simulation approach.

As an illustration of the procedure, the probabilities of failure of a column and a beam-column section were calculated using assumed data. The data considered in the examples are given in Table 7.2 with assumed statistical parameter for each variable. More than 1,000,000 random variables were generated to estimate the probability of failure.

Table 7.2: Assumed values of variables and their statistical parameters.

Variables	Mean (μ)	Coefficient of Variation (CV= σ/μ)	Distribution
f_c' (MPa)	30	0.18	Lognormal
f_y (MPa)	460	0.10	Lognormal
h (mm)	300	0.05	Normal
Initial diameter of steel reinforcement D (mm)	16	0.02	Lognormal
e/h	0.2	0.01	Normal
Clear concrete cover (mm)	40	0.05	Normal
Corrosion current density			
I_{corr} (μA/cm^2)	1.0	0.2	Normal
	1.5	0.2	Normal
	2.5	0.25	Normal
	5.0	0.3	Normal

The plot of probability of failure, P_f with T, determined from numerical simulation of limit sate function (Eq. 7.3a), is shown in Figure 7.8a for the column and in Figure 7.8b for beam-column which has an assumed eccentricity ratio of e/h = 0.20. It is observed that an early corrosion period would exist within which the probability of failure is virtually nil. This meaning the member's residual load capacity is sufficient to exclude any probability of failure. Likewise, as P_f increases with T, a time exists beyond which the corrosion is large enough to imply 100 % probability of failure. For a given problem

with all necessary data, P_f - T plot as shown in Figure 7.8, can be constructed for chosen value of ω or n ($n = 1/\omega$) to statistically present prediction of failure.

The two factors that affect P_f at a given mean, I_{corr}, are T and n. It is of interest to have probability plots for given T from which, at a value of P_f, decided in an assessment problem, the required value of n can be obtained. Figure 7.9 shows such plots for different values of T using the data in Table 7.2, for the example column and beam-column. The plots in Figure 7.9 have multiple uses as follows:

(a) For a chosen P_f, and corrosion period T, the required value of n can be determined.

(b) For chosen value of n and P_f, the corresponding critical time T can be determine for rehabilitation or repair.

For example, for I_{corr} = 1.0 μA/cm^2 and e/h = 0.2, if P_f = 0.22 and T = 8 years, the minimum value of n = 1.2 (ω = 0.83). If n = 1.35 and the acceptable probability of failure is 0.1, the maximum period is 12 years.

The histogram or the distribution of limit state of safety function of reinforced concrete columns and beam-columns, g, obtained from Monte Carlo simulation, is plotted in Figure 7.10 for different value of n. $g(\boldsymbol{X})$ values are normalized with respect to its maximum value which is 3500 kN and 1321 kN for column and beam-column, respectively . As expected from Figure 7.10, the positive values of g and consequently lower value of P_f can be achieved by increasing the value of n.

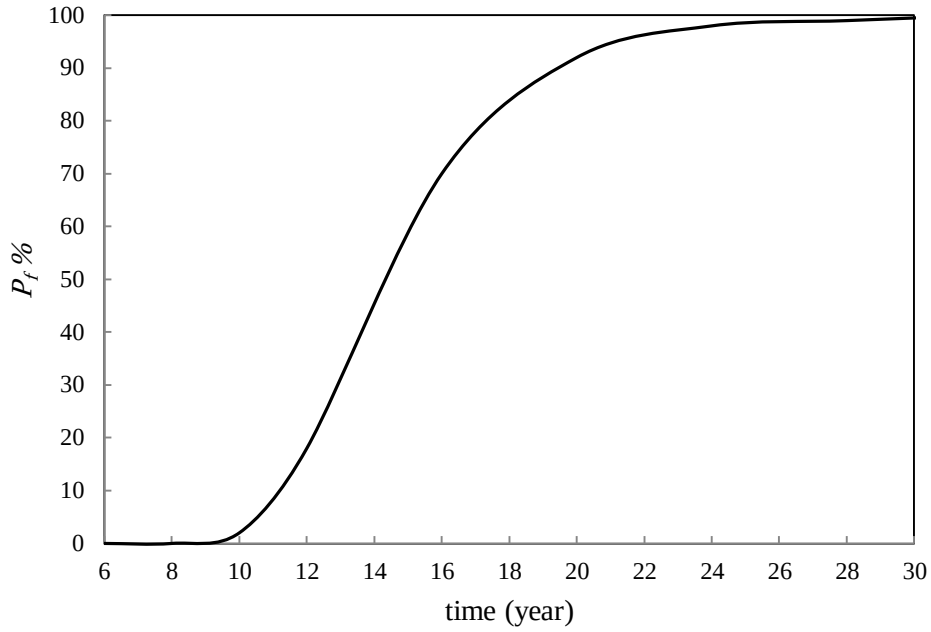

(a) Column (n= 1.4)

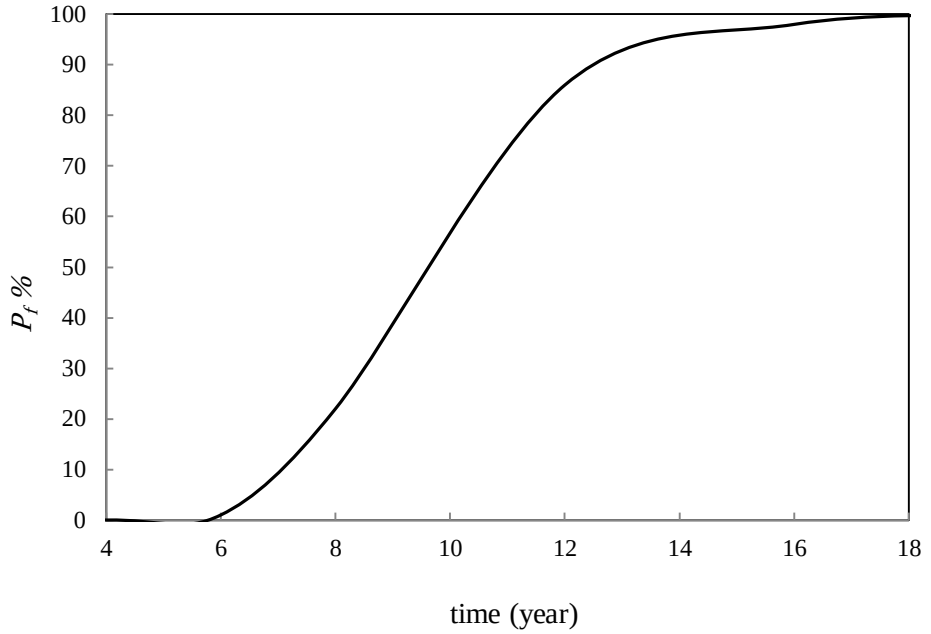

(b) Beam-column (n =1.2 and e/h =0.2)

Figure 7.8: Evolution of probability of failure of the corroded column and beam-column for mean corrosion current density 1 μA/cm^2.

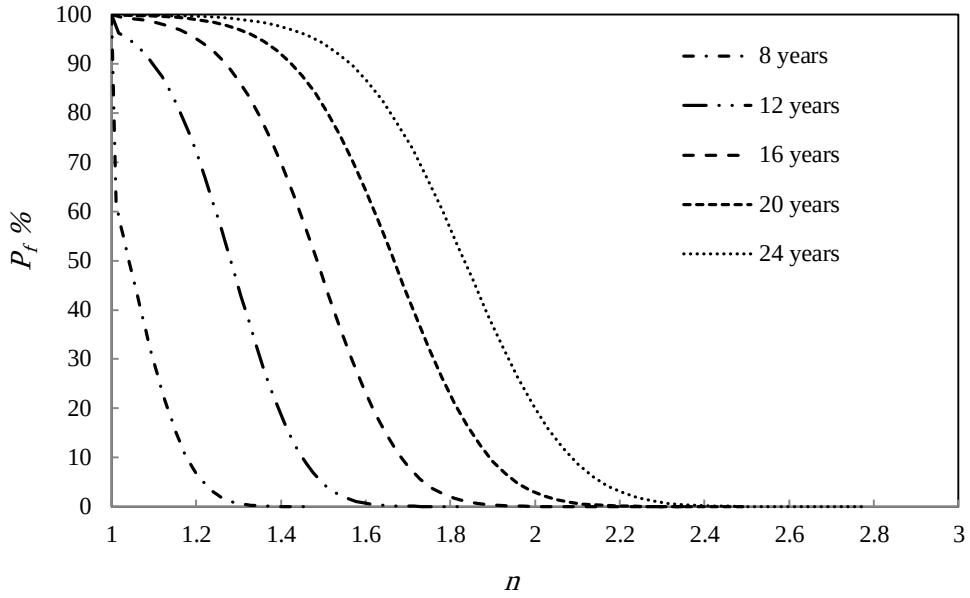

(a) Column

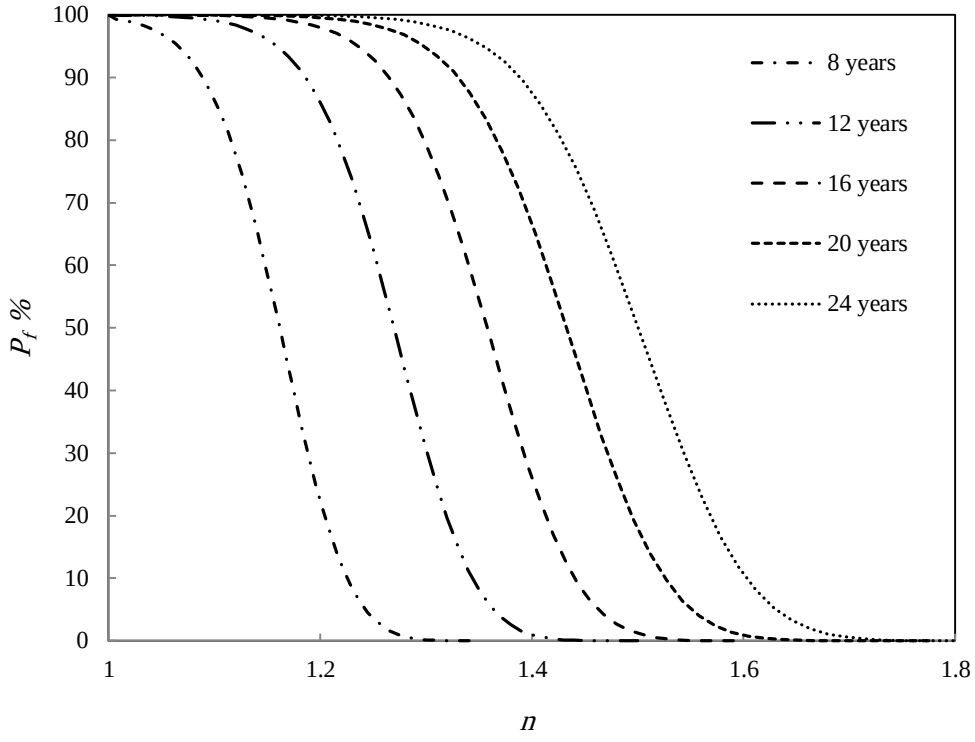

(b) Beam-column (e/h =0.2)

Figure 7.9: Evolution of probability of failure of the corroded column and beam-column for mean corrosion current density 1 μA/cm^2 and different values of T.

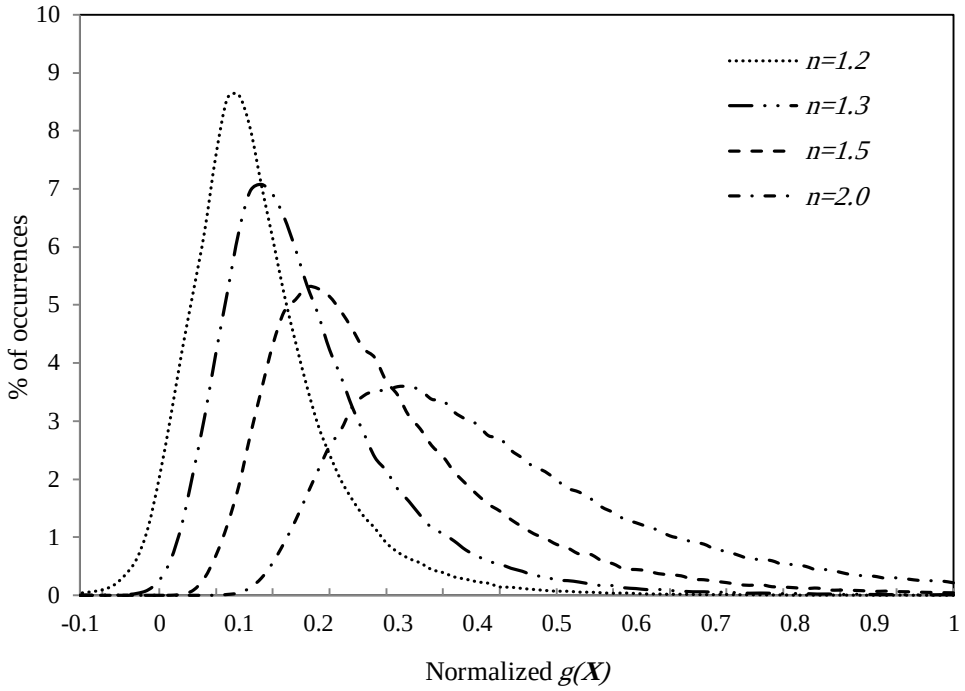

(a) Column

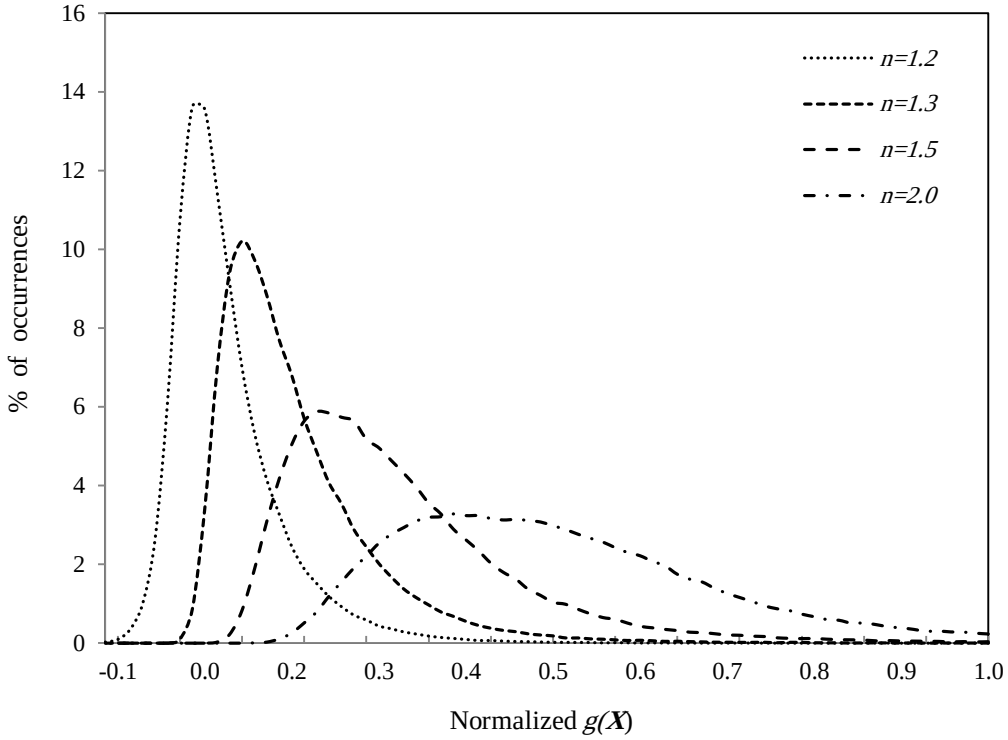

(b)Beam-column (e/h = 0.25)

Figure 7.10: Reliability function (g) for different values of factor of safety n, mean corrosion current density 1 μA/cm^2 and time T= 8 years.

7.2.5 Sensitivity Analysis

The sensitivity analysis of the model's input parameters is performed to identify the most important parameters affecting the probability of failure. The sensitivity with respect to change in the mean of the random variables is examined by varying the mean values over a wide range of values. The five parameters are I_{corr}, h, D, e/h and f_c'. Figures 7.11-7.15 show the effect of these parameters on P_f. As it can be seen from Figure 7.11, for a given value of n, the probability of structural failure increases as the corrosion current density I_{corr} increases. As expected, the change in mean value of cross-section dimensions of column and beam-column members has more effect on the probability of failure of columns than that for beam-columns (Figure 7.12). This due to the fact that the core of concrete, which is not affect by the corrosion, increases with increasing the cross-section dimensions of column and accounts for a high percentage of the axial load capacity. Figures 7.13 and 7.14 show that the probability of failure of corroded columns and beam-columns marginally changes with change the mean values of compressive strength of concrete f_c' and the bar diameter. The effect of e/h on the probability of failure of corroded beam-columns is plotted in Figure 7.15. It is noted that for a given value of n, the probability of failure of corroded beam-columns decreases as the ratio of e/h increases. From plots shown in Figures 7.11 to 7.15, it is observed that the corrosion current density I_{corr} and cross-section dimensions are the most important factors that affect the probability of failure for columns. However, the probability of failure of beam-columns is sensitive to change the value of the corrosion current density I_{corr} and the ratio of e/h.

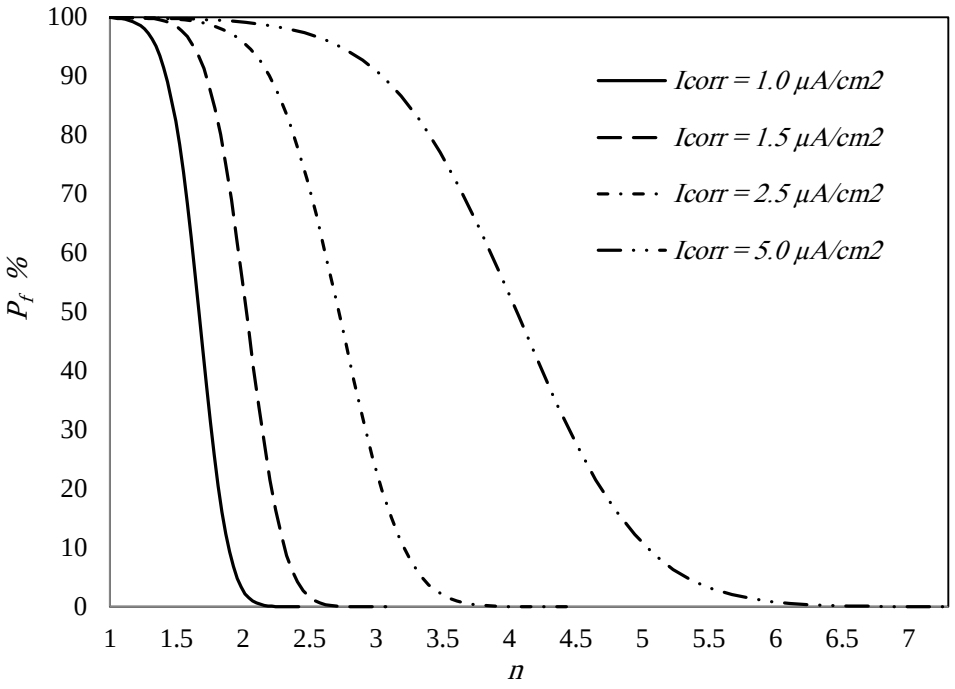

(a) Column

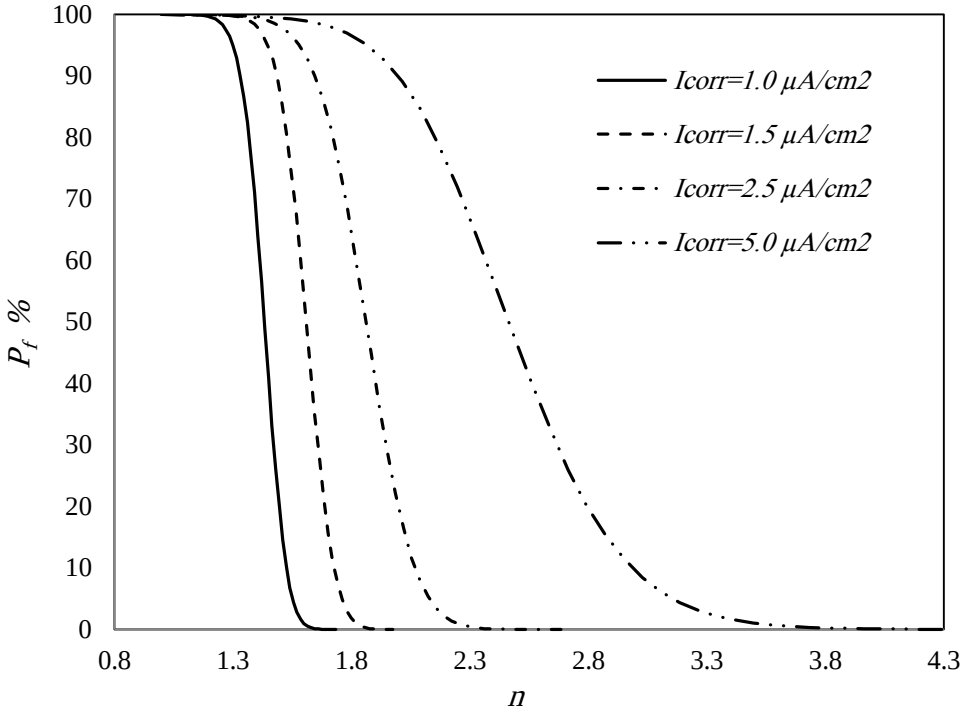

(b) Beam-column (e/h =0.2)

Figure 7.11: Evolution of probability of failure of the corroded column and beam-column for different values of corrosion current density (T = 20 years; h = 300 mm; D = 16 mm; f_c'= 30 MPa and f_y = 460 MPa).

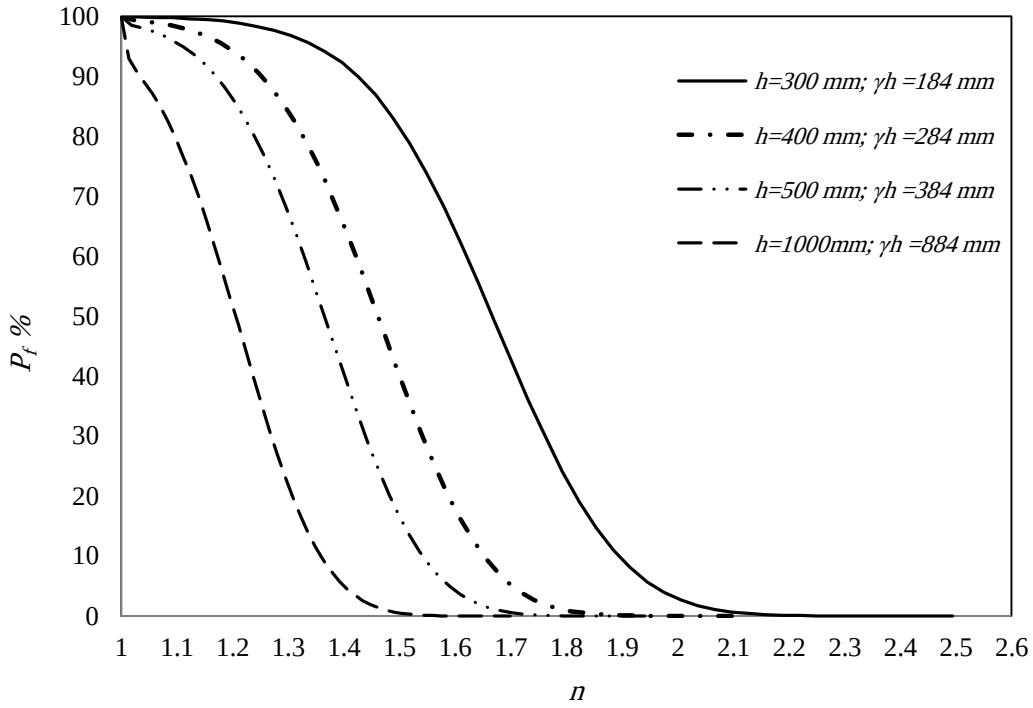

(a) Column

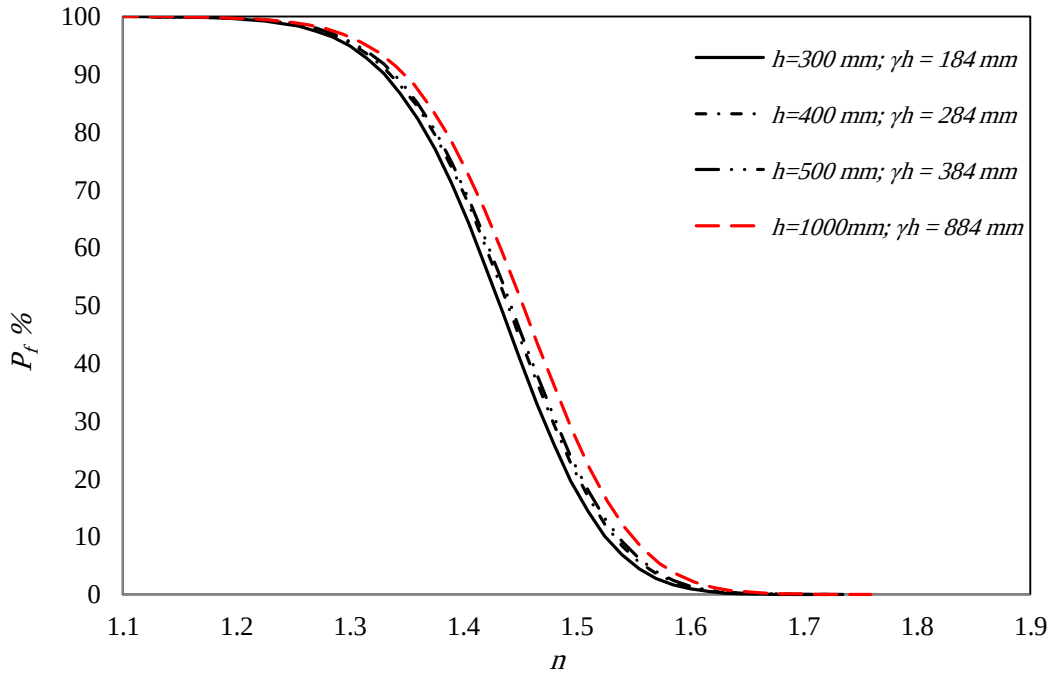

(b) Beam-column (e/h =0.2)

Figure 7.12: Evolution of probability of failure of the corroded column and beam-column for different values of cross-section (T= 20 years; I_{corr} = 1µA/cm^2; D = 16 mm; f_c'= 30 MPa and f_y = 460 MPa).

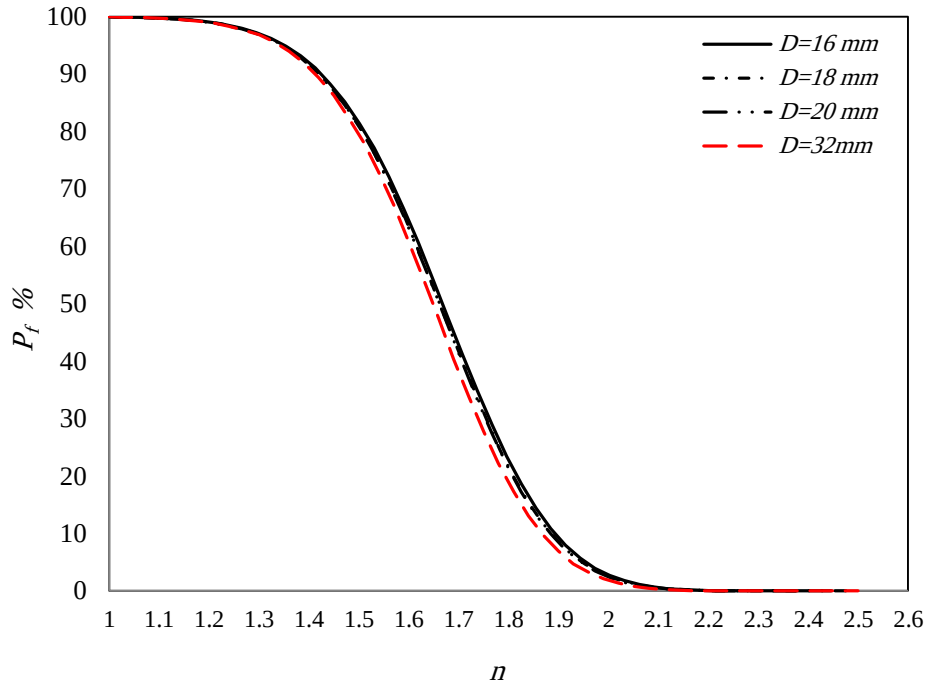

(a) Column

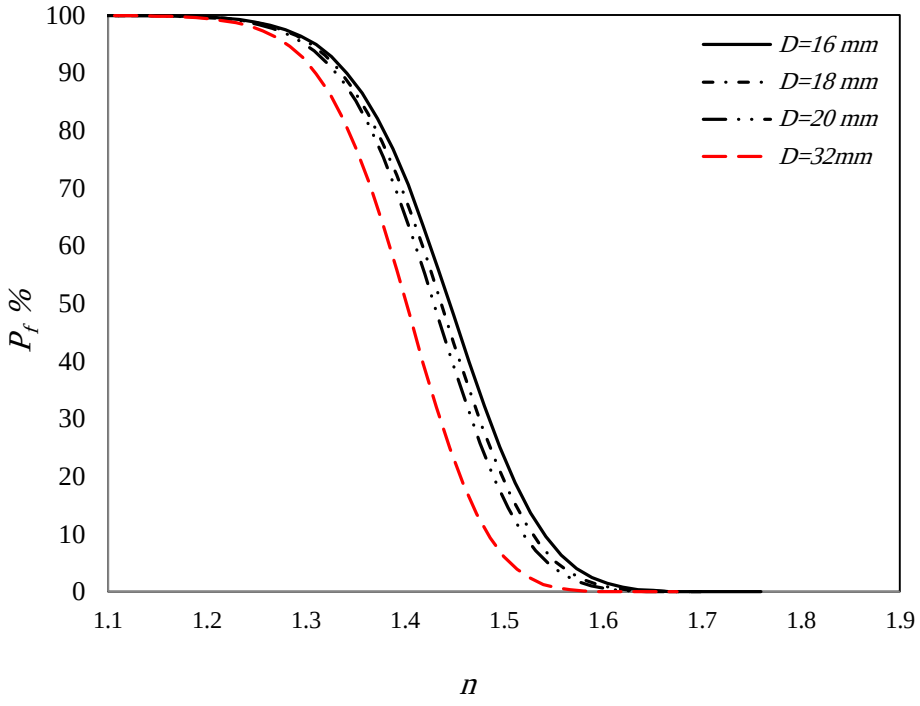

(b) Beam-column (e/h =0.2)

Figure 7.13: Evolution of probability of failure of the corroded column and beam-column for different values of diameter bar (T = 20 years; I_{corr} = 1µA/cm^2; h = 600 mm; f_c'= 30 MPa and f_y = 460 MPa).

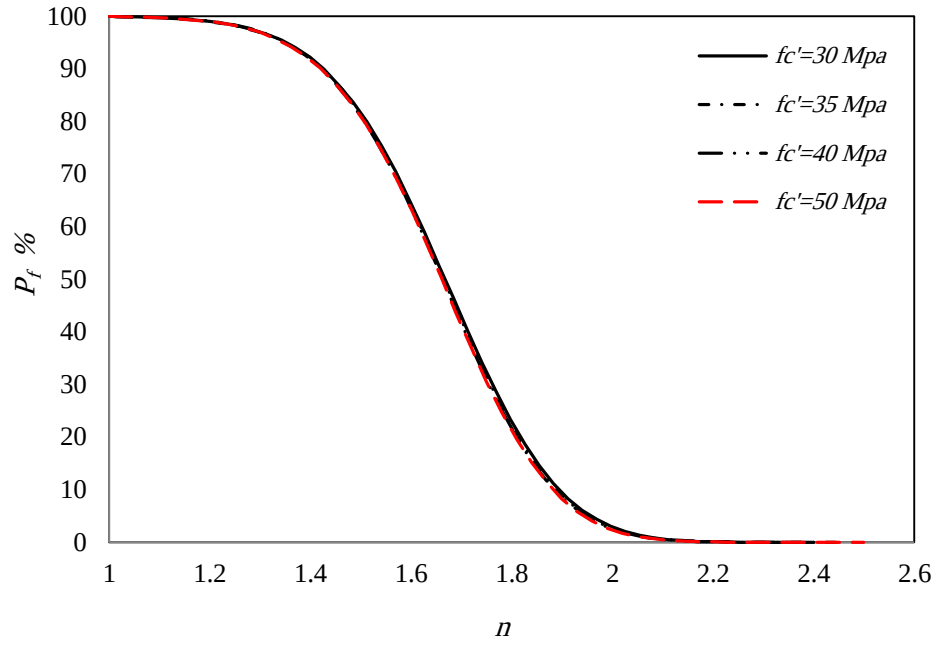

(a) Column

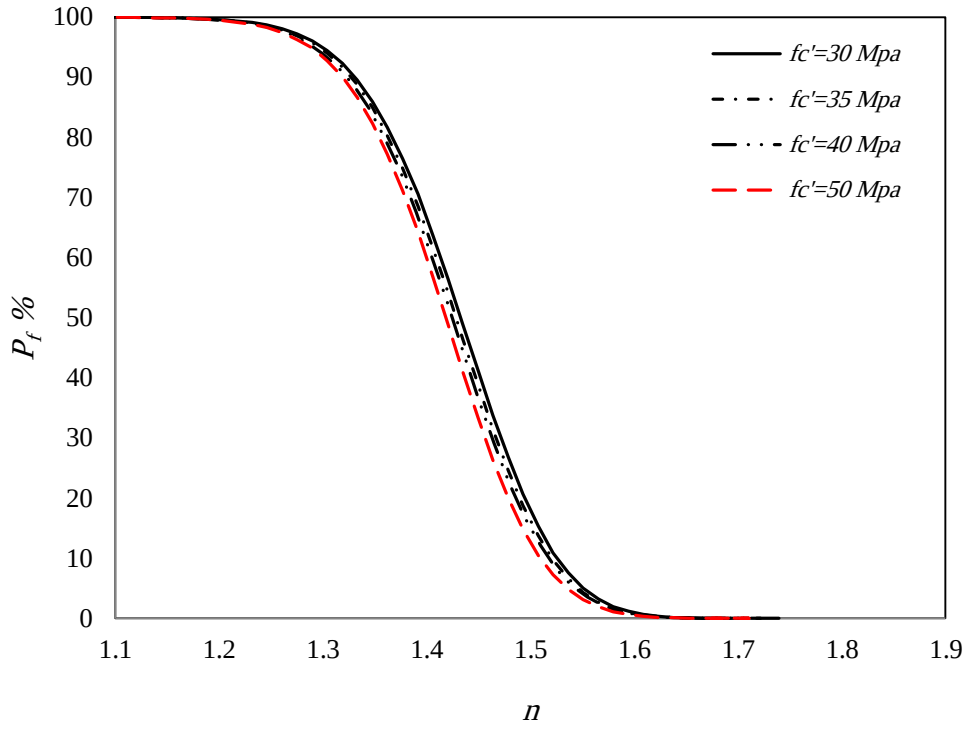

(b) Beam-column (e/h =0.2)

Figure 7.14: Evolution of probability of failure of the corroded column and beam-column for different values of concrete strength fc' (T = 20 years; I_{corr} = 1µA/cm^2; D = 16 mm; h= 300 mm and f_y = 460 MPa).

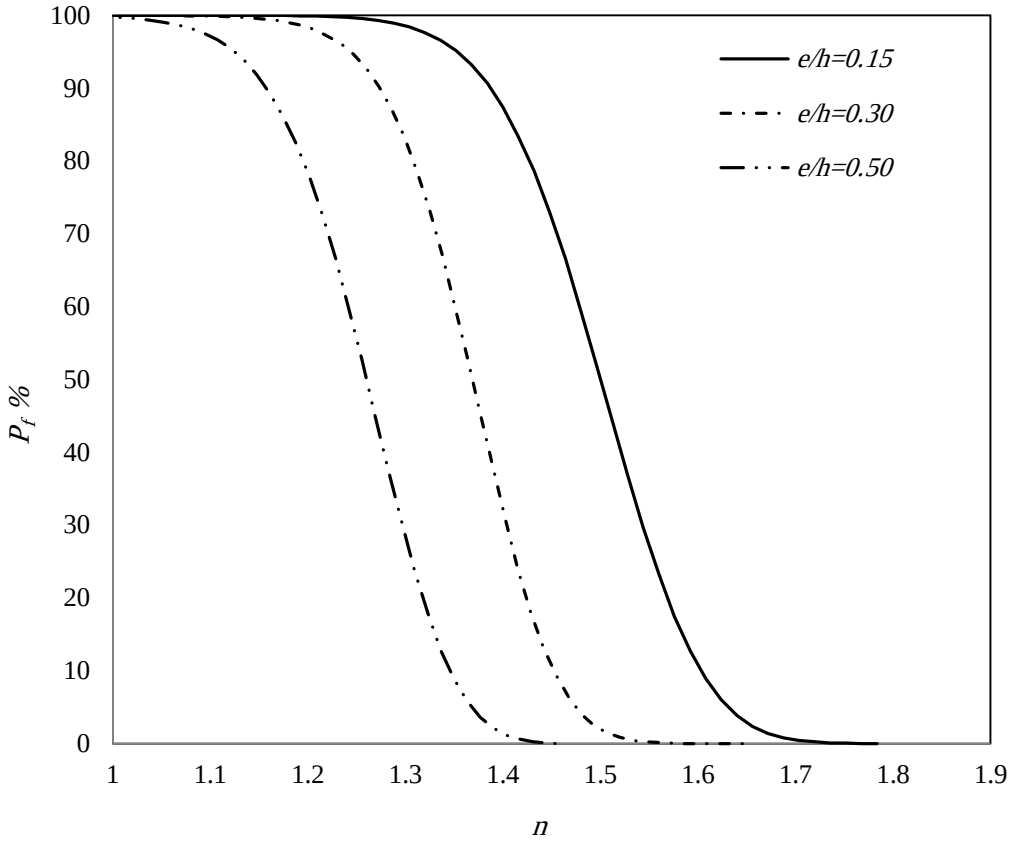

Figure 7.15: Evolution of probability of failure of the corroded beam-column for different values of *e/h* (T = 20 years; I_{corr} = 1µA/cm^2; D = 16 mm; h= 300 mm f_c'= 30 MPa and f_y = 460 MPa).

7.2.6 The Reliability Index

Structural performance can be determined by means of reliability index β, or the probability of failure. The probability of failure, P_f that the undesired performance will occur was determined by using MCS. The reliability index β, for limit state function defined by Eq. (7.1) can also be estimated as follows:

If P_{res} and the required strength demand, $Q = \omega P_{thu}$, are assumed to be normally distributed then

$$\beta = \frac{\mu_{P_{res}} - \mu_Q}{\sqrt{\sigma^2_{P_{res}} + \sigma^2_Q}} \tag{7.6}$$

$$\beta = -\left[\Phi^{-1}(P_f)\right] \tag{7.7}$$

where:

$\mu_{P_{res}}$ and μ_Q are the mean of the predicted strength and the required strength Q, respectively; $\sigma_{P_{res}}$ and σ_Q are the standard deviation of the predicted strength and the required strength Q, respectively and $\Phi(.)$ represents the cumulative distribution function (CDF) of the standard normal random variable.

Table 7.3 presents the reliability index β of corroded columns and beam-columns that approximated by using Eq. (7.7) for different values of n as given in Figure7.10.

Table 7.3: Estimated value of β of columns and beam-columns at T = 8 years.

n	β	
	Column	Beam-column
1.2	1.69	1.72
1.3	2.65	3.83
1.5	4.42	∞
2.0	∞	∞

Table 7.4 gives the reliability index β for different values of probability of failure P_f.

Table 7.4: Relation between the probability of failure P_f and reliability index β.

P_f	β
10^{-1}	1.28
10^{-2}	2.33
10^{-3}	3.09
10^{-4}	3.71
10^{-5}	4.26
10^{-6}	4.75
10^{-7}	5.19
10^{-8}	5.62
10^{-9}	5.99

Nowak and Kaszynska (2011) reported the recommended values of the target reliability index for beams in flexure and shear, slabs and columns. The target reliability index β should be higher for shear failure of concrete than that for flexure failure as the shear failure is a more brittle failure. Since the failure of columns can be more dangerous than beam failure, the target reliability index β should be higher. Table 7.5 lists the recommended values of the target reliability indices for three importance levels based on Nowak and Kaszynska (2011).

Table 7.5: Recommended target reliability indices for different importance levels (Nowak and Kaszynska, 2011).

Importance	New Design	Existing	Historical
Low priority	3.00 - 3.50	2.00 -2.50	3.25 - 3.50
Medium priority	3.50 - 4.00	2.50 - 3.00	3.50 - 4.50
High priority	3.75 -4.50	2.75 - 3.50	3.75 - 4.75

In general, if the reliability index is too small, the probability of failure P_f is large indicating safety problems, even to an extent that structural collapse is possible. However, if the reliability index is too large, the corrosion damage has to be minor so that ω is relatively small (bigger n).

7.3 Probability of Failure Using Finite Element Analysis

7.3.1 The ANSYS Probabilistic Design System (PDS)

In this thesis, an effort was made to carry out probability of failure of Eq. 7.1 by using the finite element analysis software ANSYS and PDS (probabilistic design) module. Both values of P_{res} and P_{thu} in Eq. 7.1 were determined by using the FEA. In ANSYS, the PDS is based on the Advanced Parametric Design Language (APDL). This APDL can be used to parametrically build a finite element model and to solve probabilistic problems. Furthermore, the APDL can represent the input variables as well as the result parameters in arithmetic expressions and the possibility to use do-loops and if-then-else constructs (Reh S et al., 2005). The use of APDL language is an essential tool for reliability analysis governed by the MCS since FEM model needs to be repeated thousands of times with

changing the input variables. This is almost impossible manually using Graphical User Interface (GUI).

In general, the utilization of the finite element model (FEM) to carry out the reliability analysis of column and beam column member is a rather complicated task and represents a challenge itself especially for a 3-D non-linear finite element model as each simulation step needs more than three hours. To perform reliability analysis, the 3-D finite element model of column and beam-column member was constructed by using the APDL. The FEM model for 3-D member assessment model was written to have capabilities to automatically and randomly repeat the selected input variables for each Monte Carlo simulation step. Each simulation step includes the construction of the nodes and elements, selection of the boundary condition, application of load, and computation the real constant, material properties and reliability function analysis (Konecný, 2007).

The use of MCS in finite element is illustrated for a column shown in Figure 7.16 and computed by using the following assumed data:

Cross-section: 180 x 180 mm

Main reinforcement: 4-20 mm dia. bars

Effective cover = 60 mm

Concrete compressive strength, f_c' = 32 MPa

Yield strength of steel, f_y = 555 MPa

T = 12 years.

Maximum permitted reduction factor ω = 0.714

7.3.2 Random Input Variables

For simplicity and illustration, the model was simulated by considering only 2 parameters that are regarded as random input variables. These random variables are I_{corr} and diameter of main reinforcement D as given in Table 7.6. Figure 7.17 shows the distribution of the random variables I_{corr} and D.

Table 7.6: Random input variable specifications used in finite element.

Variables	Mean (μ)	Coefficient of Variation (CV= σ/μ)	Distribution
Initial diameter of steel reinforcement D (mm)	20	0.02	Lognormal
Corrosion current density			
I_{corr} (µA/cm^2)	1	0.2	Normal

7.3.3 Cumulative Distribution of *g(X)*

The cumulative distribution curve of the limit state function ***g(X)*** is plotted in Figure 7.18 by using the sample size as the number of points. For Monte Carlo simulation methods, a confidence level of 95% is used to plot confidence bounds around the cumulative distribution function.

7.3.4 Sensitivity Plot

The sensitivity plot gives the valuable information about the effect of uncertainties of the input variables (I_{corr} and D) to the limit state function ***g(X)***. In Figure 7.19, the input

variables are divided into two groups: those that are significant and those that are insignificant for the output ***g(X)***. It is shown that the important variable is the I_{corr} as expected.

7.3.5 Scatter Plot of *g(X)*

The scatter plot in Figure 7.20 shows that the relationship between the ***g(X)*** and I_{corr}. It can be seen that a linear correlation between ***g(X)*** and I_{corr} is obtained for this example.

7.3.6 Probability Result of Response Parameter *g(X)*

The probability of ***g(X)*** to be smaller or larger than a certain limit value can be obtained from ANSYS. The probability of failure of this column for the assumed data is equal to 1.

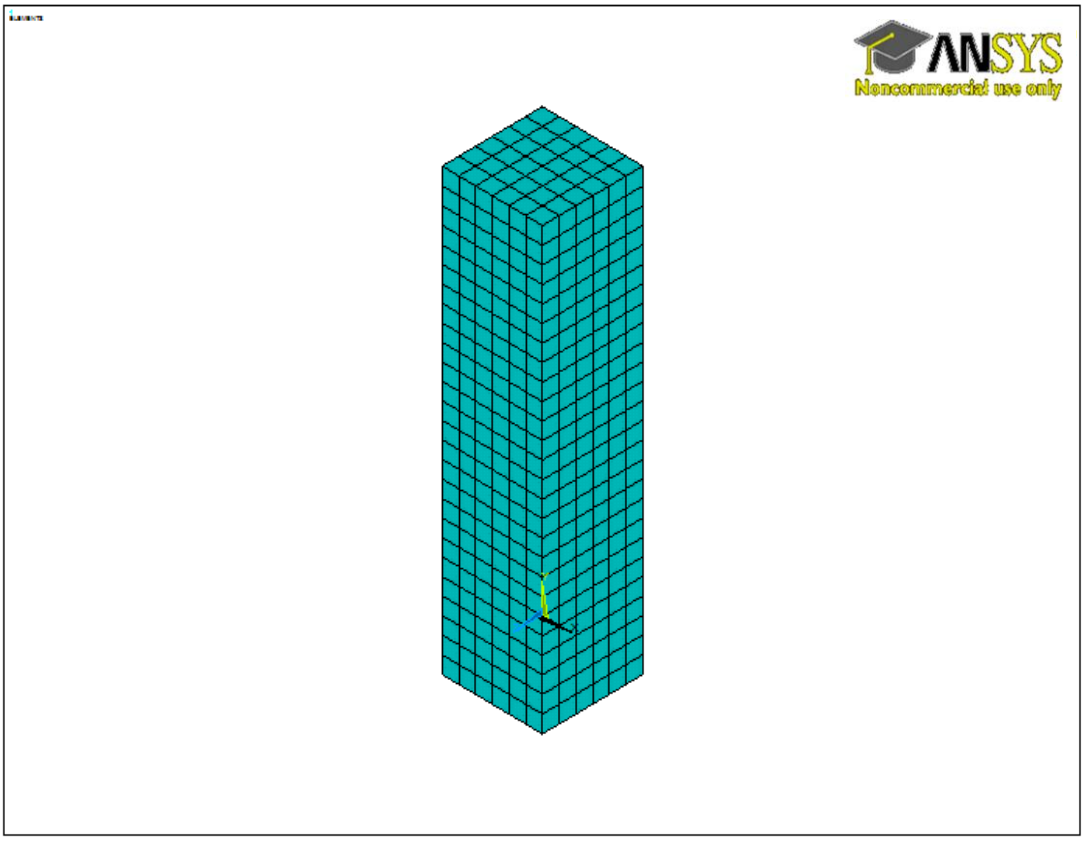

Figure 7.16: Column model used in probability analysis in finite model.

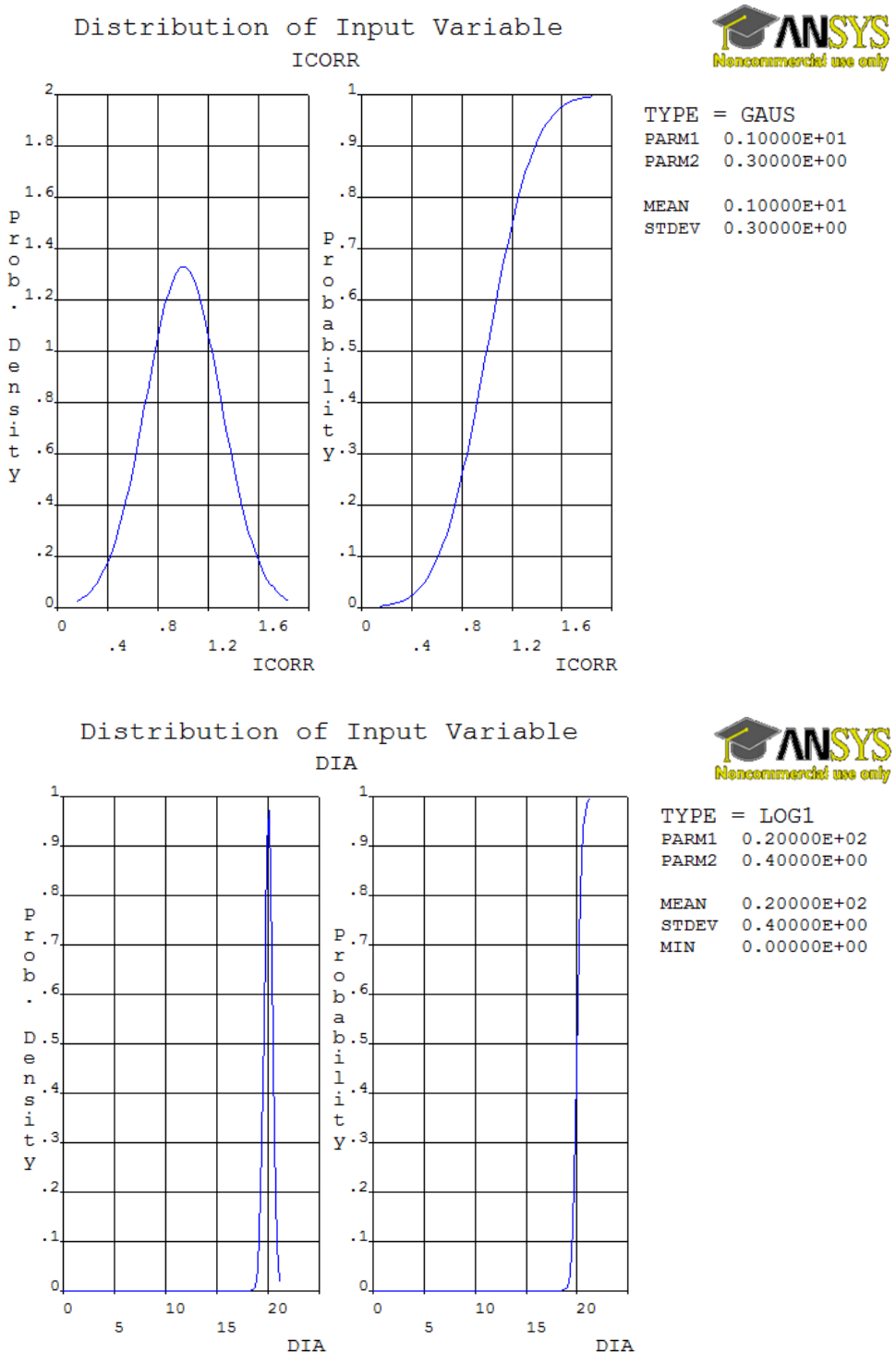

Figure 7.17: Distribution of input variables I_{corr} and D.

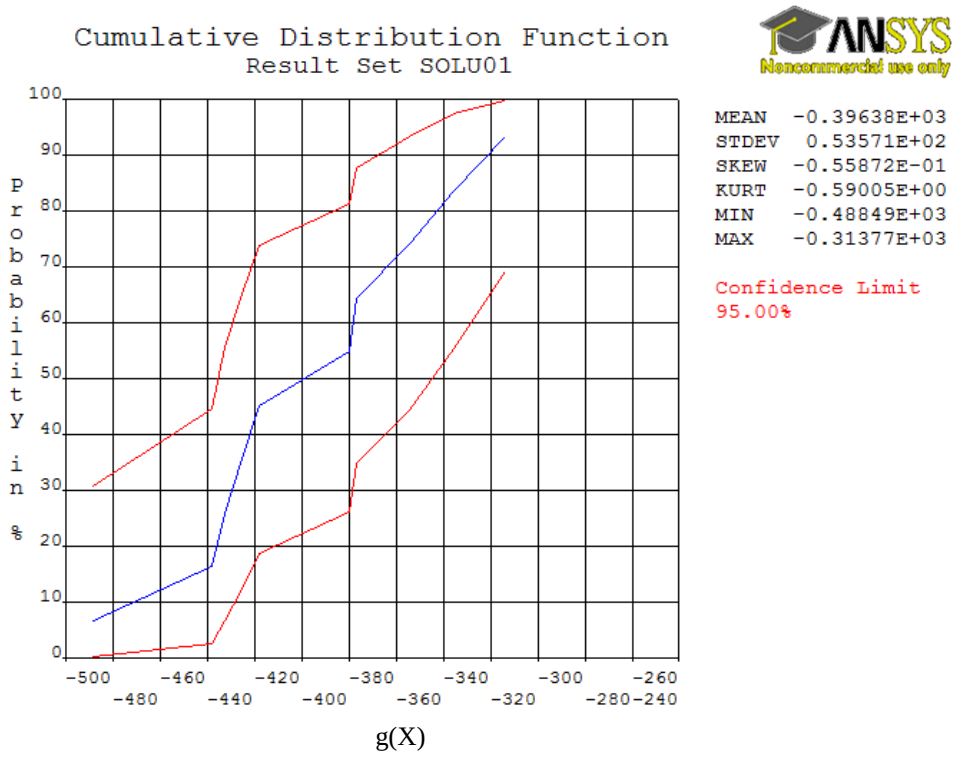

Figure 7.18: Cumulative distribution of limit state function *g(X)*.

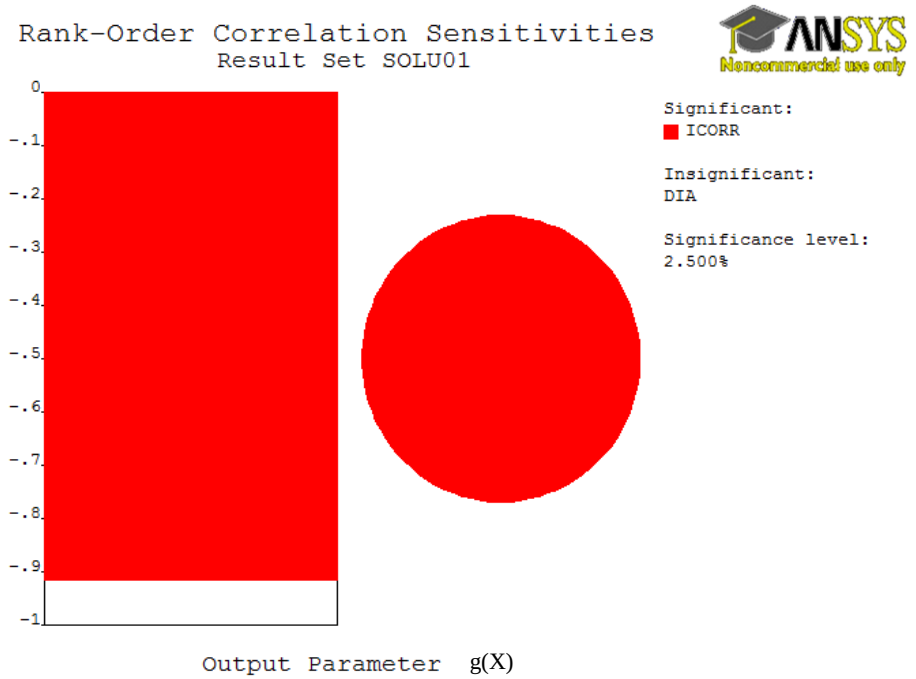

Figure 7.19: The results from the sensitivity analysis of the I_{corr} and D in limit state function *g(X)* for significance level 2.5%.

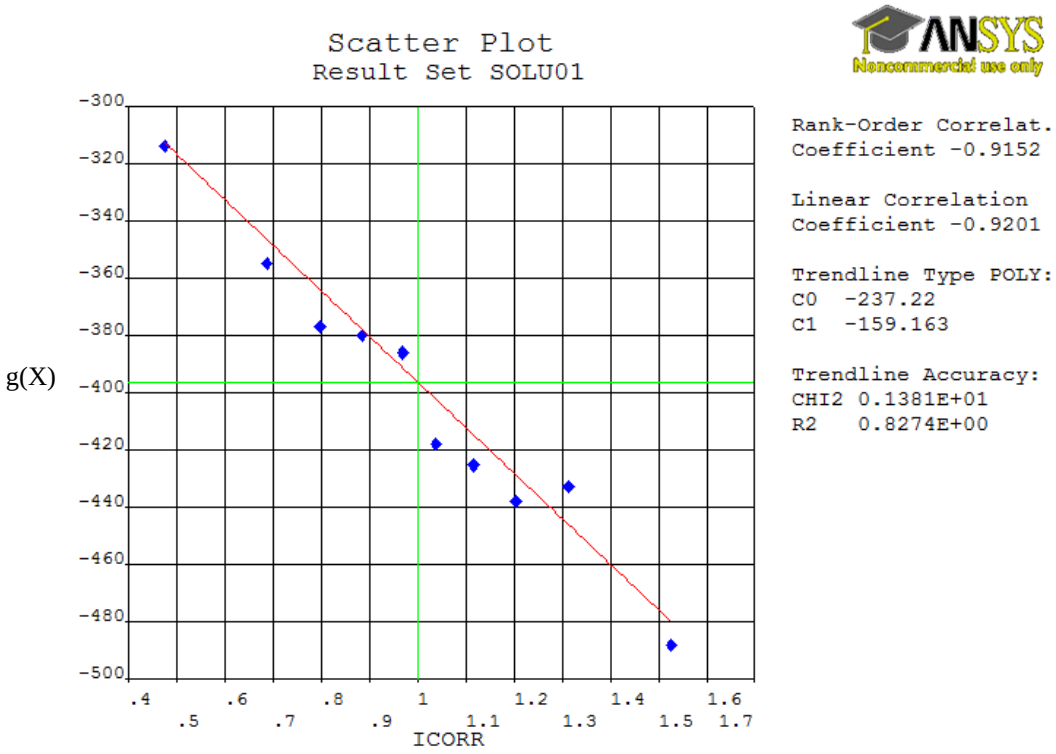

Figure 7.20: Scatter plot of *g(X)* versus I_{corr} (µA/cm^2).

CHAPTER 8

CONCLUSIONS

In this experimental study, a total of 82 reinforced concrete columns and beam-columns specimens were tested to study the effect of corrosion damage and develop predictive model for the estimation of the residual strength of corroded columns and beam-columns. Out of 82 specimens, 64 specimens were used in developing the predictive model, 4 specimens were used for verification and the remaining were repeated specimens. The following variables were used: two diameters, two cross-sections, three different corrosion durations and three different eccentricities for eccentric loading for beam-column specimens. A two-step analytical approach has been developed on the basis of experimental correlation to predicate residual strength along with a finite element modeling for estimation of strength. Using Monte Carlo simulation of the predictive model, probability of failure of corroded column and beam-column has been estimated.

8.1 Conclusions

Based on the findings of this study, the following conclusions are drawn:

1. Corrosion damage leads to reduction in strength of reinforced concrete columns and beam-columns. The significant factor of corrosion damage is $I_{corr}T$, the higher values of which result in higher reduction in the strength of columns and beam-columns.

2. The reduction in the load carrying capacity of a column relatively is more than that of an eccentrically loaded column (beam-column) for a given $I_{corr}T$, as the crack-induced damage to concrete cover significantly reduces the contribution of concrete strength to load capacity of a column.
3. The residual strength of a corroded column or beam-column cannot be predicted by using only the reduced area of reinforcement A_s' from Eq. 6.3, as the residual strength is also affected by other corrosion-induced damaging effects.
4. The proposed two-step approach for prediction of residual strength using the suggested correction factors, α_1 for columns and α_2 for beam-columns, appear to yield satisfactory results that show acceptable agreement with test data and other available information. This lends confidence in the applicability and acceptability of the proposed method for prediction of residual strength or loss of strength for corroded columns and beam-columns.
5. The proposed finite element modeling of corroded columns or beam-columns using modification of the concrete strength due to cracking of concrete, the reduction of steel area, modification of bond-slip properties, the reduction in yield strength of steel and its modulus of elasticity appears to predict the load with reasonable accuracy and can therefore serve as an acceptable analytical tool for estimation of residual strength.
6. Probability of failure and hence reliability can be estimated using Monte Carlo simulation (MCS).

7. The reliability analysis using Monte Carlo simulation (MCS) shows that the corrosion current density I_{corr} and cross-section dimensions are the most significant factors that affect the probability of failure of corroded columns. I_{corr} and *e/h* are the two key variables that have significant effect on the probability of failure of corroded beam-columns.
8. The reliability analysis using 3-D finite element technics with non-linear analysis is time consuming.

8.2 Suggestion for Future Research

The following suggestions can be made for further research in this area:

1. This work can be extended in a future research to capture the effect of dynamic loading on the corroded columns and beam-columns.
2. Further research is needed to study the effect of the clear covers relative to size of the column on the residual strength.
3. Further study on the effect of biaxial bending and compression on the corroded beam-columns should be carried out.
4. In this experimental study, the corrosion damage of reinforced concrete columns and beam-columns was achieved by using the accelerated corrosion technique. On the other hand, in real structures, the corrosion damage of the member is different. It would be desirable to collect data from natural corrosion and to check the validity of the proposed methods.

References

1. Aboutaha R. S.;, "Guide for maintenance, and rehabilitation of concrete bridge components with FRP composites-research into practice," TIRC & NYSDOT, NY, USA, 2004.

2. ACI 318-08, American Concrete Institute, Building Code Requirements for Structural Concrete, *ACI*, Farmington Hills, Mich, USA, 2008.

3. Al-Gohi, B. H.;, "Time-dependent modeling of loss of flexural strength of corroding RC beams," *M.S. Thesis*, King Fahd Univ. of Petroleum & Minerals, May. 2008.

4. Amleh, L.; and Mirza, S.;, "Corrosion influence on bond between steel and concrete," *ACI Structural Journal*, vol. 96, no. 3, pp. 415-423, 1999.

5. Almusallam, A. A.; Al-Gahtani, A. S.; Aziz, A. R.; and Rasheeduzzafar;, "Effect of reinforcement corrosion on bond strength," *Construction and Building Materials*, vol.10, no. 2, pp. 123-129, 1996.

6. Almusallam, A. A.;, "Effect of degree of corrosion on the properties of reinforcing steel bars," *Construction and Building Materials*, vol.15, no.8, pp. 361-368, 2001.

7. Al-Sulaimani, G. J.; Kaleemullah, M.; Basunbul, I. A.; and Rasheeduzzafar;, "Influence of corrosion and cracking on bond behavior and strength of reinforced concrete members," *ACI Structural journal*, vol. 87, no. 7, pp. 220-231, 1990.

8. Apostolopoulos, C. A.; Papadopoulos, M. P.; and PantelakisSp, G.;, "Tensile behavior of corroded reinforcing steel bars BSt 500s," *Construction and Building Materials*, vol.20, no.9, pp. 782–789, 2006.

9. Araújo M. J.;, "Probabilistic analysis of reinforced concrete columns," *Advances in Engineering Software*, vol.32, no.12, pp. 871- 879, 2001.

10. Arun, C. O.; and Pillai, T. M. M.;, "Reliability studies of deteriorating reinforced concrete flexural members," *Journal of Institution of Engineers* (India), vol. 86, pp. 139-143, 2006.

11. ASTM G 1;, "Standard Practice for Preparing, Cleaning and Evaluating Corrosion Test Specimens," *ASTM International*, West Conshohocken, Pa., 1990.

12. Auyeung, Y.; Balaguru, P.; and Chung, L.;, "Bond behavior of corroded reinforcement bars," *ACI Materials Journal*, vol. 97, no. 2, pp. 214-220, Mar.-Apr. 2000.

13. Azad, A. K.; and Ahmad, S.;, "A study of the size-effect of corroded reinforced concrete beams in prediction of residual strength," *Final Report, SABIC 2005/03*, KFUPM, JUL 2007.

14. Azad, A. K.; Ahmad, S.; and Azher, S. A.;, "Residual strength of corrosion-damaged reinforced concrete beams," *ACI Materials Journal*, vol. 104, no. 1, pp. 303-310, Jan.- Feb. 2007.

15. Azad, A. K.; Ahmad, S.; and Al-Gohi, B.;, "Flexural strength of corroded reinforced concrete beams," *Magazine of Concrete Research*, vol. 62, no. 6, pp. 405-414, Jun. 2010.

16. Aziz, A. R.;, "Reduction in bond and the strength of slabs due to corrosion of reinforcement," *M.S. Thesis*, King Fahd University of Petroleum and Minerals, Jun. 1994.

17. Azher, S.A.;, "Prediction model for the residual flexural strength of corroded reinforced concrete beams," *M.S. Thesis*, King Fahd Univ. of Petroleum & Minerals, Jan. 2005.

18. Ballim, Y.; and Reid, J. C.;, "Reinforcement corrosion and deflection of RC beams- an experimental critique of current test methods", *Cement and Concrete Composites*, vol. 25, no. 6, pp. 625-632, 2003.

19. Berra, A.; Castellani, D.; Coronelli, S.; Zanni, and Zhang, G.;, "Steel-concrete bond deterioration due to corrosion: finite-element analysis for different confinement levels," *Magazine of Concrete Research*, vol. 55, no. 3,pp. 237-247, 2003.

20. Bhargava, K.; Ghosh, A. K.; Mori, Y.; and Ramanujam, S.;, "Suggested empirical models for corrosion-induced bond degradation in reinforced concrete," *Journal of Structural Engineering*, vol.134, no. 2, pp. 221-231, Feb. 2008.

21. Bhargava, K.; Ghosh, A. K.; Mori, Y.; and Ramanujam, S.;, "Model for cover cracking due to rebar corrosion in RC structures," *Engineering Structures*, vol. 28, no. 8, pp. 1093-1109, 2006.

22. Bhargava, K.; Mori, Y.; and Ghosh, K. A.;, "Time-dependent reliability of corrosion-affected RC beams-Part 1: Estimation of time-dependent strengths and associated variability," *Nuclear Engineering and Design*, vol. 241, no.5,pp. 1371–1384, 2011.

23. Bhargava, K.; Mori, Y.; and Ghosh, K. A.;, "Time-dependent reliability of corrosion-affected RC beams-Part 2: Estimation of time-dependent failure probability," *Nuclear Engineering and Design* vol. 241, no.5,pp. 1385–1394, 2011.

24. Cabrera, J. G.;, "Deterioration of concrete due to reinforcement steel corrosion," *Cement & Concrete Composites*, vol.18, no.1, pp. 47-59, 1996.

25. Cabrera, J. G.; and Ghoddoussi, P.;, "The effect of reinforcement corrosion on the strength of the steel/concrete bond," *International Conference on Bond in Concrete*, Riga, Latvia, pp. 10/11-10/24, 1992.

26. Capé, M.;, "Residual service-life assessment of existing R/C structures," *M.S thesis*, Chalmers University of Technology, Gothenburg, Sweden, and Milan University of Technology, Milan, Italy, 1999.

27. Carlsson, F.; Jeppsson, J.; and Thelandersson, S.;, "Reliability analysis or corroded bridge columns," *RILEM Publication*, no. 12, pp. 271-276, 2000.

28. Castel, A.; Francois, R.; and Arliguie, G.;, "Mechanical behavior of corroded reinforced concrete beams – Part 1: bond and notch effects," *Materials and Structures/Materiauxet Constructions*, vol. 33, no. 233, pp. 539-544, 2000.

29. Castel, A.; Francois, R.; and Arliguie, G.;, "Mechanical behavior of corroded reinforced concrete beams – Part 2: bond and notch effects," *Materials and Structures/Materiauxet Constructions*, vol. 33, no. 233, pp. 545-551, 2000.

30. Capozucca, R.; and Cerri M. N.;, "Influence of reinforcement corrosion in the compressive zone on the behavior of RC beams," *Engineering Structures*, vol.25, no. 13, pp. 1575-1583, 2003.

31. Cheung, M. S.; and Kyle B. R.;, "Service life prediction of concrete structures by reliability analysis," *Construction and Building Materials*, vol. 10, no.1, pp. 45-55, 1996.

32. Chung, L.; Najm, H.; and Balaguru, P.;, "Flexural behavior of concrete slabs with corroded bars," *Cement and Concrete Composites*, vol.30, no. 3, pp. 184–193, 2008.

33. Coronelli, D.;, "Corrosion cracking and bond strength modeling for corroded bars in reinforced concrete," *ACI Structural Journal*, vol. 99, no. 3, pp. 267-275, 2002.

34. Coronelli, D.; and Gambarova, P.;, "Structural assessment of corroded reinforced concrete beams: modeling guidelines," *Journal of Structural Engineering*, vol. 130, no. 8, Aug. 2004.

35. Darmawan, S. M.;, "Pitting corrosion model for reinforced concrete structures in a chloride environment," *Magazine of Concrete Research*, vol. 62, no. 2, pp. 91-101, Feb. 2008.

36. Du, Y.; Clark, L. A.; and Chan A.;, "Impact of reinforcement corrosion on ductile behavior of reinforced concrete beam," *ACI Structural Journal*, vol.104, no.3, pp. 285-293, 2007.

37. Du, Y. G.; Clark, L. A.; and Chan, A. H. C.;, "Residual capacity of corroded reinforcing bars," *Magazine of Concrete Research*, vol.57, no.3, pp. 135-147, 2005.

38. Ely, T.; Soudki, K.; and Tropper, T.;, "Long-term performance of corrosion-damaged reinforced concrete beams," *ACI Structural Journal*, vol.102, no. 5, pp. 649-656, 2005.

39. Emhamed, K. M.; "Reliability analysis of reinforced concrete beams," *M.S. Thesis*, Heriot-Watt University, Aug. 2010.

40. Enright, P. M.; and Frangopol, M. D.;, "Probabilistic analysis of resistance degradation of reinforced concrete bridge beams under corrosion," *Engineering Structures*, Vol. 20, No.11, pp. 960-971, 1998.

41. Esmaeilpoursaee A.;, "An analysis of the factors influencing electrochemical measurements of the condition of reinforcing steel in concrete structures" *PhD Thesis*, Waterloo, Ontario, Canada. 2007.

42. Fu, X.; and Chung, D.D.L.;, "Effect of corrosion on the bond between concrete and steel rebar," *Cement and Concrete Research*, vol. 27, no. 12,pp. 1811-1815, 1997.

43. Gonzalez, J. A.; Andrade, C.; Alonso, C.; and Feliu, S.;, "Comparison of rates of general corrosion and maximum pitting penetration on concrete embedded steel reinforcement," *Cement and Concrete Research*, vol. 25, no. 2, pp. 257-264, 1995.

44. Hanjari, K. Z.; Kettil, P.; and Lundgren, K.;, "Analysis of mechanical behavior of corroded reinforced concrete structures," *ACI Structural Journal*, vol. 108, no. 5, pp. 532-541, Sep.-Oct. 2011.

45. Huang, R.; and Yang, C.C.;, "Condition assessment of reinforced concrete beam relative to reinforcement corrosion," *Cement and Concrete Composites*, vol.19, no. 2, pp.131-137, 1997.

46. Hui, Y.; Li, R.; and Lin, Z. S.; Quan M.;, "Experimental studies on the property before and after reinforcement corrosions in basic concrete members," *Industrial Construction*, vol.27, no. 6, 1997, pp. 14-18.

47. Ijsseling, F. P.;, "Application of electrochemical methods of corrosion rate determination to system involving corrosion product layers," *British Corrosion Journal*, vol. 21, no. 2, pp. 95-101, 1986.

48. ISO 2394: "General principles on reliability for structures," *Genève, Switzerland*: ISO, 1998.

49. Jia, M.;, "Finite element modeling of reinforced concrete beams strengthened with FRP composite sheets," *M.S. Thesis*, University of Alabama in Huntsville, 2003.

50. Jin, W.L.; and Zhao, Y.X.;, "Effect of corrosion on bond behavior and bending strength of reinforced concrete beams," *Journal of Zhejiang University (Science)*, vol. 2, no. 3, pp. 298-308, Jul.-Sep. 2001.

51. Kachlakev, D. I.; Miller, T. H.; Yim, S. C. S.; Chansawat, K.; and Potisuk, T.;, "Finite element modeling of concrete structures strengthened with FRP laminate, " *Rep. SPR316*, United States Department of Transportation Federal Highway Administration and the Oregon Department of Transportation, United States, 2001.

52. Konecný, P.;, "Reliability of reinforced concrete bridge decks with respect to ingress of chlorides," *PhD Thesis*, Technical University of Ostrava, 2007.

53. Lee, C.; Bonacci, J.F.; Thomas, M.; Maalej, M.; Khajehpour, S.; Hearn, N.; Pantazopoulou, S.; and Sheikh, S.;, "Accelerated corrosion and repair of reinforced concrete columns using carbon fibre reinforced polymer sheets," *Canadian Journal of Civil Engineering*, vol.27, no.5, pp. 941-948, 2000.

54. Lee, S. H.; Noguchi, T.; and Tomosawa, F.;, "Evaluation of the bond properties between concrete and reinforcement as a function of the degree of reinforcement corrosion," *Cement and Concrete Research*, vol. 32, no.8, pp. 1313–1318, 2002.

55. Lee, S. H.; Noguchi, T.; and Tomosawa, F.;, "FEM analysis for structural performance of deteriorated RC structures due to rebar corrosion," *Proceedings of the Second International Conference on Concrete under Severe Conditions*, Norway: Tromsø, pp. 327–336, 1998.

56. Li, C. Q.;, "Life-cycle modeling of corrosion-affected concrete structures: propagation," *Journal of Structural Engineering*, ASCE, vol. 129, no. 6, pp. 753-761, Jun. 2003.

57. Li, C. Q.;, "Reliability based service life prediction of corrosion affected concrete structures," *Journal of Structural Engineering*, vol. 130, no.10, pp. 1570-1577, Oct. 2004.

58. Li, C. Q.; and Zheng, J. J.;, "Propagation of reinforcement corrosion in concrete and its effect on structural deterioration," *Magazine and Concrete Research*, vol. 57, no. 5, pp. 261-271 , Jun. 2005.

59. Liu, Y.; and Weyers, R. E.; "Modeling the time-to-corrosion cracking in chloride contaminated reinforced concrete structures," *ACI Materials Journal*, vol. 95, no. 6, pp. 675-681, Nov.-Dec. 1998.

60. Malumbela, G.; Alexander, M.; and Moyo, P.;, "Variation of steel loss and its effect on the ultimate flexural capacity of RC beams corroded and repaired under load," *Construction and Building Materials*, 2009.

61. Mangat, P. S.; and Elgarf, M. S.;, "Flexural strength of concrete beams with corroding reinforcement," *ACI Structural Journal*, vol. 96, no.1, pp. 149-158, Jan.-Feb. 1999.

62. Maslehuddin, M.; Al-Mehthel, M.; Alidi, S.; Shameem, M.; and Ibrahim, M.;, " Effect of dust in coarse aggregates on reinforcement corrosion in concrete," *Construction and Building Materials*, vol. 24, no.3, pp. 326-331, Mar. 2010.

63. MEC;, "As solid as concrete," *Middle East Construction*, pp. 20-21, Apr.-May 1987.

64. Mirza, S. A.; and MacGregor, J. G.;, "Variability of mechanical properties of reinforcing bars," *Journal of the Structural Division*, vol.105, no.5, pp. 921-937, 1979.

65. Mirza, S. A.; MacGregor, J. G.; and Hatzinikolas, M.;, "Statistical descriptions of strength of concrete," *Journal of the Structural Division*, vol.105, no.6, pp. 1021-1037, 1979.

66. Molina, F. J.; Alonso, C.; and Andrade, C.;, "Cover cracking as a function of rebar corrosion 2-numerical model," *Materials and Structures*, vol. 26, no. 163, pp. 532-548, 1993.

67. Mohammed, A. M., Almansour, H. H.; and Martín-Pérez B.;, "Combined effect of reinforcement corrosion and seismic loads on RC bridge columns: modeling," *2nd International Engineering Mechanics and Materials Specialty Conference Ottawa*, Ontario, pp. 1-10, Jun. 2011.

68. N o w a k, A. S.; and K a s z y ń s k a, M.;, "Target reliability for new, existing and historical structures," *IX Conference on Renewal of Historical Structures*, pp.219-228, 2011.

69. Nokhasteh, M. A.; Eyre, J. R.; and Mcleish, A.;, "The effect of reinforcement corrosion on the strength of reinforced concrete members," *Structural Integrity Assessment, Elsevier Applied Science*, pp. 314- 325, 1992.

70. Nowark, A. S.; and Collins, K. R.;, "Reliability of structures," *McGraw Hill*, New York, 2000.

71. Pantazopoulou, S. J.; and Papoulia, K. D.;, "Modeling cover-cracking due to reinforcement corrosion in RC structures," *Journal of Engineering Mechanics*, ASCE, vol. 127, no. 4, pp. 342-351, 2001.

72. Potisuk, T.; Higgins, C.; Miller, H. T.; and Yim, C. S.;, "Finite element analysis of reinforced concrete beams with corrosion subjected to shear," *Advances in Civil Engineering*, Vol. 2011, 2011.

73. Pozolo, A. M.;, "Transfer and development lengths of steel strands in full-scale prestressed self-consolidating concrete bridge girders," *M.S. Thesis*, University of Illinois at Urbana-Champaign, 2010.

74. Reh, S.; Beley, J.; Mukherjee, S.; and Khor, E.;, "Probabilistic finite element analysis using ANSYS," *Structural Safety*, vol. 28, pp. 17-43, 2005.

75. Revathy, J.; Suguna, K.; and Raghunath, P. N.;, "Effect of corrosion damage on the ductility performance of concrete columns," *American Journal of Engineering and Applied Sciences*, vol. 2, no.2, pp. 324-327, 2009.

76. Ravindrarajah, R.; and Ong, K.;, "Corrosion of steel in concrete in relation to bar diameter and cover thickness," *ACI Special Publication*, vol. 100, no.4, pp. 1667-1678, Apr. 1987.

77. Rasheeduzzafar; Dakhil, F. H.; and Al-Gahtani, A. S.;, "Deterioration of concrete structures in the environment of the Middle East," *ACI Journal*, vol. 81, no. 1, pp. 13-20, Jan. 1984.

78. Rodriguez, J.; Ortega, L. M.; and Casal, J.;, "Load carrying capacity of concrete structures with corroded reinforcement," *Construction and Building Materials*, vol.11, no. 4, pp. 239-249, 1997.

79. Saito, Y.; Michiaki, O.; Kanakubo, T.; and Yamamoto, Y.;, "Structural performance of corroded RC column under uniaxial compression load," http://www.kz.tsukuba.ac.jp/~rclab/protect2007s.pdf.

80. SAS. ANSYS 12.1 Finite element analysis system manual, SAS IP Inc., Pittsburgh, PA, Unites States, 2009

81. Shang, F.; An, X.; Mishima, T.; and Maekawa, K.;, "Three-dimensional nonlinear bond model incorporating transverse action in corroded RC members," *Journal of Advanced Concrete Technology*, vol. 9 , no. 1 , pp. 89-102 , Feb. 2011.

82. Stanish, R. D.; Hooton; and Pantazopuolou, S. J.;, "Corrosion effects on bond strength in reinforced concrete," *ACI Structural Journal*, vol. 96, no. 6, pp. 915-921, 1999.

83. Stewart, M. G.;, "Mechanical behavior of pitting corrosion of flexural and shear reinforcement and its effect on structural reliability of corroding RC beams," *Structural Safety*, vol.31, no. 1, pp. 19-30, 2009.

84. Stewart, M. G.; and Rosowsky, D. V.;, "Structural safety and serviceability of concrete bridges subject to corrosion," *Journal of Infrastructure System*, ASCE, vol. 4, no. 4, pp. 146-155, 1998.

85. Tachibana, Y.; Maeda, K-I; Kajikawa, Y.; and Kawamura, M.;, "Mechanical behavior of RC beams damaged by corrosion of reinforcement," *Third International Symposium on Corrosion of Reinforcement in Construction*, Wishaw, UK, pp.178-187, 1990.

86. Tapan, M.; and Aboutaha, R. S.;, "Strength evaluation of deteriorated RC bridge columns," *Journal of Bridge Engineering*, ASCE, vol. 13, no. 3, pp. 226-236, May-Jun. 2008.

87. Tavarez, F.A.;, "Simulation of behavior of composite grid reinforced concrete beams using explicit finite element methods," *M.S. Thesis*, University of Wisconsin-Madison, Madison, Wisconsin, 2001.

88. Thomas, J.; and Ramaswamy, A.;, "Nonlinear analysis of shear dominant prestressed concrete beams using ANSYS," http://www.ansys.com/staticassets/ANSYS/staticassets/resourcelibrary/confpaper/2006-Int-ANSYS-Conf-30.pdf

89. Ting, S. C.; and Nowak, A. S.;, "Effect of reinforcing steel area loss on flexural behavior of reinforced concrete beams," *ACI Structural Journal*, vol. 88, no. 3, pp. 309-314, May-Jun. 1991.

90. Torres-Acosta, A. A.; Fabella-Gallegos, M. J.; Munoz-Naval, A.; Vasquez-Vega, D.; Hernandez-Jimenez, J. R.; and Martinez-Madrid, M.;, "Influence corrosion on the structural stiffness of reinforced concrete beams," *Corrosion*, vol. 60, no. 9, pp. 862-872, 2004.

91. Torres-Acosta, A. A.; Navarro-Gutierreza, S.; and Teran-Cullen, J.;, "Residual flexure capacity corroded reinforced concrete beams," *Engineering Structures*, vol. 29, no.6, pp. 1145-1152, 2007.

92. Uomoto, T.; and Misra, S.;," Behavior of concrete beams and columns in marine environment when corrosion of reinforcing bars takes place," *ACI Special Publication SP-109*, pp. 127-145, 1988.

93. Val, D. V.;, "Deterioration of strength of RC beams due to corrosion and its influence on beam reliability," *Journal of Structural Engineering*, vol. 133, no.9, pp. 1297-1306, Sep. 2007.

94. Val, D. V.; and Chernin, L.;, "Serviceability reliability of reinforced concrete beams with corroded reinforcement," *Journal of Structural Engineering*, vol. 135, no. 8, pp. 896-905, Aug. 2009.

95. Val , D. V.; and Melchers, R. E.;, "Reliability of deteriorating RC slab bridges," *Journal of Structural Engineering*, ASCE, vol.123, no.12, pp.1638-1644, 1997.

96. Vu, K. A. T.; and Stewart, M. G.;, "Structural reliability of concrete bridges including improved chloride induced corrosion models," *Structural Safety*, vol. 22, no. 4, pp. 313-333, 2000.

97. Wang, C.; Salman, C. G.; and Pincheira, J. H.;, "Reinforced concrete design," *John Wiley* & Sons, Inc., 2007.

98. Wang, W. L.; and Chen, J.;, "Residual strengths of reinforced concrete beams with heavy deterioration," *Research Journal of Applied Sciences, Engineering and Technology*, vol. 2, no. 8, pp. 798-805, 2011.

99. Wang, X.; and Liang, Fa-Yun;, "Performance of RC columns with partial length corrosion," *Nuclear Engineering Design*, vol. 238, no.12, pp. 3194-3202, 2008.

100. Wang, X.; and Liu, X.;, "Bond strength modeling for corroded reinforcements," *Construction and Building Materials*, vol. 20, no. 3, pp. 177-186, 2005.

101. Wang, X.; and Liu, X.;, "Simplified methodology for the evaluation of the residual strength of corroded reinforced concrete beams," *Journal of Performance for Constructed Facilities*, vol. 24, no. 2, pp. 108-119, 2010.

102. Wolanski, A. J.;, "Flexural behavior of reinforced and prestressed concrete beams using finite element analysis," *M.S. Thesis*, Marquette University, 2004.

103. Xiao-hui, W. and Xi-la, L.;, "Modeling the flexural carrying capacity of corroded RC beam," *Journal of Shanghai Jiaotong University (Science)*, vol. 3, no. 2, pp. 129-135, 2008.

104. Xiaoming, Y.; and Hongqiang, Z.;, "Finite element investigation on load carrying capacity of corroded RC beam based on bond-slip," *Jordan Journal of Civil Engineering*, vol. 6, no. 1, pp. 134-146, 2012.

105. Xue, X.; and Seki, H.;, "Influence of longitudinal bar corrosion on shear behavior of RC beams, " *Journal of Advanced Concrete Technology*, vol. 8, no. 2, pp. 145-156, 2010.

106. Xu, S.;, "The models of deterioration and durability evaluation of reinforced concrete structure[D]," *XI'an University of Architecture and Technology*, 2003.

107. Yamamoto, T.; Sato, Y.; Hattori, A.; and Miyagawa, T.;, "Studies on the shear behavior of RC beams with corroded reinforcement," *Proceedings of the Japan Concrete Institute*, vol. 27, no. 1, pp. 913-918, 2005. (In Japanese).

108. Yeung, H. W.;, "Canopy and balcony collapses – lessons from the past', safety in buildings," *Hong Kong Institution of Engineers Materials Division*, Hong Kong Exhibition and Conference Centre, Mar. 1999.

109. Yoon, S.; Wang, K.; Weiss, W.J.; and Shah, S.P., "Interaction between loading, corrosion, and serviceability of reinforced concrete," *ACI Materials Journal*, vol. 79, no. 3, pp. 637-644, Nov.-Dec. 2000.

110. Yubun, A.; Balaguru, P.; and Lan, C.;, "Bond behavior of corroded reinforcement bars," *ACI Materials Journal*, vol. 97, no.2, pp. 214-220, Mar.-Apr. 2000.

111. Zangeneh, P.;, "Finite element modeling of steel- concrete composite beams strengthened with prestressed FRP laminates," *M.S. Thesis*, Calgary University, September, 2011.

112. Zhang, P.S.; Lu, M.; and Li, X.Y.;, "Mechanical property of rustiness in reinforcement steel," *Industrial Construction*, vol. 25, no. 9, pp. 41-44, 1995.

Vitae

Name :Mohammed Ali Mohammed Al-Osta

Nationality :Yemeni

Date of Birth :5/2/1975

Email :malosta@kfupm.edu.sa; nasser20022009@gmail.com

Address :King Fahd University of Petroleum and Minerals (KFUPM), Dhahran, 31262, Saudi Arabia.

Academic Background :B.Sc. in Civil Engineering, Sana'a Univ., Sana'a, Yemen 1999. (First rank with honour). M.S., King Fahd University of Petroleum & Minerals, Dhahran, Saudi Arabia, June 2009. (First rank with honour). Obtained the highest GPA (3.97/4.00) among the graduate Civil and Applied Civil Engineering students. PhD, King Fahd University of Petroleum & Minerals 2013. Obtained the highest GPA (3.940/4.00)